

## Development of a green hypergolic propellant based on hydrogen peroxide and ionic liquids

Felix Lauck

Deutsches Zentrum für Luft- und Raumfahrt  
Institut für Raumfahrtantriebe  
Lampoldshausen

# **Forschungsbericht 2024-29**

## **Development of a green hypergolic propellant based on hydrogen peroxide and ionic liquids**

Felix Lauck

Deutsches Zentrum für Luft- und Raumfahrt  
Institut für Raumfahrtantriebe  
Lampoldshausen

172 Seiten  
62 Bilder  
42 Tabellen  
243 Literaturstellen



Deutsches Zentrum  
DLR für Luft- und Raumfahrt





*Herausgeber:*

Deutsches Zentrum  
für Luft- und Raumfahrt e. V.  
Wissenschaftliche Information  
Linder Höhe  
D-51147 Köln

ISSN 1434-8454  
ISRN DLR-FB-2024-29  
Erscheinungsjahr 2024  
DOI: [10.57676/fvc3-5w76](https://doi.org/10.57676/fvc3-5w76)

## **D 93 (Dissertation der Universität Stuttgart)**

### **Erklärung des Herausgebers**

Dieses Werk wird unter den Bedingungen der Creative Commons Lizenz vom Typ Namensnennung 4.0 International, abrufbar über <https://creativecommons.org/licenses/by/4.0/legalcode> , zur Nutzung überlassen.

### **Lizenz**



Creative Commons Attribution 4.0 International

Felix LAUCK  
DLR, Institut für Raumfahrtantriebe, Lampoldshausen

***Entwicklung eines grünen, hypergolen Treibstoffs basierend auf Wasserstoffperoxid und ionischen Flüssigkeiten***

Dissertation Universität Stuttgart

Das Ziel dieser Arbeit ist es, eine grüne, hypergole Treibstoffkombination zu entwickeln. Die neue Treibstoffkombination soll eine vergleichbare Leistung zu herkömmlichen hypergolen Treibstoffen bieten, dabei jedoch ein erheblich reduziertes Gefahrenpotential aufweisen.

Hypergole Treibstoffe, wie beispielsweise die Kombination aus Hydrazin oder einem seiner Derivate mit Distickstofftetroxid, sind in der Raumfahrt weit verbreitet. Sie sind für den Antrieb im Weltraum hervorragend geeignet, da sie nahezu unbegrenzt wieder gezündet werden können, gut lagerfähig sind und eine hohe Leistung aufweisen. Diese Treibstoffe haben jedoch erhebliche Nachteile: der Oxidator Distickstofftetroxid ist hochgiftig und flüchtig. Zudem sind die Brennstoffe basierend auf Hydrazin und seinen Derivaten giftig und stehen im Verdacht krebserregend zu sein, was zukünftig zu einer Einschränkung der Verwendung in Europa führen könnte. Der Einsatz herkömmlicher, lagerfähiger Treibstoffe ist kostspielig und zeitaufwendig, da er eine umfangreiche Schutzausrüstung und Aufwand bei der Handhabung erfordert. Daher werden derzeit in vielen Forschungszentren alternative "grüne" Treibstoffe entwickelt. Jedoch gibt es derzeit noch keinen allgemein akzeptierten Ersatz für herkömmliche hypergole Treibstoffe. Diese Arbeit zielt darauf ab, diese Lücke zu schließen.

Der Entwicklungsprozess begann mit der Definition der Anforderungen und Randbedingungen für die neue Treibstoffkombination. Als Oxidator wurde Wasserstoffperoxid ausgewählt, das eine Alternative zu den herkömmlichen Oxidatoren darstellt. Als Brennstoffkandidaten wurden ionische Liquide ausgewählt, da sie bei Umgebungsbedingungen eine vernachlässigbare Dampfphase haben, was die Handhabung erheblich erleichtert. In der nächsten Entwicklungsphase wurde ein Screening nach geeigneten Treibstoffkandidaten durchgeführt, wobei sich auf kommerziell erhältliche Substanzen konzentrierte wurde. Auf der Grundlage dieses Screenings wurde eine Auswahl an vielversprechenden ionischen Flüssigkeiten getroffen. Anschließend wurden diese im Tropftest untersucht, mit dem bestimmt werden kann, ob zwei Substanzen hypergol sind. Ionische Liquide mit dem Thiocyanat-Anion erwiesen sich als hypergol mit hochkonzentriertem Wasserstoffperoxid. Im Tropftest betrug der Zündverzug von 1-Ethyl-3-methylimidazoliumthiocyanat 25-30 ms. Durch die Zugabe eines Additivs, wie z. B. Kupferthiocyanat, konnte der Zündverzug auf etwa 13 ms reduziert werden. Eine Studie über den Einfluss verschiedener Parameter im Tropftest ergab, dass der vielversprechendste Brennstoff in Bezug auf den Zündverzug aus dem ionischen Liquid 1-Ethyl-3-methylimidazoliumthiocyanat mit 5 Gew.-% Kupferthiocyanat (E5C) besteht. Das Zündverhalten dieses Treibstoffs wurde unter relevanteren Bedingungen in speziell entwickelten Injektoren untersucht. Dabei wurden Zündverzögerungen in der Größenordnung von einigen Millisekunden beobachtet, was für eine zuverlässige Zündung in Triebwerken ausreichend ist. Der Treibstoff E5C wurde in Bezug auf Dichte, Viskosität und thermisches Verhalten charakterisiert. Es wurde ein maximaler theoretischer spezifischer Impuls von 323 s (eingefrorene Überschall-expansion, Brennkammerdruck 10 bar, Expansionsverhältnis 330) berechnet. Damit ist der spezifische Impuls um 5 % niedriger als bei der herkömmlichen hypergolen Treibstoffkombination Monomethylhydrazin und Distickstofftetroxid. Der spezifische Dichteimpuls ist jedoch 10 % höher. Schließlich wurde die Anwendung des gewählten ionischen Liquids in einem Dual-Mode-Antriebssystem untersucht, wobei ein elektrischer Modus die ionische Flüssigkeit als Treibstoff verwendet wurde. Für eine geostationäre Mission wurde festgestellt, dass ein Dual-Mode-System im Vergleich zu einer vollständig chemischen Lösung erhebliche Masseneinsparungen bietet.

Zusammenfassend lässt sich festhalten: die Gruppe der ionischen Flüssigkeiten mit dem Thiocyanatanion hat sich als eine vielversprechende Klasse von hypergolen Substanzen in Kombination mit Wasserstoffperoxid erwiesen. Der Treibstoff E5C ist in Bezug auf Leistung und Hypergolizität der beste Kandidat, um herkömmliche hypergole Treibstoffe zu ersetzen.

Felix LAUCK

German Aerospace Center (DLR), Institute of Space Propulsion, Lampoldshausen

***Development of a green hypergolic propellant based on hydrogen peroxide and ionic liquids***

Doctoral thesis University of Stuttgart

This thesis aims to develop a green hypergolic propellant combination with similar performance compared to conventional hypergolic propellants but at a reduced hazard potential.

Hypergolic propellants are widely used in space propulsion because they are well-suited for in-space propulsion, as they offer virtually unlimited restarts, good storability and excellent performance. However, such propellants have significant drawbacks: the oxidizers, based on nitrogen tetroxide and its derivatives, are highly toxic and volatile, and the fuels, based on hydrazine and its derivatives, are toxic and suspected to be carcinogenic, which may lead to restricted use in Europe. Operations associated with conventional storable propellants are costly and time consuming as they require extensive protective equipment and special procedures. To overcome these limitations, alternative "green" propellants are currently being developed at many research centres, but there is still no widely accepted replacement for conventional hypergols. This thesis aims to fill this gap.

The development process began by defining the novel propellant's requirements and boundary conditions. The oxidizer selected was hydrogen peroxide, a green alternative to the conventional oxidizers. The fuel candidates were selected among ionic liquids since they have a neglectable vapour phase at ambient conditions, which facilitates handling, and they can be tuned by selecting a combination of anions and cations. In the next development phase, suitable fuel candidates were screened, focusing on commercially available substances. Based on the screening, a selection of promising ionic liquid was made. Next, these ionic liquids were tested in a lab-scale drop test. This procedure allows the initial evaluation of the hypergolicity of two substances. Ionic liquids with the thiocyanate anion were found to be hypergolic with highly concentrated hydrogen peroxide. In the drop test, the ignition delay of 1-ethyl-3-methylimidazolium thiocyanate was 26-32 ms. Adding an additive, such as copper thiocyanate, reduced the ignition delay to about 13 ms. A study on the influence of various parameters in the drop test showed that the most promising fuel is based on the ionic liquid 1-ethyl-3-methylimidazolium thiocyanate with 5 wt% copper thiocyanate (E5C). The ignition behaviour of this fuel was studied under more relevant conditions in specifically designed impinging injectors. Here, ignition delays in the order of several milliseconds were observed, which is expected to be sufficient to provide smooth ignition in thrusters. The fuel E5C was characterized in terms of density, viscosity and thermal behaviour. A maximum theoretical specific impulse of 323 s (frozen supersonic expansion, combustion chamber pressure 10 bar, expansion ratio 330) was calculated. Thus, the specific impulse is 5 % lower compared to the conventional hypergolic propellant combination of monomethyl hydrazine and dinitrogen tetroxide. However, the density-specific impulse is 10 % higher. Finally, the application of the ionic liquid fuel selected in a dual-mode propulsion system was investigated, with an electrical mode using the ionic liquid as a propellant. For a geostationary mission, it was found that a dual-mode system offers significant mass savings compared to a full chemical solution.

To conclude, the group of thiocyanate ionic liquids is a promising class of hypergolic substances with hydrogen peroxide. Further, the fuel E5C is the best candidate in terms of performance and hypergolicity to substitute conventional hypergolic propellants.

# Development of a green hypergolic propellant based on hydrogen peroxide and ionic liquids

A thesis approved by the Faculty of Aerospace Engineering and Geodesy of the University of Stuttgart in fulfilment of the requirements for the degree of Doctor of Engineering Sciences (Dr.-Ing.)

by  
**Felix Lauck**  
born in  
Quierschied

Main referee: Prof. Dr.-Ing. Stefan Schlechtriem  
Co-referee: Prof. Angelo Pasini  
Date of defence: 07.11.2024

Institute of Space Systems  
University of Stuttgart  
2024



*By the nature of research more tests are going to fail than are going to succeed,  
and more combinations are going to ignite slowly than are going to light off in a hurry.  
And when the result of each delayed ignition is a demolished motor,  
a screening program can become a bit tedious and more than a bit expensive.*

John Clark, IGNITION!



# Danksagung

Ein großer Dank geht an Herrn Prof. Dr.-Ing. Stefan Schlechtriem, für die Möglichkeit meine Promotion am Institut für Raumfahrtantriebe durchzuführen und für die Betreuung der Arbeit. Außerdem bedanke ich mich bei Herrn Prof. Angelo Pasini für die Begutachtung dieser Arbeit. Besonders möchte ich mich bei Dominic Freudenmann und Michele Negri bedanken. Ihr habt mich auf dieses spannende Thema gebracht und mir die Möglichkeiten gegeben, es nach meinen Vorstellungen zu bearbeiten. Außerdem habt ihr mich mit vielen Anregungen und dem Teilen von Kenntnissen sehr unterstützt und weitergebracht. Mein Dank geht auch an Sophie Stölzle für die vielen Austausche und erleuchtenden Einblicke in die Welt der Chemie.

Ein weiterer Dank geht an Lukas Werling und Christoph Kirchberger für eure Unterstützung und Verständnis, sodass es möglich war, dass dieses schriftliche Werk entstehen konnte.

Ich möchte mich herzlich bei dem Labor-Team der Abteilung Chemische Treibstofftechnologie und dem M11-Team der Abteilung Satelliten- und Orbitalantriebe bedanken. Durch eure Hilfe und Unterstützung konnte ich meine Versuche aufbauen und durchführen, sowie die vielen Ergebnisse produzieren.

Danke auch an die fleißigen Studenten, die mich mit ihrer Tatkraft in den vergangenen Jahren unterstützt haben. Namentlich waren das Jan, Jakob und Julian. Ja, das "J" im Vornamen war Einstellungsvoraussetzung.

Ich freue mich, dass das Resultat der Arbeit HIP\_11 ein vielversprechender Treibstoff ist weiterverfolgt wird. Danke an Philipp Teuffel, Florian Merz, Marc Gritzka und die KollegInnen von M11 und ISPTech, dass wir HIP\_11 weiter vorantreiben.

Danke an Sophie, Dominic, Lukas und Michele für das Reviewen meiner Arbeit und für eure Fragen und Anmerkungen.

Vielen Dank auch an meine Familie, für den Rückhalt in den vergangenen Jahren. Der größte Dank geht an meine Frau Carina, die mich immer unterstützt hat. Vor allem danke für dein Verständnis, dass ich die ein oder andere Urlaubswoche in den vergangenen Jahren zu einem großen Teil am PC verbracht habe.





# Contents

<b>Abstract</b>	<b>vi</b>
<b>Kurzfassung</b>	<b>ix</b>
<b>List of Figures</b>	<b>ix</b>
<b>List of Tables</b>	<b>xi</b>
<b>1 Introduction and motivation</b>	<b>1</b>
1.1 Motivation . . . . .	2
1.2 Green propellants . . . . .	3
1.3 Objective . . . . .	4
1.4 Research methodology . . . . .	4
1.5 Outline . . . . .	5
<b>2 Fundamentals and background</b>	<b>7</b>
2.1 Fundamentals of rocket propulsion . . . . .	7
2.1.1 Performance analysis with CEA . . . . .	9
2.2 Hypergolic ignition . . . . .	11
2.2.1 Qualitative models of hypergolic ignition . . . . .	11
2.2.2 Ignition theories . . . . .	12
2.2.3 Ignition delay . . . . .	14
2.3 Test methods . . . . .	16
2.3.1 Drop tests . . . . .	16
2.3.2 Injector tests . . . . .	16
2.3.3 Thruster tests . . . . .	17
2.4 State of the art: Green propellants . . . . .	17
2.4.1 Hydrogen peroxide . . . . .	17
2.4.2 Hypergolic fuels with hydrogen peroxide . . . . .	20
2.4.3 Ionic liquids: definition and properties . . . . .	21
2.4.4 Ionic liquids for space propulsion . . . . .	21
2.5 Injection . . . . .	24
2.5.1 Impinging injector . . . . .	25
2.5.2 Swirl injector . . . . .	27
2.5.3 Pintle injector . . . . .	27
<b>3 Methods</b>	<b>29</b>
3.1 Definition and screening . . . . .	29
3.1.1 Performance calculation . . . . .	29
3.2 Experimental setups . . . . .	30
3.2.1 Drop test . . . . .	30
3.2.2 Hypergolic injection test setup . . . . .	38
3.2.3 Diagnostics . . . . .	44
3.2.4 Materials . . . . .	45

<b>4</b>	<b>Definition and screening</b>	<b>47</b>
4.1	Detailed objective . . . . .	47
4.2	Definition of criteria . . . . .	48
4.3	Requirements . . . . .	49
4.3.1	Physical and chemical properties . . . . .	49
4.3.2	Performance potential . . . . .	51
4.3.3	Safety aspects . . . . .	52
4.3.4	Application related properties . . . . .	52
4.3.5	Cost . . . . .	53
4.3.6	Others . . . . .	54
4.3.7	Relevant for the screening . . . . .	54
4.4	Data set . . . . .	54
4.5	Performance calculation . . . . .	56
4.6	Evaluation and selection . . . . .	59
<b>5</b>	<b>Drop test</b>	<b>61</b>
5.1	Part 1: initial testing . . . . .	61
5.1.1	Neat ionic liquids . . . . .	61
5.1.2	Reduction of the IDT . . . . .	62
5.2	Part 2: testing in the hypergolic drop test setup . . . . .	66
5.2.1	Detailed investigation of [Cu][SCN] . . . . .	66
5.2.2	Drop test parametric study . . . . .	69
5.2.3	Environmental factors on the ignition . . . . .	71
5.2.4	Influence of cation structure . . . . .	82
5.2.5	Reference test . . . . .	84
5.3	Summary of the drop tests . . . . .	85
<b>6</b>	<b>Injection test</b>	<b>87</b>
6.1	Injector design . . . . .	87
6.2	Preparation . . . . .	88
6.2.1	Discharge coefficient calibration . . . . .	88
6.3	Initial testing of green hypergolic fuels . . . . .	90
6.3.1	Block 0 . . . . .	90
6.3.2	E5C . . . . .	91
6.4	Second test campaign: fuel screening and low pressure ignition verification . . . . .	97
6.4.1	E5C ambient pressure variation . . . . .	97
6.4.2	E1C pressure variation . . . . .	100
6.4.3	[EMIm][SCN] ignition verification . . . . .	102
6.4.4	Swirl injector . . . . .	104
6.5	Test anomalies . . . . .	107
6.6	Summary of the injector tests . . . . .	109
<b>7</b>	<b>HIP_11</b>	<b>111</b>
7.1	Properties of HIP_11 . . . . .	111
7.1.1	Physical properties . . . . .	111
7.1.2	Thermodynamic properties . . . . .	114
7.1.3	Propulsive potential . . . . .	115
7.1.4	Toxicity . . . . .	117
7.2	Perspective use of HIP_11 in a multimode propulsion system . . . . .	118
7.3	Summary . . . . .	120

<b>8</b>	<b>Conclusion and outlook</b>	<b>121</b>
8.1	Summary and conclusion . . . . .	121
8.2	Outlook . . . . .	123
<b>9</b>	<b>Annex</b>	<b>125</b>
9.1	Injectors . . . . .	125
9.2	Hypergolic ionic liquids with hydrogen peroxide . . . . .	126
	<b>References</b>	<b>130</b>



# Abstract

This thesis aims to develop a green hypergolic propellant combination with similar performance compared to conventional hypergolic propellants but at a reduced hazard potential.

Hypergolic propellants are widely used in space propulsion because they are well-suited for in-space propulsion, as they offer virtually unlimited restarts, good storability and excellent performance. However, such propellants have significant drawbacks: the oxidizers, based on nitrogen tetroxide and its derivatives, are highly toxic and volatile, and the fuels, based on hydrazine and its derivatives, are toxic and suspected to be carcinogenic, which may lead to restricted use in Europe. Operations associated with conventional storable propellants are costly and time-consuming as they require extensive protective equipment and special procedures. To overcome these limitations, alternative "green" propellants are currently being developed at many research centres, but there is still no widely accepted replacement for conventional hypergols. This thesis aims to fill this gap.

The development process began by defining the novel propellant's requirements and boundary conditions. The oxidizer selected was hydrogen peroxide, a green alternative to the conventional oxidizers. The fuel candidates were selected among ionic liquids since they have a neglectable vapour phase at ambient conditions, which facilitates handling, and they can be tuned by selecting a combination of anions and cations. In the next development phase, suitable fuel candidates were screened, focusing on commercially available substances. Based on the screening, a selection of promising ionic liquid was made. Next, these ionic liquids were tested in a lab-scale drop test. This procedure allows the initial evaluation of the hypergolicity of two substances. Ionic liquids with the thiocyanate anion were found to be hypergolic with highly concentrated hydrogen peroxide. In the drop test, the ignition delay of 1-ethyl-3-methylimidazolium thiocyanate was 26-32 ms. Adding an additive, such as copper thiocyanate, reduced the ignition delay to about 13 ms. A study on the influence of various parameters in the drop test showed that the most promising fuel is based on the ionic liquid 1-ethyl-3-methylimidazolium thiocyanate with 5 wt% copper thiocyanate (E5C). The ignition behaviour of this fuel was studied under more relevant conditions in specifically designed impinging injectors. Here, ignition delays in the order of several milliseconds were observed, which is expected to be sufficient to provide smooth ignition in thrusters. The fuel E5C was characterized in terms of density, viscosity and thermal behaviour. A maximum theoretical specific impulse of 323 s (frozen supersonic expansion, combustion chamber pressure 10 bar, expansion ratio 330) was calculated. Thus, the specific impulse is 5 % lower compared to the conventional hypergolic propellant combination of monomethyl hydrazine and dinitrogen tetroxide. However, the density-specific impulse is 10 % higher. Finally, the application of the ionic liquid fuel selected in a dual-mode propulsion system was investigated, with an electrical mode using the ionic liquid as a propellant. For a geostationary mission, it was found that a dual-mode system offers significant mass savings compared to a full chemical solution.

To conclude, the group of thiocyanate ionic liquids is a promising class of hypergolic substances with hydrogen peroxide. Further, the fuel E5C is the best candidate in terms of performance and hypergolicity to substitute conventional hypergolic propellants.



# Kurzfassung

Das Ziel dieser Arbeit ist es, eine grüne, hypergole Treibstoffkombination zu entwickeln. Die neue Treibstoffkombination soll eine vergleichbare Leistung zu herkömmlichen hypergolen Treibstoffen bieten, dabei jedoch ein erheblich reduziertes Gefahrenpotential aufweisen.

Hypergole Treibstoffe, wie beispielsweise die Kombination aus Hydrazin oder einem seiner Derivate mit Distickstofftetroxid, sind in der Raumfahrt weit verbreitet. Sie sind für den Antrieb im Weltraum hervorragend geeignet, da sie nahezu unbegrenzt wieder gezündet werden können, gut lagerfähig sind und eine hohe Leistung aufweisen. Diese Treibstoffe haben jedoch erhebliche Nachteile: der Oxidator Distickstofftetroxid ist hochgiftig und flüchtig. Zudem sind die Brennstoffe basierend auf Hydrazin und seinen Derivaten giftig und stehen im Verdacht krebserregend zu sein, was zukünftig zu einer Einschränkung der Verwendung in Europa führen könnte. Der Einsatz herkömmlicher, lagerfähiger Treibstoffe ist kostspielig und zeitaufwendig, da er eine umfangreiche Schutzausrüstung und Aufwand bei der Handhabung erfordert. Daher werden derzeit in vielen Forschungszentren alternative "grüne" Treibstoffe entwickelt. Jedoch gibt es derzeit noch keinen allgemein akzeptierten Ersatz für herkömmliche hypergole Treibstoffe. Diese Arbeit zielt darauf ab, diese Lücke zu schließen.

Der Entwicklungsprozess begann mit der Definition der Anforderungen und Randbedingungen für die neue Treibstoffkombination. Als Oxidator wurde Wasserstoffperoxid ausgewählt, das eine Alternative zu den herkömmlichen Oxidatoren darstellt. Als Brennstoffkandidaten wurden ionische Liquide ausgewählt, da sie bei Umgebungsbedingungen eine vernachlässigbare Dampfphase haben, was die Handhabung erheblich erleichtert. Zudem können die Eigenschaften dieser Substanzen durch die Wahl einer Kombination von Anionen und Kationen gezielt beeinflusst werden. In der nächsten Entwicklungsphase wurde ein Screening nach geeigneten Treibstoffkandidaten durchgeführt, wobei sich auf kommerziell erhältliche Substanzen konzentrierte wurde. Auf der Grundlage dieses Screenings wurde eine Auswahl an vielversprechenden ionischen Flüssigkeiten getroffen. Anschließend wurden diese im Tropftest untersucht, mit dem bestimmt werden kann, ob zwei Substanzen hypergol sind. Ionische Liquide mit dem Thiocyanat-Anion erwiesen sich als hypergol mit hochkonzentriertem Wasserstoffperoxid. Im Tropftest betrug der Zündverzug von 1-Ethyl-3-methylimidazoliumthiocyanat 25-30 ms. Durch die Zugabe eines Additivs, wie z. B. Kupferthiocyanat, konnte der Zündverzug auf etwa 13 ms reduziert werden. Eine Studie über den Einfluss verschiedener Parameter im Tropftest ergab, dass der vielversprechendste Brennstoff in Bezug auf den Zündverzug aus dem ionischen Liquid 1-Ethyl-3-methylimidazoliumthiocyanat mit 5 Gew.-% Kupferthiocyanat (E5C) besteht. Das Zündverhalten dieses Treibstoffs wurde unter relevanteren Bedingungen in speziell entwickelten Injektoren untersucht. Dabei wurden Zündverzögerungen in der Größenordnung von einigen Millisekunden beobachtet, was für eine zuverlässige Zündung in Triebwerken ausreichend ist. Der Treibstoff E5C wurde in Bezug auf Dichte, Viskosität und thermisches Verhalten charakterisiert. Es wurde ein maximaler theoretischer spezifischer Impuls von 323 s (eingefrorene Überschallexpansion, Brennkammerdruck 10 bar, Expansionsverhältnis 330) berechnet. Damit ist der spezifische Impuls um 5 % niedriger als bei der herkömmlichen hypergolen Treibstoffkombination Monomethylhydrazin und Distickstofftetroxid. Der spezifische Dichteimpuls ist jedoch 10 % höher. Schließlich wurde die Anwendung des gewählten ionischen Liquids in einem Dual-Mode-Antriebssystem untersucht, wobei ein elektrischer Modus die ionische Flüssigkeit als Treibstoff verwendet wurde. Für eine geostationäre



Mission wurde festgestellt, dass ein Dual-Mode-System im Vergleich zu einer vollständig chemischen Lösung erhebliche Masseneinsparungen bieten kann.

Zusammenfassend lässt sich festhalten: die Gruppe der ionischen Flüssigkeiten mit dem Thiocyanatanion hat sich als eine vielversprechende Klasse von hypergolen Substanzen in Kombination mit Wasserstoffperoxid erwiesen. Der Treibstoff E5C ist in Bezug auf Leistung und Hypergolizität der beste Kandidat, um herkömmliche hypergole Treibstoffe zu ersetzen.

# List of Figures

1.1	Artemis I in lunar orbit on Dec. 5, 2022, Credit: NASA / ESA . . . . .	1
1.2	Liquid chemical rocket propulsion for in-space applications . . . . .	2
1.3	Development process for a novel green hypergolic propellant . . . . .	5
2.1	Rocket principle . . . . .	7
2.2	Qualitative temperature evolution according to [27] . . . . .	11
2.3	Semenov theory: rate of heat generation and heat loss of gaseous reaction in a closed vessel at different pressures according to [38] . . . . .	14
2.4	Possible applications of hydrogen peroxide as propellant . . . . .	18
2.5	Different injector types; a) impinging injector, b) swirl injector, c) pintle injector . . . . .	25
3.1	Left: scheme of the initial drop test setup, right: photograph . . . . .	30
3.2	Drop test setup in laboratory . . . . .	31
3.3	Drop test chamber, left: scheme; right: picture . . . . .	32
3.4	Example snapshot shortly after ignition, test run 544 . . . . .	34
3.5	Example analysis of a drop test, test run 544 . . . . .	35
3.6	Example analysis of time to vapour generation determination, test run 544 . . . . .	35
3.7	Determination of drop size and velocity . . . . .	36
3.8	P&ID of the HIT set up . . . . .	38
3.9	Left: HIT reaction chamber; right: HIT integrated at M11.2 . . . . .	39
3.10	Absolute and relative deviation form reference pressure adapted from [179] . . . . .	43
3.11	Absolute and relative deviation form reference temperature adapted from [179] . . . . .	43
4.1	Flowchart of the screening of ionic liquids . . . . .	55
4.2	Screening vacuum $I_{sp}$ over ROF at chamber pressure 10.35 bar, frozen supersonic expansion, $\epsilon=330$ , 98 % $H_2O_2$ . . . . .	56
5.1	[BMIm][Ac] with a submerged drop of $H_2O_2$ , no reaction visible after 250 ms . . . . .	62
5.2	Drop test of [BMIM][SCN] and $H_2O_2$ . . . . .	63
5.3	[EMIm][SCN] with different amounts of additive [Cu][SCN] . . . . .	66
5.4	Drop tests with different amounts of additive [Cu][SCN] . . . . .	68
5.5	Upper: Drop test [EMIm][SCN] in air, lower: in argon . . . . .	73
5.6	Left: IDT over initial pressure, right: TVG over initial pressure . . . . .	75
5.7	Ignition of [EMIm][SCN] at different initial pressures, upper: 0.42 bar, lower: 0.25 bar . . . . .	76
5.8	Ignition at different initial temperatures, a) IDT for [EMIm][SCN], b) duration of the vapour phase of [EMIm][SCN], c) ratio viscosity and TVG for [EMIm][SCN], d) IDT for E5C, e) duration of the vapour phase of E5C f) ratio viscosity and TVG for E5C . . . . .	77
5.9	Arrhenius plot of [EMIm][SCN] and E5C . . . . .	80
5.10	Different $H_2O_2$ concentration vs IDT . . . . .	81
5.11	Different cationic structures . . . . .	82
5.12	Ignition of [EMIm][DCA] and WFNA . . . . .	84
6.1	2-on-1 Injector, left: drawing, right: picture . . . . .	88

6.2	Discharge coefficient, left: real system, right: assumption . . . . .	89
6.3	Mass flow over $\Delta p$ 2-on-1 injector . . . . .	90
6.4	Ignition of E5C under flowing condition . . . . .	92
6.5	Pressure slopes HIT test . . . . .	93
6.6	Flames during combustion, times from ox valve signal . . . . .	94
6.7	Ignition of E5C and H <sub>2</sub> O <sub>2</sub> with 3-on-1 injector times from ox valve signal . . . . .	96
6.8	Pressure of E5C and H <sub>2</sub> O <sub>2</sub> with 3-on-1 injector times from ox valve signal . . . . .	96
6.9	Flame during stationary condition at different pressures left: ambient pressure, right: 50 mbar . . . . .	99
6.10	Flame during stationary condition at different pressures left: ambient pressure, right: 100 mbar . . . . .	101
6.11	Ignition of [EMIm][SCN] and H <sub>2</sub> O <sub>2</sub> with 2-on-1 injector times from ox valve signal	102
6.12	Pressure of [EMIm][SCN] and H <sub>2</sub> O <sub>2</sub> with 2-on-1 injector times from ox valve signal	102
6.13	Swirl injector, taken from [179] . . . . .	104
6.14	Ignition of E5C and H <sub>2</sub> O <sub>2</sub> with swirl injector at OP 3 times from ox valve signal	105
6.15	Pressure of E5C and H <sub>2</sub> O <sub>2</sub> with swirl injector at OP 3 from ox valve signal . . . . .	105
6.16	Ignition of E5C and H <sub>2</sub> O <sub>2</sub> with swirl injector at OP 4 times from ox valve signal	106
6.17	Pressure of E5C and H <sub>2</sub> O <sub>2</sub> with swirl injector at OP 4 from ox valve signal . . . . .	106
6.18	Pressure and temperature data of anomaly test 004_001 3-on-1, left: pressure, right: temperature . . . . .	108
6.19	High speed recording of the anomaly with 3-on-1 injector during test 004_001 . . . . .	108
7.1	Lines: density of various concentrations of [Cu][SCN] dissolved in [EMIm][SCN] over temperature according to [50], dotted line interpolated values for 5 wt% [Cu][SCN] content, points: own measurements . . . . .	112
7.2	Lines: viscosity of various concentrations of [Cu][SCN] dissolved in [EMIm][SCN] over temperature according to [50], dotted line interpolated values for 5 wt% [Cu][SCN] content, points: own measurements; left: wide temperature range, right: zoom around the measurement . . . . .	112
7.3	IR spectra from [EMIm][SCN] and E5C . . . . .	113
7.4	TGA/DSC of a) [EMIm][SCN] and b) E5C . . . . .	114
7.5	Performance variation depending on ROF for different fuels, a) $I_{sp}$ , b) adiabatic temperature, c) $c^*$ , d) average molecular mass of exhaust . . . . .	116
8.1	Hot firing test of battleship thruster with HIP_11 E5C . . . . .	123
9.1	Pressure drop and $c_d$ of 3on1 injector . . . . .	125
9.2	Pressure drop and $c_d$ of 2on1 injector in 2nd test campaign . . . . .	125
9.3	Pressure drop and $c_d$ of the swirl injector . . . . .	126
9.4	2-on-1 injector drawing . . . . .	126

# List of Tables

2.1	Monopropellant H <sub>2</sub> O <sub>2</sub> performance at different concentrations, decomposition chamber pressure 10bar, expansion ratio 80, frozen at throat . . . . .	19
3.1	Uncertainties of high speed recoding evaluation . . . . .	37
3.2	Comparison simulants and propellant components at 25 °C . . . . .	41
3.3	Sequence of HIT Test . . . . .	42
4.1	Requirements with desired and acceptable ranges . . . . .	50
4.2	Data set of different commercially available ionic liquids . . . . .	57
4.3	Results of screening with different IL and 98 % hydrogen peroxide as oxidizer . . . . .	59
5.1	Initial test with different ionic liquid fuel candidates and 95 % hydrogen peroxide . . . . .	61
5.2	Drop test results with different amounts of [Co][SCN] <sub>2</sub> as additive . . . . .	64
5.3	Drop test results with different amounts of [BMIm][FeCl <sub>4</sub> ] as additive . . . . .	64
5.4	Drop test results with different amounts of [Cu][SCN] as additive . . . . .	65
5.5	Drop test results of [EMIm][SCN] and different amounts of the additive [Cu][SCN] . . . . .	65
5.6	Drop test results of [EMIm][SCN] and different amounts of the additive [Cu][SCN] . . . . .	67
5.7	Drop test results of different free fall distances . . . . .	70
5.8	Drop test results of different drop orders . . . . .	70
5.9	Drop test results of different drop amounts . . . . .	71
5.10	Drop test results of different inert atmospheres . . . . .	72
5.11	Arrhenius factors of the pressure dependent IDT fitting curve . . . . .	74
5.12	Empirical constants for viscosity [50] . . . . .	78
5.13	Arrhenius factors . . . . .	79
5.14	Arrhenius factors of the concentration fitting curve . . . . .	80
5.15	Drop test results of different concentrations H <sub>2</sub> O <sub>2</sub> for [EMIm][SCN] and E5C . . . . .	81
5.16	Drop test results of storage stored fuels . . . . .	82
5.17	Drop test results of different cations . . . . .	83
6.1	Test matrix with fuels and injectors . . . . .	88
6.2	Block 0 operating condition and ignition delay time . . . . .	90
6.3	Different operating points 2-on-1 injector during stationary conditions, tank supply pressure p <sub>tank</sub> , mass flow $\dot{m}$ , and injection velocity v <sub>inj</sub> for oxidizer and fuel; resulting ROF . . . . .	91
6.4	Ignition delay at different operating points, 2-on-1 injector, E5C 96.7 % H <sub>2</sub> O <sub>2</sub> . . . . .	94
6.5	Different operating points 3-on-1 injector during stationary conditions, tank supply pressure p <sub>tank</sub> , mass flow $\dot{m}$ , and injection velocity v <sub>inj</sub> for oxidizer and fuel; resulting ROF . . . . .	95
6.6	Results of ignition tests with different operating points 3-on-1 injector . . . . .	96
6.7	Operation points for tests with E5C and 2-on-1 injector at different ambient conditions, $\Delta p$ pressure difference from tank to ambient, v <sub>inj</sub> calculated injection velocity of the jet and resulting ROF . . . . .	98
6.8	Results of ignition tests with E5C and 2-on-1 injector at different pressure environments and operating conditions . . . . .	98

6.9	Operation points for tests with E1C and 2-on-1 injector at different ambient conditions, $\Delta p$ pressure difference form tank to ambient, $v_{inj}$ calculated injection velocity of the jet and resulting ROF . . . . .	100
6.10	Results of ignition tests with E1C and 2-on-1 injector at different ambient conditions ans operating conditions . . . . .	100
6.11	Operation points for tests with [EMIm] [SCN] and 2-on-1 injector, $\Delta p$ pressure difference form tank to ambient, $v_{inj}$ calculated injection velocity of the jet and resulting ROF . . . . .	103
6.12	Results of ignition tests with [EMIm] [SCN] and 2-on-1 injector at different operating conditions . . . . .	103
6.13	Operating points swirl injector . . . . .	104
6.14	Results swirl injector $IDT_{HS}$ - high speed recording, $IDT_{pr}$ - pressure rise . . . .	106
7.1	Surface tension of [EMIm][SCN] and E5C . . . . .	114
7.2	Maximum values of the theoretical performance . . . . .	116
7.3	Different mission scenarios . . . . .	120
9.1	Hypergolic ionic liquids with hydrogen peroxide (no DLR developments included), status from January 2023 . . . . .	127

# List of symbols

Symbol	Description	Unit
A	area	[m <sup>3</sup> ]
A'	pre-exponential factor	[-]
$c_e$	exhaust velocity	[m/s]
c	concentration	[mol/m <sup>3</sup> ]
$c^*$	characteristic velocity	[m/s]
$c_d$	discharge coefficient	[-]
CF	conversion factor	[mm/pixel]
$c_p$	molar heat capacity at constant pressure	[J/mol K]
$E_A$	activation energy	[J]
F	thrust	[N]
$g_0$	gravity on Earth	[m/s <sup>2</sup> ]
H	the heat of reaction	[J]
I	impulse	[Ns]
$I_{sp}$	specific impulse	[s]
k	reaction rate	[1/s]
l	length	[m]
$\bar{M}$	average molecular mass	[g/mol]
$\dot{m}$	mass flow	[g/s]
m	mass	[kg]
p	pressure	[bar]
R	universal gas constant	[J/mol K]
Re	Reynolds number	[-]
S	surface	[m <sup>2</sup> ]
t	time	[s]
T	temperature	[K]
u	uncertainty	diverse
v	velocity	[m/s]
V	volume	[m <sup>3</sup> ]
We	Weber number	[-]

## Greek symbols

Symbol	Description	Unit
$\alpha$	heat transfer coefficient	[W/m <sup>2</sup> K]
$\Delta$	difference	diverse
$\epsilon$	expansion ratio of the nozzle	[-]
$\eta$	viscosity	[Pa s]
$\kappa$	specific heat ratio	[-]
$\rho$	density	[g/cm <sup>3</sup> ]
$\sigma$	surface tension	[Nm]

## Subscripts

Subscript	Description
0	initial
ad	adiabatic
c	combustion chamber
fu	fuel
gen	generation
inj	injection
loss	loss
mix	mix
ox	oxidizer
t	throat
total	total
vac	vacuum

# List of Abbreviations

## General Abbreviations

Abbreviation	Meaning
ABH	Aluminium borohydride
ADN	Ammonium dinitramide
AF-315E	Propellant blend developed by AFRL, now called ASCENT
AFRL	Air Force Research Laboratory
AN	Ammonium nitrate
ASCENT	Advanced Spacecraft Energetic Non-Toxic
CEA	Chemical Equilibrium and Applications
COTS	Commercial off the shelf
DLR	Deutsches Zentrum für Luft- und Raumfahrt / German Aerospace Center
ECHA	European Chemicals Agency
EIL	Energetic ionic liquid
ESA	European Space Agency
ESD	Electrostatic discharge
Fc	Ferrocenyl
FDL	Feedline
fps	Frames per second
FTIR	Fourier-transform infrared spectroscopy
GHS	Globally Harmonized System of Classification, Labelling and Packaging of Chemicals
HAN	Hydroxylammonium nitrate
HEHN	2-Hydroxyethylhydrazinium nitrate
HIL	Hypergolic ionic liquid
HP	Hydrogen peroxide
HTP	High test peroxide
IDT	Ignition delay time
IL	Ionic liquid
IRFNA	Inhibited red fuming nitric acid
JAXA	Japan Aerospace Exploration Agency
LMP-103S	Propellant blend developed by SSC - liquid monopropellant 103S
MMH	Monomethylhydrazine
MON	Mixed oxides of nitrogen
NASA	National Aeronautics and Space Administration
NOFB	Nitrous oxide fuel blend
NTO	Dinitrogen tetroxide
OP	Operation point
PTFE	Polytetrafluoroethylene
REACH	Registration, Evaluation, Authorisation and Restriction of Chemicals
RFNA	Red fuming nitric acid
RGHP	Rocket grade hydrogen peroxide



Abbreviation	Meaning
ROF	Mixture ratio (O/F)
SCAPE	Self Contained Atmospheric Protective Ensemble
SHP163	Propellant blend developed by the company <i>IHI</i>
SoA	State of the art
SSC	Swedish Space Cooperation
THTDP	Trihexyltetradecylphosphonium
TNK	Tank
TRL	Technology readiness level
TVG	Time to vapor generation
UDMH	Unsymmetrical dimethylhydrazine
USEF	Unmanned Space Experiment Free Flyer by JAXA
WFNA	White fuming nitric acid
RCS	Reaction control system

---

## Abbreviations related to the ionic liquids

### Cations

Abbreviation	Meaning
[EMIm] <sup>+</sup>	1-ethyl-3-methylimidazolium
[BMIm] <sup>+</sup>	1-butyl-3-methylimidazolium
[AMIm] <sup>+</sup>	1-allyl-3-methylimidazolium
[diMIm] <sup>+</sup>	1,3-dimethylimidazolium
[AElm] <sup>+</sup>	1-allyl-3-ethyl imidazolium
[THTDP] <sup>+</sup>	trihexyltetradecylphosphonium

### Anions

Abbreviation	Meaning
[Ac] <sup>-</sup>	acetate
[DCA] <sup>-</sup>	dicyanamide
[EtOSO <sub>3</sub> ] <sup>-</sup>	ethyl sulfate
[MeOSO <sub>3</sub> ] <sup>-</sup>	methyl sulfate
[FeCl <sub>4</sub> ] <sup>-</sup>	tetrachloroferrate
[SCN] <sup>-</sup>	thiocyanate
[TCM] <sup>-</sup>	tricyanomethanide
[BH <sub>3</sub> CN] <sup>-</sup>	cyanoborohydride
[Al(BH <sub>4</sub> ) <sub>4</sub> ] <sup>-</sup>	aluminium borohydride



# 1 Introduction and motivation

Currently, humans are returning to the moon with the Artemis program [1]. With the Orion capsule propelled by the European service module, Artemis I flew to the moon and back in 2022. The module uses conventional hypergolic propellants. The grey cones in figure 1.1 are the nozzles of the different engines of the propulsion system. The large nozzle belongs to the main engine, an AJ10 by Aerojet Rocketdyne. This exact engine flew on several space shuttle missions as part of the Orbital Manoeuvring System (OMS) [2]. An earlier variant of the engine propelled the Apollo spacecraft around the moon. The development of the initial version of the AJ10 started in the 1950s [3]. This shows that the technology in the 21st century, which is used to return humans to the moon, is still the same as in the early days of space flight.

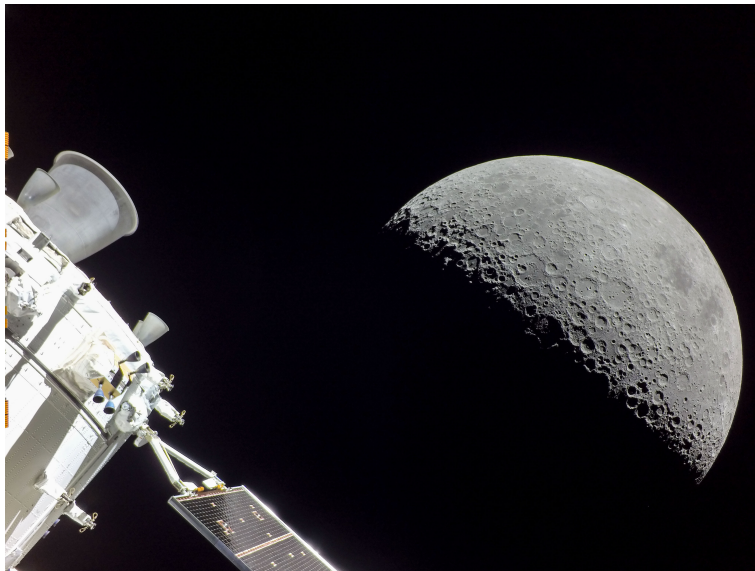


Figure 1.1: Artemis I in lunar orbit on Dec. 5, 2022, Credit: NASA / ESA

Today, spaceflight and its services are part of our everyday life. Some pervasive examples are the weather forecast based on satellite data, navigation with a system like GPS or Galileo, TV broadcasts, and now evolving satellite constellations providing internet access. Further, space flight enables scientific progress and findings. Here, important areas are: earth observation and the status of climate change, exploration of our solar system or fundamental research on the universe. For all of these activities, different spacecraft are needed.

The space flight economy is undergoing a significant change. For many decades, governmental programs were the main driver of space flight. But this is now changing: more and more commercial providers become operational. These companies have business models based on offering services provided with space resources. The recent commercialization activities of space services are called *NewSpace*. In the frame of *NewSpace*, the focus lies on fast and cost-effective solutions, allowing early revenues and profitable services in the long term.

With more active players using space infrastructure, also new challenges arise. The low earth orbits get crowded with new operational satellites, particularly new satellite constellations and space debris. If more objects are in low orbits, the risk of collisions increases. Further, a collision produces more debris objects, and a cascade with more collisions can be triggered [4]. Therefore,

every spacecraft should be equipped with a propulsion system to perform collision avoidance and de-orbit manoeuvres. Without a propulsion system, a spacecraft is a passive device in orbit, similar to space debris. The propulsion system can conduct manoeuvres necessary for the mission, such as attitude and reaction control, orbit manoeuvres, and manoeuvres to avoid space debris and de-orbiting at the end of the lifetime. The latter is becoming more critical because space debris threatens the use of certain orbits. Consequently, ESA announced a Zero Debris approach [5], of which active debris removal will be a part. This can be accomplished if every spacecraft is equipped with a propulsion system.

## 1.1 Motivation

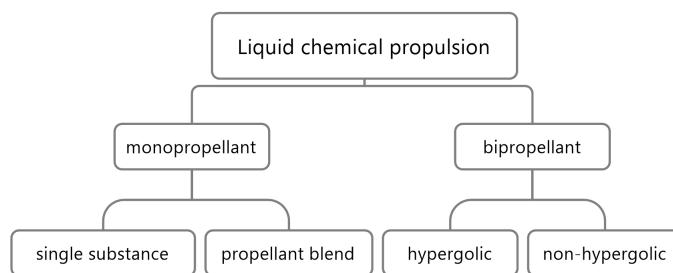


Figure 1.2: Liquid chemical rocket propulsion for in-space applications

Figure 1.2 shows a classification of commonly used storable, liquid chemical propellants for in-space propulsion. The first distinction is made based on the number of liquids that need to be stored to generate thrust by chemical reactions of the propellant. The propulsive performance of a monopropellant results from one single liquid. The liquid can either be a single liquid substance or a mixture of different substances. In the case of single substances, an exothermic decomposition reaction of the substance generates hot gaseous products, which are expanded in a nozzle to convert the released energy into thrust. The decomposition can be enabled by a suitable catalyst or thermally. The most commonly used monopropellant of this type is hydrazine ( $\text{N}_2\text{H}_4$ ). Other examples are highly concentrated hydrogen peroxide  $\text{H}_2\text{O}_2$ , nitrous oxide ( $\text{N}_2\text{O}$ ) or nitromethane ( $\text{CH}_3\text{NO}_2$ ). Some monopropellant blends were developed and demonstrated in orbit during the past two decades. Examples are LMP-103S, AF-315E (now ASCENT for Advanced Spacecraft Energetic Non-Toxic) or SHP163. These propellants are mixtures of a solid energetic compound dissolved in suitable liquids, such as fuel and water [6]. Typically, a preheated catalyst is needed to ignite these blends. Bipropellants consist of two liquid components that are stored separately. One component is the oxidiser, the second one is the fuel. The two components are brought together in the combustion chamber. Here, they either ignite spontaneously shortly after contact or they require a suitable external ignition source. The spontaneous ignition is called hypergolic ignition. Commonly used hypergolic propellants are based on hydrazine or one of its derivatives, monomethylhydrazine (MMH) or unsymmetrical dimethylhydrazine (UDMH), and a dinitrogen tetroxide (NTO) based oxidiser. Currently, hypergolic propellants are widely applied in propulsion systems for spacecraft or as propellants for launcher applications [7]. An example of a bipropellant combination requiring an external ignition is the combination of nitrous oxide and propane, where a spark plug can be used as an ignition source [8].

As mentioned above, the fuel of conventional hypergolic propellants is hydrazine or one of its

derivatives. Hydrazine is a carcinogenic and toxic substance with the following classification [9]: Carcinogenicity (category 1B, H350 May cause cancer); acute toxicity oral and dermal (Category 3, H301+H311 toxic if swallowed or in contact with skin); acute toxicity inhalation (category 2, H330 fatal if inhaled). Further,  $N_2H_4$  is skin corrosive and sensitive, flammable and hazardous to the aquatic environment [9]. Due to its carcinogenic potential, hydrazine has been included in the REACH (Registration, Evaluation, Authorisation and Restriction of Chemicals) candidate list of substances of very high concern by the European Chemicals Agency since 2011 [10]. A possible next step could be the ban on the use of hydrazine in Europe. Since MMH and UDMH are also toxic and suspected to cause cancer [11, 12], they could be treated in the same way as hydrazine and be banned in Europe in the future.

The conventional oxidiser for storable hypergolic propulsion systems is based on dinitrogen tetroxide  $N_2O_4$  (NTO). The vapour phase of NTO mainly consists of  $NO_2$  [13]. There is an equilibrium between the liquid and gas phase.  $NO_2$  has a very characteristic brown colour. As an oxidiser, NTO is used pure or in mixtures with other nitrogen oxides. Those mixtures are referred to as mixed oxides of nitrogen (MON). The solutions are named mixed oxides of nitrogen (MON-i), where i indicates the percentage of nitric oxide NO in  $N_2O_4$  /  $NO_2$ . Commonly used mixtures are MON-1 or MON-3.  $N_2O_4$  and  $NO_2$  are toxic (H330, acute toxicity, category 1) and corrosive (H314) [14]. Further, NTO's boiling point is at 21.1 °C [14]. Therefore, the vapour pressure of  $N_2O_4$  is high (around 1000 mbar) at ambient conditions, and the vapour is classified as fatal if inhaled (H330) [14].

SCAPE (Self Contained Atmospheric Protective Ensemble) suits are necessary to handle conventional hypergolic propellants safely. This is time-consuming and costly. Further, the life cycle of these toxic substances, from production, storage, transportation, testing, and qualification of hardware until the fuelling of a spacecraft, generates high expenses due to extensive precaution and safety measures. This results in high overall costs, even if the production of the propellant components and raw materials is relatively inexpensive. Moreover, the unintended release of hypergolic substances is hazardous. Over the last decades, several accidents with conventional hypergolic propellants endanger personnel and the public. Nufer brought together a summary of accidents and incidents in the US [15, 16].

To overcome the adverse issues attributed to conventional propellants' toxicity and carcinogenic potential, alternatives, the so-called "green" propellants, are researched and developed.

## 1.2 Green propellants

There is no general definition of what a 'green' propellant is. The term has been used since the late 1990s for alternative propellants, which are "environmentally friendly" [17] and low toxic [18, 19]. The least common denominator is the definition based on the comparison with conventional toxic propellants. Green propellants should be less toxic and non-carcinogenic [20]. From a European perspective, a green propellant should not be considered in REACH. In chapter 4, a more detailed definition of 'green' is given. This definition of 'green' is very different from many uses of 'green' in today's public discussions, where 'green' stands for a more sustainable, environmentally friendly or  $CO_2$ -neutral approach. Therefore, the two 'greens' have a divergent meaning and should not be confused.

Due to the reduced toxicity of green propellants, handling is facilitated compared to conventional propellants. This means handling is possible without a SCAPE suit which accelerates procedures and has a high cost-saving potential. Especially in the cost-driven NewSpace economy, low-cost green propulsion can be an enabler for new business models.

Liquid storable oxidisers for space propulsion applications are rare. The following list provides liquid oxidisers as an alternative to NTO:

- white fuming nitric acid –  $\text{HNO}_3$
- red fuming nitric acid – mixture of  $\text{HNO}_3$  and  $\text{NO}_2$
- nitrous oxide –  $\text{N}_2\text{O}$
- highly concentrated hydrogen peroxide –  $\text{H}_2\text{O}_2$

Based on the preliminary definition of a green propellant, the toxicities of the alternative liquid oxidisers are compared:

- White and red fuming nitric acid based oxidisers are highly toxic (H330: fatal if inhaled, acute toxicity, category 1) and corrosive [21]. Therefore, they should not be considered as a 'green' alternative for NTO based oxidisers.
- Nitrous oxide is gaseous at ambient conditions. But it can be liquefied with pressure of around 50 bar at ambient temperature. Nitrous oxide is not toxic but may cause drowsiness or dizziness (H336) [22]. Nitrous oxide can be considered as a 'green' oxidiser.
- Highly contracted hydrogen peroxide is also toxic and corrosive. The toxicity is classified as acute toxicity, category 4, H302 and H332 harmful if swallowed or inhaled [23]. Following, the toxicity of  $\text{H}_2\text{O}_2$  is several categories lower compared to the conventional oxidiser NTO. Because of the reduced toxic potential of hydrogen peroxide, it can be considered as a 'green' choice.

For this thesis, hydrogen peroxide was set as the relevant oxidiser because it is the only green oxidiser liquid at ambient conditions.

### 1.3 Objective

Developing green propellant solutions is necessary due to the adverse effects of conventional propellants. Green technologies can potentially substitute high-performing conventional solutions if they are economically advantageous. Currently, there are no green hypergolic solutions available. Therefore, as the objective of this thesis, the aim is to overcome the gap of a missing green hypergolic propellant. Further, the novel development should be able to substitute conventional hypergolic propellants.

For the development, highly concentrated hydrogen peroxide is chosen as the relevant oxidiser, offering lower toxicity than conventional oxidisers. Ionic liquids (ILs) are the relevant class of potential fuels. ILs have a neglectable vapour pressure at ambient conditions in common and, therefore, a reduced hazard potential compared to conventional fuels. A more detailed explanation of the rationales of this selection is given in chapter 4.

The objective in short: **Development of a green, hypergolic propellant to substitute conventional hypergolic propellants.**

### 1.4 Research methodology

The propellant development process is conducted in several steps, as shown in figure 1.3. In the beginning, the definition of requirements is necessary. A crucial factor is the definition of the meaning of 'green' in green propellants. Furthermore, the discussion on the needed properties for the evaluation of different candidates is necessary. Here, the class where potential fuels are coming from is defined and the rationales behind this selection are explained.

The second step involves screening for potential fuel candidates according to the requirements

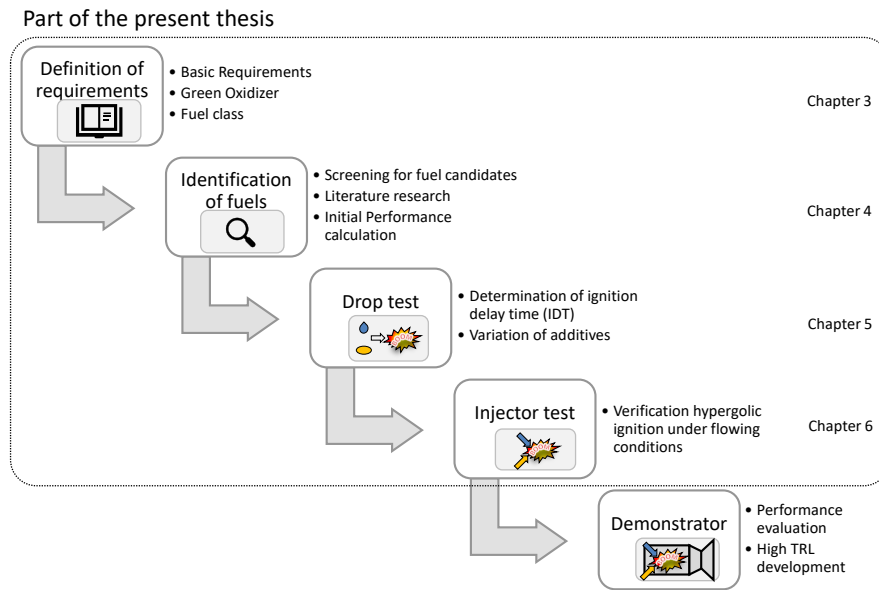


Figure 1.3: Development process for a novel green hypergolic propellant

and boundary conditions of the previous phase. Potential fuel candidates are identified, and their properties and theoretical performance are evaluated. The selection of interesting fuel candidates for an initial experimental investigation is made.

The first evaluation of the hypergolic behaviour is conducted in lab-scale drop tests. In these tests, the two components of the propellant are brought together when a falling drop of the first component hits a pool of the second component. If the substances are hypergolic with each other, the ignition delay can be determined by studying the dropping, mixing and reaction with a high-speed camera. In this stage, additives can be dissolved in one of the components to evaluate their effect on the ignition delay time. Suitable fuel candidates should provide a short ignition delay time with the oxidiser. The desired ignition delay is in the order of a few milliseconds, similar to conventional hypergolic propellants. The drop test differs from the conditions in a thruster where the propellants are intended to be applied.

Therefore, injection tests are necessary to validate the hypergolic ignition under more realistic conditions. In this phase, the promising propellant combinations are studied using different injectors and varying significant parameters such as injection velocity or pressure environment. Finally, with the results of the injection study, a thruster can be designed with a suitable injector. Following, experiments can be conducted to evaluate the performance of the propellant in a combustion chamber.

## 1.5 Outline

Chapter 2 covers the state-of-the-art (SoA) of hydrogen peroxide, green hypergolic propellants. Further, relevant fundamentals regarding rocket propulsion, ignition theories and testing methods are summarized. The development approach is explained in chapter 3 as well as the theoretical and experimental methods relevant to this thesis. Chapter 4 describes the initial selection process of fuel candidates, and based on this procedure, seven suitable candidates were found. These candidates were tested on hypergolic ignition with the lab-scale drop test. The results are presented in chapter 5. Further optimization of the most promising candidate and evaluation of different parameters on the ignition delay is also presented. Chapter 6 discusses the results



of injection tests at different operating conditions of the most promising fuel combination. In chapter 7, propellant properties and the perceptive use of the novel hypergolic propellant combination are presented. The conclusion of the conducted work is given in chapter 8 as well as an outlook on further developments.

## 2 Fundamentals and background

In this chapter essential fundamentals on rocket propulsion and hypergolic ignition are given. Moreover, an overview of the state of the art of green hypergolic propellants is given.

### 2.1 Fundamentals of rocket propulsion

The fundamental principle of rocket propulsion is the application of Newton's laws. A force is applied to the rocket or spacecraft by the change in the momentum of a mass. For a rocket engine: the mass is gaseous decomposition or combustion products which are accelerated and ejected by a nozzle. This generates a force in the opposite direction that propels the spacecraft or rocket.

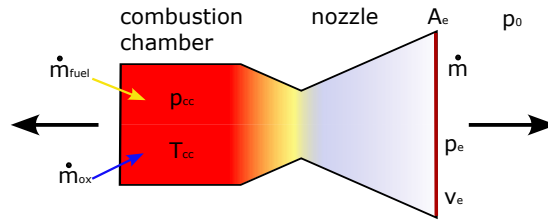


Figure 2.1: Rocket principle

For the rocket engine shown in figure 2.1 the following equation for the thrust  $F$  can be derived, by the assumption of a constant velocity at the nozzle exit:

$$F = \dot{m} v_e + (p_e - p_0)A_e = \dot{m} c_e \quad (2.1)$$

with the total mass flow  $\dot{m}$ , the velocity of the fluid at the nozzle exit  $v_e$ , the pressure at the nozzle exit  $p_e$ , the ambient pressure  $p_0$  and the effective exhaust velocity  $c_e$ .

The total impulse of a rocket is defined as the integral of the thrust  $F$  over time  $t$

$$I_{\text{total}} = \int_0^t F dt \quad (2.2)$$

For a constant thrust, the total impulse is the product of the thrust and the duration when the thrust is applied  $\Delta t$

$$I_{\text{total}} = F \Delta t \quad (2.3)$$

Following, the weight-specific impulse can be written as

$$I_{\text{sp}} = \frac{\int_0^t F dt}{g_0 \int_0^t \dot{m} dt} = \frac{I_{\text{total}}}{g_0 m_{\text{propellant}}} \quad (2.4)$$

with the total mass of the propellant  $m_{\text{propellant}}$  and the gravitational acceleration at sea level

$g_0 = 9.8066 \text{ m/s}^2$  [7]. For a constant mass flow rate and thrust, the specific impulse becomes

$$I_{sp} = \frac{F \Delta t}{g_0 \dot{m} \Delta t} = \frac{F}{g_0 \dot{m}} \quad (2.5)$$

The unit of the specific impulse  $I_{sp}$  is second. Therefore, the  $I_{sp}$  value can be compared independently from the systems of units [7]. The specific impulse is a term for the efficiency of a propellant to generate thrust. With equation (2.1) and (2.5) the effective exhaust velocity  $c_e$  can be written as:

$$c_e = I_{sp} g_0 = \frac{F}{\dot{m}} \quad (2.6)$$

In the following, a few other terms are defined as necessary for the understanding of the initial performance evaluation of a propellant.

The ratio of oxidiser to fuel mass flows (ROF) is defined as the name reveals:

$$ROF = \frac{\dot{m}_{ox}}{\dot{m}_{fuel}} \quad (2.7)$$

with oxidiser mass flow  $\dot{m}_{ox}$  and fuel mass flow  $\dot{m}_{fuel}$ . In other references, the ROF can also be referred to as mixture ratio, mass ratio or O/F.

The characteristic velocity  $c^*$  is defined as the product of the combustion chamber pressure  $p_c$  and the nozzle throat area  $A_t$  divided by the total mass flow  $\dot{m}$ :

$$c^* = \frac{p_c A_t}{\dot{m}} \quad (2.8)$$

The characteristic velocity is independent of the nozzle. Therefore, it is possible to assess the combustion quality on ground tests without a thrust measurement.

## Ideal rocket

The concept of the ideal rocket is a model based on thermodynamic principles and their mathematical relationships to express terms important for rocket propulsion. There are several assumptions and simplifications made, but useful results can be achieved [7]:

- the model is one-dimensional and assumes frictionless flows with only axial velocity components
- chemical equilibrium is established, and a frozen flow in the nozzle
- steady-state conditions are reached
- substances are homogeneously distributed
- all substances behave like ideal gases

With the assumption of an ideal rocket and a nozzle adapted to the ambient pressure, the following expression can be derived [7]:

$$I_{sp} = \frac{1}{g_0} \sqrt{\frac{2\kappa}{\kappa-1}} \sqrt{\frac{RT_0}{\bar{M}}} \sqrt{1 - \left(\frac{p_e}{p_0}\right)^{\frac{\kappa-1}{\kappa}}} \quad (2.9)$$

with the specific heat ratio  $\kappa$ , the universal gas constant  $R$ , the combustion chamber pressure  $T_0$ , the average molecular mass  $\bar{M}$ , the pressure at the nozzle exit  $p_e$  and the ambient pressure

$p_0$ . This expression shows that the  $I_{sp}$  depends on the term  $T_0/\bar{M}$ . For a high  $I_{sp}$ , high combustion temperature and low average molecular mass are necessary. In addition, a low ratio of the exit pressure to the combustion chamber pressure is favourable for a high  $I_{sp}$ . The  $c^*$  can be expressed as

$$c_{ideal}^* = \frac{\sqrt{\kappa \frac{R}{\bar{M}} T_0}}{\kappa \sqrt{\left(\frac{2}{\kappa+1}\right)^{\frac{\kappa+1}{\kappa-1}}}} \quad (2.10)$$

### 2.1.1 Performance analysis with CEA

In the frame of the present thesis, novel propellant combinations are screened, and their potential performance is assessed. For this assessment, the NASA program 'Chemical Equilibrium and Applications' (CEA) developed by McBride and Gordon is used [24]. As the name already suggests, the combustion is modeled and calculated based on the assumption of chemical equilibrium in the combustion chamber, and this can be applied to combustion inside a rocket combustion chamber. Further assumptions are [7]:

- isobaric, adiabatic combustion
- reactions are fast
- the reactions are in equilibrium, so reversible reactions between products and reactants occur
- all substances are behaving like ideal gases
- perfect mixing and homogeneous distribution of the substances

In a rocket combustor, several factors are unknown, such as the composition of products and reactants in the equilibrium state, the combustion temperature, and the pressure. To solve the problem, CEA sets up a system of equations based on energy balance, mass balance, and equilibrium relations [7]. A combustion pressure is assigned. With an estimated combustion temperature, the system of equations is solved, and the composition of the substances is calculated. If the resulting system reaches an energy balance between the heat of the reaction and the heat absorbed by the gasses, the problem is solved. If not, a new temperature is estimated in an iterative process, and the equation system is solved again. When the solution converges, the calculation can be stopped.

When the system's equilibrium state was iteratively calculated, the program calculated several parameters relevant to the rocket propulsion regarding the nozzle flow. The challenge is the nozzle's shifting equilibrium state due to the fluid's changing pressure and temperature during the acceleration of the flow. Different cases can be chosen to solve this: equilibrium or frozen calculation. In the equilibrium case, the equilibrium composition is recalculated for the nozzle flow. This method overestimates the performance of  $I_{sp}$  or  $c^*$  typically by 1 % to 4 % [7]. The second method, the 'frozen flow', assumes no change in the composition of the products in the nozzle. This means the composition is 'frozen' in the combustion chamber or throat (depending on the user's selection). This method tends to underestimate the performance by 1 % to 4 % [7].

For the chemical equilibrium calculation of a rocket combustion chamber, the input parameters are:

- propellant composition with the molecular formula of each substance
- enthalpy of formation of each substance
- initial temperature

- mixture ratio (ROF)
- combustion chamber pressure
- expansion ratio  $\epsilon = A_e/A_t$

The calculation output is the condition at three locations: inside the combustion chamber, at the throat, and at the nozzle exit. The relevant parameters for the performance assessment are:

- temperature in the combustion chamber  $T_{cc}$
- average molecular mass of the exhaust  $\bar{M}$
- characteristic velocity  $c^*$
- specific impulse in vacuum  $I_{sp,vac}$
- specific impulse regarding nozzle exit pressure  $I_{sp,nozzle}$

$I_{sp,vac}$  refers to vacuum conditions and considers the pressure difference between the exit plane of the nozzle and vacuum, compare equation (2.1).  $I_{sp,nozzle}$  is calculated assuming an ambient pressure equal to the pressure of the exit plane of the nozzle.

## 2.2 Hypergolic ignition

The processes leading to an ignition after the contact of two substances are essential for hypergolic propellants. An overview of different hypergolic ignition models is given in the following sections.

### 2.2.1 Qualitative models of hypergolic ignition

The ignition delay time (IDT) for this work is defined as the duration between the initial contact of fuel and oxidiser and the self-ignition of the mixture. The succession leading to ignition includes physical processes and chemical reactions.

The process of hypergolic ignition starts with the primary contact of fuel and oxidiser. After the contact, physical mixing processes and diffusion are dominant. In this phase, reactants are liquid and mixed with each other. Following, initial reactions in the liquid phase occur. These reactions release energy and heat the mixture. The release of vapour from the reacting mixture can be observed at some point. Thus, the heat release of the liquid phase reactions produced enough heat to evaporate the mixture. The liquid phase reactions further release heat and vaporise more of the mixture. However, reactions in the gaseous phase also raise the local temperature. Finally, the self-ignition temperature in the gas phase is reached and an ignition kernel forms. Afterwards, the flame rapidly propagates in the gaseous phase, and a combustion can be observed.

This process for hypergolic ignition was described in several references [25–29] and also observed in many different experiential tests presented in chapters 5 and 6. Figure 2.2 shows the qualitative temperature evolution during the hypergolic ignition process according to [27]. At time 0, the initial contact of fuel and oxidiser occurs, and the physical mixing and diffusion occur. The liquid phase reaction starts to heat the mixture. At point A, the reaction rate increases drastically until, at time B, vaporisation becomes visible. Finally, in the vapour phase, the ignition temperature is reached at point C and ignition and combustion are observed. In the present study, the time from 0 to B will be referred to as the time to vapour generation (TVG). The duration from 0 to C is the ignition delay time.

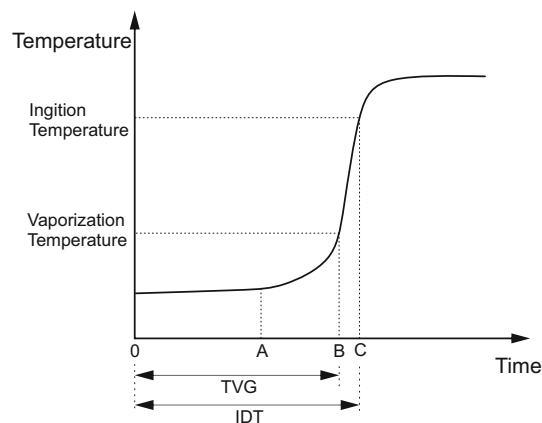


Figure 2.2: Qualitative temperature evolution according to [27]

Different authors named the phases differently. Dadiou et al. referred to a 'physical' and 'chemical' delay time [27]. The physical delay time is described as the duration of 0 to B because, in this period, physical processes like mixing, diffusion and convection occur. The chemical delay time is the duration between B and C, where the vapour phase reactions happen. The addition of both times leads to the ignition delay time. The terms of physical and chemical delay are not very favourable because, during the physical delay, significant chemical processes need to take place to vaporise the mixture. Also, during the chemical phase, interactions of the vapour with

the surroundings influence the duration. The term of the chemical delay time was also adapted by other authors [29, 30]. Kang et al. proposed to differentiate between the liquid and gas phase reactions [28].

Recent investigations regarding hypergolic ionic liquids with dicyanamide anions and white fuming nitric acid exhibit a slightly different process [31–33]. Liquid phase reactions lead to the vapourisation of WFNA. Simultaneously, interactions of the fuel droplet and the WFNA lead to vapour formation between the fuel droplet and the WFNA pool. Further gas-liquid-phase reactions occur, and small fuel droplets are expelled in a so-called micro-explosion. By the atomisation due to the explosion, the ignition finally occurs when the auto-ignition temperature of a small drop in the nitric acid vapour is reached. The authors distinguish between two characteristic times: the explosion delay time (EDT) and the ignition delay time (IDT). The EDT is similar to the previously introduced TVG: It is the time interval between the contact and the instant when the significant vapour release starts and the micro-explosion happens.

### 2.2.2 Ignition theories

A chemical reaction is a process where reactants are transformed by their interaction into other chemical substances called products of the reaction. This transformation can consume or release energy. The conversion from reactants to products elapses with a particular reaction rate. A certain amount of energy, the so-called activation energy, is needed to initiate a chemical reaction. The combustible substances or reactants of a combustion process in a bipropellant rocket engine are fuel and oxidiser. With the addition of activation energy, the ignition occurs. Gaseous products are generated, and energy is released in the form of heat. These products can be accelerated in a Laval nozzle to generate thrust in rocket engines. For hypergolic propellants, the activation energy is not provided externally, for example, by an ignition device. The initial energy is provided by the interaction and reaction of fuel and oxidiser after the primary contact.

#### Reaction rate

The reaction rate of a chemical conversion depends on the temperature and pressure. In 1889, the Swedish scientist Svante Arrhenius described a relationship between the reaction rate and the temperature. The so-called Arrhenius law in exponential form is given [34]:

$$k(T) = A e^{\left(\frac{-E_a}{RT}\right)} \quad (2.11)$$

where  $k$  is the reaction rate constant,  $A$  is the frequency or the pre-exponential factor,  $E_a$  is the activation energy of the reaction,  $R$  is the universal gas constant and  $T$  is the absolute temperature.

The time  $t$  required for a certain fraction of the reaction is proportional to  $1/k$ , and the resulting equation is [26]:

$$t = A' e^{\left(\frac{E_a}{RT}\right)} \quad (2.12)$$

Assuming the global reaction of a hypergolic ignition characterised by the ignition delay time, the equation can be written as:

$$IDT = A'' e^{\left(\frac{E}{RT}\right)} \quad (2.13)$$

where  $A''$  is the pre-exponential factor of the global hypergolic reaction,  $E$  is the global activation energy of the hypergolic reaction,  $R$  is a constant and  $T$  is the absolute temperature.

This global consideration significantly simplifies the processes leading to the hypergolic ignition. The processes include physical processes such as mixing and a succession of reactions between

fuel, oxidiser, intermediate species, and products. Different research groups examined this simplified approach. Aggarwal [35] described it for auto-igniting propellants. Kapusta et al. applied this on a green hypergolic combination and found a linear relationship between the IDT and the reciprocal fuel temperature [36]. Smith [30] and Black et al. [37] applied this to the duration of the gas phase of the hypergolic ignition process. Smith found that the activation energies of the hypergolic ignition of MMH and hydrazine with RFNA are in the same order [30].

### Thermal ignition theory

The thermal ignition theory by Nikolai Semenov 1935 considers a reaction of gaseous reactants homogeneously distributed in a vessel. The reaction is exothermal, and heat is generated during the conversion of the reactants into the products. The generated heat  $\dot{q}_{gen}$  in the vessel can be expressed as:

$$\dot{q}_{gen} = -V \left( \Delta H \frac{dc}{dt} \right) \quad (2.14)$$

where  $V$  is the volume of the vessel,  $\Delta H$  is the heat of reaction and  $\frac{dc}{dt}$  is the reaction rate. With the Arrhenius expression of the reaction rate, the term becomes [26]:

$$\dot{q}_{gen} = -V \Delta H \left( A C_{ox}^a C_{fuel}^b \exp \left( \frac{-E}{R T_{mix}} \right) \right) \quad (2.15)$$

where  $C_{ox}$  is the concentration of the oxidiser,  $C_{fuel}$  is the concentration of the fuel,  $a, b$  are empirical constants and  $T_{mix}$  is the assumed homogeneous temperature of the reaction system. The rate with that heat is transferred to the surrounding  $\dot{q}_{loss}$  can be expressed with:

$$\dot{q}_{loss} = \alpha S (T_{mix} - T_0) \quad (2.16)$$

where  $\alpha$  is the heat transfer coefficient,  $S$  is the surface of the vessel,  $T_0$  is the wall temperature. Heat generation is an exponential function of the mixture temperature, whereas heat loss to the surroundings is linear. An example of the influence of different initial pressures is shown in figure 2.3. The figure shows different heat fluxes over the temperature: heat generation slopes for three different initial pressures and the linear heat loss. It should be noted that the generation term in equation (2.15) is dependent on the concentration of fuel and oxidiser. The concentration is a function of the density and, therefore, of the initial pressure. The heat loss relies on the heat transfer coefficient, which is less sensitive to the initial pressure.

At  $T_1$ , the heat generation and the heat loss of the reaction at  $p_3$  are equal; therefore, no heating of the mixture occurs. The temperature is stable at this point. If, due to external factors,  $T_3$  is reached at  $p_3$ , ignition can occur if further heat is added. The temperature will decrease to  $T_1$  if not.  $T_2$  is not stable due to a small perturbation, which can lead to a higher heat flux and lead to ignition. For  $p_1$ , ignition will be achieved because the heat loss is always lower than the heat generation.

Pourpoint applied Semenov's theory on catalytic hypergolic propellants and derived an expression for the IDT [26]. The formula is given as follows:

$$\tau = \frac{R^2 T_0^3}{E A \Delta H (p_{fuel} + p_{ox})} \left( 1 + \frac{p_{fuel}}{p_{ox}} \right) \left( C p_{fuel} + \frac{p_{ox}}{p_{fuel}} C p_{ox} \right) \exp \left( \frac{E}{R T_0} \right) \quad (2.17)$$

with activation energy  $E$ , pre-exponential factor  $A$ , the heat of reaction  $\Delta H$ , the universal gas constant  $R$ , the initial temperature  $T_0$ , the partial pressures of the fuel  $p_{fuel}$  and oxidiser  $p_{ox}$  and the molar heat capacities of fuel  $C p_{fuel}$  and oxidiser  $C p_{ox}$ .

Pourpoint concluded that this equation is helpful to get an impression of which factors influence



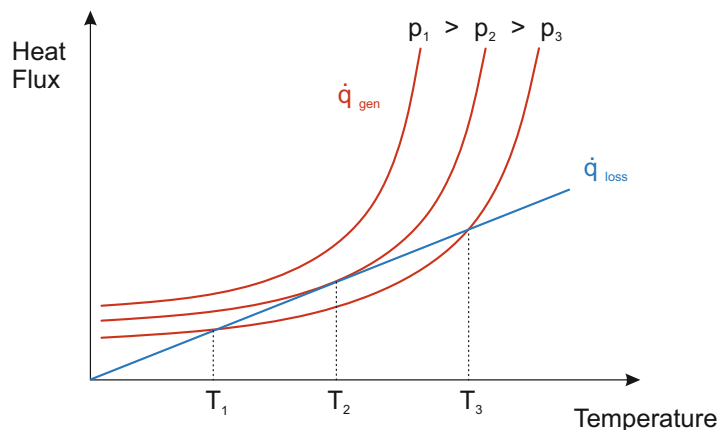


Figure 2.3: Semenov theory: rate of heat generation and heat loss of gaseous reaction in a closed vessel at different pressures according to [38]

the ignition delay time [26]: "The IDT becomes short if the mixture has a low volumetric heat capacity, a high heat of combustion, and a high initial reaction rate." Besides, the process is highly dependent on the initial temperature. Seamans et al. also derived equation (2.17) [39]. They compared the equation's results to actual ignition delay measurements in thrusters operated with NTO and UDMH at vacuum conditions. The predicted ignition delays were shorter than the experimental values.

### 2.2.3 Ignition delay

A qualitative overview of the processes leading to hypergolic ignition was given in the previous section. Different factors influencing the ignition delay can be derived from these fundamental processes. These factors can be optimised for shorter ignition delays. The following list names the considered points influencing the IDT:

- Physical factors:
  - Mixing energy
  - Miscibility
  - Viscosity
  - Ambient factors
- Thermal / chemical factors:
  - Temperature
  - Additive concentration
  - Hydrogen peroxide concentration
  - Stability
  - Vapour pressure

**Mixing energy** The initial mixing phase can be influenced by the energy put into the mixing. Several investigations showed that the IDT in injection tests is shorter than in drop tests [26, 40, 41]. An influencing factor is that the mixing between the two components is enhanced with the injection and forced impinging of fuel and oxidiser. The impingement reduces the initial

duration of the mixing phase compared to drop tests where only single drops accelerated by the gravity field are brought together. Impinging jet velocities in the order of 10 m/s are used in thruster injectors [42]. But if the mixing is poor or too much mixing energy is applied, it is also possible that an ignition is not achieved or a longer ignition delay results [26, 43, 44].

**Miscibility** The miscibility of the propellant's components also facilitates the ignition process. Substances that are not miscible with each other can separate after initial contact, prohibiting an ignition. Such a behaviour was observed in experiments with an ionic liquid that was not miscible with hydrogen peroxide [45].

**Viscosity** The viscosity influences the initial mixing. Higher viscosities can lead to longer ignition delay times [41]. The viscosity also has an impact on the spray behaviour of the substances.

**Ambient conditions** The ambient conditions can also influence the ignition delay time. Equation (2.16) shows if the surrounding medium has a higher heat transfer coefficient, the losses are higher, leading to a longer ignition delay time or even prohibiting the ignition. Pourpoint showed that helium as the surrounding medium prolongs the IDT compared to air or argon [25, 26]. A low-pressure environment extends the ignition delay time [26, 46]. At some point, the ignition is not achieved any more. The expression (2.17) shows the influence of lower pressures extending the IDT. Higher pressures have the opposite effect and can shorten the IDT [36]. The impact of the low pressure on the ignition delay is considerable regarding the application of hypergolic propellants in space. There, the initial pressure of a thruster is the vacuum of space. Conventional hypergolic propellants work in space environment. Due to the high vapour pressure of NTO and the confinement of the combustion chamber, a pressure increase in the combustion chamber occurs shortly after opening the flow control valve [47]. This leads to ignitable conditions within a short time. In the space environment, further factors influence the IDT, such as the interaction of the inflowing propellant with surfaces such as the combustion chamber walls, the liquid-vapour transition and initial cooling and freezing due to evaporation, condensation of pre-ignition products [48].

**Temperature** The initial temperature of the propellant also influences the ignition delay [26, 49]. The initial reaction rate is an exponential function of the temperature, compare equation (2.17). Further, the temperature influences other parameters, such as viscosity [41, 50], vapour pressure or density of the substances [50]. Also, the solubility of additives is influenced by the temperature.

**Additives** Additives are widely used for hypergolic propellants using hydrogen peroxide as oxidiser to introduce a hypergolic behaviour because only very few pure substances are hypergolic with hydrogen peroxide. The additive can induce a reaction between the fuel and hydrogen peroxide. In many cases, the IDT depends on the additive's concentration. With a higher amount, the IDT can be shortened [25, 51]. But additives must be dissolved in liquid fuels, and the dissolution needs to be stable [52, 53]. The additives can also become saturated in a fuel when dissolved.

**Stability** Sufficient thermal stability and stability against stimuli such as friction, electrostatic discharge (ESD), and impact are essential for the safe handling of substances [54]. Conversely, very stable substances may be less reactive and have a long IDT.

**Hydrogen peroxide concentration** The hydrogen peroxide concentration significantly impacts the hypergolic behaviour of a propellant combination. The higher the concentration, the faster the hypergolic ignition occurs [26, 52, 55]. Further, with a high concentration, the performance of a propellant combination also increases.

**Vapour pressure** The vapour pressure influences the IDT according to equation (2.17). This work focuses on ionic liquids, which do not have a significant vapour pressure [56]. At higher temperatures, the ionic liquid decomposes instead of vaporising [57].

## 2.3 Test methods

Different test methods are used to evaluate the hypergolic behaviour of different substances. The test methods can be divided into three groups:

1. drop tests
2. injection tests
3. thruster tests

The different methods and examples are presented in the following sections.

### 2.3.1 Drop tests

The drop test is a procedure where single drops of the two components of interest are brought together, and their interaction is observed. In most cases, one component is provided as a small pool, and the second is dropped into the pool. This process can be recorded with a high-speed camera or other diagnostics such as light barriers and photodiodes to detect the falling drop and the ignition.

Such a setup can be implemented quickly and easily and is suited to provide an initial quantification of the hypergolic behaviour of the tested components. With more advanced setups allowing, for instance, the control of the ambient medium or pressure, an evaluation of the hypergolic behaviour under different conditions is possible. There is no standardisation regarding the drop test. The results obtained in drop tests may not be replicated on a different setup in a different lab. Reviews on historic setups are described by Dadiou et al. [27], Pourpoint [26], Hampton et al. [29, 30] or Davis et al. [58]. More recent setups were developed by research groups in China [31–33, 59–61], South Korea [28, 62, 63], Poland [36, 64, 65], USA [37, 66, 67], Israel [68, 69] and Japan [70]. Some of these setups can apply different initial conditions, such as elevated temperature or pressure [36, 65], use other diagnostics than only high-speed imaging to detect the IDT [28, 62] or apply high-speed infrared imaging [33, 61].

### 2.3.2 Injector tests

A reliable hypergolic ignition in a thruster depends on the injection and mix of the propellant's components. Therefore, it is necessary to verify the hypergolic ignition under flowing conditions after identifying and characterising suitable propellant candidates. Different injector configurations or the influence of various parameters, such as ambient pressure or medium, can also be studied with such tests. Reviews on historic setups can be found in Dadiou's [27] and Pourpoint's [26] work. More recent setups were described by researchers from Poland [64], South Korea [40, 71, 72], Japan [70], USA [73–75] and Taiwan [51, 76]. Injection test setups are much fewer compared to drop tests. This may be related to more extensive procedures and infrastructure which is needed to safely perform hypergolic injection tests.

### 2.3.3 Thruster tests

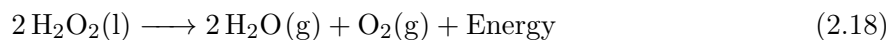
Finally, to conclude the development of a novel hypergolic propellant thruster, firings are necessary to demonstrate the fuel's suitability and characterise its performance. Such tests require even more infrastructure and higher amounts of propellants have to be handled. In the 2000s, some initial work on hypergolic thrusters with hydrogen peroxide as oxidiser was published [77–81]. Only very few institutions recently conducted such tests. Among them are *KAIST*, South Korea [40, 55], *Institute of Aviation*, Poland [82], *National Institute for Space Research*, Brazil [83] and private companies such as *NewRocket* [68, 69].

## 2.4 State of the art: Green propellants

This section summarises recent developments in green propulsion with a focus on hydrogen peroxide and hypergolic fuels developed in the last decade. Further, an overview of ionic liquids and their typical properties is given. The SoA regarding the application of ionic liquids in space propulsion is summarised.

### 2.4.1 Hydrogen peroxide

Hydrogen peroxide (HP) is a colourless liquid typically available in an aqueous solution at variable concentrations. The formula of the hydrogen peroxide molecule is  $\text{H}_2\text{O}_2$ . Hydrogen peroxide can decompose into water and oxygen; see the reaction equation (2.18). The decomposition reaction is exothermic. Starting from a concentration of 65 %, the released energy is high enough that all decomposition products are gaseous [84].



At ambient conditions, hydrogen peroxide is subjected to a slow decomposition reaction. The reaction rate of this self-decomposition depends on various factors, such as purity, contamination, material compatibility, surface (of the container wall) to volume (of the peroxide) ratio, temperature, pH value or radiation [85]. In a clean environment at ambient temperature, decomposition rates below 1 % per year can be achieved [86]. In disadvantageous conditions, e.g. due to contamination with a catalytic material, self-heating due to the exothermal decomposition of HP accelerates the reaction rate, generating large amounts of gaseous products. This can lead to a significant rise in pressure in closed vessels until the rupture of the vessel. Therefore, confinement of hydrogen peroxide should be avoided, or safety devices must be installed to prevent pressure build-up above a certain level.

Many materials promote the decomposition reaction; therefore, selecting highly compatible materials for storage of  $\text{H}_2\text{O}_2$  is essential [86, 87]. Highly compatible materials are PTFE, polyethylene, pure aluminium or certain stainless steels after passivation [88]. Stabilisers are added after the production to prevent the accelerated decomposition of hydrogen peroxide. These stabilisers are added in small amounts (in the order of ppm) and act on the removal or inactivation of catalytic ions [88].

Hydrogen peroxide is a widely used chemical in different applications. In 2018, the global  $\text{H}_2\text{O}_2$  production was 4.9 megatons [89]. HP at low concentrations (0.5 – 3 wt%) can be found in households as a disinfection solution. Concentrations up to 50 % are used in a variety of industrial applications, e.g. chemical purification, pulp and paper bleaching, hydrometallurgy and metal finishing, bleaching of textiles, or water treatment [89, 90]. The production of paper and use of hydrogen peroxide as a bleaching agent is the largest single application of HP [90]. Hydrogen peroxide of high concentrations (typically 70 – 99.9 wt%) can be used as a versatile

propellant for rockets or gas generators. For these types of applications,  $\text{H}_2\text{O}_2$  can be referred to as rocket grade hydrogen peroxide (RGHP), high test peroxide (HTP) or highly concentrated hydrogen peroxide. Typical concentrations of RGHP, which are available in Europe, are 87.5 wt% or 98 wt%.

Hydrogen peroxide was first used as a propellant during the Second World War in Germany. Here, HP was referred to as T-Stoff. The first HP-powered rocket was fired in June 1937 [91]. Later, HP was used to propel torpedoes, submarines, rocket planes, rockets and turbo pumps of rocket engines [27]. An example is the turbo pump of the V2 rocket, which was driven by decomposed hydrogen peroxide. A fuel with the alias C-Stoff was developed to be hypergolic with hydrogen peroxide. C-Stoff is composed of hydrazine hydrate and methanol and powered the rocket plane Messerschmitt Me 163B Komet [27, 91]. After World War II, different programs in the UK and the US utilised hydrogen peroxide as a propellant. A prominent example from the UK is the Black Arrow, which was an orbital launch vehicle. The engines of the launcher were powered by the combination of 85 wt% hydrogen peroxide and kerosene [92]. In the US, several satellites in the early 60s were equipped with hydrogen peroxide based reaction control systems, such as the SYNCOM I-III satellites [92] or the capsules of the mercury program [93]. In the second half of the 1960s, new effective catalysts for hydrazine became available [92]. Following, hydrazine was chosen to be used as a monopropellant for in-space propulsion because of its higher performance compared to HP. The  $I_{sp}$  of hydrazine is up to 240 s [94], which is more than 50 s higher than highly concentrated hydrogen peroxide. Furthermore, hypergolic bipropellants with hydrazine based fuels and dinitrogen tetroxide outperform bipropellant solutions with HP. At that time, the performance and storage advantages were regarded as more crucial than the hydrazine's adverse effects of toxicity, environmental issues or operating expenses [94]. Therefore, John Clark concluded in his book *Ignition* that hydrogen peroxide is "the oxidiser that never made it" and stays "always a bridesmaid" [95]. It is worth mentioning that the reaction control system of the Soyuz re-entry module uses hydrogen peroxide as a monopropellant for many decades until today [96].

The interest in hydrogen peroxide as a propellant returned in the 1990s, when first studies were conducted to identify less toxic propellants than hydrazine due to more stringent environmental regulations [97]. Since then, the interest has increased.

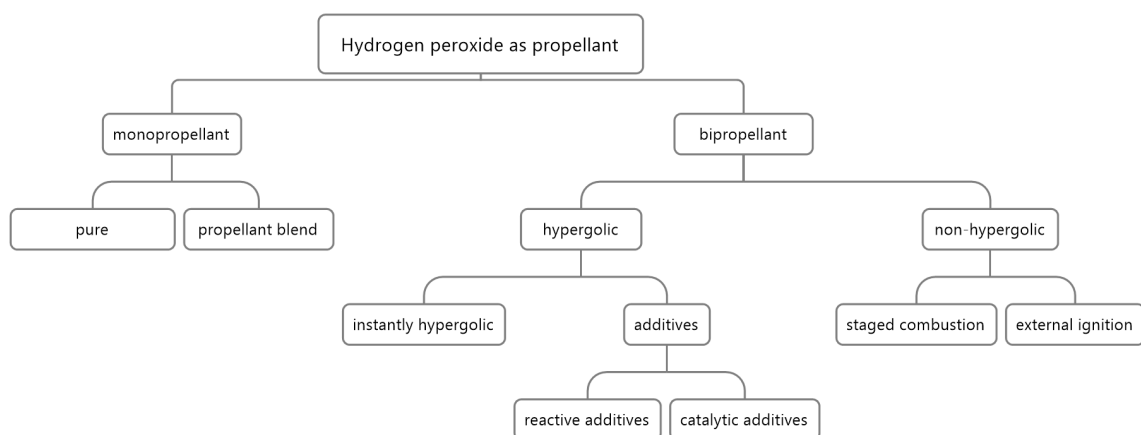


Figure 2.4: Possible applications of hydrogen peroxide as propellant

Figure 2.4 shows the possible ways to apply  $\text{H}_2\text{O}_2$  as a propellant for rocket propulsion. The left side of 2.4 shows the monopropellant applications of hydrogen peroxide. As described above, the

exothermic decomposition can be utilised to produce hot gaseous products, which are expanded to generate thrust. The theoretical performance of different hydrogen peroxide concentrations is shown in table 2.1. The calculation was performed with NASA CEA assuming a chamber pressure of 10 bar, an expansion ratio of the nozzle of 80 and frozen supersonic expansion. Pure hydrogen peroxide has the highest theoretical performance, with an  $I_{sp}$  of 193 s. The  $I_{sp}$  and adiabatic decomposition temperatures are reduced with higher water contents. The decomposition reaction of hydrogen peroxide can be introduced by a catalyst. Examples of suitable catalytic materials are silver, platinum, or manganese oxides [98–102]. The use of a specific material depends on the decomposition temperature of the hydrogen peroxide concentration. For example, silver has a melting point of 962 °C. As displayed in table 2.1, the adiabatic decomposition temperature of 98 %  $H_2O_2$  is 952 °C. Due to the low mechanical strength close to the melting point, a silver catalyst can only be used with HP up to 90 %. Typically, a high-temperature resistant carrier material is coated with a catalytic active phase because of the high temperatures and need for noble metals. As carrier materials, alumina pellets are often used. Catalysts can degrade over the service time due to mechanical failure of the carrier material or deactivation of the catalytic surface due to impurities and stabilisers. A second option is the thermal initiation of the decomposition reaction [103, 104]. Another monopropellant approach is a blend of HP with a liquid fuel. The safe operation of such a blend is very challenging because HP can become very sensitive if mixed with hydrocarbons, and the blend can detonate if triggered [105].

Table 2.1: Monopropellant  $H_2O_2$  performance at different concentrations, decomposition chamber pressure 10bar, expansion ratio 80, frozen at throat

$H_2O_2$ concentration	$I_{sp \text{ vac}}^a$	$T_{ad}^b$
[%]	[s]	[K]
100	193	1275
98	190	1225
90	120	1030
87.5	117	968

<sup>a</sup> vacuum specific impulse

<sup>b</sup> adiabatic decomposition temperature

Bipropellant propulsion systems using hydrogen peroxide as an oxidiser can be either non-hypergolic or hypergolic, depending on the fuel selected. Non-hypergolic fuel-oxidiser combinations can be ignited after mixing fuel and HP with a suitable ignition source, such as a torch igniter, pilot flame or pyrotechnic charge. Another possibility is to decompose  $H_2O_2$  via a catalyst bed into hot vapour and oxygen. The fuel is then injected into the hot decomposition products, and ignition occurs because the autoignition temperature is exceeded. This concept is often referred to as staged combustion. The hypergolic ignition occurs when the HP is mixed with a hypergolic fuel. Only very few pure substances are hypergolic with HP. To overcome this, suitable additives can be dissolved in a liquid fuel. The additive introduces and promotes a reaction between the fuel blend and the HP. Finally, due to reaction and heat generation, the ignition is achieved. There are two types of additives: reactive and catalytic [106]. Reactive additives are strong reducing agents, which directly react with  $H_2O_2$ , releasing heat and leading to ignition. Catalytic additives decompose HP after contact. The decomposition releases heat, and reactive vapours occur. When the autoignition temperature of the fuel is reached, an ignition occurs in the gas phase.

Many research groups and development teams are working on different green propellant solutions. Diverse approaches are currently under development, and the first solutions have already been proven in space and are commercially available. Benchmark Space Systems offers monopropellant

and bipropellant thrusters using hydrogen peroxide [107]. The approach for the development of alternative monopropellants is blending an energetic compound such as ammonium dinitramide (ADN) or hydroxylammonium nitrate (HAN) with a liquid fuel. Examples are LMP-103S [108–110], AF-315E/ASCENT [111–114] or SHP163 [115]. Further, premixed blends of liquid fuel and oxidiser are investigated. There are nitrous oxide fuel blends (NOFB) [116–119]. Moreover, alternative bipropellants are under development or already flight-proven. Here, self-pressurizing systems with nitrous oxide as oxidiser and a light hydrocarbon as fuel are promising [8].

### 2.4.2 Hypergolic fuels with hydrogen peroxide

As mentioned earlier, highly concentrated hydrogen peroxide is a space-proven propellant which has been in use for many decades. But there are very few pure liquid substances which are hypergolic with hydrogen peroxide at an ignition delay in the order of 10 ms or below.

During the Second World War, the first hypergolic propellants were developed in Germany. At that time, 80 % hydrogen peroxide was used as an oxidiser and called T-Stoff. The hypergolic fuel was a blend of methanol, hydrazine, and water and, as an additive for the hypergolic ignition, potassium tetracyanocuprate(I). The fuel was called C-Stoff. This combination was used in the Walter engine of the airplane Me 163B [27]. The ignition delay of the C-Stoff/T-Stoff combination is 90 ms in drop tests and 40 ms in injection tests [27]. During this time, an ignition delay of 50 ms was considered as sufficient short to provide reliable ignitions [27]. After World War II, the "Hunting of the Hypergol" began [95], and many combinations of fuels and oxidisers were tested. Pure hydrazine ignites hypergolically with hydrogen peroxide. The ignition delays were around 10 ms in the modified open-cup test apparatus [41]. In a small-scale rocket engine, ignition delays between 9 ms and 34 ms were observed [41]. Further, the ignition delay of hydrazine with 84.75 %  $\text{H}_2\text{O}_2$  in a closed volume reaction is reported to be 1.4 - 3.5 ms [120]. Another pure substance to ignite with hydrogen peroxide is pentaborane  $\text{B}_5\text{H}_9$ . Although the combustion is smooth, the ignition delay is too long for practical application [27].

To conclude from historical studies, only hydrazine is a liquid substance which can ignite with hydrogen peroxide fast enough for an application in a rocket engine. In the 1950s and 1960s, the hypergolic combinations based on hydrazine or a derivative and NTO prevailed and were implemented in propulsion systems despite their drawbacks, such as high toxicity.

An interest in the development of less toxic alternatives to the now 'conventional' propellants started in the 1990s in the US. Due to the lack of pure hypergolic substances with hydrogen peroxide, additives were dissolved in fuels to introduce hypergolic behaviour. In general, there are two kinds of additives which differ from their reaction with hydrogen peroxide: catalytic and reactive additives [106].

Catalytic additives decompose hydrogen peroxide. Typically, transition metal salts are dissolved in a fuel. After contact of the fuel with hydrogen peroxide, the decomposition reaction starts. The decomposition releases heat, and after some time, vapour containing fuel, hydrogen peroxide and decomposition products is generated. Finally, an ignition occurs in the vapour phase. Typical catalytically active transition metals salts have  $\text{Co}^{2+}$ ,  $\text{Co}^{3+}$ ,  $\text{Cu}^+$ ,  $\text{Cu}^{2+}$ ,  $\text{Fe}^{2+}$ ,  $\text{Fe}^{3+}$ ,  $\text{Mn}^{2+}$ , or  $\text{Mn}^{3+}$  cations [121]. An example of a catalytic active hypergolic fuel is the so-called Block 0. It was developed in the 1990s by the US Navy [106]. The fuel consists of manganese acetate tetrahydrate (22 wt%) dissolved in methanol. Further investigation with Block 0 and other hypergolic catalytic fuels can be found in the following references [26, 51, 73, 76–81, 83]

Reactive additives are strong reducing agents dissolved in a suitable fuel. The agents are typically metal- or borohydrides. The hydrides directly react with the hydrogen peroxide after initial contact, generating heat and leading to the ignition of the mixture. A widely used reactive additive is sodium borohydride. Recent studies on reactive hypergolic propellant were published

by groups from Poland [64], South Korea [40, 55, 72, 122], Japan [70] and Israel [68, 69]. A challenge regarding reactive additives is their high sensitivity to moisture [64].

### 2.4.3 Ionic liquids: definition and properties

Ionic liquids (ILs) are salts that have a melting point below 100°C [123]. Further, many ionic liquids have been found, which are liquid at room temperature and below. Therefore, they are called room-temperature ionic liquids (RTILs) or molten salts. ILs are composed of anions and cations. The cations are usually large asymmetric organic molecules which can contain a positively charged nitrogen atom, and the anions can be inorganic or organic [124, 125]. Because of the ionic composition, the vapour pressure of ionic liquids is neglectable at ambient conditions [56]. The viscosity of ionic liquids is, in general, considerably higher compared with water or other molecular liquids such as solvents and conventional propellants. But 'low viscous' ionic liquids are available, which have a dynamic viscosity in the order of some ten mPa s at ambient temperature (see chapter 4). In addition, the viscosity can be strongly dependent on the temperature of the ionic liquid [50]. The density of ionic liquids is typically higher than 1 g/cm<sup>3</sup> [54]. Due to the ionic composition, a charge can be transported in the medium, but the conductivity is limited by the bulky molecules and relatively high viscosity [56]. Many properties of ionic liquids, such as density, viscosity or enthalpy of formation, directly depend on the combination of the cation and anion of the ionic liquid. Further, by specific manipulation of the structure of the cation or anion, the desired property can be tailored. Therefore, ionic liquids are a highly versatile group of substances and very attractive as novel fuel candidates.

The first room-temperature ionic liquid ethylammonium nitrate was described in 1914 by Paul Walden [126], whereas other ionic liquids (with higher melting points than room temperature) were already described in the late 19th century [125]. During the 20th century, few researchers worked in the field of ionic liquids, but new ionic liquids were synthesised and characterised. Until the mid-1990s, ionic liquids were only present in a small scientific community. Since the end of the 1990th and the beginning of the 20th century, ionic liquids have emerged as a new class of substance to provide novel solutions in the aspect of 'green chemistry' [127]. The versatility of ionic liquids provides solutions for more sustainable chemical processes. Moreover, in the last 20 years, many ionic liquids have become commercially available.

In recent years, certain ionic liquids have been found to be hypergolic with different oxidisers. In 2008, the first work on the hypergolic behaviour of an ionic liquid based on the dicyanamide anion was published [128, 129]. Since then, a high interest in the development of a hypergolic combination based on ionic liquids and suitable oxidisers has been ongoing. The state of the art of this development is presented in the following section

### 2.4.4 Ionic liquids for space propulsion

#### Motivation for ionic liquids in space propulsion

The aim of the present development is the substitution of highly toxic conventional hypergolic propellants. Ionic liquids are promising candidates because there are already hypergolic ILs with different liquid oxidisers known [54, 125]. Further, as earlier mentioned, the group of ILs offers a high versatility and following the possibility to optimize the IL to a certain application. Moreover, ILs do not have a vapour phase at ambient conditions. This can facilitate handling procedures compared to conventional hypergolic propellants because there is no need for SCAPE suits. This has a high potential to save costs and time during the development and qualification of propulsion hardware until the final preparation of a mission. Finally, production, transporta-



tion and storage of the propellant are facilitated. This reduces the overall lifetime costs of such a fuel compared to hydrazine and its derivatives.

### ILs in space

Certain ionic liquids already found their way into space as propellant of propulsion systems. ILs can be applied in chemical and electrical propulsion. The following section gives a brief overview of current space proven ionic liquid propellants.

**Chemical propulsion** Energetic ionic liquids are components of monopropellant blends that substitute the conventional monopropellant hydrazine. In Europe, the monopropellant LMP-103S developed by the Swedish Space Cooperation (SSC) and commercialised by ECAPS has flown on numerous missions [109, 110]. Therefore, the propellant and the 1N thruster reached TRL9. LMP103S is a blend consisting of 63 wt% ammonium dinitramide (ADN,  $[\text{NH}_4][\text{N}(\text{NO}_2)_2]$ ), 18.4 wt% methanol, 4.6 wt% ammonia and 14.0 wt% water [110]. The ionic liquid ADN with a melting point of 93 °C serves as the oxidiser. Since ADN is not liquid at room temperature, it is dissolved in the above-mentioned liquids. In this blend, methanol and ammonia are the fuel components that combust with ADN. Ammonia also serves as a stabiliser. Water is added to reduce the combustion temperature of the blend and to reduce the sensitivity [130, 131]. The propellant is ignited using a heated catalyst bed. The  $I_{\text{sp}}$  of LMP-103S is 254 s and hence, 5 % higher compared to hydrazine [132]. The density-specific impulse is 24 % higher compared to hydrazine [110, 132].

In the US and Japan, comparable fuel blends were developed based on hydroxylammonium nitrate (HAN,  $[\text{NH}_3\text{OH}][\text{HNO}_3]$ ) as an energetic component. The most mature blend currently is ASCENT (Advanced SpaceCraft Energetic Non-Toxic propellant), which was formerly known as AF-M315E. This blend is composed of HAN dissolved in water and a hygroscopic fuel [94]. The detailed composition of the propellant is not public. The propellant offers a 12 % higher  $I_{\text{sp}}$  and is 45 % more dense compared to hydrazine [111]. AF-M315E was successfully demonstrated in space on NASA's GMIP mission in 2019, and 2020 [112–114]. Several thrusters are currently under development.

The propellant SHP163 developed in Japan is composed of 73.6 wt% HAN, 3.9 wt% ammonium nitrate (AN), 16.3 wt% methanol, and 6.2 wt% water [115]. The propellant has flown on a Japanese demonstrator mission USEF in 2019 - 2020, and a 1 N thruster demonstrated an  $I_{\text{sp}}$  of 209 s in space [115].

**Electric propulsion** ILs are suitable for electric propulsion because of their ionic composition and their neglectable vapour pressure. Hence, there is no need to ionize the propellant, and the IL stays liquid in the vacuum of space without boiling. Electrical propulsion systems using ionic liquids as propellant are called colloid or electrospray thrusters. In this type of thruster, the ionic liquid is fed from a reservoir to the emitter. Above the emitter, an extractor is located. The extractor is a perforated or porous structure such as a mesh or perforated plate. Between the emitter and the extractor, a voltage is applied, which results in an electric field. Due to the electric field, the ionic liquid forms a cone shape, where the perforations of the extractor are. This is referred to as a Taylor cone. At the tip of the cone, single ions or droplets are extracted from the liquid surface and accelerated by the electric field [133].

Several colloid and electrospray thrusters are already flight-proven proven, and more are under development by different companies and start-ups. In the late 1990s and early 2000s, *Busek* developed a colloid thruster for the *LISA Pathfinder* mission. This thruster used the ionic liquid 1-ethyl-3-methylimidazolium bis(trifluoromethylsulfonyl)imid as propellant [134]. They were

operated successfully on the mission for more than 2400 hours [135, 136]. *Accion Systems* developed electrospray propulsion modules for CubeSats and has several modules in orbit [137]. The applied ionic liquid is not disclosed. The  $I_{sp}$  of their systems is given with 1650 s [138]. A start-up from Spain *Ienai Space* is currently developing an electrospray propulsion unit. They are aiming for a propulsion system with an  $I_{sp}$  of 1600 - 2000 s at 30-50  $\mu\text{N/W}$ . Another company named *ION-X* from France is also developing electrospray propulsion modules with up to 5000 s of  $I_{sp}$  [139].

### Hypergolic ionic liquids

The first hypergolic ionic liquids (HILs) were described by Schneider and Chambreau et al. of AFRL in 2008 [128, 129]. In their work, dicyanamide (DCA) ionic liquids were found to be hypergolic with IRFNA (ignition delays in the order of some 100 ms) and WFNA (IDs in the order of some 10 ms) in simple lab-scale drop tests. From then on, different research groups started to explore hypergolic ionic liquids. Researchers from different countries found many hypergolic ionic liquids with different oxidisers in the last 15 years. Researchers from China, India, the USA, Israel, and Europe contributed. Many HILs are hypergolic with WFNA; some were assessed with NTO or  $\text{H}_2\text{O}_2$ . This section will focus on HILs with hydrogen peroxide as the oxidiser. For the other HILs, the following review articles are recommended [54, 125, 140–142].

The first hypergolic ionic liquid with highly concentrated hydrogen peroxide was described by Schneider et al. in 2011 [143]. The HILs with dicyanamide, nitrocyanoamide, and azide anions are hypergolic with nitric acid but do not ignite with highly concentrated hydrogen peroxide. Therefore, Schneider et al. synthesised an IL with an aluminium borohydride (ABH) based anion  $[\text{Al}(\text{BH}_4)_4]^-$  and the trihexyltetradecylphosphonium  $[\text{THTDP}]^+$  cation. This ionic liquid had an ignition delay with 90 % and 98 % hydrogen peroxide of less than 30 ms. The IL is highly hygroscopic and needs to be handled in a glove box [143].

Schneider et al. patented mixtures of different ionic liquids that are hypergolic with  $\text{H}_2\text{O}_2$  [144]. The fuel has two components; the first component contains an IL with a transition metal anion, which serves as a catalyst for the decomposition of hydrogen peroxide. The second component is another IL, which is the actual fuel. In the patent, the lowest IDT of 50 ms is given for a mixture of 22 wt%  $[\text{BMIm}][\text{FeCl}_4]$  as the catalyst and 78 wt% 2-hydroxyethylhydrazinium nitrate (HEHN).

Kim et al. investigated mixtures of 2-hydroxyethylhydrazine and different ionic liquids. The ILs with the anions such as azide  $[\text{N}_3]^-$ , cyanide  $[\text{CN}]^-$ , iodide  $[\text{I}]^-$ , or tetrachloroaluminate  $[\text{AlCl}_4]^-$  reached ignition delay times between 8 ms and 33 ms in drop test [145].

Weiser et al. investigated 1-allyl-3-methylimidazolium dicyanamide  $[\text{AMIm}][\text{DCA}]$ . To introduce a hypergolic behaviour with hydrogen peroxide, 15 wt% of a catalytic copper salt was dissolved in the IL. With hydrogen peroxide of a concentration of 94.7 %, an ignition delay of 9 ms was reached [146]. Weiser et al. used a setup where a certain amount of oxidiser was injected into a polyethylene coquille containing the ionic liquid.

Wang et al. investigated additives to the ionic liquids 3-ethyl-1-methylimidazolium cyanotrihydroborate  $[\text{EMIm}][\text{H}_3\text{BCN}]$  and  $[\text{MIm}][\text{BH}_3]$ . The additives were needed as promoters for the hypergolic reaction because the neat IL have IDTs with 95 %  $\text{H}_2\text{O}_2$  of more than 300 ms and 1000 ms, respectively. As promoters, four different iodocuprate-containing ionic liquids (CuIL) were tested. With an amount of 10wt% of the promoter IDTs from 14 - 38 ms were observed [147].

Chinnam et al. investigated different promoters for  $[\text{EMIm}][\text{BH}_3\text{CN}]$ . The promoters were salts containing  $[\text{B}_{12}\text{I}_{12}]$  or iodine  $[\text{I}]^-$  anions. The cations were organometallic, containing copper and ferrocene. In drop tests of the mixtures with 8 wt% of the promoter and 95 %  $\text{H}_2\text{O}_2$ , ignition delays between 17 ms and 243 ms were reached [148].

Further, Wang et al. tested the ILs  $[\text{EMIm}][\text{DCA}]$ ,  $[\text{EMIm}][\text{BH}_3\text{CN}]$ ,  $[\text{AMIm}][\text{BH}_3\text{CN}]$ , 1-ethyl-3-

methylimidazolium dimethylboranophosphate [EMIm][DMPB] with “tandem-action” inorganic-organometallic hybrid promoters  $[\text{FcCH}_2\text{N}(\text{CH}_3)_3]_2[\text{Cu}_2\text{I}_4]$  (P1) (Fc = ferrocenyl) and  $[\text{FcCH}_2\text{N}(\text{CH}_3)_3]_n[\text{Cu}_2\text{I}_3]_n$ . The most promising results were reached with a combination of base IL [EMIm][BH<sub>3</sub>CN] and 10 wt%  $[\text{FcCH}_2\text{N}(\text{CH}_3)_3]_n[\text{Cu}_2\text{I}_3]_n$  with an IDT of 31 ms. The combination also ignites with H<sub>2</sub>O<sub>2</sub> at low temperatures down to -40°C. Another interesting result is that IL with the [AMIm] cation showed slightly higher IDT than the IL with the [EMIm] cations [149].

Recent work of Wang et al. investigated the influence on the ignition delay of different solid energetic complexes containing copper, nickel and manganese [150]. The shortest IDT was achieved with compound 2  $[\text{Cu}(\text{AIM})]_4[\text{NO}_3]_2$  of 3 ms. Further work focused on a promoter for the ionic liquids [AMIm][DCA] and [BMIm][DCA]. Most promising was the additive containing copper and boron namely  $[\text{Bis}(1\text{-allyl-1H-imidazole-3-ium-3-yl)-dihydroboronium}]_2[\text{Cu}_4\text{I}_6]$  (P-Al). [AMIm][DCA] with 20 wt% P-Al achieved an ignition delay of 34 ms with 90 % H<sub>2</sub>O<sub>2</sub> [151].

Bhosale et al. conducted a theoretical screening of ionic liquids and their performance potential with different oxidisers [152]. Here, from the screened ILs [EMIm][BH<sub>3</sub>CN] offered the highest performance. Later, Bhosale et al. tested different borane-based fuels in drop tests with hydrogen peroxide [153]. The pure ionic liquids 1-ethyl-3-methyl imidazolium cyanoborohydride [EMIm][BH<sub>3</sub>CN] and 1-allyl-3-ethyl imidazolium cyanoborohydride [AEIM][BH<sub>3</sub>CN] had an IDT of more than 1000 ms. The IL [EMIm][BH<sub>4</sub>] is solid at room temperature and has a melting point of 50 °C. It shows an IDT of 18.5 ms. It was also used as an additive in a fuel blend and accelerated the hypergolic ignition.

Further work of Bhosale et al. showed a reduction of the ignition delay time of the IL [EMIm][BH<sub>3</sub>CN] by promoters based on dissolved iodine-rich additives based on 1,3-dimethyl imidazolium copper iodide ( $[\text{diMIm}]_n[\text{Cu}_2\text{I}_3]_n$ ). Depending on the drop test conditions and the amount of the dissolved promoter IDTs between 126 and 13 ms were reached [63].

As a next step Bhosale et al. characterised the hypergolicity of copper complexes of imidazole cyanoborohydrides  $[\text{Cu}^{\text{II}}(1\text{-Himidazole})_4([\text{BH}_3\text{CN}])([\text{BH}_3\text{CN}])]$  (Cu-P1) and  $[\text{Cu}^{\text{II}}(1\text{-methylimidazole})_4([\text{BH}_3\text{CN}]_2)]$  (Cu-P2). These two substances are solid at room temperature, but ignition occurs within 3.8 ms and 8.5 ms after contact with hydrogen peroxide. The additive Cu-P1 dissolved in [EMIm][BH<sub>3</sub>CN] at 13 wt% led to an ignition delay of 9.5 ms [154].

This review shows that, at the moment, other research groups are working on the development of hypergolic ionic liquids on boron fuels with copper and iodine-containing additives. The table 9.1 in the annex displays the mentioned hypergolic substance. When the present work started, no pure liquid metal-free hypergolic ionic liquid with H<sub>2</sub>O<sub>2</sub> was known.

For completeness, the publications of my colleague Sophie Ricker are quoted here. This work is based on the initial findings regarding the hypergolicity of thiocyanate ionic liquids [155–157]. Also, Park et al. studied the influence of additives dissolved in hydrogen peroxide with thiocyanate ionic liquids [158].

## 2.5 Injection

As mentioned in 2.3, different test methods exist for hypergolic propellants. They are suited for different development phases due to their need for time and effort. For a reliable, smooth ignition and stable combustion in a combustion chamber or thruster, the injection is critical. Therefore, only with a suitable injector can a thruster work properly.

The task of the injector is to introduce the propellant into the combustion chamber. Further, the propellant’s components need to be atomised and mixed so that the hypergolic reaction can be initiated. After the energy is released by the hypergolic reaction, stable combustion can follow,

and the gaseous reaction products are accelerated through the nozzle to generate thrust. There are different types of injectors which are suited for different physical conditions of the propellant at the injection. For the present work, the propellant components will be liquid at the instance of injection. Suitable injector elements for liquid / liquid injection include impinging, showerhead, swirl, pintle, or concentric tube injectors [159]. For hypergolic propellants, impinging, swirl and pintle elements are commonly used and will be discussed shortly in the following paragraph. The principal layout of the three injector types is provided in figure 2.5.

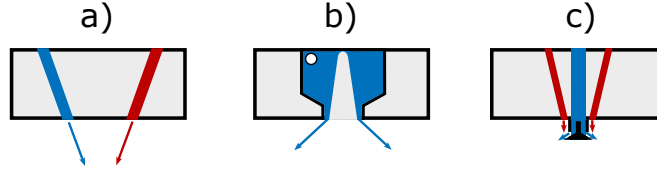


Figure 2.5: Different injector types; a) impinging injector, b) swirl injector, c) pintle injector

The following relationships are important for the characterisation of injectors. The mass conservation in an injector is given by:

$$\dot{m} = A \rho v_{inj} \quad (2.19)$$

with the mass flow  $\dot{m}$ , the area of the injection orifice  $A$ , the fluid density  $\rho$  and velocity of the flow  $v_{inj}$ .

The mass flow through an orifice can be employed by applying the pressure difference  $\Delta p$  across the orifice

$$\dot{m} = c_d A \sqrt{2\rho\Delta p} \quad (2.20)$$

where  $c_d$  is the discharge coefficient of the orifice. The flow can be characterised by the Reynolds number, a dimensionless number relating inertial and viscous forces. The Reynolds number  $Re$  is defined as

$$Re = \frac{\rho v_{inj} l}{\eta} \quad (2.21)$$

with the the fluid density  $\rho$  and velocity of the flow  $v_{inj}$ , a characteristic length  $l$  and the dynamic viscosity  $\eta$ . For circular orifices the characteristic length is the diameter of the orifice. A second dimensionless number, characterising the interaction of a flow which is injected, is the Weber number  $We$ . It is the ratio of the fluid's inertia and the surface tension.

$$We = \frac{\rho v_{inj}^2 l}{\sigma} \quad (2.22)$$

with the the fluid density  $\rho$  and velocity of the flow  $v_{inj}$ , a characteristic length  $l$  and the surface tension of the fluid  $\sigma$ .

### 2.5.1 Impinging injector

In general, in impinging injectors, at least two jets of fluid impinge each other. Atomisation occurs after the impingement point due to the different momentum of the single jets. Depending on the flow condition, a spray sheet and/or many atomised droplets form. There are two different types of impinging elements: like and unlike. Impinging elements have two or more jets of the same component of the propellant, which impinge at one point. Unlike elements, jets of the fuel

and oxidiser directly impinge at one point. Here, the mixing of fuel and oxidiser occurs at the instance of the impingement.

Unlike impinging elements are commonly used with hypergolic propellants. For these elements, the impingement point of the propellant components is known. With the impingement and mixing, the hypergolic reaction starts. The mixing of the components is critical to realise a fast and smooth ignition of the hypergolic propellant.

The phenomena of reactive stream separation (RSS) can occur for hypergolic propellants [42, 159, 160] with unlike impinging elements. At RSS, the fuel and oxidiser do not mix properly, and zones with unmixed fuel and oxidiser occur. Between these zones, the hypergolic reaction is forming hot gaseous reaction products, which again prevent mixing. RSS can lead to low combustion efficiencies and performance. This phenomenon should be avoided by a suitable injector design and injection conditions.

An important geometric factor for this kind of injector element is the impingement angle. A commonly used angle is  $60^\circ$ . A high impingement angle can lead to a backflow of the propellant in the direction of the injector plate. This can result in high heat flux at the injector face plate. A low impingement angle can result in poor mixing and atomisation of the propellant. This can also promote RSS [42].

Another geometric factor is the injection orifice size and geometry. The size of the orifice determines the injection jet velocity at a given mass flow of the liquid propellant. Low velocities can lead to poor mixing and atomisation behaviour. High velocities can mix too violently, leading to long ignition delays for hypergolic propellants [26]. Further, the momentum ratio of the impinging jets depends on the injection velocity and mass flow. Over the orifice, a certain pressure loss should also be generated to decouple the injection and propellant feed from the combustion chamber pressure and pressure fluctuation. A coupling can trigger instabilities. Typical values are 10 % - 25 % of  $\Delta p$  across the injection orifice in relation to the combustion chamber pressure [7]. The pressure loss of smaller thrusters for orbital propulsion is typically higher.

Unlike impinging elements were used in the Apollo SPS engine, lunar module ascent engine [159], Space Shuttle OMS [160], and reaction control thrusters of Apollo [161], Space Shuttle [162] or ATV/ESM [2, 163].

Several investigations have been conducted with impingement injectors and hypergolic hydrogen peroxide based propellants in recent years. At Purdue University, Mahakali et al. tested hypergolic combinations with sodium borohydride as a reactive additive and different fuels [164]. An unlike impinging injector was tested in open space and with a combustion chamber. The injector had a central fuel bore and around these four oxidiser bores. The angle between the central bore and the oxidiser bores was  $30^\circ$ . The injector alone provided fast hypergolic ignition with IDTs between 7 ms and 12 ms. The injector was also able to ignite the combustion chamber [164]. Later, Kan et al. [165] investigated a hypergolic fuel consisting of triglyme with 8 wt% sodium borohydride and 90 %  $H_2O_2$ . They conducted tests in a combustion chamber with and without a nozzle section to characterise the ignition at different conditions. The chosen injector consisted of three, unlike impinging elements. Each element had a central fuel bore and three surrounding oxidiser bores. Hypergolic ignition was achieved with an IDT in the combustion chamber of 5 ms [165].

Kang et al. performed several tests with a 500N battleship combustion chamber [52, 166]. The injector was an unlike impinging element with a central fuel bore and four surrounding oxidiser bores, a so-called unlike pentad or 4on1 injector. The impingement angle between the fuel bore and the oxidiser bore was  $30^\circ$ . This injector provided reliable and fast ignition with their Stock 2 (tetraethylene glycol dimethyl ether, tetrahydrofuran, toluene and sodium borohydride) fuel and concentrations of hydrogen peroxide between 95 % and 98 % [55]. Recently, Kim et al. investigated the RSS of a hypergolic combination in an unlike pentad injector [72]. The propel-

lant consisted of 1,2-propanediamine with 6.5wt%  $\text{NaBH}_4$  and 3.5wt%  $\text{NH}_4\text{I}$  as additives and 95 % hydrogen peroxide. The hypergolic combustion in an open optical accessible combustion chamber was analysed, and different combustion regimes were identified [72].

### 2.5.2 Swirl injector

In swirl injectors, the moving fluid has an axial movement component and a second tangential (swirling) component. When this fluid exits the injector element, the tangential component leads to the formation of a cone-shaped spray sheet. Due to instabilities in the flow which grow after leaving the swirl exit, the spray atomises [159]. The swirl injector consists of a swirl chamber with one closed and an open end. At the closed end are one or more tangential holes, where the fluid is injected into the chamber and flows along the wall. Along the axis of the swirl chamber, a gaseous core is formed. The fluid exits the chamber at the open end, and the sheet widens due to the tangential movement component. There are two types of swirl chambers: open and simplex swirl. The chamber of the open swirl is cylindrical. The simplex swirl has a chamber with a tapered design. With this, the tangential velocity of the fluid is increased due to the reduction of the swirl chamber diameter. A certain opening angle of the spray cone is formed depending on the swirl geometry, the fluid properties and the mass flow. The design and manufacturing of swirl injectors is more complex compared to impinging injectors. Design criteria for swirl injectors can be found in [167].

Swirl injectors can also be arranged coaxial, where the inner swirl provides one propellant component, and the outer swirl provides the second component. This design is used in many European orbital propulsion thrusters from *ArianeGroup* [168–170]. The coaxial swirl design also provides a fuel film cooling at the chamber wall.

Some investigations with swirl injectors and hypergolic hydrogen peroxide-based propellants are published. Long investigated different swirl configurations with the propellant combination Block 0 and 98 % hydrogen peroxide in a 42 lbf (187 N) thruster [81]. Injectors in different configurations were able to provide smooth hypergolic ignitions. The injectors showed relatively low  $c^*$  efficiencies. Further, it was pointed out that a coaxial design is challenging regarding dimensions for this thrust class.

A variation of a swirl injector was tested by Yuan et al. [51]. Here, a cyclonic injector was used with a fuel called W2 (a mixture of kerosene, manganese acetate tetrahydrate, methanol, and an undisclosed dispersion medium) and hydrogen peroxide. The cyclonic injector has a chamber where liquid fuel and oxidiser are tangentially injected. They mix, and a hypergolic reaction starts to vaporise the mixture. This injector provided ignition delays between 18 and 4 ms [51].

### 2.5.3 Pintle injector

The pintle injector is an injector for bipropellants. It consists of a central cylindrical structure, the pintle, see figure 2.5 c). At the tip, some kind of opening exists. One component of the propellant is delivered by an internal channel to the tip and discharged through bores or a slit or something similar in the radial direction. Around the bottom of the pintle, the second component is injected through a slit and flows along the outside of the pintle wall. Both components meet and mix at the pintle's tip, and atomisation occurs. Pintle injectors are particularly well suited for throttleable applications because the areas of the propellant outlet is variable. Some design rules can be found in [159].

Pintle injectors have been applied in several hypergolic rocket engines [171]. An eminent example is the Lunar Module Descent Engine of the Apollo program.

Austin et al. tested a pintle injector inside a 150 lbf (667 N) combustion chamber [78]. The

propellant was Block 0 and 98 % hydrogen peroxide. With the developed pintle injector, rapid reproducible ignitions were demonstrated.

## 3 Methods

This chapter gives an overview on the selection process of suitable fuel candidates. Further, the experimental methods are described.

### 3.1 Definition and screening

The research objective is the development of a green hypergolic alternative to conventional propellants for use in typical orbital propulsion applications. With this objective, several boundary conditions are defined. Further critical parameters for the development of a novel fuel combination are derived and assessed. A suitable oxidiser is chosen in the initial step, and a class of fuels is identified. Following, the requirements necessary for the application of the potential fuel candidates are gathered. With this information in the next step, performance calculation can be conducted. Finally, a selection of suitable fuel candidates can be made.

#### 3.1.1 Performance calculation

To estimate the performance potential of a novel fuel / oxidiser combination, a primary calculation with the program *Chemical equilibrium and Applications*(CEA) by NASA is performed [24]. The basic principles and assumptions are explained in 2.1.1.

For the present investigation, the *rocket* problem was used. The supersonic expansion in the nozzle was regarded as frozen. As mentioned by Sutton, this case underestimated the actual performance in the order of a few percent [7] but has proven to be useful especially for low thrust rocket engines.

As reference case the 400 N bipropellant apogee motor of ArianeGroup is chosen. This thruster uses MMH as fuel and as oxidiser NTO, MON-1 or MON-3. At the nominal conditions, a thrust of 425 N is produced at a specific impulse of 321 s and a nozzle expansion ratio (by area) of 330. The combustion chamber pressure is 10.35 bar at a nominal oxidiser to fuel ratio (ROF) of 1.65. The input for the performance calculations are: pressure in the combustion chamber, nozzle expansion ratio  $\epsilon$ , ROF and the propellant specific data such as molecular formula, heat of formation, initial temperature of the propellant. For each calculation, the pressure in the combustion chamber and nozzle expansion ratio  $\epsilon$  are set to 10.35 bar and 330, which are the values from the reference thruster. The composition of the oxidiser is based on the highest concentration commercially available at the moment. Therefore, 98 wt% hydrogen peroxide and 2 wt% water are considered. The specific data such as enthalpy of formation of  $H_2O_2$  and water are provided in the CEA database. The fuel is assumed as a pure substance with the molecular formula and enthalpy of formation provided in table 4.2. The initial temperature of the propellant is 298.15 K. The calculation assumes frozen conditions from the throat on.

The performance is computed for different oxidiser to fuel ratios because the optimum ROF for the highest  $I_{sp}$  is not known yet. The range of the considered ROF is from 1 to 8 with an increment of 0.1. The output of the calculation considered for this screening for each ROF step are the  $I_{sp}$  values referring to the nozzle and vacuum conditions, the  $c^*$  value, the adiabatic flame temperature inside the combustion chamber and the average molecular mass of the exhaust products.



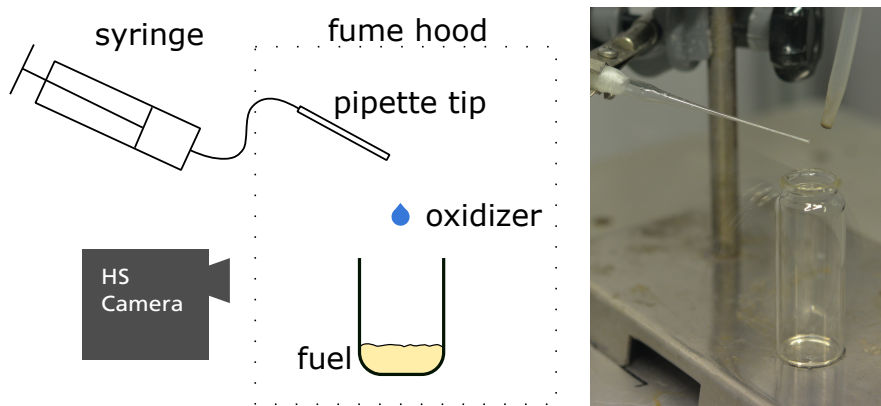


Figure 3.1: Left: scheme of the initial drop test setup, right: photograph

## 3.2 Experimental setups

In this section, the experimental setups are described, developed and applied during the different phases of the thesis.

### 3.2.1 Drop test

#### Basic drop test setup

The drop test is a fast and straightforward method to evaluate the reactivity of two substances. During a drop test, small amounts (i.e. drops) of the two substances are brought together by dropping one component onto the other. Since only small quantities are used, these tests can be performed with little effort compared to tests with an injector or a thruster, where extensive infrastructure is needed. Therefore, the drop test is suited for an initial assessment of the hypergolic potential of a new propellant combination. Besides, the drop test is a suitable tool to evaluate the effect of additives dissolved in the propellant in terms of their influence on the ignition behaviour.

The sequence of a drop test with hypergolic substances starts with providing one component of the propellant in a vessel. The second component is dropped into the vessel and encounters the first component. The two components mix and start to react, and at some point, ignition and flame propagation can be observed. This process can be recorded utilizing a high-speed camera. Via the analysis of the high-speed recordings, the moment of the first contact of the two components, the moment of the initial vapour release, and the moment of the ignition can be determined.

During this thesis, two different drop tests setups were applied. For initial tests, a simple setup consisting of a pipette from where the drop is released and a watch glass or test vial which contains a small pool of the second component. A setup scheme is shown in Figure 3.1 on the left, and a picture of the setup is shown on the right. After a drop test, the additional tube above the test vial can provide water to suppress the hypergolic reaction.

All drop tests were executed inside a fume hood with a closed front panel for safety reasons. For releasing the drop, a syringe connected to a hose with a pipette tip was used. By operating the syringe in front of the fume hood, the drop was released from the pipette tip. Most of the drop tests were conducted with a fuel as pooling component and a hydrogen peroxide droplet. The height of the falling drop above the pool in the initial setup was 80 mm. The diameter of the pipette was 1 mm. The tests were recorded with two high-speed cameras by *Photron* (SA-X2 or Fastcam 1.1). The frame rate was chosen between 2000 and 5000 frames per second.

With this setup, 239 drop tests were performed. From the experience gained during these tests,



Figure 3.2: Drop test setup in laboratory

a new chamber was designed, to allow a control of the ambient conditions. In addition, further experiments were carried out under a protective atmosphere or lower pressure.

#### Advanced drop test setup - HYPED UP

Based on the experience with the initial drop tests, an advanced drop test setup was designed and put into operation. This task was executed within a master's thesis project by J. Balkenhohl [172]. The following requirements were defined for the novel setup:

1. a closed volume with the possibility to control ambient pressure in the range of 0.1 – 2 bar and the surrounding medium (air or inert atmosphere) should be implemented
2. optical access to the reaction chamber with the optical high-speed camera
3. automated drop generation system with good repeatability
4. measurement of temperature and pressure inside the chamber

The novel setup, the so-called 'HYPERgolic Drop test setUP' or 'HYPED UP', should be able to control the initial conditions of the drop test, such as initial pressure or surrounding medium. Therefore, a design with closed volume and optical access was necessary. It was also assumed that the repeatability of the drop tests is increased with a closed volume and controlled environment. During the use of HYPED UP, several minor optimizations were applied. The setup presented in the following is the latest configuration used for the bulk of the drop tests. With the setup, more than 670 tests were conducted.

Figure 3.2 shows the complete assembly of the drop test setup inside a fume hood, high-speed camera, control and measuring computers in the lab of M3. The setup has several subsystems:

- drop chamber assembly
- conditioning infrastructure
- measurement and test controlling

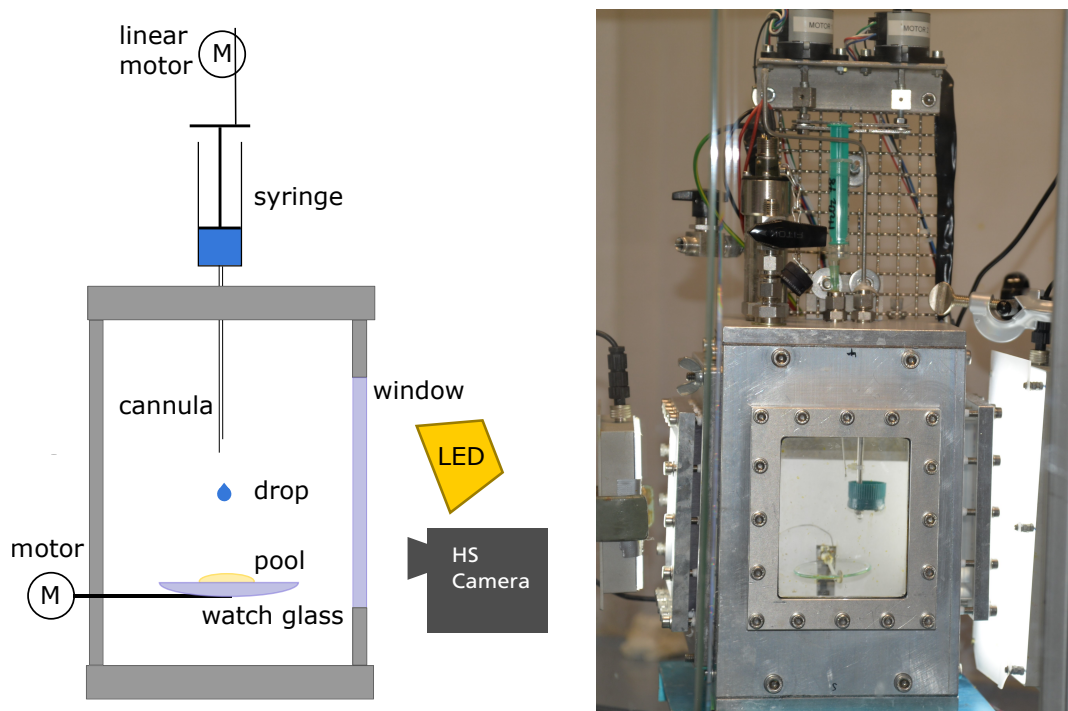


Figure 3.3: Drop test chamber, left: scheme; right: picture

- high-speed camera and control
- *optional: additional measurement such as spectrographic devices*

**Drop test chamber assembly** Figure 3.3 shows the reaction chamber of the drop test setup in more detail. The chamber itself consists of a square aluminium profile. The inner volume is  $216 \times 140 \times 140 \text{ mm}^3$ . The top and bottom are closed with aluminium plates. There are three cut-outs in three of the four side walls. One of those cut-outs has a removable side panel to allow fast and easy access into the chamber. Windows are mounted directly on the other two openings. On the top of the chamber, a syringe pump assembly is mounted. Further, connectors to inert gas or vacuum pump, to the pressure transducer and support for safety devices are placed there. From the syringe, a cannula leads into the chamber. Inside the chamber, a watch glass is placed in the middle. A shaft connects the holder of the watch glass to a motor. With the motor, the watch glass can be turned. A beaker is filled with water and placed below the watch glass (not visible in Figure 3.3). The beaker is used as a reservoir to catch wastewater after a drop test and to suppress further reactions. Additionally, a small cup (green cup inside the chamber in Figure 3.3) can be placed below the cannula to catch any released drops when it is not desired. This allows safe operation inside the chamber to prepare and post-process a drop test. The cup can be turned to a side position. This allows the free passage of the drop from the cannula to the watch glass.

The syringe pump assembly consists of a medical syringe connected to a cannula and a linear motor. The syringe plunger can be moved in or out by activating the linear motor. The cannula ends inside the reaction chamber above the watch glass. Hence, to conduct a drop test, a single drop of one component can be released from the tip of the cannula. The drop falls into a pool of the second component located in the watch glass.

**Conditioning infrastructure** Sealing the chamber to conduct tests at reduced pressure or under an inert atmosphere is possible. For this purpose, a vacuum pump and a gas bottle supply can be connected to the chamber. Argon was used as an inert gas. The chamber was designed to withstand pressures between 0.1 and 2 bar.

**Measurement and test control** The control and data acquisition is accomplished with a *LabVIEW* routine and a *NI Compact DAQ* with several modules. The syringe pump is controlled with a digital output module *NI 9472*. This module is connected to a *SAMOTronic* stepper motor controller, which operates the linear motor. The signal of the pressure transducer is measured with an analogue input module *NI 9219*. A *NI 9214* thermocouple module is used for the temperature measurement. In *LabVIEW*, a routine with an user interface was programmed, which allowed the control of the stepper motor, visualised and saved the data. For the pressure measurement, a *PR3102 Protran* pressure transducer by *Althen* with a range from 0-10 bar is used. Moreover, a type K thermocouple can be placed inside the chamber to measure the temperature. It is also possible to place the thermocouple inside the pool component to measure the pool temperature. The data acquisition rate of the pressure sensor was 250 Hz. The thermocouple was sampled at 20 Hz.

**High-speed camera and control** The high-speed recording is necessary for the evaluation of the ignition delay of the tested hypergolic combination. The instance of the first contact of fuel and oxidiser can be determined by analysing the high-speed recording. Following the initial vapour generation, ignition with flame propagation is also recorded. The records were conducted with a *Photron SA-X2* camera. For sufficient illumination, one or two LED panels were used (compare Figure 3.3). The frame rate was between 3600 and 5000 frames per second (fps). The *Photron* software PFV Viewer 3.50 controlled the high-speed camera. The high-speed camera was located outside the fume hood (see Figure 3.2). A lens with a focal length of 100 mm was used to record the processes inside the reaction chamber. The field of view focused on the pooling component. The camera was triggered manually before a drop test.

**Test execution** Here, a short explanation of the execution of a drop test with the HYPED up is given. In most test runs, hydrogen peroxide was the dropping component, and the ionic liquid was the pool component. For the preparation, the hydrogen peroxide was taken from the storage, and an amount of roughly 30-50 ml was transferred to a beaker. The peroxide in the beaker was used as a reservoir for the drop test and concentration determination. From the beaker, a syringe of a nominal size of 5 ml was filled with 1 ml of hydrogen peroxide and inserted into the syringe pump. Then, the syringe pump was activated to fill the cannula. For this, some drops of peroxide were caught from the cannula in a beaker or with a wet tissue. In the next step, the watch glass was turned in the right position and the fuel was positioned in the centre of the glass. A certain amount of fuel was dosed with an Eppendorf pipette on the watch glass. Then, the chamber was closed, and the setup was ready for testing when the 'safety cup' was turned into the open position. The drop test is executed by starting the high-speed camera and activating the syringe pump to release a drop of hydrogen peroxide. After the drop test and successful ignition, the 'safety cup' is turned below the cannula to prevent further drops from falling on the watch glass. The high-speed camera is stopped, and the record is stored. The watch glass is turned into a position allowing the test residuals to run into the beaker at the bottom of the chamber. This also suppresses further hypergolic reactions. When the hypergolic reaction is over, the reaction chamber can be opened, allowing the flow inside the fume hood to draw the combustion products. After the vapours have vanished, the watch glass can be cleaned with water and a new drop test can be prepared. Before another drop test, some drops of  $\text{H}_2\text{O}_2$

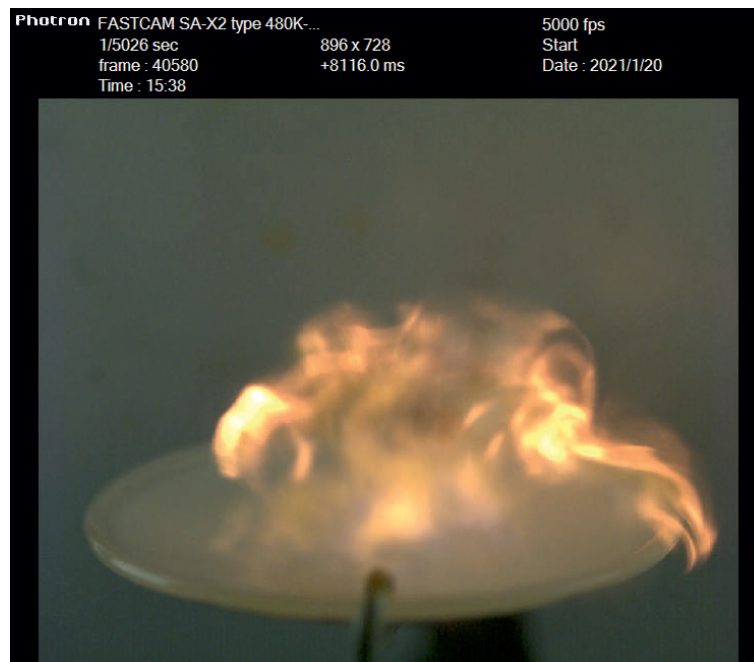


Figure 3.4: Example snapshot shortly after ignition, test run 544

were released from the cannula and caught to ensure that the next drop test was conducted with a fresh hydrogen peroxide drop.

The reaction chamber was evacuated after the chamber was closed for tests at reduced pressures. When the desired pressure was reached, the valve to the vacuum pump was shot, and the test was executed. The reaction chamber was evacuated to 0.2 bar for tests with the inert gas and filled with the inert gas to 1 bar. Then, the chamber was evacuated again to 0.2 bar and refilled with the inert gas. This was repeated five times to reach a low remaining partial air pressure in the order of 0.05 %.

### Exemplary evaluation

This section shows an exemplary analysis of the high-speed recording to determine the TVG and IDT. Figure 3.4 shows a snapshot of the high-speed recording shortly after the ignition. In the header of the recording, some information is given, such as the resolution, frame rate, shutter speed, frame number and time stamp of the present frame. The timestamp of the frame is counted from the triggering of the high-speed camera. In this case, the camera was triggered manually approximately 8 seconds before the drop test.

**Determination of ignition delay** Figure 3.5 shows selected frames of the high-speed recording of test run '544'. In this test, a drop of hydrogen peroxide falls into a pool of the ionic liquid [EMIm][SCN] (slight yellow fluid at the bottom inside the watch glass). The times are derived from the time stamps of the corresponding frames. The falling drop is visible in frame a) 5 ms before impact. The impact is shown in frame b). This initial contact of fuel and oxidiser is also defined as time 0 for the determination of the TVG and IDT. After the impact, the drop of hydrogen peroxide merges with the fuel pool, mixing occurs, and initial reactions start. The reactions generate heat. Between frames c) and f), vapour is released from the reacting mixture. Frame c) shows the instance shortly before the vapour is released. In frame d), the initial vapour core becomes visible, and the vapour cloud develops and expands in frames e) and f). In frame



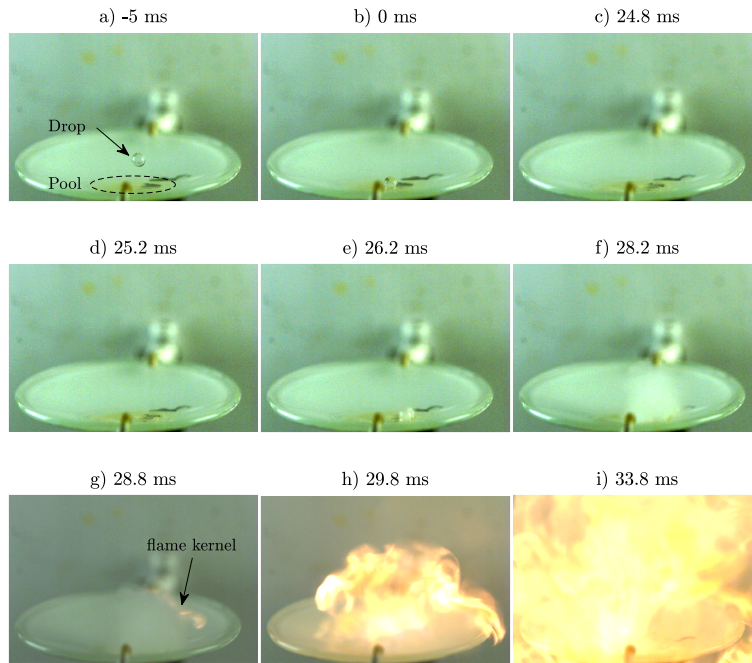


Figure 3.5: Example analysis of a drop test, test run 544

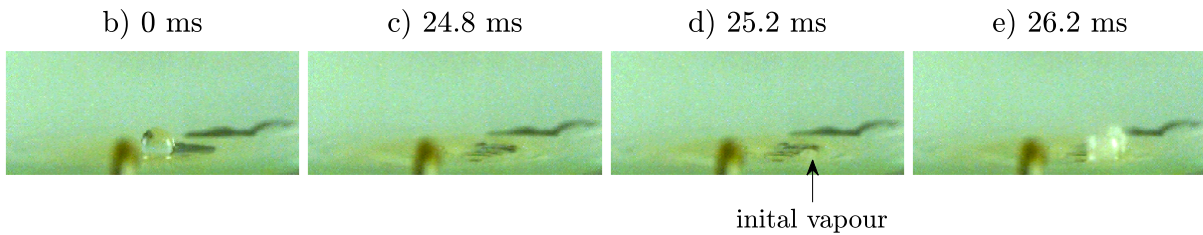


Figure 3.6: Example analysis of time to vapour generation determination, test run 544

g), the initial ignition becomes visible in the vapour phase. The flame propagates, and frames h) and i) show the flame 1 and 5 ms after ignition.

Figure 3.6 shows the initial contact and the time around the vapour generation in more detail. The TVG is measured from the initial contact until frame d), where the vapour gets firstly visible; here, the TVG is 25.2 ms. As can be seen, determining the initial vapour is not a simple task. However, the determination is less complicated if the video is analysed compared to the single frame displayed here. The determination of the IDT is easier because of the bright appearance of the flame. The IDT in this drop test is 28.8 ms and determined with the following equation (3.1).

$$IDT = t_{ignition} - t_{contact} \quad (3.1)$$

**Determination of drop size and velocity** The high-speed recordings were also used to determine the drop size and the velocity prior to impact. The drop size was determined by assuming a spherical drop and measuring the drop diameter in terms of pixels. The diameter was measured in x ( $l_x$ ) and y ( $l_y$ ) direction by confining the falling drop with the cross cursor, as displayed in the left picture of figure 3.7. The average value  $l_{av}$  of  $l_x$ ) and y  $l_y$  is taken to calculate the drop diameter. A known reference length was used to convert the measurement from pixels to

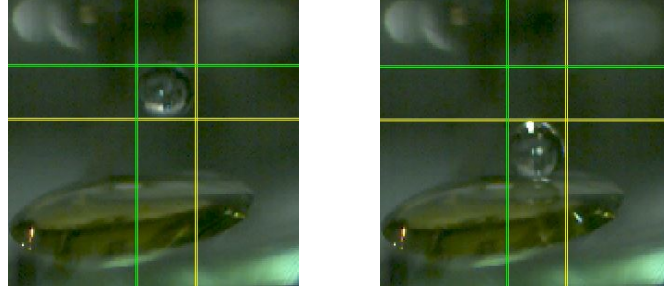


Figure 3.7: Determination of drop size and velocity

a physical length. As a reference, the diameter of the watch glass was used; compare figure 3.5. The diameter is known as 50 mm. The diameter  $l_{\text{ref}}$  was measured from a frame of the high-speed recording, and a conversion factor  $CF_{\text{px/mm}}$  (mm per px) was determined. The diameter of the drop  $D_{\text{Drop}}$  was calculated:

$$D_{\text{drop}} = \frac{l_{\text{av}}}{CF_{\text{px/mm}}} \quad (3.2)$$

The volume of the drop  $V_{\text{drop}}$  can be calculated with:

$$V_{\text{drop}} = \frac{1}{6}\pi D_{\text{drop}}^3 \quad (3.3)$$

The velocity of the falling drop was determined shortly before impact. As shown in the left picture of figure 3.7, roughly one diameter before impact, a square was defined around the drop. As the first time  $t_1$  reference for the velocity determination, the time stamp, then the drop firstly touches the yellow line was used. The second time  $t_2$  is taken when the drop lastly touches the yellow line. The velocity is calculated:

$$v_{\text{drop}} = \frac{l_y}{t_2 - t_1} \quad (3.4)$$

This velocity determination is only a rough estimation since the drop is permanently accelerated.

**Uncertainty** Combined quantities, which are calculated from different measurement values or constants, are determined with the combined standard uncertainty  $u_c^2$  according to the Gaussian error propagation:

$$u_c^2 = \sum_{i=1}^N \left( \frac{\partial f}{\partial x_i} \right)^2 u^2(x_i) \quad (3.5)$$

where  $f$  is a function which is dependent on the quantity  $x_i$  and  $u(x_i)$  is the uncertainty of the quantity  $x_i$ .

As presented, ignition delays and time to vapour generation are determined with the high-speed camera recordings of their time stamp. The camera's internal time generator has a resolution of 100 ns. This is several orders lower than the typical ignition delays and, therefore, neglectable for the error determination. The determination of IDT and TVG relies on the frame-by-frame evaluation of the high-speed recording. To determine the initial contact of the drop with the surface of the propellant, an uncertainty of the duration of one frame can be assumed. The determination of the vapour phase rising from the mixture is not always obvious. Therefore, an uncertainty of the duration of 2 frames is assumed. Generally, the ignition kernel can be spotted

Table 3.1: Uncertainties of high speed recoding evaluation

instance	name	uncertainty [s]
contact	$u_{t_0}$	$1/fps$
vapour generation	$u_{t_v}$	$2/fps$
ignition	$u_{t_I}$	$1/fps$

reliably. Here, an uncertainty of the duration of one frame can be assumed. The uncertainties are displayed in table 3.1.

The uncertainty in the determination of the IDT is calculated with the Gaussian error propagation applied to equation (3.1):

$$u_{IDT} = \sqrt{u_{t_I}^2 + u_{t_0}^2} = \frac{\sqrt{2}}{fps} \quad (3.6)$$

Similar, the uncertainty for the TVG is:

$$u_{TVG} = \sqrt{u_{t_v}^2 + u_{t_0}^2} = \frac{\sqrt{5}}{fps} \quad (3.7)$$

For the uncertainty of CF  $u_{CF}$  caused by the measurement of the reference length, an uncertainty of three pixels is assumed. The uncertainty of  $l_{av}$  ( $u_l$ ) is assumed with two pixels. The uncertainty of the drop diameter  $u_{dia\ drop}$  is

$$u_{diadrop} = \sqrt{\left(\frac{1}{CF_{px/mm}}\right)^2 u_l^2 + \left(\frac{l_{av}}{CF_{px/mm}^2}\right)^2 u_{CF}^2} \quad (3.8)$$

The uncertainty of the velocity measurement is:

$$u_{velocity} = \sqrt{\left(\frac{1}{\Delta t}\right)^2 u_{diameter}^2 + \left(\frac{l_y}{(\Delta t)^2}\right)^2 u_{\Delta t}^2} \quad (3.9)$$

With  $\Delta t = t_2 - t_1$  and  $u_{\Delta t}$  is the duration of 2 frames at the corresponding frame rate.



### 3.2.2 Hypergolic injection test setup

The **H**ypergolic **I**njection **T**est setup (HIT) is designed to perform hypergolic ignition investigations with propellants under flowing conditions using different injectors. Figure 3.8 shows the piping and instrumentation diagram (P&ID) of the HIT setup. HIT consists of a propellant supply, a modular injector, an atmospheric reaction chamber and the measurement instrumentation, see figure 3.8. Figure 3.9 left shows a picture of the reaction chamber and the equipment. The HIT setup is supplied by the infrastructure of the test bench M11.2, which also provides the measurement and data acquisition system. In the upper part of Figure 3.8, the propellant supply can be seen, which consists of two stainless steel tanks for oxidiser (volume of 1 l) and fuel (volume of 0.5 l) and separate feeding lines to the injector. Both tanks can be pressurized from the top with nitrogen. Nitrogen pressurization can be independently chosen for fuel and oxidiser. The tank's supply pressure is used to set the operating conditions for the injection tests. PID pressure regulators regulate the supply pressures.

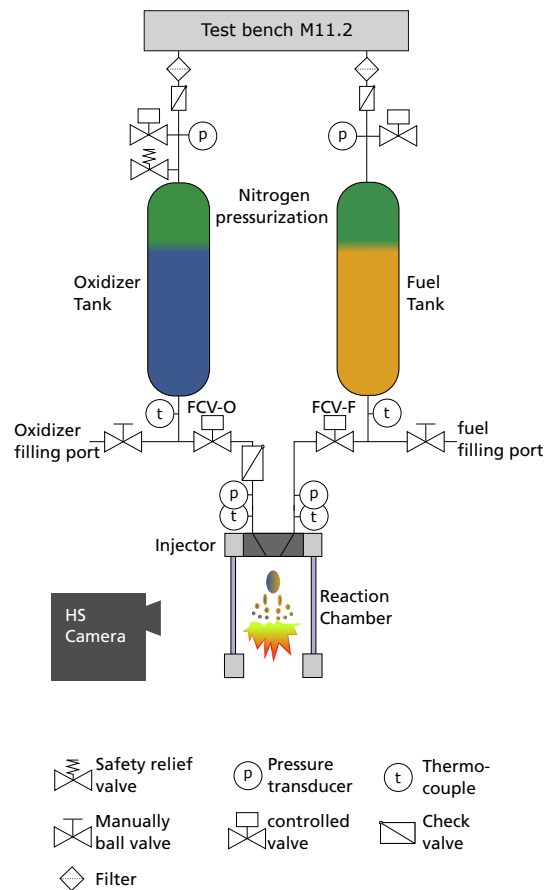


Figure 3.8: P&ID of the HIT set up

The P&ID shows that a pressure transducer and valve for venting are placed on top of each tank. Additionally, a safety relief valve with an opening pressure of 30 bar is placed at the oxidiser side to avoid over pressure building up due to a possible decomposition reaction of the hydrogen peroxide. Each tank can be filled from the bottom side via a manually operated ball valve. The feeding line to the injector is equipped with a solenoid valve from Buschjost, which serves as a flow control valve (FCV). Temperature and pressure are measured in the line behind the valve just before the injector head. The injector head is modular, and different injectors

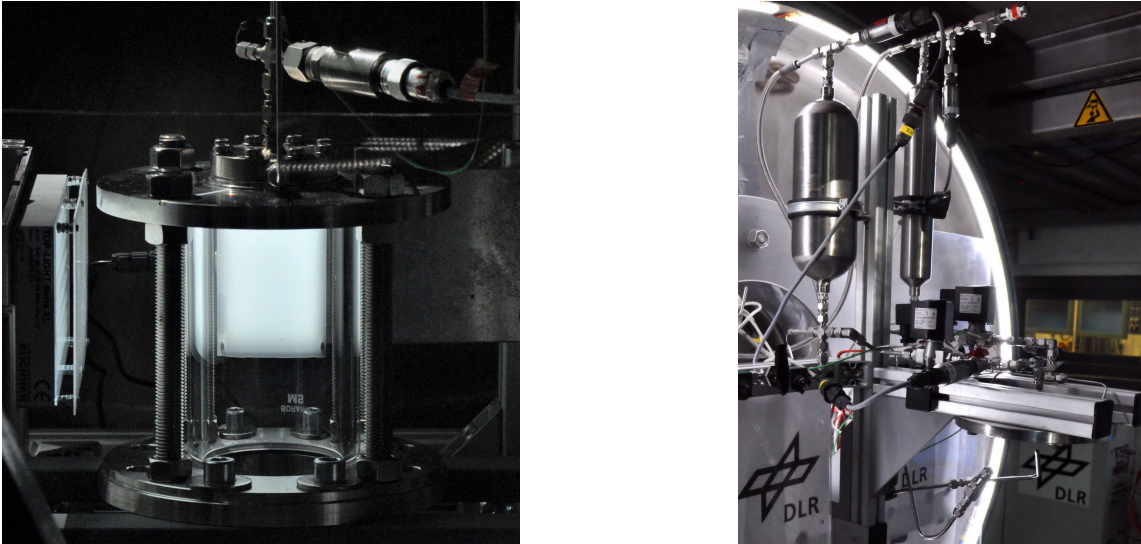


Figure 3.9: Left: HIT reaction chamber; right: HIT integrated at M11.2

can be tested. For the initial investigation of the hypergolic ignition ability of the propellant candidates under flowing conditions, an impinging injector is used. An optical accessible reaction chamber is mounted below the injector; see Figure 3.9 left. The chamber is open on the bottom side, so tests at atmospheric pressure can be conducted in this configuration.

For the second test campaign, where the influence of the ambient pressure on the ignition delay was evaluated, the HIT setup was integrated into the vacuum chamber of the test bench M11.2. The P&ID is identical to the initial test campaign. In the initial test campaign, the glass of the reaction chamber was contaminated with fuel and combustion residuals after some tests. This reduces the visibility, and a cleaning of the glass was necessary after a few test runs. Therefore, the reaction chamber was removed due to the limited accessibility of the setup inside the vacuum chamber. A picture of the setup integrated HIT setup at M11.2 is shown in Figure 3.9 right.

### Control and data acquisition

The test position M11.2 is equipped with a versatile control and data acquisition system based on a real-time processing module *ADwin-Pro II* rack with a *Pro-CPU-T12* processor by *Jäger*. This system is connected to a control and measurement PC, and the user interface is implemented in a *LabVIEW* program. The program allows control of the test bench, automated sequence runs, visualizes the measured data, and saves the data in a .txt file. The *ADwin* rack is equipped with different modules for control (*ProII-TRA-16*) and data acquisition.

**Pressure** The pressures in the HIT setup are measured with P913-G003 pressure transducers by Measurement. The range of the sensors is 0 – 50 bar absolute pressures. The mV signal of the pressure sensors is amplified by *DAQP-STG Dewetron* amplifiers. The resulting signal between 0 – 10V is sampled by the DAQ system with an analogue input module at the *ADwin* rack. Before the test campaign, the pressure sensors were calibrated in the DLR measurement lab with a reference measurement sensor and a sensor polynomial was derived. The polynomial is implemented in *LabVIEW* to convert the measured signal into a physical value. The sampling rate for the pressure sensors was 1 kHz.

**Temperature** The temperatures are measured with type K thermocouples with a diameter of 1 mm. The outer material of the thermocouples, which is in contact with the fuel or oxidiser, is stainless steel. The signals of the thermocouples are sampled by the DAQ using a thermocouple measuring module. The sampling rate was set to 100 Hz.

**High-speed imaging** For the evaluation of the ignition behaviour, two high-speed cameras are aligned towards the injector. The view fields of the two cameras are perpendicular to each other: one camera focuses on the plane where the liquid sheet of the impinging injector forms. The other camera's field of vision is perpendicular to this plane and looks at the injector orifices. LED panels are mounted behind the reaction chamber for illumination. The frame rate was 10000 fps. The high-speed cameras were controlled by the *Photron* software *PFV Viewer 3.50* which was run on a second computer (independently of the control and DAQ PC). In the test sequence, a trigger signal was issued 100 ms before the opening of the first FCV to start the recording. Only one high-speed camera was used for the test campaign inside the vacuum chamber.

#### Test preparation

For a safe operation with hydrogen peroxide, special care must be given to material compatibility and cleanliness of the supply system. The materials in direct contact with hydrogen peroxide should be highly compatible to avoid self-decomposition. Further, organic compounds mixed with hydrogen peroxide can become a sensitive mixture that may detonate. Therefore, it is important that the system is clean, especially free from organic materials such as oil or grease. Most of the components in the feeding system were made from stainless steel, such as SS316 for the fittings or 1.4571 for the tubing. This material has good compatibility with hydrogen peroxide and is declared as a class 2 material [88]. This means the material is recommended for short-term use with hydrogen peroxide. If a stainless steel is properly passivated, the compatibility increases. All other parts in direct contact with hydrogen peroxide, such as flow control, check, or pressure relief valves, were purchased in a condition suitable for oxygen operation. This means the components are free from oil or organic grease, and an oxygen-compatible lubricant such as *Krytox* is used.

When the whole feeding system was assembled, the hydrogen peroxide line was subjected to a cleaning and passivation procedure. The cleaning is necessary to eliminate possible oil and grease films in the tubing. The passivation leads to a less active surface on the decomposition of the hydrogen peroxide. For this purpose, treatment with an acid and hydrogen peroxide creates a passive layer which is less active in terms of the decomposition of  $\text{H}_2\text{O}_2$ . The passivation procedure was developed based on literature [88, 173] and in discussions with industry representatives. In the first step, the lines were assembled in a way that no dead ends were present. Then, a four-step procedure was performed to prepare the system for use with hydrogen peroxide. In the beginning, the system was treated with a degreasing solution. For this purpose, a solution containing 24 g/l trisodium phosphate and sodium metasilicate was used. This solution was filled into the system and pumped around for 4 hours with a hose pump. After that, the system was flushed with distilled water until the water was pH neutral again. The second step is a pickling solution to provide a better surface for the following passivation step. The pickling solution is 5 wt% solution of caustic soda diluted with water. This solution was kept in the system for one hour. Afterwards, the system was flushed until the flushing water was pH-neutral. The actual passivation step is a treatment with 65 % nitric acid for 5 hours. In this step, free iron on the surface is removed [174]. Then, the system is flushed with water until the pH of the water is neutral. Finally, a solution of 30 % hydrogen peroxide is filled into the system for 8 hours to complete the passivation. In the end, the system is flushed with water and purged with nitrogen until it is dry. Hereafter, the system can be reassembled in a clean environment and is ready for testing after a successful leak check. For the reassembling process, special care should be given

to cleanliness. For the second test campaign with HIT inside the vacuum chamber of the M11.2, a citric acid-based solution called *CitriSurf 3050* was applied. The citric acid solution provides similar results but facilitates handling procedures and waste management.

### Test execution

Two different test modes are performed: cold flow testing and hot fire testing. At cold flow tests, only non-reactive substances are used, for example, for commissioning, function, or calibration tests. Water can be used as a non-reactive simulant for hydrogen peroxide. Highly concentrated hydrogen peroxide (98 %) has a higher density ( $1.44 \text{ g/cm}^3$ ) than water ( $1.0 \text{ g/cm}^3$ ) and a higher viscosity (dynamic viscosity 30 % higher) compared to water. But these values are still in the same order; see table 3.2. Further, there are no hazards due to contamination of the feeding system if distilled water is used. The ionic liquid fuel for the injector tests has a much higher viscosity. Therefore, a solution of 30 % glycerol and 70 % water was used as a simulant. This solution has a viscosity and density similar to the neat ionic liquid. The relevant properties of simulant and propellant components are compared in table 3.2.

Table 3.2: Comparison simulants and propellant components at 25 °C

	density [g/cm <sup>3</sup> ]	viscosity [m Pa s]	surface tension [mN/m]	
H <sub>2</sub> O <sub>2</sub> 98 %	1.42	1.156	80.1	[88]
water	0.997	0.89	72	[175]
[EMIm][SCN]	1.12	22.6	46.3	[50, 176]
70 wt% glycerine - 30 wt% water	1.18	23.1	67	[177, 178]

For a test run, a certain pressure is set in the tank. The mass flow through the injector results from the pressure difference between the supply pressure in the tank and the ambient pressure. The mass flow can be estimated for a certain pressure difference if the discharge coefficient ( $c_d$ ) of the injector is known; see equation (2.20). The  $c_d$  value can be determined in calibration tests conducted with the simulants. The simulants are used because they are much simpler to handle, do not generate hazards and are cheap. To conduct the calibration test, one simulant was filled into the tank. Then, the tank was pressurised to the desired supply pressure level. Next, a test sequence was started with an opening time of the flow control valve of 10 – 20 s. The fluid ejected by the injector was cached in a beaker. The mass of the fluid was determined with a scale. The mass divided by the opening time of the flow control valve gives the average mass flow at the corresponding supply pressure.

With the known mass flow and pressure difference across the injector, the according  $c_d$  value can be calculated according to equation (2.20). With the calibration for different pressure levels and mass flows, the characteristics of the injector are known, and operation conditions for the hot fire test can be estimated.

For the hot fire tests, fuel and oxidiser are filled into the tanks separately and successively to avoid any hazardous situation where fuel and oxidiser could come into contact unintentionally. Before the first hot test run, fuel and oxidiser feeding lines are filled successively. For this, the supply pressure of the tanks is set to a slight overpressure such as 1.3 to 1.5 bar. Then, one of the flow control valves is opened manually and closed in the instance when the first fluid flowing out of the injector becomes visible. This is repeated for the second feed line of the other component. After filling the lines, the setup is ready for testing. For the hot fire tests, the run time of the test is chosen. The run time is the duration when both FCVs are open. Further, the opening order of the FCVs can be defined as the opening of both valves at the same time or with a lead time on

one side. Moreover, an operation point for the test is selected. The needed supply pressures can be determined according to the injector calibration. The pressure regulators set this pressure. The test sequence can be started if the desired pressure is reached in the tanks. The sequence is executed as follows:

Table 3.3: Sequence of HIT Test

sequence start:	regulation of the pressure during the whole sequence
- 3.5 s:	start of the data storage
- 0.1 s:	trigger high speed camera
0 s:	FCV(s) opens
$0s + x$ :	<i>FCV 2 opens if lead time was chosen</i>
0 s + run time:	FCVs close
8 s:	data storage stops

During the test sequence, the pressure is regulated. 3.5s before the first valve opens, the data storage begins. 100 ms before the initial valve opening, the high-speed cameras are triggered. At 0s, the signal to open the valves is given. If a lead time is chosen, the second valve will be triggered after the lead time. When the run time is over, the signal to the valves stops. 8 s after the initial valve signal, the data storage is stopped.

### Uncertainty

Combined quantities such as the average mass flow,  $c_d$ , injection velocity and ROF were calculated with equation (3.5).

**Pressure** The pressure measurement was compared to a calibrated reference sensor to analyse the uncertainty in the measurement chain. A *Beamex MC5* multifunction calibrator with *EXT 20C* sensor was used. The analysis was performed with all sensors connected to a calibration setup, which submits the same pressure to all sensors. The setup allows the setting of pressure via a manual pressure regulator. When the system reaches a steady pressure, a measurement for 10 seconds is started. The average values of the sensor over the 10 s are compared to the reference sensor, and the variation can be derived. The calibration was conducted for pressure levels of 1, 5, 10, 15 and 20 bar. The results are displayed in the following figure 3.10 taken from [179]. Figure 3.10 shows that the maximum relative deviation from the reference pressure is below 0.7 %.

**Temperature** The thermocouples and their measurement chain were also compared with a calibrated reference unit, a *Beamex FB660* field temperature block. For this, the tip of the thermocouples was placed inside the oven, and a measurement was conducted over 30 seconds when a steady temperature was reached. Temperatures between 25 and 40 °C were tested. The results are displayed in Figure 3.11. The absolute deviation from the reference is around 0.5 K. This corresponds to a relative deviation of around 0.4 %.

**IDT** The ignition delays are determined with the high-speed camera recordings. The uncertainty is depending on the frame rate, see section 3.2.1.

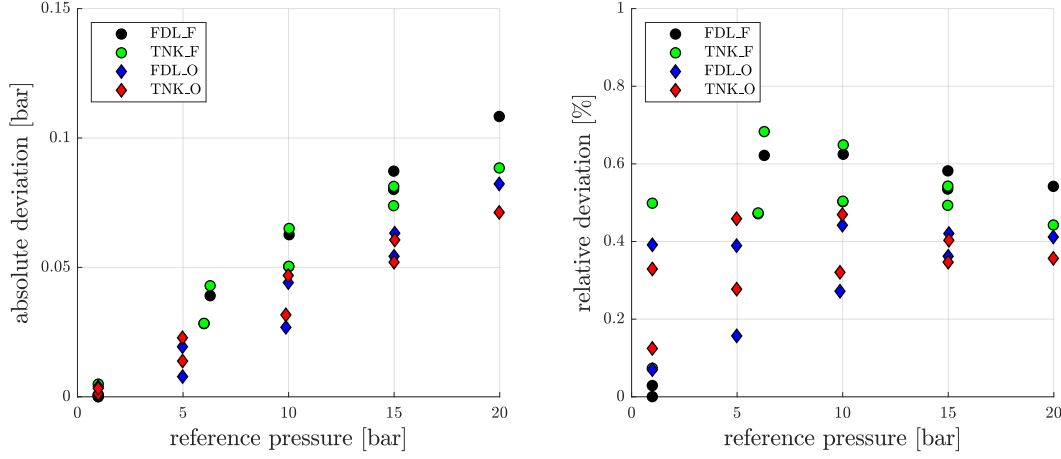


Figure 3.10: Absolute and relative deviation from reference pressure adapted from [179]

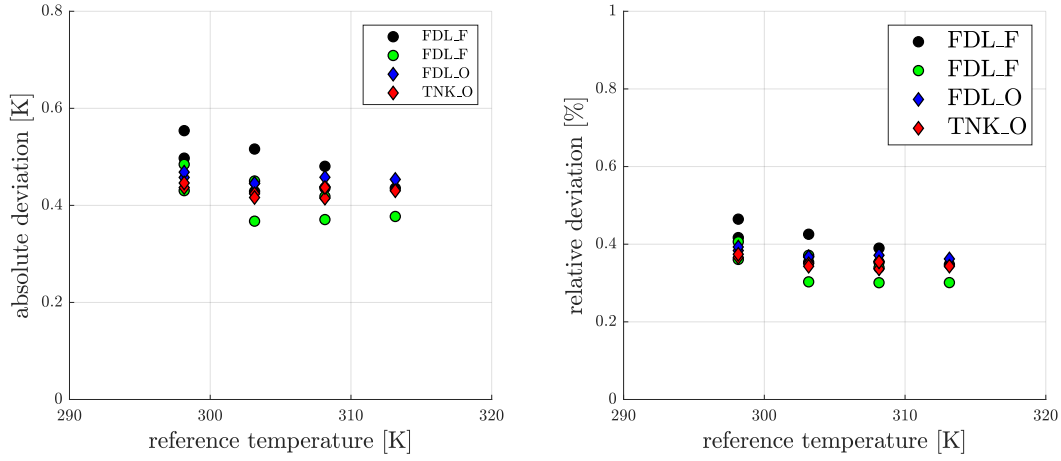


Figure 3.11: Absolute and relative deviation from reference temperature adapted from [179]

**Mass flow I** The mass flow is determined during the calibration tests by measuring the mass which flowed through the injector over a time of 10 or 20 s. The fluid was caught in a beaker and the mass of fluid was determined with a scale. The average mass flow is calculated with:

$$\dot{m} = \frac{\text{measured mass}}{\text{opening time of the valve}} \quad (3.10)$$

The uncertainty of the measured mass  $u_{\text{mass}}$  is 0.4 g, which is the specified uncertainty of the calibrated scale (Kern PES 31000). The uncertainty of the valve open time  $u_{\text{time}}$  is assumed with 0.02s. The combined standard uncertainty of the mass flow is:

$$u_{\dot{m}_I}^2 = \left(\frac{1}{t}\right)^2 u_{\text{mass}}^2 + \left(-\frac{m}{t^2}\right)^2 u_{\text{time}}^2 \quad (3.11)$$

**Discharge coefficient  $c_d$**  The discharge coefficient is calculated with equation (2.20). The uncertainty of the mass flow is  $u_{\text{mass flow}}$  is given above. The uncertainty of the area of the injection orifice  $u_A$  assumes that the nominal diameter has a tolerance of  $\pm 0.01$  mm. The uncertainty of the density  $u_\rho$  is assumed to be  $5 \text{ kg/m}^3$  due to a slight variation of the temperature around  $25^\circ\text{C}$ , the reference temperature for the density value. The uncertainty  $u_{\Delta p}$  is based on

the calibration measurement described above and assumed with 0.7 % of the sensor reading. The following uncertainty  $u_{c_d}$  is derived from (3.5): :

$$u_{c_d}^2 = \left( \frac{1}{A\sqrt{2\rho\Delta p}} \right)^2 u_{mass\ flow}^2 + \left( -\frac{\dot{m}}{A^2\sqrt{2\rho\Delta p}} \right)^2 u_A^2 + \left( -\frac{\dot{m}\Delta p}{A(2\rho\Delta p)^{3/2}} \right)^2 u_\rho^2 + \left( -\frac{\dot{m}\rho}{A(2\rho\Delta p)^{3/2}} \right)^2 u_{\Delta p}^2 \quad (3.12)$$

**Mass flow II** For the hot firing tests, the mass flow is calculated with the determined  $c_d$  value of the injector during the calibration test and equation (2.20). The uncertainty of the mass flow  $u_{\dot{m}_{II}}$  depends on the uncertainty of the discharge coefficient  $u_{c_d}$ , uncertainty of the density  $u_\rho$ , uncertainty of the area of the injection orifice  $u_A$  and the uncertainty of the  $\Delta p$  value  $u_{\Delta p}$ . The values are given above.

$$u_{\dot{m}_{II}}^2 = \left( A\sqrt{2\rho\Delta p} \right)^2 u_{c_d}^2 + \left( c_d\sqrt{2\rho\Delta p} \right)^2 u_A^2 + \left( \frac{Ac_d\sqrt{\Delta p}}{\sqrt{2\rho}} \right)^2 u_\rho^2 + \left( \frac{Ac_d\sqrt{\rho}}{\sqrt{2\Delta p}} \right)^2 u_{\Delta p}^2 \quad (3.13)$$

**Injection velocity** The injection velocity is calculated with equation (2.19). The uncertainty of the injection velocity depends on the uncertainty of the mass flow  $u_{\dot{m}_{II}}$ , uncertainty of the density  $u_\rho$  and uncertainty of the area of the injection orifice  $u_A$ . The values are described above.  $u_{\dot{m}_{II}}$  is calculated:

$$u_{v_{inj}}^2 = \left( \frac{1}{A\rho} \right)^2 u_{\dot{m}_{II}}^2 + \left( -\frac{\dot{m}}{\rho A^2} \right)^2 u_A^2 + \left( -\frac{\dot{m}}{A\rho^2} \right)^2 u_\rho^2 \quad (3.14)$$

**ROF** The uncertainty of the oxidiser to fuel ratio depends on the uncertainties of the oxidiser and fuel mass flow, determined as above. The result is:

$$u_{ROF}^2 = \left( \frac{1}{\dot{m}_{fuel}} \right)^2 u_{\dot{m}_{ox}}^2 + \left( \frac{\dot{m}_{ox}}{\dot{m}_{fuel}^2} \right)^2 u_{\dot{m}_{fuel}}^2 \quad (3.15)$$

The presented uncertainties are used to calculate the uncertainties of the operation points in chapter 6.

### 3.2.3 Diagnostics

Several diagnostic methods for the characterisation of fuels and oxidisers were applied. This section gives a short overview of the methods and apparatus in the laboratory. The measurement of surface tension, the thermogravimetric analysis and infrared spectroscopy were conducted by colleagues from the lab team.

**Density** Density measurements were performed to characterise novel ionic liquid fuels. Moreover, density measurements were used to determine the concentration of the hydrogen peroxide. Density measurements were conducted with a density meter *Easy D40* by *Mettler-Toledo* at ambient pressure and a temperature of 25°C. The density meter is temperature regulated, and its measurement uncertainty is  $\pm 0.0005$  g/cm<sup>3</sup>. For every data point, three measurements were performed, and the average value is given.

For the  $\text{H}_2\text{O}_2$  concentration determination, the measured density was compared to the relation of density and concentration in table A.3 of [88]. These values are based on data collected by Easton et al. [180]. The uncertainty of the measurement is 0.2 %.

**Viscosity** The viscosities were measured with an Ubbelohde viscometer class II. The viscometer was placed in a water bath with a temperature regulated to  $25^\circ\text{C} \pm 0.5^\circ\text{C}$ . Three measurements were performed for each data point, and the average value was used. The maximum relative uncertainty of the measurement is 0.8 % based on uncertainties of the viscometer, the time measurement, the density and the standard deviation.

**Surface tension** Surface tension measurements were performed with a *Krüss EasyDyne* tensiometer using the Wilhelmy plate method. The measuring temperature was regulated to  $25^\circ\text{C} \pm 0.6^\circ\text{C}$ . For each data point, three measurements were performed, each with a fresh sample. The maximum relative uncertainty of the measurement is 0.5 %, based on uncertainties of the tensiometer and the standard deviation.

**Thermogravimetric analysis** The thermogravimetric analysis (TGA) with differential scanning calorimetry (DSC) was performed with a *Netzsch STA 449 F3 Jupiter®R* thermal analyser. The tests were conducted with the samples in closed aluminium crucibles in a nitrogen atmosphere at a heating rate of 10 K per minute from 30 – 600°C.

**Infrared spectroscopy** Attenuated total reflection Fourier-transform infrared (ATR- FTIR) spectra were measured with a *Shimadzu IRAFFINITY-1S* spectrometer. The samples were directly placed on a diamond crystal for the measurement.

### 3.2.4 Materials

The ionic liquids used for this work were all commercially available and purchased from the *Iolitec GmbH*. The ionic liquids had a purity specified by the supplier of >98 %, if not differently stated. Generally, the ILs were used as purchased without any in-house purification. If a further purification step was needed, it is stated in the relevant text passage.

For the hydrogen peroxide, two different suppliers were used. The majority of the drop tests and all injection tests were conducted with *Propulse 980* by *Evonik*. It was stored at ambient conditions for one year and, since then, at  $5^\circ\text{C}$  in a refrigerator. Before and during the test campaigns, the hydrogen peroxide concentration was determined by measuring the density and referring this measurement to available literature data [85, 88]. The actual hydrogen peroxide concentration is stated in the passages. The drop test investigation in 5.2.3 and 5.2.4 on the initial temperature, concentration, storage, and cation structure were performed using highly concentrated hydrogen peroxide supplied by *Jakusz Space Tech*. The  $\text{H}_2\text{O}_2$  has a nominal concentration of 98 % and is conform with the specification MIL-PRF-16005F on hydrogen peroxide as a propellant [181]. The hydrogen peroxide was stored at  $5^\circ\text{C}$ . For tests at reduced  $\text{H}_2\text{O}_2$  concentration, the highly concentrated hydrogen peroxide was diluted with a certain amount of deionized water and the resulting concentration was determined.

Two commercially available additives were tested to reduce the ignition delay time. Copper(I)thiocyanate and cobalt(II)thiocyanate were purchased by *Alfa Aesar* with a purity of >96 % and 98 %, respectively.





## 4 Definition and screening

This chapter describes the screening process for the identification of hypergolic fuel candidates. In the first step, the group of substances of interest is selected. Then, requirements for the candidate fuels are defined. These requirements are prerequisites for the selection of an ionic liquid as a fuel. In the next step, a data set with the most important physical and chemical properties is generated by a literature study. This is the basis for the evaluation of the different fuel candidates. Further, the theoretical performance of the fuel candidate with hydrogen peroxide as oxidizer is calculated using NASA's Chemical Equilibrium and Applications code [24]. Finally, the different aspects are evaluated, and suitable substances are selected for further examination.

### 4.1 Detailed objective

The project aims to develop a green hypergolic alternative to conventional propellants for typical orbital propulsion applications. From this objective, certain top-level requirements can be derived:

- hypergolic
- green
- liquid
- storable

**Hypergolicity** The novel propellant combination should be hypergolic. Hypergolic ignition is preferred for space propellants because it supersedes ignition systems and allows reliable and repeatable ignitions in a thruster. Hypergolic propellant combinations have been proven in space since the 1960s and are still used on many satellites and other spacecraft. An alternative hypergolic propellant would be able to replace established propellants. Hypergolic ignition is crucial for transitioning from the conventional toxic propellant to new alternatives.

**Green** There is no universal definition of 'green' or green substances. There is the term 'green chemistry'. An important field of these developments is devoted to the design of new, more environmentally friendly solvents [124, 182]. These substances should be non-toxic, biodegradable and synthesized by an environmentally friendly procedure [124, 183]. The substances of conventional hypergolic propellants are highly toxic and carcinogenic (in the case of the fuels) and endanger personnel who handles them. In general, in the space domain, a 'green' propellant is seen as a less toxic substance than NTO, hydrazine and its derivatives.

**Liquid** Liquid propellants can offer high performance and densities. Also, they are transferable from tank to thruster by applying a pressure difference. Precise, reliable, and repeatable firings of thrusters are feasible. Further, liquid propellants have high energy densities.

**Storable** For space missions, where there are no refuelling stations (yet), the propellant required for the manoeuvres over the entire mission duration must be on board the spacecraft from the beginning. Therefore, the propellants must be storable over the whole mission duration as long as propulsion is needed. Hence, suitable propellants that are stable during the period of use in the space environment are needed. The storage period strongly depends on the mission. It can typically last from several months up to 15 years.

As for the mentioned objectives, additional boundary conditions were set for this work regarding the choice of fuel and oxidizer. The oxidizer relevant for this thesis is highly concentrated hydrogen peroxide. The development focuses on suitable hypergolic fuels from the group of ionic liquids. ILs are very versatile substances which have a low or negligible vapour pressure at ambient temperature in common. Therefore, the handling is facilitated compared to conventional hypergolic propellants. Further, in the frame of green chemistry, ionic liquids are regarded as a suitable alternative to conventional problematic substances because of the following properties: non-volatility (reduced air pollution), non-flammability (process safety) and excellent stability (recycling and reusing potential) [124].

It was estimated from the known anions and cations that there are  $10^{18}$  possible room temperature ionic liquids [124, 184]. About  $10^3$  are described in the literature, and some hundreds are available commercially [185]. Because of the high numbers, a structured process is needed to find suitable fuel candidates. The first step is the definition of relevant criteria.

## 4.2 Definition of criteria

In the section above, some top-level requirements and boundary conditions were derived from the objective of the present work. In addition to these boundary conditions, which the new propellant must meet, a substance should fulfil other relevant criteria and requirements. The relevant criteria and requirements for this thesis for novel fuels include:

- physical properties
  - density
  - viscosity
- thermal properties
  - melting point
  - decomposition temperature
- performance potential
  - hypergolic behaviour
  - enthalpy of formation
  - specific impulse
  - eligibility for different operation modes (e.g. pulse mode, steady state, throttling)
- safety
  - vapour pressure
  - toxicity
  - environmental hazard
  - sensitivity to electronic discharge, impact, friction

- application-related properties
  - storability
  - material compatibility
  - operation
- costs
  - availability
  - procurement
  - handling
  - components

The presented criteria originate from different literature sources [54, 125, 186] as well as experience and exchange during the *High-Performance Propellant Development* or *New Green Propellant Propulsion Concepts for Space Transportation* Projects with ESA [6, 187]. Details on each requirement are presented below. It must be mentioned that this list has no claim to be complete but tries to give a first impression of essential points to be considered during the development of novel propellants. Moreover, it is impossible to consider all these criteria for the screening since some aspects or data are not known yet. Later in this section, a focus will be on essential criteria suitable for a first selection of novel fuel candidates.

## 4.3 Requirements

In this section the criteria for the requirements are explained. Following, suitable requirements are derived. Table 4.1 shows an overview of the relevant requirements, including desired and acceptable values. As a comparison, some data points of conventional propellants are given.

### 4.3.1 Physical and chemical properties

#### Density

The density is an essential property for propellants suitable for in-space operation. The reason is that the higher the density, the more energy is confined in a specific volume. For spacecraft where masses should always be as low as possible, propellants with higher densities can reduce tank sizes and mass. However, a high density alone is only beneficial if the performance of the propellant is high. Therefore, the density-specific performance should also be considered in evaluating fuel candidates. Conventional hypergolic fuels based on hydrazines have a density between 0.8 and 1 g/cm<sup>3</sup>. Novel fuels should have a density of more than 1 g/cm<sup>3</sup> to gain an advantage over conventional propellants. Many ionic liquids based on the imidazolium cation have a higher density than 1 g/cm<sup>3</sup>, which makes them a promising group of candidate substances in terms of density. A density similar to conventional propellants (0.8 g/cm<sup>3</sup>) would still be acceptable.

#### Viscosity

Another parameter with a high impact on pressure losses and the mixing of the components of the propellant is viscosity. For a hypergolic fuel, a low viscosity is desirable. A low viscosity can facilitate the mixing with the oxidizer. Also, the injection and spray of a low viscous fluid is beneficial to generate small drops, good mixing and allow a high combustion efficiency [125]. Due to the mentioned reasons, the viscosity of a fuel should be as low as possible. However, ionic liquids typically have higher viscosities than molecular fluids such as solvents or conventional fuels. Many ionic liquids have viscosities of more than 20 mPa s, whereas the hydrazine based

Table 4.1: Requirements with desired and acceptable ranges

requirement	desired	acceptable	comparison
<b>physical properties</b>			
density	$[g/cm^3]$ > 1	> 0.8	MMH: 0.875 ; N <sub>2</sub> H <sub>4</sub> : 1
viscosity	$[mPa s]$ < 1	< 250	N <sub>2</sub> H <sub>4</sub> : 0.9
<b>thermal properties</b>			
melting point	$[°C]$ < -40	0	MMH: -52, N <sub>2</sub> H <sub>4</sub> : 2, N <sub>2</sub> O <sub>4</sub> : -11
decomposition temperature	$[°C]$ > 140	> 100	
<b>performance potential</b>			
hypergolic behaviour	yes	with additive	
enthalpy of formation	$[kJ/mol]$ positive	<0	N <sub>2</sub> H <sub>4</sub> : 50, MMH 54
theoretic $I_{sp}$	$[s]$ >320	300	MMH- N <sub>2</sub> O <sub>4</sub> : 335
<b>safety</b>			
vapour pressure	neglectable	low	
toxicity	non-toxic	low-toxic	
environmental hazard	none	low impact	
sensitivity to ED, impact, friction	none	some	
<b>application related properties</b>			
storability	15 yr	1 yr	
material compatibility	no limitations	some limitations but PTFE, certain stainless steel possible	
different operation modes	Steady state, short minimum impulse bit	steady state, longer minimum impulse bit	
<b>costs</b>			
availability	commercially available	on-demand production	
procurement	worldwide	only from special supplier	
handling	simple	no SCAPE suit	
components	COTS	COTS with adaptation	

fuels have a viscosity of 0.6 – 0.9 mPa s at room temperature [188]. The composition of anion and cation influences the viscosity of ionic liquids. For imidazolium ionic liquids and a certain anion, the viscosity can be tuned by choosing the proper side chains of the imidazolium cations. For example, longer hydrocarbon side chains lead to higher viscosities [189]. This requirement aims to find ionic liquids with viscosities that are as low as possible.

### Thermal properties

Important parameters in terms of the thermal properties of ionic liquids for their potential use as fuel are melting point and decomposition temperature. Ionic liquids are defined as salts with a melting point below 100 °C. Still, for the application as a liquid propellant, the melting point of a suitable ionic liquid should be at least below room temperature. A melting point below 0 °C is better. The viscosity of the ionic liquid is highly dependent on the temperature. Therefore, it is beneficial for low viscosities to have a margin between the melting point and the temperatures typical during operation. Typically, propellants on a spacecraft are conditioned to ambient temperature. As a comparison, the melting point of the commonly used hydrazine is 2 °C, and its derivatives MMH and UDMH have a melting point of -52.4 °C and -58 °C, respectively [27]. Since ionic liquids have a neglectable vapour phase, the IL will likely decompose before ignition. Therefore, a high thermal stability of an ionic liquid may result in unfavourable ignition characteristics. Reference values for the thermal stability of conventional fuels are not comparable to the processes leading to ignition between ionic liquids and hydrogen peroxide. Therefore, the comparison is set aside at this stage. The fuel should be stable over a range of temperatures to ensure safe handling at ambient conditions. Stability up to 100 °C is acceptable, and stability better than 140°C is desired.

### 4.3.2 Performance potential

#### Enthalpy of formation

The enthalpy of formation  $\Delta_f H^0$  of a fuel is an important factor needed for the performance calculation of the propellant. High positive values are beneficial for better performance. On the other side, substances with high positive  $\Delta_f H^0$  can become sensitive [190]. The enthalpy of formation can be calculated using software tools [67] or it can be determined using bomb calorimetry [191]. Typical values for the conventional hydrazine based fuels range from 48 to 54 kJ/mol [24]. For the novel fuels, a positive enthalpy of formation is desired, but a small  $\Delta_f H^0$  value is still acceptable.

#### Hypergolic behaviour

The hypergolic behaviour is a key parameter for this investigation. However, only very few pure substances are known to be hypergolic with hydrogen peroxide. Therefore, it could be necessary to dissolve additives into the fuel. These solutions need to be stable for space storage conditions. Additives such as transition metal salts are proven to introduce a hypergolic behaviour to a non-hypergolic fuel [121]. It is beneficial if the salt additive and the ionic liquid share the same anion. Then, a high amount can be dissolved, and the solution is expected to be stable [50]. On the other hand, the addition of transition metal ions to introduce or improve the hypergolic behaviour will adversely affect the specific impulse. This is caused by the higher average molecular mass of the exhaust products, compare equation (2.9). Further, solid metal oxides might be formed in the plume, which can have a sandblast effect on surfaces such as solar panels or optical surfaces. Therefore, if additives are needed, an optimization between hypergolic behaviour and metallic content must be conducted.

### 4.3.3 Safety aspects

#### Toxicity

The toxicity is a critical property regarding an alternative green propellant. The term 'green' in this scope is derived from comparing alternative and conventional rocket propellants. According to the European Space Agency, a "green propellant can be defined as a propellant with reduced toxicity for the environment or the personnel that may come in contact with the propellant" [20].

Thus, green propellants for space applications should be less toxic than hydrazine based fuels and oxidizers based on dinitrogen tetroxide. The parameters related to the toxicity are: "First, the [alternative] propellant must not cause or induce carcinogenic effects on humans in contact with the propellant. In addition, the propellants shall have higher exposure limits than conventional propellants (typically one order of magnitude higher) and/or low toxic vapour pressures. Other parameters that must be considered are mutagenicity or harm to reproduction." [20].

Moreover, the elements contained in the ionic liquid should be considered. Elements which can form toxic reaction products should be avoided, if possible, to facilitate the testing effort. Such elements leading to toxic reaction or decomposition products are, e.g., fluorine or boron [192].

#### Vapour pressure

The vapour pressure of ionic liquids is neglectable at ambient conditions [56]. This is a significant advantage over commonly used propellants. No hazardous or flammable vapours are generated in case of a spill or a leakage. Conventional propellants have high vapour pressures [14], leading to atmosphere contamination after releasing these substances. Therefore, SCAPE suits are needed for the handling of conventional propellants. In contrast, ILs can be handled easily without the need for a SCAPE suit or respirator. This also makes ionic liquids interesting to substitute toxic or flammable solvents in other industrial processes.

#### Environmental hazard

The environmental hazard of ionic liquids cannot be evaluated simultaneously for all substances. It needs to be assessed specifically for each single substance. For example, initial investigations on the effects of the ecotoxicity towards *Vibrio fischeri* show some groups of ionic liquids are harmless; others can be slightly or moderately toxic [193]. Hydrazine is hazardous to the aquatic environment, acute and chronic, with category 1 (H400 and H410) [9].

#### Sensitivity to electronic discharge, impact, friction

Substances should be insensitive to electronic discharge, impact, and friction for safe and simple handling. A general statement on the class of ionic liquids cannot be made, and the behaviour of the specific IL needs to be evaluated. Certain ILs are energetic and therefore referred to as energetic ionic liquids (EIL). An example is ammonium dinitramide (ADN), the energetic component in LMP103s. The EILs can be sensitive to external factors such as electronic discharge, impact, and friction [141].

### 4.3.4 Application related properties

#### Storability

The novel fuel should be storable for extended periods. In the best case, the storage should be possible in the order of ten years at space conditions. Additionally, a shelf life of several years at ambient conditions on the ground should be possible. The fuel should also be stable, and changes

in its composition should be minor or non-existent. This is especially of concern if additives are dissolved in the fuel. Stratification or re-crystallization of the additive should be avoided. The propellant should be stable over a broad temperature range. Conventional propellants have demonstrated storability over decades in many missions. An outstanding example of the reliability of hydrazine technology is the successful thruster firing of the Voyager 1 spacecraft in 2017, 40 years after its launch. The thruster had been dormant for 37 years and operated as expected [194].

### Material compatibility

The novel fuels should have good material compatibility with typical aerospace construction materials. Ideally, the fuel available or commercial off-the-shelf (COTS) materials and components can be used. This simplifies the introduction and adaptation of a novel fuel into the application. The available COTS components and materials are designed for use with hydrazine based propellants. Therefore, these components are compatible with hydrazines or NTO. For green propellants based on hydrogen peroxide, particular care must be given to the material selection. A material that is not suitable can accelerate the self-decomposition of hydrogen peroxide and lead to catastrophic failures. Compatibility with aerospace construction materials has not been assessed yet for many ionic liquids. After identifying promising fuel candidates, a screening must be performed to identify compatible materials.

### Operation

The novel propellant with the ionic liquid as fuel and the associated propulsion hardware should perform similarly to the conventional hypergolic propulsion solutions. This applies not only to the  $I_{sp}$  values but also to operation modes such as repeatable short pulses and efficient steady-state combustion. The actual performance requirements depend on the operational regimes of the spacecraft demanded by the mission.

#### 4.3.5 Cost

A new propulsion technology's overall life cycle costs need to be addressed. These costs cannot be evaluated at this stage since the fuel is unknown. However, a novel green propellant offers general advantages, leading to lower costs for a propulsion solution over its life cycle. Some considerations associated with green propellants are given below.

### Availability and procurement

A factor regarding the life cycle costs is the price of the fuel substance. The class of ionic liquids is not widely spread over a broad range of applications (yet). Therefore, many ionic liquids are produced in lab-scale amounts and only on demand. Therefore, the prices are quite high per kilogram. Especially if only a small amount is bought for initial testing of different substances. The price for the initial samples of ionic liquid bought for this thesis was in the range of €500 to €2000 per kg for the procurement of samples in the 100 g order. The base substances are available in large quantities. The price of larger batches is expected to scale down. The prices of the base chemicals and the solvents needed during the synthesis are low, e.g., imidazolium, solvents like ethanol, acetone, or fluids needed during the synthesis steps, such as HCl. Moreover, the procedure for the production is not very extensive in most cases. Fuel procurement is only a small amount of the total life cycle cost.

Some providers in Europe can already supply ionic liquids on scales up to several hundred kg. But only hundreds of IL are currently commercially available.



### Handling

The handling of ionic liquid fuels does not require a SCAPE suit. Therefore, a large cost-saving potential during fuel production, storage, transportation, and handling is expected. Furthermore, the operation can be conducted more time efficiently, for example, during the satellite integration and fuelling, leading to further cost reductions.

Due to the reduced hazardous potential of a hypergolic propellant in combination with hydrogen peroxide and ionic liquid fuels, development, testing, and qualification costs can be reduced. This can result in lower costs for the whole propulsion solution compared to a conventional solution.

### Components

The use of COTS components simplifies the introduction of a novel solution. As mentioned above, the novel propellant with hydrogen peroxide and the ionic liquid fuel needs to be assessed regarding material compatibility.

#### 4.3.6 Others

Other requirements with minor importance for the initial screening step are presented here. It can be beneficial for ionic liquids if they are mixable with water. If a substance is mixable with water, it is likely also mixable with hydrogen peroxide [85]. Further, it is beneficial to facilitate handling and storage requirements if the ionic liquid is not sensitive to moisture or water.

#### 4.3.7 Relevant for the screening

For the following screening, certain requirements for fuel candidates are selected to narrow the choice of suitable fuels based on ionic liquids down. The selected requirements include physical and thermodynamic properties. These factors are important to evaluate the applicability of a substance as a liquid fuel. In detail, the regarded properties in this stage are:

- density
- viscosity
- thermal properties
- enthalpy of formation
- potential hypergolic behaviour

### 4.4 Data set

Suitable ionic liquids must be identified from the requirements described in 4.3. As a starting point for the identification of candidates, it was decided to focus on commercially available ionic liquids. The advantage is that the needed data for evaluating many of these ionic liquids is already available in the literature. Further, the ionic liquids can be purchased in small quantities, and initial drop tests can be conducted. So, the evaluation of hypergolic behaviour can be conducted easily and quickly. The alternative would be to design and synthesise ionic liquids, with an additional effort for quality assurance. The most important physical and chemical properties would have to be determined in-house, which is very time-consuming and can be prevented by accessing public data and commercial products. For the longer term, it is possible to synthesise novel ionic liquids after a group of promising fuel candidates is identified. The properties of these

second-generation fuels can be tuned for a better performance. But in this first step, the focus is on commercially accessible ionic liquids.

The company *Iolitec GmbH* offers more than 300 ionic liquids in their product repertoire. Essential properties such as melting point, density, and viscosity are listed in the catalogue for many of their products. Therefore, this catalogue was the initial screening source for finding suitable ionic liquids. The flowchart of the selection process is shown in figure 4.1. In the first step, the selection was focused on imidazolium-based ionic liquids. McCrary et al. showed that imidazolium-based ionic liquids have better or equal ignition properties than other rings of the cations [195]. Besides, the imidazolium-based ionic liquids are widely described in the literature, and a lot of data can be found. The commitment to imidazolium-based ionic liquids reduced the number of suitable candidate substances to 191.

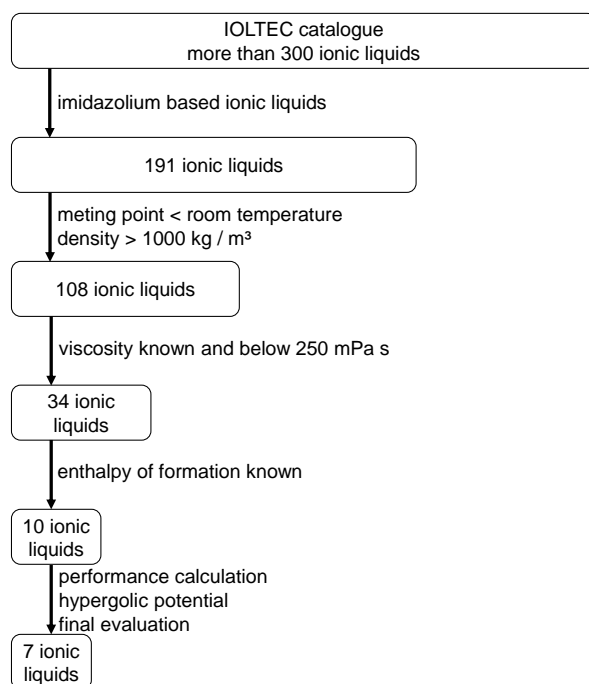


Figure 4.1: Flowchart of the screening of ionic liquids

In the next step, the melting point and density requirement was applied. The ionic liquids must have a melting point below room temperature and a density of more than  $1 \text{ g/cm}^3$ . This reduced the number of candidates to 108. At this stage, ionic liquids with the following anions were in the selection:

bis(trifluoromethylsulfonyl)imides, bis(pentafluoroethylsulfonyl)imides, triflates, tetrafluoroborates, perfluorobutanesulfonates, 1,1,2,2-tetra-fluoroethanesulfonates, chlorides, bromides, iodides, sulfates, dimethyl/ethyl/butyl phosphates, thiocyanates, dicyanamides, acetates, tricyanomethanides, tetrachloroferrates, hexafluorophosphates, tetrathiocyanocobaltates.

Following, a criterion on the viscosity was applied. The viscosity for the use of fuel should be as low as possible. The cut-off value of viscosity was defined at around  $250 \text{ mPa s}$ , and 34 ionic liquids remained.

To calculate a fuel's performance, the formation's enthalpy must be known. The literature was intensively screened for enthalpy of formation values for the remaining set of ionic liquids. The relevant data set for the ionic liquids is presented in the table 4.2. This table shows that the values of the properties come from many sources. Moreover, a variation of single reported values is possible. For example, the viscosity of  $[\text{BMIm}][\text{Ac}]$  varies between  $208$  and  $485 \text{ mPa s}$  at a

temperature of 25°C. This is a variation of the factor of more than two.

After the performance calculation, which is presented in the next section, and an evaluation, seven ionic liquids for initial testing were chosen.

## 4.5 Performance calculation

The performance calculation was conducted with the dataset from table 4.2 and executed with the Chemical Equilibrium and Applications code by Gordon and McBride [24]. As mentioned in 3.1.1 the reference was the 400 N bipropellant apogee motor of ArianeGroup using the conventional propellant monomethyl hydrazine and dinitrogen tetroxide. The calculation assumed frozen supersonic expansion.

Figure 4.2 shows the vacuum  $I_{sp}$  values over the different ROF for the imidazolium ionic liquid fuels and 98 % hydrogen peroxide. Further, the conventional hypergolic propellant MMH/NTO is also shown as reference, see grey dashed line.

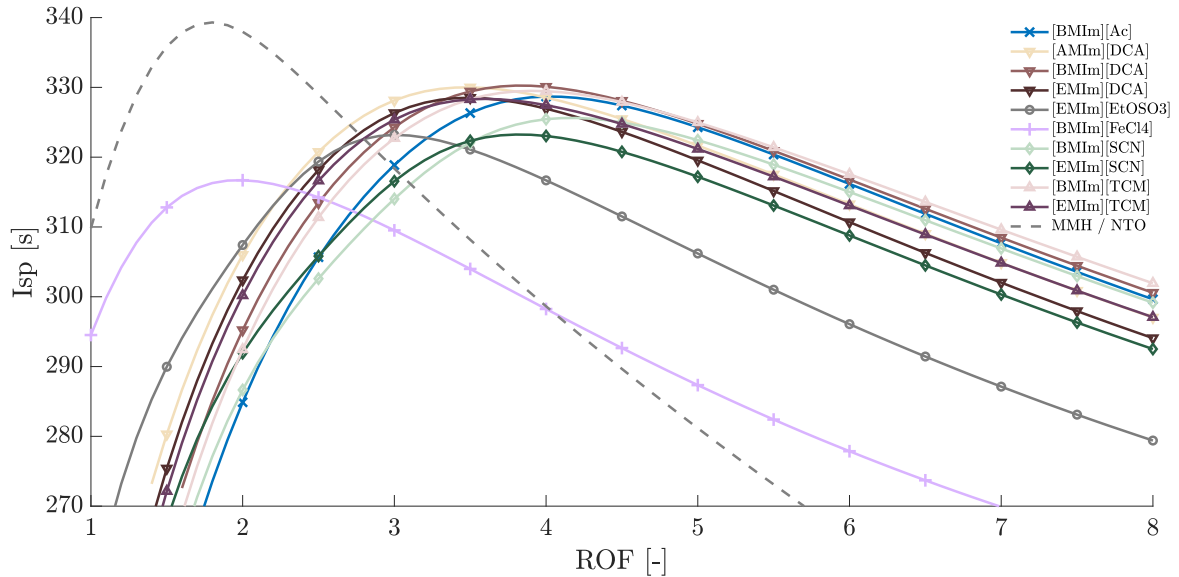


Figure 4.2: Screening vacuum  $I_{sp}$  over ROF at chamber pressure 10.35 bar, frozen supersonic expansion,  $\epsilon=330$ , 98 %  $H_2O_2$

It stands out in figure 4.2 that all ionic liquids with the  $[Ac]^-$ ,  $[DCA]^-$ ,  $[TCM]^-$  and  $[SCN]^-$  have a very similar characteristic in terms of the  $I_{sp}$  dependence on the ROF. For the ionic liquids with the mentioned anions, the maximum  $I_{sp}$  is around 330 s, and the corresponding ROF varies between 3.4 and 4.1.  $[EMIm][EtOSO_3]$  and  $[BMIm][FeCl_4]$  show a slightly lower maximum  $I_{sp}$  at a lower ROF. The conventional propellant has the highest  $I_{sp}$  with 339 s at an ROF of 1.8. Table 4.3 shows the different values at the maximum  $I_{sp}$  of the screened ionic liquids and the conventional reference propellant. As mentioned above, almost all ionic liquids have a maximum  $I_{sp, vac}$  of around  $325 \text{ s} \pm 5 \text{ s}$ . The maximum difference between  $[EMIm][SCN]$  and  $[BMIm][DCA]$  is 2.2 %. The exhaust products of the ionic liquids also have almost the same average molecular mass between 22.3 g/mol and 23.2 g/mol. The adiabatic flame temperature is also very similar between 2803 °C and 2883 °C. This results in comparable  $c^*$  values of around 1600 m/s. An exception is  $[BMIm][FeCl_4]$  with a maximum  $I_{sp, vac}$  of 316.7 s. This ionic liquid contains heavy iron, which results in a relatively high average molecular mass of the exhaust products

Table 4.2: Data set of different commercially available ionic liquids

Cation	Anion	Short name	Molecular formula	Density [g/cm <sup>3</sup> ]	Meting point [°C]	Viscosity [mPa s]	Enthalpy of formation [kJ/mol]
1-Butyl-3-methylimidazolium	acetate	[BMIm][Ac]	C <sub>10</sub> H <sub>18</sub> N <sub>2</sub> O <sub>2</sub>	1.05 <sup>a</sup>	-7 <sup>b</sup>	393.3 <sup>a</sup> ; 485 <sup>b</sup> ; 208 <sup>c</sup>	-452 <sup>d</sup>
1-Allyl-3-methylimidazolium	dicyanamide	[AMIm][DCA]	C <sub>9</sub> H <sub>11</sub> N <sub>5</sub>	1.12 <sup>e</sup>	< -80 <sup>e</sup>	20.5 <sup>e</sup>	382 <sup>e</sup>
1-Butyl-3-methylimidazolium	dicyanamide	[BMIm][DCA]	C <sub>10</sub> H <sub>15</sub> N <sub>5</sub>	1.06 <sup>e</sup>	-6 <sup>e</sup>	29.3 <sup>e</sup>	244 <sup>e</sup> ; 206.2 <sup>f</sup>
1-Ethyl-3-methylimidazolium	dicyanamide	[EMIm][DCA]	C <sub>8</sub> H <sub>11</sub> N <sub>5</sub>	1.1 <sup>e</sup>	-18 <sup>e</sup>	15.2 <sup>e</sup>	274 <sup>e</sup> ; 235.3 <sup>f</sup>
1-Ethyl-3-methylimidazolium	ethyl sulfate	[EMIm][EtOSO <sub>3</sub> ]	C <sub>9</sub> H <sub>18</sub> N <sub>2</sub> O <sub>4</sub> S	1.23 <sup>g</sup>	< -140 <sup>h</sup>	97.6 <sup>g</sup>	-579.13 <sup>i</sup>
1-Butyl-3-methylimidazolium	tetrachloroferrate	[BMIM][FeCl <sub>4</sub> ]	C <sub>8</sub> H <sub>15</sub> N <sub>2</sub> FeCl <sub>4</sub>	1.37 <sup>i</sup>	< RT <sup>c</sup>	41.0 <sup>i</sup>	-190 <sup>d</sup>
1-Butyl-3-methylimidazolium	thiocyanate	[BMIm][SCN]	C <sub>9</sub> H <sub>15</sub> N <sub>3</sub> S	1.0 <sup>c</sup>	-29 <sup>k</sup>	35.8 <sup>c</sup>	-5 <sup>d</sup>
1-Ethyl-3-methylimidazolium	thiocyanate	[EMIm][SCN]	C <sub>7</sub> H <sub>11</sub> N <sub>3</sub> S	1.12 <sup>l</sup>	-6 <sup>m</sup>	24 <sup>l</sup>	52.8 <sup>n</sup>
1-Butyl-3-methylimidazolium	tricyanomethanide	[BMIm][TCM]	C <sub>12</sub> H <sub>15</sub> N <sub>5</sub>	1.06 <sup>o</sup>	< RT <sup>c</sup>	31.8 <sup>n</sup>	279.2 <sup>f</sup>
1-Ethyl-3-methylimidazolium	tricyanomethanide	[EMIm][TCM]	C <sub>10</sub> H <sub>11</sub> N <sub>5</sub>	1.08 <sup>p</sup>	-11 <sup>q</sup>	14 <sup>p</sup>	342 <sup>f</sup>

<sup>a</sup> Bogolitsyn et al. [196] <sup>b</sup> Fendt et al. [197] <sup>c</sup> Iolitec catalogue [185] <sup>d</sup> Kabo et al. [198] <sup>e</sup> Sun et al. [189]  
<sup>f</sup> Emelyanenko et al. [199] <sup>g</sup> Gonzalez et al. [200] <sup>h</sup> Fernandez et al. [201] <sup>i</sup> Zhang et al. [202] <sup>j</sup> Cruz et al. [203]  
<sup>k</sup> Gruzdev et al. [204] <sup>l</sup> Vataščin et al. [205] <sup>m</sup> Prigle et al. [176] <sup>n</sup> Zaitsau et al. [191] <sup>o</sup> Carvalho et al. [206]  
<sup>p</sup> Vataščin et al. [207] <sup>q</sup> Yoshida et al. [208]

at 25.5 g/mol. This has a negative impact on the  $I_{sp}$ , although the combustion temperature is more than 100 K higher than the other ILs. The density-specific impulse of the ionic liquids is also very similar between 436 and 446 s g cm<sup>-3</sup>. Interestingly, [BMIm][FeCl<sub>4</sub>] has the highest density-specific impulse due to the higher density of the fuel.

The high similarity of the different ionic liquids in the theoretical performance calculation results from the similar composition of the various substances. The main components are carbon, hydrogen and nitrogen, which are present in the imidazolium cations. There are minor differences in the composition of the anions, where, for example, additional sulphur, iron, chlorine, or oxygen atoms are. As a result, the exhaust products all have a similar average molecular mass, except for the iron-containing IL. Moreover, the composition influences the adiabatic flame temperature. If ionic liquids with the same anion are compared regarding the different cations [AMIm]<sup>+</sup>, [BMIm]<sup>+</sup> and [EMIm]<sup>+</sup>, [BMIm]<sup>+</sup> offers the highest performance. [AMIm][DCA] has a similar performance in terms of  $I_{sp}$  as [BMIm][DCA]. In contrast to [BMIM]<sup>+</sup>, the [EMIm]<sup>+</sup> or [AMIm]<sup>+</sup> cations have a higher enthalpy of formation and combustion temperature. However, due to the additional carbon and hydrogen in the cation's butyl side chain, the exhaust products' average molecular mass is slightly lower, having an overall positive impact on the  $I_{sp}$ . However, this impact is in the order of 1 -2 s. Taking the fuel density into account, the values of the density  $I_{sp}$  between [EMIm]<sup>+</sup> and [BMIM]<sup>+</sup> are almost identical. The higher density of the IL with [EMIm]<sup>+</sup> cation compensates for the difference in the  $I_{sp}$ . For the [DCA]<sup>-</sup> ILs, [AMIM][DCA] offers the highest density-specific impulse due to a high performance and higher density. The  $I_{sp}$  is expected to slightly increase for longer side chains due to a lower average molecular mass of the exhaust products. On the other hand, the longer side chains also influence other parameters and properties, which, in total, may lead to a reduction in the performance of the propellant. From the performance perspective in terms of  $I_{sp}$ , the difference between cations with varying carbon side chains is minor. Therefore, the focus of the selection can be set on other aspects important to achieve good performance, such as short ignition delay and low viscosity.

All ionic liquids have a lower adiabatic flame temperature compared to the conventional propellant. The calculated  $I_{sp, vac}$  of MMH / NTO is 3 - 7 % higher than the ionic liquids with hydrogen peroxide as oxidizer. On the other hand, the maximum density specific impulse is 9 - 11 % higher in the case of ionic liquid fuels. A difference is also in the ROF of the maximum  $I_{sp}$ . The conventional propellant has its maximum at a ROF of 1.8, whereas the ionic liquids have their optimum at higher values than 2 and the majority between 3.5 and 4. As mentioned earlier, the nominal ROF of the MMH/NTO ArianeGroup thruster is 1.65. The thruster is not operated at the condition with the maximum  $I_{sp}$  because, at the ROF 1.65, the volume flow rates of the propellant components are similar. This means the same volume for both components is combusted at the nominal conditions. Thus, identical tank sizes can be used, facilitating production and reducing costs if only one tank size is needed.

Table 4.3: Results of screening with different IL and 98 % hydrogen peroxide as oxidizer

ionic liquid	max $I_{sp \text{ vac}}^a$ [s]	ROF [-]	T <sup>b</sup> [°C]	$\rho I_{sp \text{ vac}}^a$ [s g/cm <sup>3</sup> ]	$\bar{M}^c$ [g/mol]	c* <sup>d</sup> [m/s]
[BMIm][Ac]	328.7	4.0	2803.4	438.3	22.3	1620.8
[AMIm][DCA]	330.0	3.4	2889.9	444.0	22.5	1637.2
[BMIm][DCA]	330.3	3.8	2856.8	440.2	22.3	1635.3
[EMIm][DCA]	328.5	3.5	2862.8	440.4	22.6	1627.6
[EMIm][EtOSO <sub>3</sub> ]	323.2	3.0	2803.3	444.1	23.1	1592
[BMIm][FeCl <sub>4</sub> ]	316.7	2.0	2968.4	446.4	25.5	1563.1
[BMIm][SCN]	325.6	4.1	2827.3	436.8	22.9	1607
[EMIm][SCN]	323.2	3.8	2830.8	437.0	23.2	1595.6
[BMIm][TCM]	329.5	3.9	2869.9	439.9	22.6	1630.6
[EMIm][TCM]	328.3	3.6	2883.2	438.6	22.8	1626.3
MMH / NTO	339.3	1.8	3127.2	398.1	21.3	1740.4

<sup>a</sup>  $I_{sp}$  vacuum    <sup>b</sup> adiabatic flame temperature    <sup>c</sup> average molecular mass exhaust

<sup>d</sup> characteristic velocity

## 4.6 Evaluation and selection

The screening of the ionic liquids based on density, viscosity and liquid range are listed in table 4.2. The final selection is based on the theoretical performance and the potential of hypergolic behaviour with hydrogen peroxide.

### Performance

The above-presented calculations are the basis for selecting suitable ionic liquid fuel candidates, which are worth further evaluation in drop tests. From the performance standpoint, no considerable differences occurred in the screened ionic liquids. The ionic liquids with the dicyanamide, tricyanomethanide and acetate anion are the highest performing fuels in terms of  $I_{sp}$ . Closely behind are the thiocyanate and ethyl-sulfate ILs. The tetrachloroferrate IL has the lowest performance. Nevertheless, all these ionic liquids have a density-specific impulse, 9 - 11 % higher than conventional propellants. Therefore, from the performance criteria, all the ionic liquids are interesting to analyse their hypergolic behaviour further.

### Hypergolic potential

After the previous selection stages, the following ILs were assessed in terms of their hypergolic potential:

- Dicyanamide ionic liquids are known to be hypergolic with WFNA [128, 129, 189, 195]. Still, when the initial screening for this work was conducted, no information on the hypergolic behaviour with hydrogen peroxide as an oxidizer was available. Therefore, conducting a first drop test with a [DCA]<sup>-</sup> IL was of interest to investigate the hypergolic behaviour. For this first test, [EMIm][DCA] was chosen because it has the lowest viscosity and also a low IDT with WFNA[189].

- The tetrachloroferrate ionic liquid was used as an additive to introduce hypergolic behaviour into non-hypergolic substances by Schneider et al. [209]. No information on the behaviour of the pure IL and hydrogen peroxide was available. Therefore, as a potential hypergolic substance, [BMIm][FeCl<sub>4</sub>] was selected for further investigation.
- Block 0 was one of the first hypergolic fuels with hydrogen peroxide. As an additive, manganese acetate tetrahydrate is dissolved. This additive should also have a good solubility in the [BMIm][Ac] ionic liquid. On the other hand, [BMIm][Ac] has a relatively high viscosity. But despite this, and because of its ability to dissolve a proven hypergolic additive, [BMIm][Ac] was chosen for further investigation.
- On the thiocyanate and tricyanomethanide, no information on their hypergolic behaviour with hydrogen peroxide was available. However, these ionic liquids have a very low viscosity compared to most ILs. As mentioned earlier, a low viscosity is important for later application and can be advantageous for good spray and combustion performance. Therefore, these ILs were also considered for a first test on hypergolic ignition with hydrogen peroxide as the oxidizer.
- The 1-Ethyl-3-methylimidazolium ethyl sulfate has a higher viscosity than the [DCA], [TCM], [FeCl<sub>4</sub>] and [SCN] ionic liquids. A similar ionic liquid with the methyl sulfate anion has a viscosity of less than half the value of ethyl sulfate IL. The 1-Ethyl-3-methylimidazolium methyl sulfate is also commercially available, but no value of the enthalpy of formation has been found or published. However, the performance is anticipated to be close to the performance of the calculated ethyl sulfate ionic liquid. Besides, a lower viscosity is expected to contribute to a shorter hypergolic ignition. Therefore, for the experimental evaluation of hypergolicity 1-Ethyl-3-methylimidazolium methyl sulfate was chosen.

After the evaluation, the following ionic liquids were selected for testing on hypergolicity in the drop test with hydrogen peroxide:

- 1-Ethyl-3-methylimidazolium methyl sulfate [EMIm][MeOSO<sub>3</sub>]
- 1-Ethyl-3-methylimidazolium dicyanamide [EMIm][DCA]
- 1-Ethyl-3-methylimidazolium thiocyanate [EMIm][SCN]
- 1-Butyl-3-methylimidazolium thiocyanate [BMIm][SCN]
- 1-Butyl-3-methylimidazolium tetrachloroferrate [BMIm][FeCl<sub>4</sub>]
- 1-Butyl-3-methylimidazolium tricyanomethanide [BMIm][TCM]
- 1-Butyl-3-methylimidazolium acetate [BMIm][Ac]

## 5 Drop test

This chapter is divided into two parts. Initial drop tests with different ionic liquids are described in the first part. Furthermore, additives were introduced to study their influence on hypergolic ignition. These initial tests were conducted with the simple drop test setup (see section 3.2.1). The second part investigates the most promising fuels with the thiocyanate anion in the drop test chamber (see section 3.2.1). Here, a study of the effect of different parameters and their influence on the IDT in drop tests is also presented and discussed.

### 5.1 Part 1: initial testing

This part describes the initial drop tests performed. The first drop tests were conducted with the simple drop test described in 3.2.

#### 5.1.1 Neat ionic liquids

As described in chapter 4, many ionic liquids were screened, and seven were selected to be tested on hypergolic behaviour with hydrogen peroxide. For the initial tests, the hydrogen peroxide had a concentration of 95 %. The pure ionic liquids that were investigated are listed in table 5.1.

Table 5.1: Initial test with different ionic liquid fuel candidates and 95 % hydrogen peroxide

substance	result
[EMIm][MeOSO3]	no reaction visible
[BMIm][Ac]	no reaction visible
[EMIm][DCA]	no reaction visible
[BMIm][TCM]	late ignition after 10 s
[BMIm][FeCl <sub>4</sub> ]	late ignition after 8.2 s
[BMIm][SCN]	fast ignition 52.5 ms
[EMIm][SCN]	fast ignition 31 ms

Neat [EMIm][MeOSO<sub>3</sub>], [BMIm][Ac] and [EMIm][DCA] didn't show an obvious reaction with hydrogen peroxide. As an example, in Figure 5.1, a pool of [BMIm][Ac] is shown containing a drop of hydrogen peroxide 250 ms after initial contact. The drop of H<sub>2</sub>O<sub>2</sub> is submerged and clearly distinguishable. This indicates that the ionic liquid does not mix with hydrogen peroxide, and no fast reactions occur between the two components. This specific ionic liquid is also known for being not mixable with water. The ionic liquid with the methylsulfate anion behaves similarly.

[BMIm][FeCl<sub>4</sub>] and [BMIm][TCM] showed an interaction with hydrogen peroxide, but it needed several seconds until the signs of the reaction became visible. In the case of the [BMIm][FeCl<sub>4</sub>], an ignition occurred 8.2 s after initial contact. [BMIm][TCM] ignited after 10 s. These two substances are not suited purely as a hypergolic fuel due to the long ignition delay. Surprisingly, [EMIm][SCN] and [BMIm][SCN] ignited fast after contact with highly concentrated hydrogen peroxide. Figure 5.2 shows an example drop test where different snapshots from the high-speed recording are displayed. One millilitre of [BMIM][SCN] is at the flask's bottom. The first picture



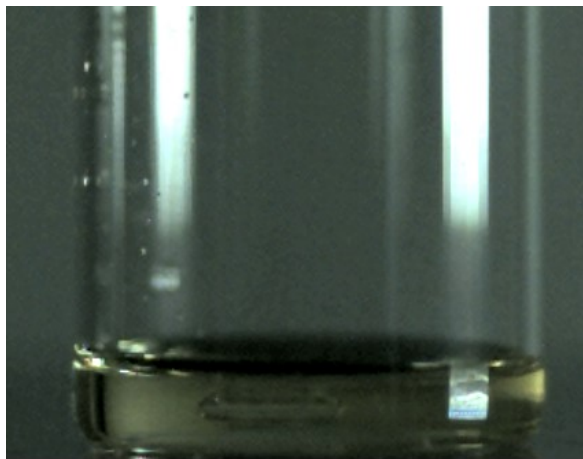


Figure 5.1: [BMIm][Ac] with a submerged drop of  $\text{H}_2\text{O}_2$ , no reaction visible after 250 ms

shows the falling  $\text{H}_2\text{O}_2$  drop 15 ms prior to initial contact of fuel and oxidiser. In the second picture, figure 5.2 b), the initial contact of fuel and oxidiser occurs. This moment is defined as 0 ms. After contact, fuel and oxidiser mix and initial reactions in the liquid phase between [BMIm][SCN] and  $\text{H}_2\text{O}_2$  begin to heat the mixture. After a certain time, the temperature is high enough that the surface of the mixture breaks up, and vapour is released. The released vapour can be seen in c). Shortly after vapour is generated, the ignition occurs in the vapour phase, and the flame propagates fast, see d) and e). The combustion almost vanishes 50 ms after the ignition, as shown in f). In this test, the ignition delay time is 56.5 ms, and the time until the vapour is generated is 51.5 ms.

The average ignition delay times in these initial tests of [EMIm][SCN] and [BMIm][SCN] were, on average, 31 ms and 52.5 ms, respectively. The difference in the ignition delay time of the two thiocyanate ionic liquids may be related to the different structures of the cation. Several investigations with ionic liquids hypergolic with WFNA have shown that the [EMIm] cation has a shorter ignition delay time than [BMIm] cation [189, 195]. For hydrogen peroxide, this may also be the case. The ignition delay time below 50 ms could be sufficient for hypergolic ignition of a rocket engine. However, a hard start induced by the accumulation of propellant can occur with a higher probability of long ignition delays.

As far as the author is aware, these were the first tests with thiocyanate ionic liquids on hypergolic behaviour with hydrogen peroxide. Therefore, the results with such a good ignitability were unexpected and surprising. Because of the encouraging results, it was decided to investigate the thiocyanate ionic liquids in more detail. In the further course of this thesis, the focus lies on thiocyanate based fuels. Strategies to reduce the ignition delay time and various factors influencing the ignition delay will be examined. Besides, a patent application about using thiocyanate based hypergolic fuels in rocket engines was filed [210].

### 5.1.2 Reduction of the IDT

The thiocyanate ionic liquids turned out to be hypergolic with highly concentrated hydrogen peroxide, and therefore, they are very promising fuel candidates. As a next step, efforts were made to reduce the ignition delay time by dissolving an additive into the ionic liquid. This investigation aimed to assess the impact of the additive on the ignition delay time. Ideally, ignition delays of around 10 ms or less should be reached. As comparison the conventional combination of MMH/NTO has an IDT of 1 ms in drop tests [129]. Hypergolic combinations with IDTs in this order are also expected to provide smooth ignitions in a rocket engine. Two transition metal salts with the thiocyanate anion were chosen: copper(I)thiocyanate ([Cu][SCN])

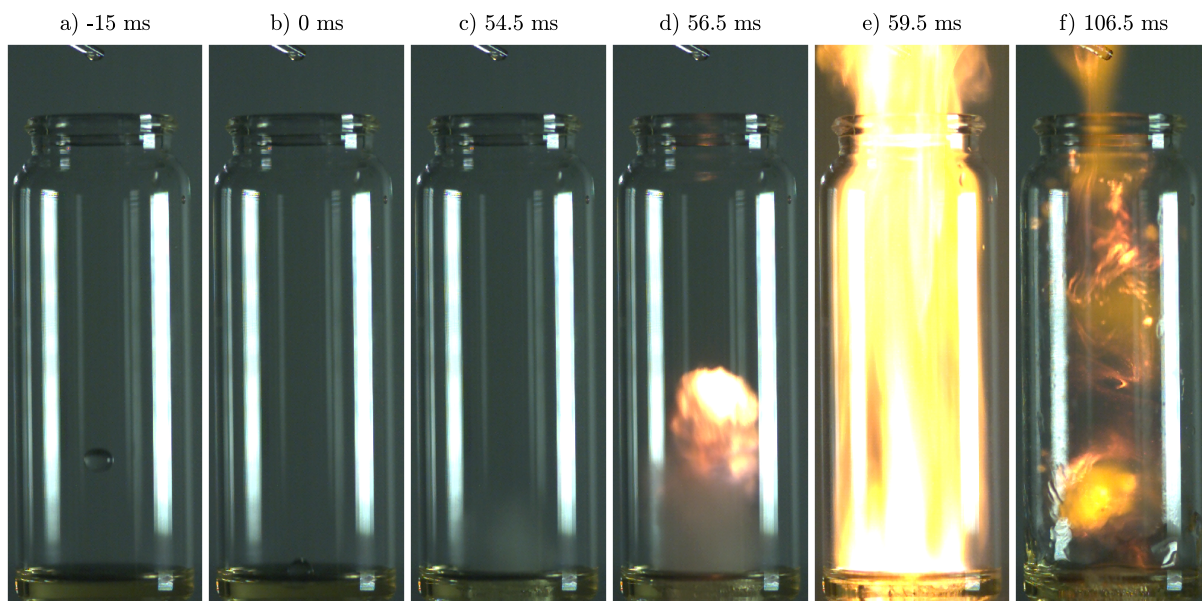


Figure 5.2: Drop test of [BMIM][SCN] and  $\text{H}_2\text{O}_2$

and cobalt(II)thiocyanate ( $[\text{Co}][\text{SCN}]_2$ ).  $[\text{Cu}]^{1+}$  and  $[\text{Co}]^{2+}$  are described as suitable catalytically active ions for the decomposition of hydrogen peroxide [121]. Furthermore, if the ionic liquid and a solid salt share the same anion, the solid salt has a good solubility in the ionic liquid [50]. Both transition metal salts were commercially available. In addition, mixtures of the thiocyanate ILs with  $[\text{BMIm}][\text{FeCl}_4]$  were also investigated because the tetrachloroferrate IL is also described as a catalytic additive to reduce the ignition delay time [209].

### Cobalt(II)thiocyanate $[\text{Co}][\text{SCN}]_2$

Cobalt(II)thiocyanate was investigated as an additive. The corresponding mixtures were produced by weighing the components with a lab scale and stirring them for two hours to dissolve the solid salt in  $[\text{BMIm}][\text{SCN}]$  and  $[\text{EMIm}][\text{SCN}]$ . The amount of additive and their ignition delay time, time to vapour generation and corresponding standard deviation are given in table 5.2. The drop tests were conducted with hydrogen peroxide of a concentration of 96.5 %. Three different mixtures with  $[\text{EMIm}][\text{SCN}]$  were investigated. The ignition delay time is much longer than in the previously described tests. The highest additive amount also has the highest ignition delay time. The IDT and TVG are similar for the 1 and 4 wt% solutions. Because of the negative influence, only one mixture with  $[\text{BMIm}][\text{SCN}]$  was tested. For the presented mixture, the ignition delay is also increased compared to the neat ionic liquid. Cobalt(II)thiocyanate does not improve the ignition delay time of thiocyanate ionic liquid. On the contrary, it tends to increase the ignition delay time for different concentrations. This additive is, therefore, not suited as an additive to accelerate the hypergolic ignition of the combination.

### 1-Butyl-3-methylimidazolium tetrachloroferrate $[\text{BMIm}][\text{FeCl}_4]$

Different amounts of the metal-containing ionic liquid  $[\text{BMIm}][\text{FeCl}_4]$  were mixed with  $[\text{EMIm}][\text{SCN}]$  and  $[\text{BMIm}][\text{SCN}]$ . The mixtures were produced by bringing the two components together and stirring. The mixture changed its colour rapidly to a dark red. Further, the resulting mixture had a much higher viscosity than the neat thiocyanate ionic liquid. The red colour indicates that

Table 5.2: Drop test results with different amounts of [Co][SCN]<sub>2</sub> as additive

IL	amount [wt%]	IDT <sup>a</sup> [ms]	SD <sub>IDT</sub> <sup>b</sup> [ms]	TVG <sup>c</sup> [ms]	SD <sub>TVG</sub> <sup>b</sup> [ms]	n <sup>d</sup> [-]
[EMIm][SCN]	1	45.0	3.9	40.6	4.4	4
[EMIm][SCN]	4	45.6	3.4	39.7	1.9	6
[EMIm][SCN]	10	61.8	5.4	56.7	5.2	3
[BMIm][SCN]	6.7	57.3	3.3	50	2.0	5

<sup>a</sup> ignition delay time    <sup>b</sup> standard deviation of n drop tests

<sup>c</sup> time to vapour generation    <sup>d</sup> number of drop tests

ferric thiocyanate has formed. The drop tests were performed with 96.5 % hydrogen peroxide. Table 5.3 lists the IDT, TVG, and corresponding standard deviations. For both ionic liquids, the additive reduces the ignition delay. But only to a certain amount. The ignition delay for [BMIm][SCN] / [BMIm][FeCl<sub>4</sub>] mixture varies on average only 1.2 ms by the addition of 4.8 to 30.3 wt% of additive. Interestingly, the TVG is the shortest with the highest additive content. In the case of [EMIm][SCN] / [BMIm][FeCl<sub>4</sub>] fuels, the average IDT and TVG are shorter for the higher additive values. But in both cases, the standard variations are quite high, which could result from the higher viscous fuels. Because of the high viscosity, the mixing of fuel and oxidiser depends more on how the falling drop interacts on the fuel's surface. It is not expected that the mixture of thiocyanate ILs and [BMIm][FeCl<sub>4</sub>] reach lower values than 18 ms.

Table 5.3: Drop test results with different amounts of [BMIm][FeCl<sub>4</sub>] as additive

IL	amount [wt%]	IDT <sup>a</sup> [ms]	SD <sub>IDT</sub> <sup>b</sup> [ms]	TVG <sup>c</sup> [ms]	SD <sub>TVG</sub> <sup>b</sup> [ms]	n <sup>d</sup> [-]
[BMIm][SCN]	4.8	19.9	0.4	17.8	0.4	5
[BMIm][SCN]	9.4	19.5	4.4	18.3	4.5	4
[BMIm][SCN]	30.3	18.7	3.7	15.9	2.7	5
[EMIm][SCN]	14.8	21.5	5.4	18.0	5.6	4
[EMIm][SCN]	34.2	18.5	3.3	13.5	4.5	3

<sup>a</sup> ignition delay time    <sup>b</sup> standard deviation of n drop tests

<sup>c</sup> time to vapour generation    <sup>d</sup> number of drop tests

### Copper(I)thiocyanate [Cu][SCN]

In this test series, copper(I)thiocyanate was added in different amounts to [EMIm][SCN]. Also, a mixture for comparison of the additive and [BMIm][SCN] was tested. The amounts of the ionic liquid and the solid salt were dosed by weighting and stirred for two hours until a homogeneous liquid resulted. Table 5.4 shows the resulting fuels and results of the drop tests. As before, tests were conducted with 96.5 % hydrogen peroxide in the basic configuration.

For the [EMIm][SCN] / [Cu][SCN] mixtures, the lowest IDT with 12.2 ms is at 6.3 wt% additive content. For the higher additive amounts, the IDT increases again. With the addition of 4.1 wt% of [Cu][SCN], the IDT is about half the value of the neat IL. The TVG shows the same behaviour as the IDT with the lowest value at 6.3 wt% additive content. The repeatability in this sequence

is good, with standard deviations of max 1.7 ms. The copper additive has also reduced the ignition delay of [BMIm][SCN]. The dissolved copper acts catalytically on the hydrogen peroxide decomposition. Thus, the overall IDT is shortened compared to the neat ILs.

Table 5.4: Drop test results with different amounts of [Cu][SCN] as additive

IL	amount [wt%]	IDT <sup>a</sup> [ms]	SD <sub>IDT</sub> <sup>b</sup> [ms]	TVG <sup>c</sup> [ms]	SD <sub>TVG</sub> <sup>b</sup> [ms]	n <sup>d</sup> [-]
[BMIm][SCN]	6.1	18.0	1.2	16.0	1.0	6
[EMIm][SCN]	1.3	19.5	0.4	17.2	0.5	3
[EMIm][SCN]	4.1	14.5	1.5	13.7	1.7	3
[EMIm][SCN]	6.3	12.2	0.2	11.2	0.5	5
[EMIm][SCN]	11.1	17.0	0.6	15.6	1.1	4

<sup>a</sup> ignition delay time    <sup>b</sup> standard deviation of n drop tests

<sup>c</sup> time to vapour generation    <sup>d</sup> number of drop tests

A second test series was conducted to find the optimum value, and catalyst concentrations of 3.3, 4.9, 6.4 and 8.1 wt% were investigated. Each fuel was tested five times. The concentration of hydrogen peroxide was 97.1 %. Table 5.5 shows the results of the drop tests. The average ignition delay time scatters below 1 ms for the catalyst content between 3.3 to 8.1 wt%. The minimal ignition delay time was achieved with 11.5 ms for the 3.3 and 4.9 wt% fuels. A lower additive content is regarded as more favourable. Therefore, a subsequent iteration should focus on the two lower catalytic contents. The results are presented in Part 2 of this chapter.

Table 5.5: Drop test results of [EMIm][SCN] and different amounts of the additive [Cu][SCN]

amount [wt%]	IDT <sup>a</sup> [ms]	SD <sup>b</sup> [ms]
3.3	13.1	1.2
4.9	12.8	1.1
6.4	12.9	0.7
8.1	13.7	1.0

<sup>a</sup> ignition delay time    <sup>b</sup> standard deviation of 5 drop tests

### Summary of initial tests

- 1-Ethyl-3-methylimidazolium thiocyanate and 1-butyl-3-methylimidazolium thiocyanate are hypergolic with highly concentrated hydrogen peroxide in the order of some tens ms
- The other tested ILs are not hypergolic or have an ignition delay of several seconds after initial contact of fuel and oxidiser
- Additives can be dissolved in the thiocyanate ionic liquids to reduce the ignition delay
- The addition of copper thiocyanate to the thiocyanate ionic liquids clearly reduces the ignition delay time

- Mixtures of [BMIm][FeCl<sub>4</sub>] and thiocyanate ionic liquids also reduce the IDT, but the effect seems to be limited
- The addition of cobalt thiocyanate does not lead to reduced IDT

Because of these preliminary tests, it was decided to investigate [EMIm][SCN] with [Cu][SCN] in further detail. The [EMIm][SCN] was chosen because of its better ignition performance and lower viscosity, which can be advantageous for later testing in injectors and combustion chambers.

## 5.2 Part 2: testing in the hypergolic drop test setup

In the initial tests, [EMIm][SCN] was identified as a potential hypergolic fuel with hydrogen peroxide. In this part, different factors of the drop test are varied to evaluate their impact on the ignition delay. From now on, the drop tests were all conducted with the hypergolic drop test setup (HypeDUp); see section 3.2.1. The chamber was implemented to have a controlled environment to test the hypergolic propellants. It also allows direct control over some environmental factors to study their influence on the ignition delay.

### 5.2.1 Detailed investigation of [Cu][SCN]

This section is dedicated to the influence of different additive concentrations on the ignition delay of [EMIm][SCN] / [Cu][SCN] mixtures in more detail. As discussed in the initial test series, the absolute lowest ignition delay time was found for an additive content of 3.3 wt% and 6.4 wt%; see table 5.5. The investigation aimed to evaluate the influence of the catalytic additive over a larger range of concentrations in the hypergolic test chamber.

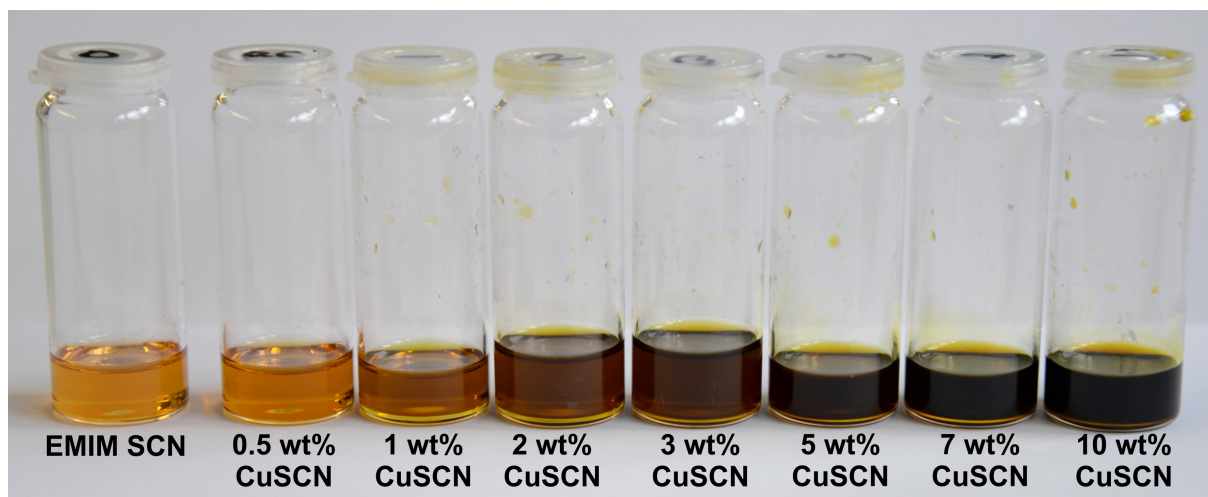


Figure 5.3: [EMIm][SCN] with different amounts of additive [Cu][SCN]

The results presented hereafter are a complete and comparable data set gathered under similar boundary conditions. A version of these results was presented in [211]. Hydrogen peroxide with a concentration of 96.1 wt% was used. The tests were recorded with a frame rate of 3600 fps. Several fuel mixtures containing 0.5 wt% up to 10 wt% of the copper additive were produced. The different fuels are shown in Figure 5.3.

Table 5.6 lists the drop test results in terms of the average IDT, TVG, the corresponding standard deviation and the number of repetitions  $n$ . Also, the difference between IDT and TVG and the

ratio of the vapour phase duration on the total ignition delay is displayed. The neat [EMIm][SCN] was also tested, and the results were presented. Figure 5.4 shows some example drop tests with different amounts of copper. In the first row, the additive content is 0.5 wt%, in the middle, 5 wt% and 10 wt% on the right. For each test, a picture before initial contact, the initial contact, a picture with vapour, the ignition, 0.3 ms and 1 ms after ignition are shown.

With the addition of 0.5 wt% [Cu][SCN], the IDT is already reduced by one-third of the initial IDT of the neat IL. At 1 wt%, the IDT is half the value. Adding more [Cu][SCN] decreases the ignition delay slightly. In this test series, the minimum ignition delay is reached for the 5 wt% additive content. If more of the catalytic substance is added the IDT rises again. The time difference between the IDT and the TVG gets shorter for higher additive contents. In other words, the vapour phase reaction is shorter; once the vapour is formed, ignition is achieved faster. Also, the vapour phase relative to the overall IDT gets shorter. This can also be seen in the high-speed recordings; see figure 5.4.

The fact that a higher additive content than 5 wt% does not shorten the ignition delay further is remarkable. One could expect that a higher additive content leads to a better reactivity between fuel and oxidiser and, therefore, shortens the IDT. But this is not the case. The IDT is longer for the higher additive contents, but the vapour phase is shorter. Hence, some effect influences the interaction between the fuel and oxidiser during the mixing and liquid reaction phase for the fuels with higher additive contents. One factor which changes considerably with the addition of copper thiocyanate is the viscosity [50]. With the measurements from [50], the viscosity of the 5 wt% fuel is already 50 % higher than the neat IL, and the viscosity of the 10 wt% fuel is almost 2.5 times the initial value; see equation (5.1). This increase in viscosity affects the mixing processes negatively, and therefore, the ignition delay is prolonged. Such an effect is also described for other hypergolic propellants by Ladanyi and Miller [41]. **There is an optimal value between the faster reaction caused by the additive amount and an impeded mixing because of the higher viscosity.** The present test series indicates that the value is close to 5 wt% [Cu][SCN] content. For further investigation, the most promising fuel in terms of ignition delay time is [EMIm][SCN] with 5 wt% [Cu][SCN] dissolved. This fuel has an average ignition delay of close to 10 ms. The scope of this fuel candidate's thesis will be evaluated in more detail. The fuel will be referred to as fuel *E5C* for [EMIm][SCN] with 5 wt% [Cu][SCN].

Table 5.6: Drop test results of [EMIm][SCN] and different amounts of the additive [Cu][SCN]

amount [wt%]	IDT <sup>a</sup> [ms]	SD <sub>IDT</sub> <sup>b</sup> [ms]	TVG <sup>c</sup> [ms]	SD <sub>TVG</sub> <sup>b</sup> [ms]	IDT-TVG [ms]	$\frac{\text{IDT-TVG}}{\text{IDT}}$ [%]	n <sup>d</sup> [-]
0	31.7	4.2	28.3	4.2	3.4	10.7	30
0.5	19.3	0.6	17.0	0.8	2.3	11.8	6
1	16.2	2.0	14.8	1.7	1.4	8.4	23
2	15.7	1.9	14.3	1.8	1.4	8.8	8
3	15.6	1.7	14.5	1.7	1.1	6.9	7
5	13.9	1.7	13.1	1.7	0.8	5.5	24
7	16.4	1.2	15.5	1.5	0.9	5.6	7
10	17.0	1.0	16.3	1.1	0.7	4.1	6

<sup>a</sup> ignition delay time    <sup>b</sup> standard deviation of n drop tests    <sup>c</sup> time to vapour generation

<sup>d</sup> number of drop tests



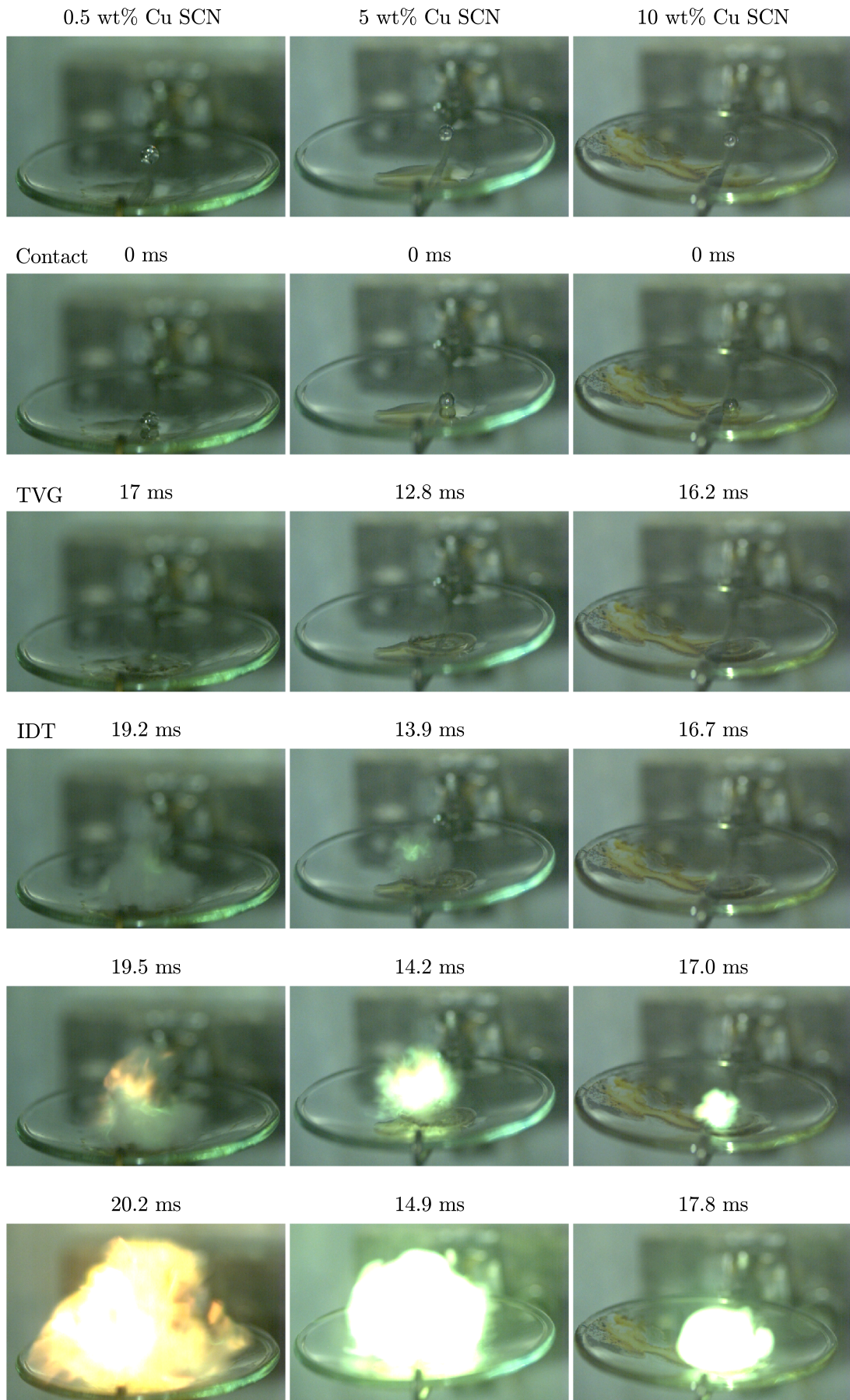


Figure 5.4: Drop tests with different amounts of additive [Cu][SCN]

### 5.2.2 Drop test parametric study

Many factors in the drop tests could influence the ignition delay. After a baseline configuration is defined, a variation of the following factors will be investigated in this section:

- drop height
- drop order
- ratio of oxidiser to fuel
- drop amount

#### Baseline configuration

Many research groups developing hypergolic fuels with hydrogen peroxide use drop tests to evaluate the hypergolic behaviour. Many drop tests are conducted with a fuel pool, meaning a drop of hydrogen peroxide falls into this fuel. With this procedure, it is described to reach shorter ignition delay times than the dropping fuel into an oxidiser pool [55]. Therefore, as a baseline configuration for our setup, a fuel pool is used, and a drop of hydrogen peroxide is added. The cannula's diameter and length predetermine the drop height and size. A cannula with a diameter of 1.1 mm and a length of 120 mm was used for the baseline configuration. This produced hydrogen peroxide drops with a volume of 14  $\mu\text{l}$  and a free fall distance of 61 mm. Fuel with a volume of 115  $\mu\text{l}$  was added for the baseline configuration. This was a good compromise with generating a drop with a surface that is large enough to ensure a high probability of hitting the pool with the peroxide drop. On the other side, it was not too much, so a small amount of fuel was needed for a drop test, and the splashing of unburned fuel was limited. This improves the chamber's operation since unburned fuel can contaminate the windows and block the view.

#### Drop height

This section compares two free fall heights of the hydrogen peroxide drop: the baseline configuration with a 61 mm free fall distance and a higher fall of 141 mm. The higher free fall was implemented using a shorter cannula with the same diameter as the baseline configuration. The higher free fall increases the impact velocity of the drop from 1 m/s to 1.6 m/s. This corresponds to 2.6 times more kinetic energy at impact. The average results of IDT and TVG are given in table 5.7.

The average ignition delay time is close to 31 ms in both cases. The standard deviations for the higher free fall distance are higher than in the baseline case. It seems that because of the higher impact velocity, the variation of the IDT increases. Despite this, there is no effect on the average IDT distinguishable. So, for higher free fall distances, the data quality is reduced. Further, a reduction of IDT in our boundary conditions set by the drop test chamber geometry is not expected. For this reason, the free fall distance of the baseline configuration was used for the further test. For such droplet impacts, the Weber number is a common dimensionless number to compare the impacts. The Weber number is the ratio of inertia of the droplet and the surface tension; see equation (2.22). An estimation of the average Weber number of the baseline configuration is 50.6. For the higher free fall, the Weber number is 107. It must be mentioned that due to the relatively low frame rate of the camera and the low resolution, the uncertainty of the velocity is relatively high. The velocity is squared in the calculation of the Weber number, compare equation (2.22). Following the uncertainty regarding the Weber number, the baseline case is in the order of 40 % and 70 % for the higher free fall. Therefore, a detailed analysis of the Weber numbers is not presented. In our boundaries, the IDT concerning the Weber number indicates that the influence on the IDT is low or not present in the tested range.



Table 5.7: Drop test results of different free fall distances

free fall height [mm]	IDT <sup>a</sup> [ms]	SD <sub>IDT</sub> <sup>b</sup> [ms]	TVG <sup>c</sup> [ms]	SD <sub>TVG</sub> <sup>b</sup> [ms]	IDT-TVG [ms]	We <sup>d</sup> [-]	n <sup>e</sup> [-]
61 (baseline)	31.2	3.8	26.3	3.6	5.0	50.6	20
141	31.4	7.4	25.0	6.3	6.0	107.0	18

<sup>a</sup> ignition delay time    <sup>b</sup> standard deviation of n drop tests    <sup>c</sup> time to vapour generation  
<sup>d</sup> Weber number    <sup>e</sup> number of drop tests

## Order

So far, the presented results all were conducted with a drop of hydrogen peroxide falling into a fuel pool. This section is dedicated to the influence of the dropping order. Tests with a drop of fuel falling into an oxidiser pool are compared to the regular configuration. The baseline is a hydrogen peroxide drop with a volume of 14  $\mu\text{l}$ , and the fuel pool has a volume of 115  $\mu\text{l}$ . Hence, the regular configuration has an excess of fuel. For the vice versa case, a 14  $\mu\text{l}$  drop of fuel is dropped into 90  $\mu\text{l}$  hydrogen peroxide. With these amounts, the mass of the pool component is roughly the same in both configurations. Pure [EMIm][SCN] and E5C were tested. The results in terms of TVG and IDT are presented in table 5.8. For the [EMIm][SCN], the baseline results can

Table 5.8: Drop test results of different drop orders

Fuel	drop	IDT <sup>a</sup>	SD <sub>IDT</sub> <sup>b</sup> [ms]	TVG <sup>c</sup> [ms]	SD <sub>TVG</sub> <sup>b</sup> [ms]	IDT-TVG [ms]	n <sup>e</sup> [-]
[EMIm][SCN]	fuel	67.6	9.3	62.9	8.2	4.6	10
[EMIm][SCN]	ox	31.2	3.8	26.3	3.6	4.9	20
E5C	fuel	21.4	2.8	20.0	2.7	1.3	7
E5C	ox	14.3	0.8	13.1	0.6	1.2	3

<sup>a</sup> ignition delay time    <sup>b</sup> standard deviation of n drop tests    <sup>c</sup> time to vapour generation  
<sup>d</sup> Weber number    <sup>e</sup> number of drop tests

be compared to the fuel drop cases. The drop tests with the oxidiser pool have an IDT, which is twice as long as the baseline case. At the same time, the vapour phase durations are similar. For the E5C fuel, an increase in the average IDT of 50 % is measured for the hydrogen peroxide pool. However, the vapour phase has a similar duration for both cases. This may indicate that similar processes occur until the ignition once vapour is generated. The difference between the two configurations is related to the interaction in the liquid phase. During the liquid phase, mixing processes take place, and the chemical reaction starts to raise the mixture's temperature until vapour is released. The longer duration of IDT for fuel dropping into  $\text{H}_2\text{O}_2$  was also described by Kang et al. [55]. The mass-specific heat capacity is different for the two pool components. Pure  $\text{H}_2\text{O}_2$  has a specific heat capacity  $c_p$  of 2.627 kJ/kg K [88] and [EMIm][SCN] 1.663 kJ/kg K [212]. Hence, the  $c_p$  of hydrogen peroxide is 60 % higher than the fuel's  $c_p$ . This also means that in the case of a  $\text{H}_2\text{O}_2$  pool, a higher amount of energy is needed to heat the mixture until the vapour is released. Following, the initial reactions and heating need more time. Further differences in the interactions and mixing processes of the two components are also possible. The fuel-rich condition is more favourable due to the shorter IDT. Hatai et al. also identified fuel-rich conditions as more favourable due to a higher probability of a smooth start up [70].

### Variation of the amounts of drop and pool

In chapter 4, initial performance calculations pointed out that the ROF for optimal  $I_{sp}$  is around 4. The drop tests are conducted with a fuel pool, resulting in a high excess of fuel. This is very different from the nominal operation of a thruster close to the  $I_{sp}$  maximum. This section will investigate the influence of varying drop and pool amounts. Table 5.9 displays the result of different test configurations. In the first row, the results are the values of the baseline tests. They were conducted with a calculated ROF of 0.19. For the tests with configuration I, a smaller hydrogen peroxide drop was used by utilizing another cannula with a diameter of 0.8 mm. The fuel pool was then reduced to half of the baseline fuel pool, configuration II. For configuration III, the fuel amount was further decreased to reach the ROF with the highest  $I_{sp}$ . In this case, the fuel pool was only 4.5  $\mu\text{l}$  and hard to hit with the hydrogen peroxide drop. Therefore, out of 8 repetitions, only four drop tests had a suitable hit of the hydrogen peroxide drop and the fuel. These four tests were used for the evaluation. The average IDTs are between 29.5 and

Table 5.9: Drop test results of different drop amounts

Conf.	pool [ $\mu\text{l}$ ]	drop [ $\mu\text{l}$ ]	ROF <sup>a</sup> [-]	IDT <sup>b</sup> [ms]	SD <sub>IDT</sub> <sup>c</sup> [ms]	TVG <sup>d</sup> [ms]	SD <sub>TVG</sub> <sup>c</sup> [ms]	IDT-TVG [ms]	n <sup>e</sup> [-]
baseline	115 $\pm$ 2.0	14 $\pm$ 2.3	0.19	31.2	3.8	26.3	3.6	4.9	20
I	115 $\pm$ 2.0	11 $\pm$ 1.9	0.15	29.5	2.6	25.2	2.3	4.3	17
II	58 $\pm$ 1.0	14 $\pm$ 2.3	0.38	30.3	2.3	25.6	1.6	4.8	8
III	4.5 $\pm$ 0.1	14 $\pm$ 2.3	4	33.3	2.4	28.3	2.2	4.9	4

<sup>a</sup> oxidiser to fuel ratio    <sup>b</sup> ignition delay time    <sup>c</sup> standard deviation of n drop tests

<sup>d</sup> time to vapour generation    <sup>e</sup> number of drop tests

33.3 ms. The maximum deviation from the baseline IDT is 2.1 ms. Considering the standard deviation, the deviations can be regarded as minor. Therefore, the ROF variation leads to similar ignition delay times. In comparison, in the first part of this chapter, results were presented, where the amount of fuel pool was in the order of 1 to 2 ml. The conducted drop tests also lead to comparable ignition delay times. This may be related to the local mixture ratio at the drop surface, where the initial interactions start. The specific contact surface and local mixture ratio are approximately equal for the different cases.

Based on these results it applies to this propellant combination: if a drop of hydrogen peroxide is dropped onto a fuel pool with an excess amount of fuel, the resulting IDTs are similarly independent of the amount of fuel. On the other side, the results of the last section showed that if fuel falls into an oxidiser pool, the IDT gets significantly longer.

### 5.2.3 Environmental factors on the ignition

In this section, several environmental factors are investigated and their influence on the ignition delay is evaluated. Environmental factors include:

- surrounding medium
- initial pressure
- initial temperature
- storage condition
- concentration of hydrogen peroxide

Table 5.10: Drop test results of different inert atmospheres

Fuel	atmosphere	IDT <sup>a</sup>	SD <sub>IDT</sub> <sup>b</sup>	TVG <sup>c</sup>	SD <sub>TVG</sub> <sup>b</sup>	IDT-TVG	n <sup>d</sup>
			[ms]	[ms]	[ms]	[ms]	[-]
[EMIm][SCN]	air	26.5	1.9	22.7	2.0	3.8	9
[EMIm][SCN]	argon	26.1	1.4	22.0	1.3	4.1	5
E5C	air	13.4	1.5	12.3	1.3	1.1	6
E5C	argon	11.5	0.7	10.4	0.7	1.1	6

<sup>a</sup> ignition delay time    <sup>b</sup> standard deviation of n drop tests    <sup>c</sup> time to vapour generation  
<sup>d</sup> number of drop tests

The drop tests investigating the surrounding medium and initial pressure were conducted within the master's thesis of J. Scholl [213].

### Surrounding medium

So far, all presented drop tests have been conducted in the air. Because air contains 21 % oxygen, the presence of gaseous oxygen could influence the hypergolic ignition. Therefore, tests in an inert atmosphere were conducted to assess if there was an influence. Argon was used as an inert gas. The procedure was as follows: The fuel was provided to the hourglass, and the drop test chamber was closed. The pressure in the chamber was reduced to 0.2 bar using the vacuum pump. Then, it was repressurised to 1 bar with Argon. The evacuation and re-pressurisation was repeated five times. After this procedure, the remaining oxygen content is in the order of 0.05 %.

The upper drop test of figure 5.5 shows a test with [EMIm][SCN] in air and the lower part a test with [EMIm][SCN] in an argon atmosphere. The flame appearance is different in the two cases. After ignition in the chamber filled with air, a bright flame develops and can still be seen more than 100 ms after ignition. In the argon case, the flame is less bright and disappears quickly. At 12 ms after the ignition, the flame is almost quenched because all the oxygen the hydrogen peroxide provides has already been used. The flame can survive much longer in the air because the vaporised fuel burns together with the oxygen from the air.

It can also be clearly seen that in the argon atmosphere, the flame ignites in the outer region of the vapour cloud. The flame is orange and propagates in the cloud. Finally, a second flame in bright yellow can be seen in the middle at the spot where the hydrogen peroxide impacted the fuel. The yellow flame burns very brightly for some milliseconds. The flame in the air also propagates in the vapour cloud. A very bright flame at the impact spot can also be seen in milliseconds after ignition; see f). This behaviour was observed in many tests with [EMIm][SCN]. The argon atmosphere makes this effect obvious. The hydrogen peroxide and [EMIm][SCN] flame may propagate in two steps, or two different mechanisms drive and supply the flame. The first flame following the initial ignition is supplied by the initial hydrogen peroxide decomposition products and vaporised fuel or decomposition products of the fuel. The second flame burns at the impact spot and may result from further liquid phase reactions. It is noticeable that this flame has a brighter appearance and needs more time to establish than the initial flame in the gaseous phase.

Table 5.10 shows the IDT and TVG for the different fuels and atmospheres. The IDT and TVG are similar for the [EMIm][SCN]. For the ignition, the oxygen present in the air does not influence the IDT. The average IDT of [EMIm][SCN] here is shorter than the one previously described in the baseline configuration, compare table 5.7. This difference is influenced by the fact that another hydrogen peroxide concentration was used, with 96.7 wt% (compared to 96.1 %

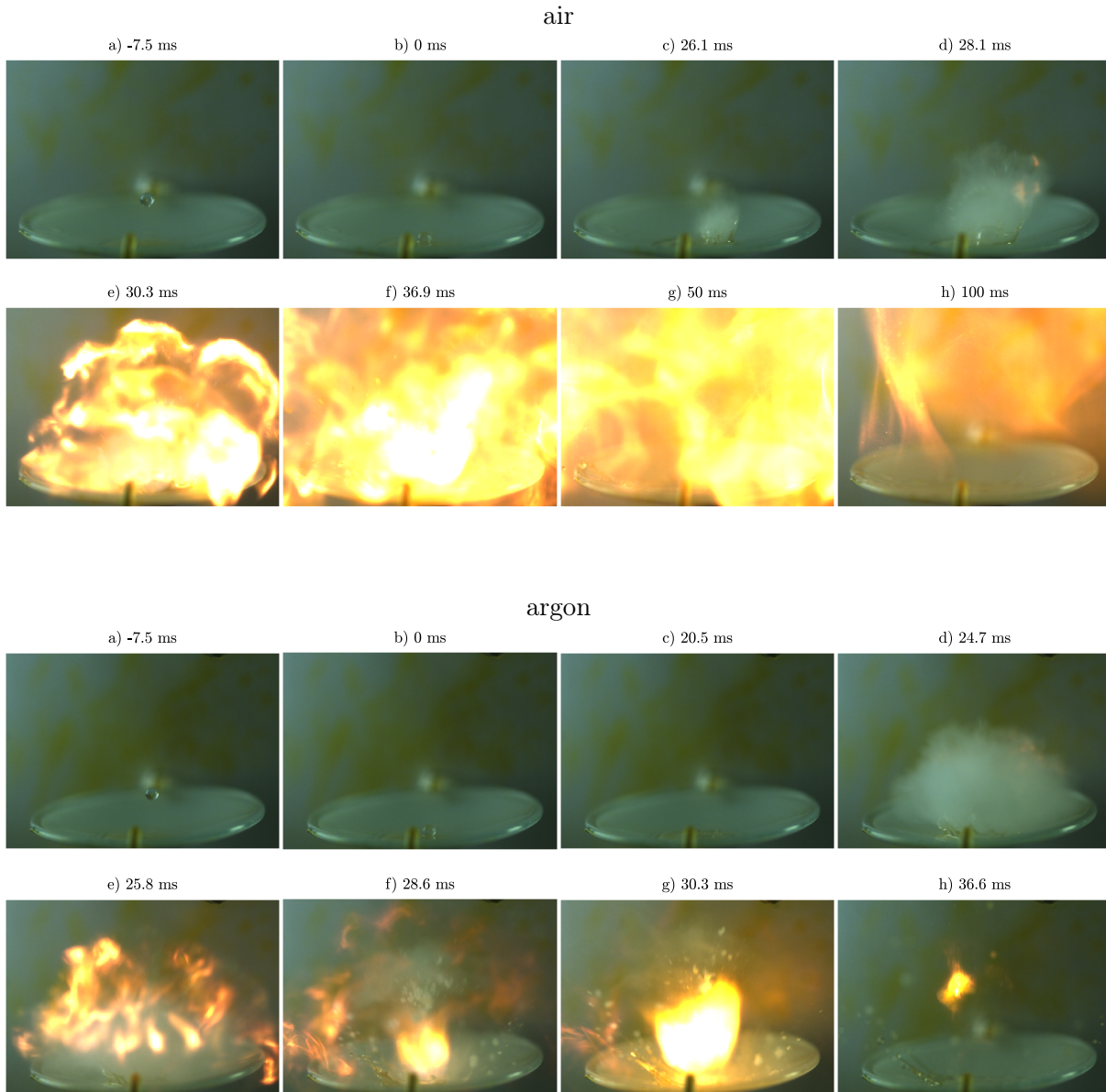


Figure 5.5: Upper: Drop test [EMIm][SCN] in air, lower: in argon

in earlier tests of section 5.2.2). Also, the tests were conducted in summer, when the ambient temperature is expected to be slightly higher.

The flame of the E5C fuel is much brighter after the ignition compared with the [EMIm][SCN]. Due to this brightness and overexposure of the high-speed video, no conclusion can be drawn if a two-step process occurs. However, it can be observed that in the argon atmosphere, the flame disappears faster than in the air. The average ignition delay in table 5.10 is shorter for the argon atmosphere. It must be mentioned that the two data points were produced on different test days. Since the IDT of the ionic liquids is sensitive to the fluid temperature, the initial temperature might have been slightly different during the hot summer days when the tests were conducted. The exact value of the ambient temperature was not documented. Concerning this and the standard deviation, there is expected to be limited or no influence of the ambient oxygen on the IDT for the E5C fuel.

According to the theory of Semenov (see section 2.2.2), the heat loss to the surroundings can

influence the ignition. The heat loss to the surrounding medium depends on the heat transfer coefficient, the surrounding surface and the ambient temperature, see equation (2.16). It is assumed that for the tests with the variation of the surrounding medium, the ambient temperature was almost constant and varied in the order of one or two Kelvin. Further, the surface where the heat loss to the surrounding occurs is also the same, since it can be seen in figure 5.5 the expansion of the initial vapour is alike. The heat loss depends linearly on the heat transfer coefficient; see equation (2.16). Air has a heat transfer coefficient of  $0.026 \frac{\text{W}}{\text{m K}}$  and argon has  $0.018 \frac{\text{W}}{\text{m K}}$  [214]. Those values are also in the same order, so a significant influence is not expected. This also agrees with observations by Pourpoint et al., where no difference in the IDT between argon and air was detected at high  $\text{H}_2\text{O}_2$  concentration [25, 26].

It can be concluded that the oxygen in the air has no relevant influence on the ignition delay time of the thiocyanate ionic liquids. Therefore, further testing can be conducted at ambient conditions, and there is no need for a protective atmosphere or falsified measurements.

### Initial pressure

The initial pressure can influence the ignition delay time, according to Semenov's theory. The influence of different initial pressures below ambient pressure is investigated in this section. The low-pressure regime is interesting because the combustion chamber of a thruster in a space environment will initially have vacuum conditions. But by injecting the propellant, the pressure will rise. The results of drop tests with [EMIm][SCN] and E5C fuel are presented. The pressure was varied in several steps from ambient down to 0.1 bar. The IDT of the drop tests in regard to the initial pressure in the drop test chamber is plotted in Figure 5.6. Also, an Arrhenius type fit of the form  $IDT(p) = A''e^{-b/p}$  is shown, where  $A''$  is the pre-exponential factor,  $b$  is the exponential constant and  $p$  the initial pressure, compare equation (2.13). The factors of the fitting curve are displayed in table 5.11.

Table 5.11: Arrhenius factors of the pressure dependent IDT fitting curve

Fuel	b [Pa]	A [s]	R <sup>2</sup>
[EMIm][SCN]	-2.414e4	18.31	0.977
E5C	-8525	11.05	0.74

The IDT of both fuels increases for low pressures. In the case of the [EMIm][SCN], the average IDT around 0.4 bar is one-third higher compared to ambient conditions. For lower pressures, the IDT increases dramatically. The longest IDT was measured for 0.202 bar with 63.1 ms in the test series. No ignition was observed at pressures of 0.197, 0.147 and 0.116 bar. For [EMIm][SCN], the ignition boundary is close to 0.2 bar at the tested conditions.

Pressures down to 0.2 bar do not influence the IDT of the E5C fuel. At initial pressures of 0.1 bar and 0.13 bar, the IDT increases to 20-30 ms. Lower pressures were not realisable in our setup. Figure 5.6 shows the TVG values of the single test runs on the right side. The TVG decreases for both fuels with lower pressures. Generally, the boiling point decreases with lower initial pressure for fluids. Therefore, this effect may be attributed to the earlier vapour release at reduced pressure. Contrarily, the vapour phase is longer with shorter TVG and increasing IDT. Figure 5.7 shows two tests with [EMIm][SCN] at two different initial pressures. After generating vapour, the cloud expands wider than at ambient pressure, compare figure 5.5. When the ignition is achieved, the flame propagates slower, and the combustion process appears less violent than at ambient pressure. The flame's intensity decreases for lower pressure; a similar effect is also

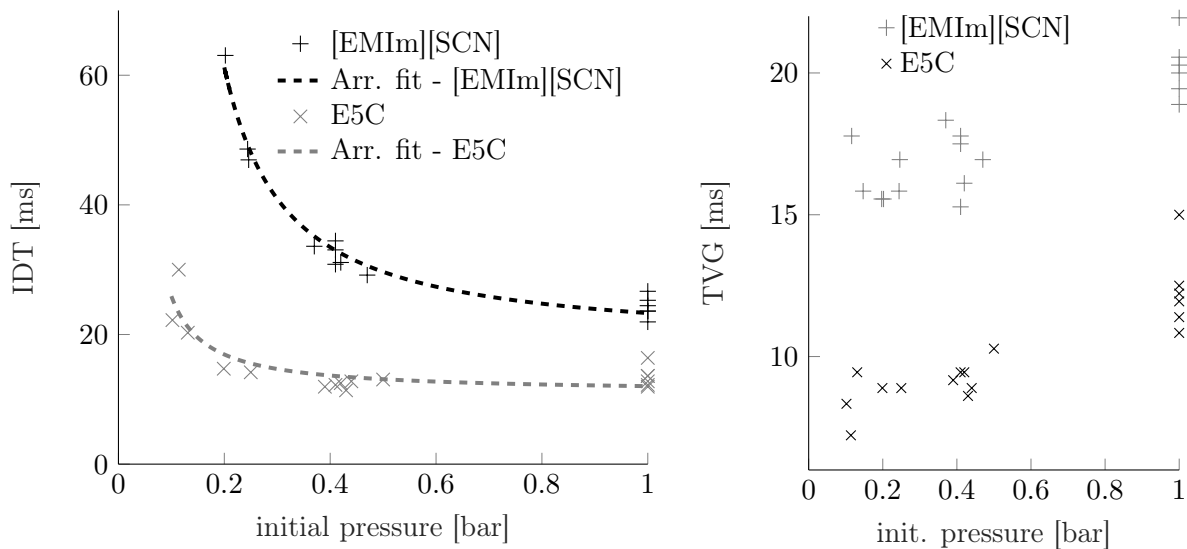


Figure 5.6: Left: IDT over initial pressure, right: TVG over initial pressure

seen in the tests with an inert atmosphere. At the reduced pressure, less oxygen from the air is present. The E5C fuel behaves similarly. At reduced pressures, before the ignition, the vapour cloud expands much wider before ignition is achieved. The flame propagation is visibly slower for the very low pressures.

According to thermal ignition theory, the heat generation is dependent on the pressure; see figure 2.3 and equation (2.15). The heat generation is also lower for lower pressures, whereas the heat loss does not change significantly. Therefore, it is possible that the heat loss to the surroundings is larger than the heat generation under certain conditions. In this case, no ignition occurs. The effect is intensified by the faster expansion of the vapour cloud at lower pressures, increasing the surface, where convection to the surrounding medium occurs.

From these drop tests, it seems more likely that the E5C fuel is less prone to late ignitions under low-pressure conditions in a space environment.

### Initial temperature

This section is dedicated to the influence of the initial fuel temperature on the ignition delay. An influence of the temperature was suspected, but unfortunately, it was systematically evaluated at the end of the test campaigns for this thesis.

For example, different IDTs were observed between different test series. The average IDT of [EMIm][SCN] in 5.10 with 26.5 ms is compared to the IDT of the baseline measurement, which was 31.2 ms, a difference of about 5 ms results. This difference is not only caused by the influence of random effects. The hydrogen peroxide concentration was slightly different with 96.7 wt% and 96.1 wt%, but it is unlikely that a significant difference of 5 ms is caused by this slight difference alone (see next section). The baseline measurements were conducted in October 2019, and the measurements presented in table 5.10 result of a warm period in the summer 2020. Until then, unfortunately, the actual temperature in the lab and of the propellant was only documented as "ambient temperature".

The test series for the variation of the initial fuel temperature was conducted with the drop test chamber. A 1 mm type K thermocouple was placed inside the fuel pool, and the actual fuel temperature was recorded. For the temperature lower than ambient, the fuel and the hourglass were cooled with ice water and then put into the chamber. During the preparation time, the fuel

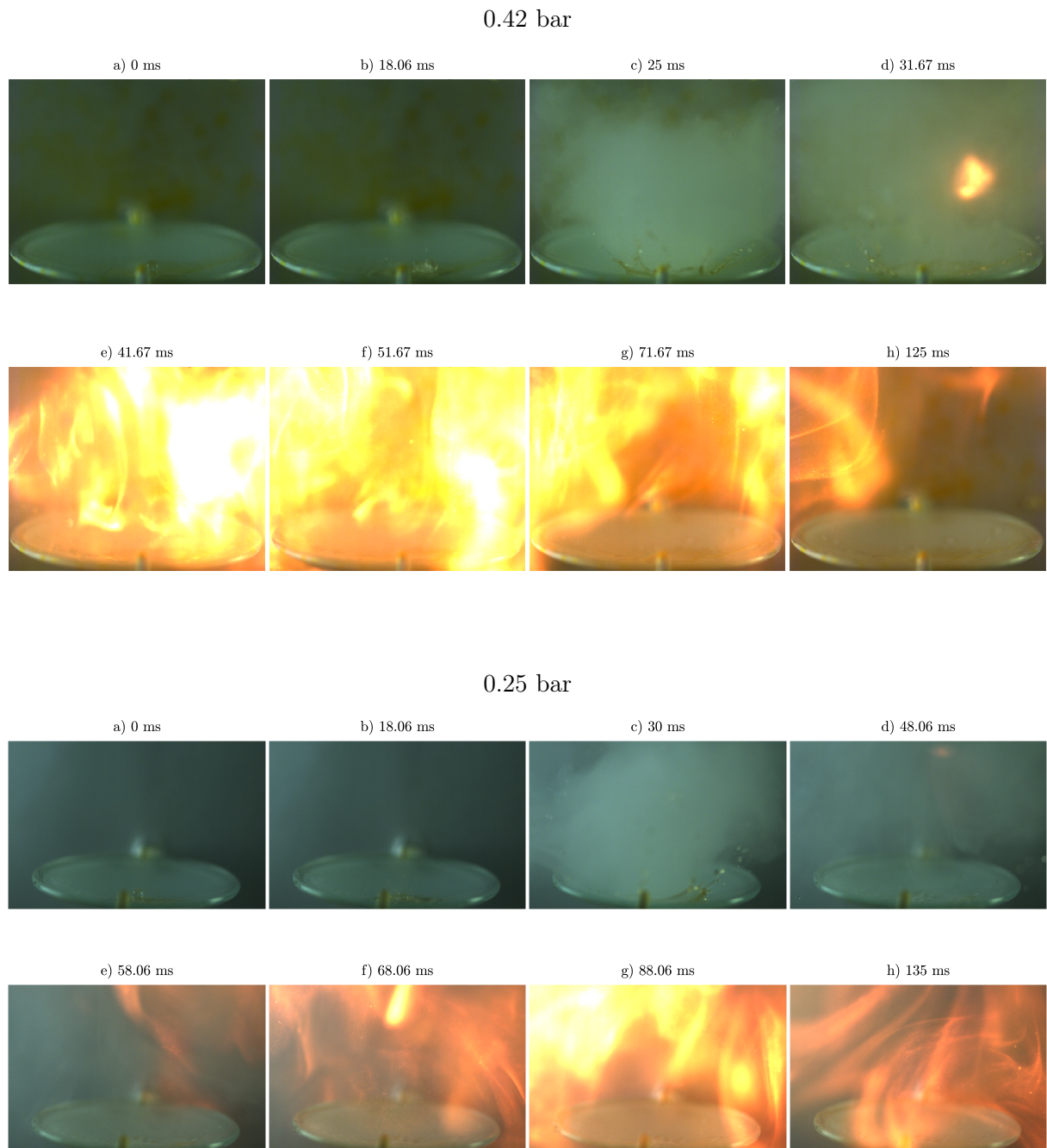


Figure 5.7: Ignition of [EMIm][SCN] at different initial pressures, upper: 0.42 bar, lower: 0.25 bar

warmed again, so the lowest temperature reached was around 12 °C. For the higher temperature, a hot air gun was used. Because the temperature was measured directly in the fuel, it was decided that this method was adequate to heat the fuel. The reproducibility is limited, but it was agreed that it is a suitable heating method in terms of effort and time efficiency. The highest temperatures were close to 80°C.

In this test series, 75 single drop tests with [EMIm][SCN] and E5C were conducted. The IDT, depending on the initial temperature, is shown in figure 5.8 a) for [EMIm][SCN] and d) for E5C.



The plots show that the initial temperature greatly influences the ignition delay. For better readability, no error bars are shown. The tests were recorded with a frame rate of 5000 fps. The uncertainty in the ignition delay is according to equation (3.6) 0.3 ms. The uncertainty of the temperature can be assumed with 1 K.

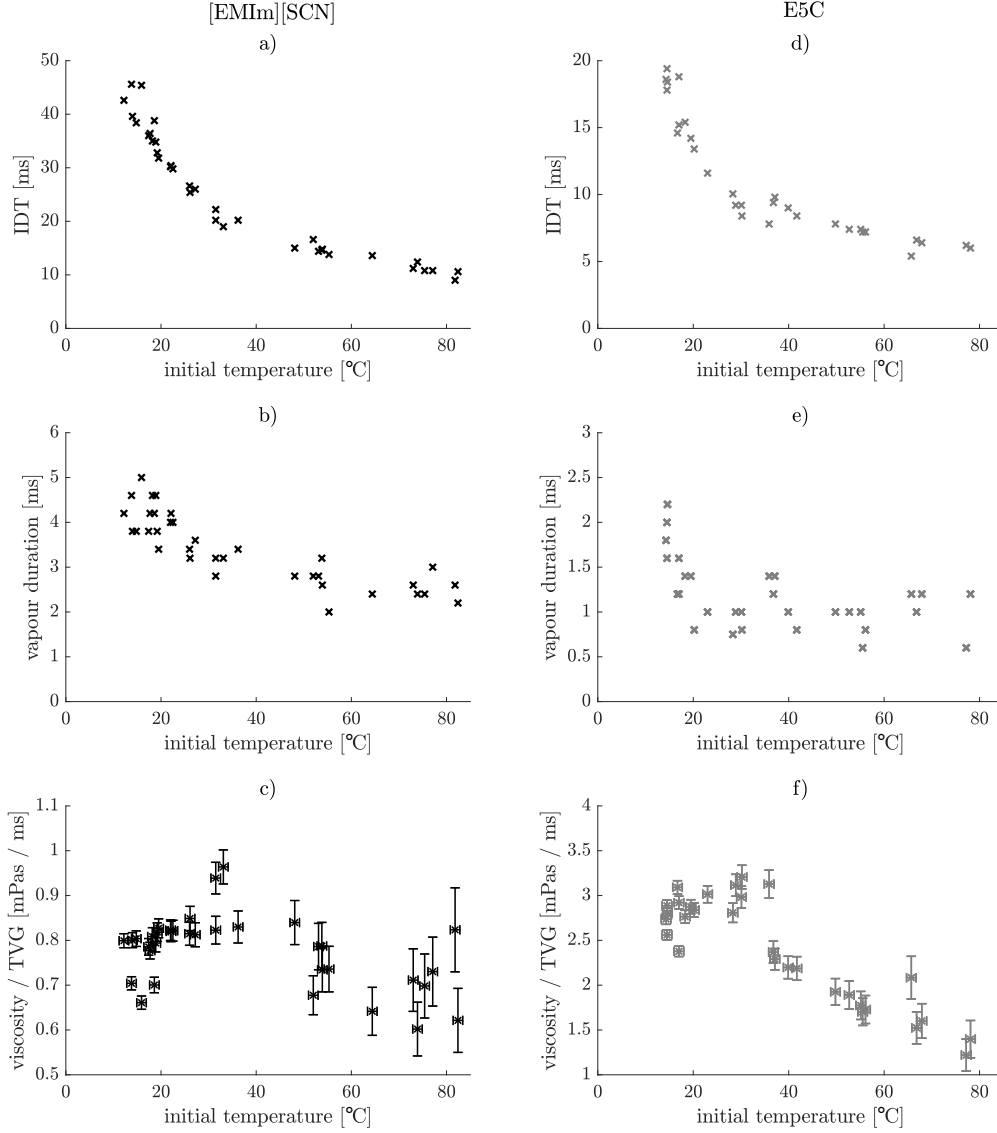


Figure 5.8: Ignition at different initial temperatures, a) IDT for [EMIm][SCN], b) duration of the vapour phase of [EMIm][SCN], c) ratio viscosity and TVG for [EMIm][SCN], d) IDT for E5C, e) duration of the vapour phase of E5C f) ratio viscosity and TVG for E5C

For low temperatures (below 30°C), the IDT changes significantly with the temperature. [EMIm][SCN] has an average IDT at 30 °C of around 20 ms and the lowest temperature (12 °C) of around 45 ms. If a linear relationship of IDT and initial temperature is assumed between 12°C and 30 °C, the IDT changes 1.2 ms per K. For the higher temperatures, the IDT is still reduced, but the gradient of the reduction is lower. The minimal ignition delay time reached is 9 ms at 81.8 °C. The IDT of E5C shows a similar behaviour for different initial fuel temperatures.



Between 14 °C and 30°C, the gradient is higher than for the higher temperatures. If, again, in this range, a linear relation is assumed, the increase in IDT is around 0.6 ms per K. The lowest ignition delay time of 6 ms was achieved at a temperature of 78°C.

The temperature dependence, especially at lower temperatures, explains the earlier observation with a difference in IDT of several ms during summer and autumn tests. Based on these results, the initial temperature during the autumn tests was roughly around 20 °C and in summer, about 23.5 °C.

**Effect of viscosity** The sensitivity of the temperature to the ignition delay time around ambient conditions is remarkable. The following gives a suggestion on the cause of this sensitivity. In figure 5.8 b), the duration of the vapour phase is shown depending on the initial temperature. At the lower temperatures, the vapour duration phase also decreases from 5 ms to 3.5 ms, whereas the change of the IDT exceeds 25 ms. Consequently, the driving factor for the temperature sensitivity is not driven by the faster reaction rates of the vapour phase leading to the hypergolic ignition. The reduction of IDT is related to the liquid phase interactions. Also, the initial temperature change, e.g. from 20 °C to 30 °C, is not expected to change the reaction rates in the liquid phase, so the IDT is reduced in the order of 10 ms. If 'chemistry' is not the driving factor, physical interactions could cause the behaviour. A physical factor that also changes significantly in the regarded temperature range is the viscosity of the ionic liquid. Zarca et al. characterised the viscosity of [EMIm][SCN] and [EMIm][SCN] / [Cu][SCN] mixtures over a broad temperature range [50]. The course of their approximation of the viscosity dependent on the temperature also has a higher gradient in the lower temperatures than in the higher temperatures. Zarca et al. approximate the temperature with:

$$\eta(T)[mPas] = A \exp\left(\frac{B}{T^3}\right) \quad (5.1)$$

where A and B are constants fitted to the measurements. The following factors in table 5.12 were used for the determination of the viscosities at the given temperature during the tests. A more detailed discussion on the viscosity is provided in 7.1.1.

Table 5.12: Empirical constants for viscosity [50]

Fuel	A [mPa s]	B [K <sup>3</sup> ]
[EMIm][SCN]	0.7842	8.52e7
E5C	0.64967	1.0118e8

$$q_{\eta/TVG}(T_i) = \frac{\eta(T_i)}{TVG(T_i)} \quad (5.2)$$

In figure 5.8 c) the quotient  $q_{\eta/TVG}$  of the viscosity and the TVG are shown for [EMIm][SCN] at the single drop test points, see equation (5.2). For the temperatures between 12 °C and 30 °C, the average value is close to 0.8 mPas /ms on a plateau with some outliers. For the higher temperatures, the value of the ratio decreases. The constant ratio on the plateau between 12 °C and 30 °C means that the TVG changes the same way as the viscosity changes. Therefore, it is assumed that the viscosity is the main driver of the IDT reduction with higher temperatures in this range. For higher temperatures, the decreasing quotient indicates a change that the TVG and viscosity are not changed in the same manner any more. Now, accelerating effects on the chemical level have also become more important. Higher viscosities in the lower temperature

range influence the physical mixing of the fuel and oxidiser after the impact. Higher viscosities negatively influence the mixing, leading to a longer liquid phase interaction and, therefore, increasing the overall ignition delay time.

Figure 5.8 e) shows the vapour duration of the E5C fuel. For the lowest temperatures, the vapour duration is close to 2 ms but decreases quickly. From 20 °C, the vapour phase duration varies at a constant level between 1.4 and 0.6 ms. Figure 5.8 f) shows the ratio of the viscosity and the TVG for E5C fuel. The E5C fuel is more viscous than the pure IL because of the addition of copper. However, the overall IDTs are significantly reduced because of the high catalytic activity, which outweighs the effects of the higher viscosity of the fuel compared to the pure [EMIm][SCN]. But a considerable influence on the IDT is observed for this fuel at the lower temperatures. In this case, from 14 °C to 30 °C, the ratio of viscosity and TVG is, on average, 3 mPas /ms, and the values of the single tests scatter around this value. For higher temperatures, the ratio decreases. Here, it is also assumed that the viscosity and its change are mainly attributed to the longer IDTs at lower temperatures. For higher temperatures, the change in the viscosity is less significant, and also other factors become an increasing influence on the ignition delay time. In conclusion, the IDT of drop tests with [EMIm][SCN] and E5C is very sensitive to the initial temperature around ambient temperature (15-30 °C). A variation of a few degrees °C in the ambient room temperature impacts the IDT. Tests should be performed with the same initial temperature to generate sound and comparable results. At least the exact initial temperature of the propellant components should be documented. From the application point of view, higher initial temperatures lead to shorter ignition delay times. This effect could be used to reduce the catalyst amount or supersede the catalyst to reach short ignition delay times.

**Arrhenius** With temperature-dependent data, an Arrhenius function can be derived. The following form of the Arrhenius function was proposed in 2.2.2:

$$IDT = A'' e^{\left(\frac{E}{RT}\right)} \quad (5.3)$$

where  $A''$  is the pre-exponential factor,  $E$  is the global activation energy,  $R$  is the universal gas constant and  $T$  the initial temperature. The Arrhenius function can be rewritten as

$$\ln(IDT) = \ln(A'') + \frac{E}{R} \frac{1}{T} \quad (5.4)$$

This represents a linear function of the inverse temperature with the natural logarithm of the constant factor as y-intercept and a slope of  $E/R$ . Figure 5.9 is an Arrhenius plot with the inverse temperature on the x-axis and the natural logarithm of the IDT on the y-axis. The IDT values have the unit of seconds. Both fuels are plotted, and their linear fits.

Table 5.13: Arrhenius factors

Fuel	E [J/mol]	A'' [s]
[EMIm][SCN]	17851	2.255 e-5
E5C	15079	3.013 e-5

Table 5.13 displays the global activation energy calculated from the slope of the Arrhenius plot for both fuels. The global activation energy is higher for the [EMIm][SCN] than the E5C. This strongly suggests that the copper additive catalyses the reaction, and roughly 15.7 % less energy is needed for the activation of the hypergolic ignition.

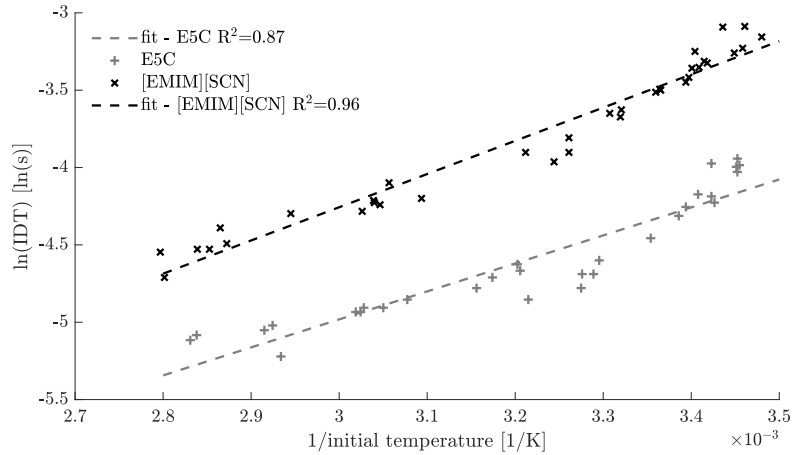


Figure 5.9: Arrhenius plot of [EMIm][SCN] and E5C

### Concentration

Drop tests with different hydrogen peroxide concentrations were conducted in a dedicated test series. The impact on the ignition delay time of different concentrations was to be investigated. The pure [EMIm][SCN] as well as E5C were tested at an initial temperature of 19°C. Figure 5.10 shows the results in terms of ignition delay of the drop tests. For clarity, no error bars are shown. Moreover, a curve is fitted through the measurement data. This fit has the Arrhenius form  $IDT(x) = Ae^{-b/x}$ , where  $A$  is the pre-exponential factor,  $b$  is the exponential constant and  $x$  the concentration. The factors of the fits are given in table 5.14.

Table 5.14: Arrhenius factors of the concentration fitting curve

Fuel	b [-]	A [s]	R <sup>2</sup>
[EMIm][SCN]	-595	0.0698	0.945
E5C	-527.6	0.0687	0.969

Table 5.15 lists the IDT, TGV and standard deviation for the different cases. Ignition was still achieved for the lowest concentration tested, around 78 % H<sub>2</sub>O<sub>2</sub>. For this H<sub>2</sub>O<sub>2</sub> concentration, the pure [EMIm][SCN] has an average IDT of about 136 ms, whereas E5C has an IDT of less than half this value. The single IDTs of [EMIm][SCN] have a high variation at the lowest concentration. With lower concentrations, the duration of the vapour phase reactions is also much longer. This can also be seen in the high-speed recordings. After ignition is achieved, the combustion is less violent compared to the higher concentration. As expected, the IDT was lowest for the highest hydrogen peroxide concentration. For the [EMIm][SCN], the matching of the Arrhenius type fit has a residual of  $R^2 = 0.94$ . The E5C has a high match, with a residual  $R^2 = 0.97$ .

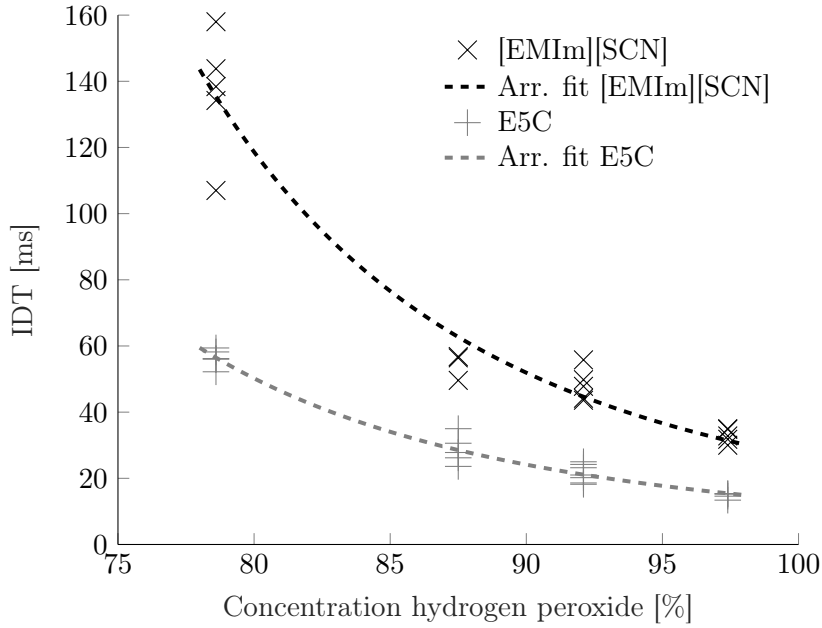
### Storage

A novel propellant must be storable on Earth and in space. Especially if additives are dissolved in a fuel, it must be assured that the additives do not crystallise or agglomerate. In this section, a brief look at aged fuel is given. Pure ionic liquids do not face the issues of additives, but the effect of storage on IDT is of interest. The pure IL is delivered in brown glass bottles. According to the datasheet, the IL should be stored in a container "closed in a dry, well-ventilated area"

Table 5.15: Drop test results of different concentrations  $\text{H}_2\text{O}_2$  for [EMIm][SCN] and E5C

concentration [%]	EMIm		E5C		EMIm		E5C	
	IDT <sup>a</sup> [ms]	SD <sub>IDT</sub> <sup>b</sup> [ms]	IDT <sup>a</sup> [ms]	SD <sub>IDT</sub> <sup>b</sup> [ms]	TVG <sup>c</sup> [ms]	SD <sub>TVG</sub> <sup>b</sup> [ms]	TVG [ms]	SD <sub>TVG</sub> <sup>b</sup> [ms]
78.6	136.3	16.7	56.4	2.5	112.6	20.4	48.4	5.6
87.5	54.3	3.3	28.6	3.9	46.7	2.6	26.6	3.8
92.1	48.2	4.4	21.5	2.5	43.0	4.2	19.6	2.0
97.4	32.8	1.8	14.6	0.8	28.8	1.5	13.5	0.6

<sup>a</sup> ignition delay time    <sup>b</sup> standard deviation    <sup>c</sup> time to vapour generation

Figure 5.10: Different  $\text{H}_2\text{O}_2$  concentration vs IDT

[215]. Moreover, it is stated as moisture sensitive. A very moisture-sensitive fuel can induce special handling and storage requirements, leading to more complex and costly procedures. To get an impression of the hygroscopic behaviour of [EMIm][SCN] and its consequence on ignition behaviour, a sample of [EMIm][SCN] was stored inside an open vial in a fume hood for ten months. Before and after the storage, the weight was taken, and over time, the sample's weight increased by 0.74 %. This additional weight is the most probable cause of air humidity and hygroscopic effects. Drop tests with [EMIm][SCN] stored closed and dry, as well as with the openly stored [EMIm][SCN], were conducted. Further, a batch of E5C was stored closed and dry for eight months, and the stability was to be investigated. The presented tests in table 5.16 were conducted on the same day so that the initial temperature can be regarded as constant.

The IDT of the two [EMIm][SCN] samples are on the same level; the TVG is slightly lower for the openly stored sample. From these few tests, a clear trend cannot be derived. However, the IDT is not highly influenced by a small amount of water captured from the air. Further, [EMIm][SCN] is hygroscopic, but the effect is only minor if standard laboratory procedures are

Table 5.16: Drop test results of storage stored fuels

fuel	storage	IDT <sup>a</sup>	SD <sub>IDT</sub> <sup>b</sup>	TVG <sup>c</sup>	SD <sub>TVG</sub> <sup>b</sup>	TVG-IDT	n
		[ms]	[ms]	[ms]	[ms]	[ms]	[-]
[EMIm][SCN]	closed and dry	31.1	3.1	26.4	2.8	4.7	7
[EMIm][SCN]	open (10 months)	30.6	4.2	24.0	2.1	6.6	5
E5C	closed and dry (8 month)	13.4	1.5	12.4	1.4	1.0	6

<sup>a</sup> ignition delay time    <sup>b</sup> standard deviation    <sup>c</sup> time to vapour generation

applied. The IDT and TVG of the E5C fuel are compared to the previously reported IDT in table 5.6 or 5.10. The values are very similar. The difference is less than 0.6 ms. The storage did not affect the ignition behaviour of E5C.

### 5.2.4 Influence of cation structure

The anion of the IL is important to introduce the hypergolic behaviour [195]. But it is known for ionic liquids that the cation influences the ignition delay [189, 195]. For certain hypergolic ionic liquids, several cation structures have been screened. For example, [189, 195] found out that in terms of IDT and  $I_{sp}$ , unsaturated allyl side chains are preferable in terms of a shorter IDT for imidazolium-based ionic liquids. In this section, [BMIm][SCN] and [AMIm][SCN] were evaluated in the drop test chamber, and the results in terms of IDT are compared with [EMIm][SCN]. The structure of the different cations is shown in 5.11. [BMIm][SCN] was already described in part 1 of this chapter, but the ionic liquid was tested again in the drop test chamber.

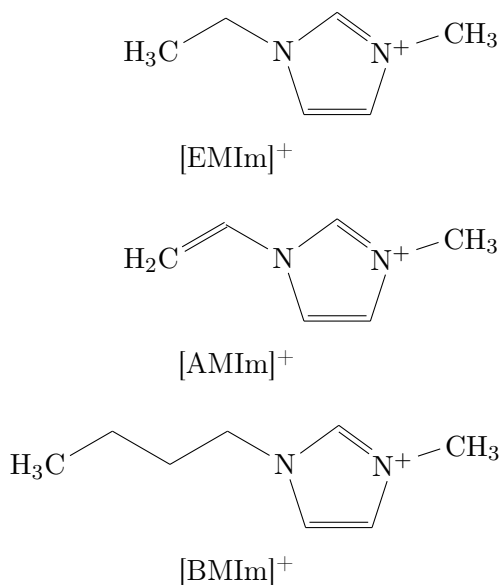


Figure 5.11: Different cationic structures

[AMIm][SCN] was purchased by *Iolitec GmbH* and specified to a purity of > 95 %. Two different configurations were tested. First, [AMIm][SCN] was used as received. Because it was suspected that water or other solvent residues were present at this specified purity, a sample was

dried for four hours at 80°C under vacuum using a rotary evaporator. The weight of the sample changed to 0.015 % during this procedure. However, both [AMIm][SCN] samples were tested. Further, two different amounts of copper thiocyanate (1 wt% and 5 wt%) were dissolved in the [AMIm][SCN] and also tested. The fuels are referred as A1C ([AMIm][SCN] + 1 wt% [Cu][SCN]) and A5C respectively.

Table 5.17: Drop test results of different cations

fuel	IDT <sup>a</sup> [ms]	SD <sub>IDT</sub> <sup>b</sup> [ms]	TVG <sup>c</sup> [ms]	SD <sub>TVG</sub> <sup>b</sup> [ms]	TVG-IDT [ms]	n [-]
[EMIm][SCN]	25.9	2.0	22.2	1.8	3.7	10
[BMIm][SCN]	59.6	3.7	52.7	4.0	6.9	8
[AMIm][SCN]	38.9	3.6	35.0	3.6	3.9	8
[AMIm][SCN] dry	39.5	3.1	36.1	2.8	3.4	5
A1C	21.3	1.2	19.6	1.5	1.7	6
A5C	16.9	0.5	16.5	0.5	0.4	5

<sup>a</sup> ignition delay time    <sup>b</sup> standard deviation    <sup>c</sup> time to vapour generation

The longest IDT has the [BMIm][SCN]. This ionic liquid was already tested and shown in 5.1. However, in the test series, where the initial temperature was 22 °C for the [BMIm][SCN], the IDT of [BMIm][SCN] is slightly longer than during the initial test campaign. This may be partly influenced by the temperature, which is not exactly known for the tests in part 1, and the different drop test setup configurations used in 5.1. At this initial temperature, [EMIm][SCN] has an IDT of about 26 ms, and the average IDT of [BMIm][SCN] is close to 60 ms, which is a factor 2 in the IDT. Also, the vapour phase reaction time is 6.9 ms for [BMIm][SCN], whereas [EMIm] has an average value of 4 ms at these conditions. The viscosity of [BMIm][SCN] at 22°C is 59.4 mPa s according to the measurements of Domańska et al. [216]. This is also almost three times higher than the viscosity of [EMIm][SCN] with 21.6 mPa s at the given temperature. The difference in the IDT is partly caused by the higher viscosity, which negatively influences the liquid interactions. Secondly, the interactions of the different side chains can negatively influence the ignition delay in the case of the butyl group.

The [AMIm][SCN] tests were conducted at an initial temperature of 25 °C. Also, reference tests with [EMIm][SCN] on the same test day under the same initial conditions were performed and are also listed in table 5.17. The ignition delay of [AMIm][SCN] and the dried sample are similar. However, the IDT of the pure [AMIm][SCN] is about 13 ms longer than the [EMIm][SCN]. The viscosities at 25°C are 23 mPa s for [AMIm][SCN] and 20.1 mPa s for [EMIm][SCN]. Consequently, the viscosities are not expected to influence the IDT to a high degree. The difference is also likely correlated to the different structures of the cation. In the case of hypergolic ionic liquids with WFNA, an allyl side chain positively affects the ignition delay time [189, 195]. For imidazolium thiocyanate ionic liquids and hydrogen peroxide, this does not apply. Further, work by Ricker et al. showed that for different cations structures, allyl groups have no positive impact on the IDT compared to ethyl functionality [155]. The vapour phase has a similar duration for [EMIm] and [AMIm][SCN].

The IDT is almost cut in half by adding 1 wt% of the copper thiocyanate to the fuels. For A5C, the IDT is slightly lower again. But these fuels stay behind the [EMIm] based fuels with the same copper additive in terms of IDT.

### 5.2.5 Reference test

To compare the performance of [EMIm][SCN], a hypergolic substance from literature, namely [EMIm][DCA], was tested. As described in 5.1 the dicyanamide ionic liquids are not hypergolic with hydrogen peroxide but with nitric acid. They were the first hypergolic ionic liquids identified in 2008 [128, 129]. [EMIm][DCA] was purchased by *Iolitec GmbH* and tested in our drop test chamber. In several references [31, 61, 66, 67, 128, 129, 189, 195, 217] drop tests with WFNA and DCA-based ionic liquids are conducted with a drop of fuel falling into the nitric acid. According to section 5.2.2, the falling drop of IL has produced significantly longer IDT for the pair  $\text{H}_2\text{O}_2$  / [EMIm][SCN] than our standard configuration. Therefore, for the first test, it was decided to test the combination WFNA / [EMIm][DCA] in our standard configuration. Surprisingly, no ignition was achieved when a drop of WFNA fell into the [EMIm][DCA] pool. About 30 ms after initial contact, brown-coloured vaporised decomposition products rose from the reacting mixture. The mixture also started to form bubbles and expelled smaller drops. When a second drop of fuel was added to the reacting mixture, no ignition occurred. Therefore, the components were switched, and a drop of IL was added to a WFNA pool. Out of 4 tests, only one ignition was observed after the initial contact of fuel and oxidiser. This ignition is shown in figure 5.12 and occurred 47 ms after initial contact. In the other cases, gaseous, brownish decomposition products rose from the reacting mixture 12 – 15 ms after the initial impact, but no ignition was observed. The ignition and flame propagation was very local around single drops of the reacting mixture that were expelled. Compared to this reference test, the [EMIm][SCN] and hydrogen peroxide combination provides a more reliable ignition, independent of the drop order or the amount of fuel and oxidiser.

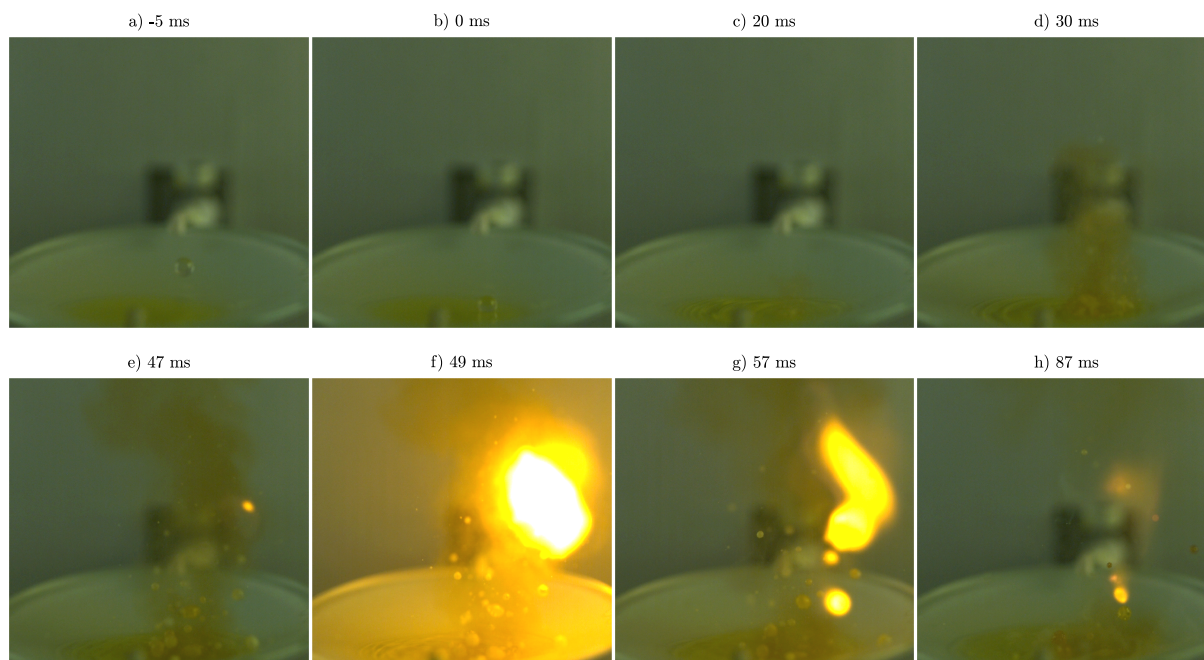


Figure 5.12: Ignition of [EMIm][DCA] and WFNA

## 5.3 Summary of the drop tests

In total, 902 drop tests were performed and analysed. Seven different ionic liquids were tested on hypergolic ignition with hydrogen peroxide. The thiocyanate ionic liquids have proven hypergolic ignition with  $\text{H}_2\text{O}_2$ . The ignition delay lies in the order of several 10 ms. It was shown that adding copper thiocyanate can reduce the ignition delay. The mixture of [EMIm][SCN] and 5 wt% [Cu][SCN] provides the shortest ignition delay time with 13 ms at ambient conditions. Therefore, the substance [EMIm][SCN] is chosen for further investigation as the most promising fuel candidate.

The following parameters of the drop test were varied to assess their potential impact on the hypergolic ignition:

- drop height
- drop order
- amounts of drop and pool
- surrounding medium
- initial pressure
- initial temperature
- $\text{H}_2\text{O}_2$  concentration

During those tests, thiocyanate ILs proved reliable ignitions. The ignition behaviour was also compared to a hypergolic reference substance known from the literature. The ignition of thiocyanate based IL and hydrogen peroxide proves to be much more robust.

The following dependencies were found:

- The drop height did not influence the IDT in the tested range
- A falling drop of fuel into a  $\text{H}_2\text{O}_2$  pool generates significantly higher ignition delays compared to a  $\text{H}_2\text{O}_2$  drop falling into a fuel pool
- Different amounts of drop and pool do not change the ignition delay
- The influence of Argon as an inert gas on the IDT was studied. In terms of the ignition delay, no significant change was observed.
- The ignition delay depends on the ambient pressure. The IDT increases at lower pressures. The influence was tested between 0.1 bar and 1 bar. [EMIm][SCN] does not ignite below 0.2 bar. E5C ignited down to 0.1 bar. At this pressure, the IDT of E5C was doubled compared to ambient conditions.
- It was found that the fuel's initial temperature significantly impacts the ignition delay in the drop tests. This is most likely related to the viscosity, which depends on temperature. Documenting the initial temperature of the ionic liquid based fuel is recommended. With elevated temperatures, the ignition delay can be significantly reduced.
- The  $\text{H}_2\text{O}_2$  concentration has an impact on the ignition delay. The ignition delay increases for lower hydrogen peroxide concentrations. Reliable ignitions were observed in tests with the lowest concentration of 78 %. The IDT for [EMIm][SCN] and E5C are about four times higher for the low concentration compared to  $\text{H}_2\text{O}_2$  with a concentration of 97 %.



- The shortest ignition delays were observed with [EMIm][SCN]; different ionic liquids with other cations, such as [AMIm][SCN] or [BMIM][SCN], have higher IDTs.
- The fuel E5C demonstrated repeatable ignition delays after storage for 10 months.

The conditions leading to the ignition in a drop test differ from a later application of the propellant in a rocket engine. Therefore, the following chapter will evaluate the possibility of ignition of [EMIm][SCN] based fuels with hydrogen peroxide under flowing conditions.

## 6 Injection test

The ignition characterisation of the previous chapter was conducted with a laboratory drop test, where single drops were brought together, and the reaction was observed. In an application of hypergolic propellants in a thruster, the propellant components are injected by an injector into the combustion chamber. Both components converge, and mixing occurs. Finally, the mixture reacts and ignites if the conditions are properly set. The injection of the propellant sets the conditions to achieve a fast, reliable ignition. This chapter is dedicated to investigating the ignition delay of the hypergolic propellant candidates under more relevant conditions, i.e. flowing conditions using injectors. A baseline injector was designed to evaluate the hypergolic ignition of different propellant configurations. Further, two more injectors were tested. In section 6.4, the influence of the ambient pressure on the ignition was investigated.

The presented tests were conducted in two different test campaigns. As described in chapter 3 the first campaign was with the atmospheric setup. The tests of the second campaign were conducted inside the vacuum chamber at M11.2 at atmospheric conditions and with lower ambient pressures.

### 6.1 Injector design

An impinging injector was chosen for the first ignition investigations due to its simple design. Moreover, impinging injectors are also widely used in hypergolic thrusters [2, 159–163]. A 2-on-1 or unlike triplet impinging injector design was selected because the maximum  $I_{sp}$  of our fuel candidate with 98 % hydrogen peroxide is around a ratio of oxidizer to fuel mass flow of 4, see 4.5. Therefore, a 1-on-1 impinging injector was not considered due to the high difference in the mass flows. A 2-on-1 injector is a better choice regarding the orientation of the injector orifices. The injector bores are located on one plane, and the development of the liquid sheet after impinging lies on a plane perpendicular to the orifice plane. Thereby, suitable optical accessibility was expected. The unlike triplet injector was designed with the provided correlation from Eleverum et al. for an impinging angle of 60° [218]:

$$\left(\frac{\dot{m}_{ou}}{\dot{m}_c}\right)^2 \frac{\rho_c}{\rho_{ou}} \left(\frac{A_c}{2A_{ou}}\right)^{1.75} = 0.66 \quad (6.1)$$

With the area of the central orifice  $A_c$ , the area of the outside individual orifice  $A_{ou}$ , the density of outer  $\rho_{ou}$  and the central  $\rho_c$  substance, the total mass flow through the outer  $\dot{m}_{ou}$  and central  $\dot{m}_c$  orifices. For the designed injector, the angle between the axes of the two outer orifices is 60°, the most common design for impinging injectors [159]. The angle between the central orifice axis and the outer orifices is 30°. The minimal orifice size was set to 0.5 mm, the lowest size that could be manufactured in-house. This size was chosen for the central fuel orifice, and considering a ROF of 4, the density of 98 % hydrogen peroxide (1430 kg/m<sup>3</sup>) and the pure ionic liquid (1120 kg/m<sup>3</sup>) results in an outer orifice diameter of 0.82 mm. Consequently, an orifice diameter of 0.8 mm was selected for manufacturing. For the injector orifice, a ratio of the length of the orifice  $L$  to the diameter  $d$   $L/d$  of 4 was picked so that a full flow can develop in the injector bore [159]. The impinging distance was 12 times the diameter of the oxidizer orifices to ensure good

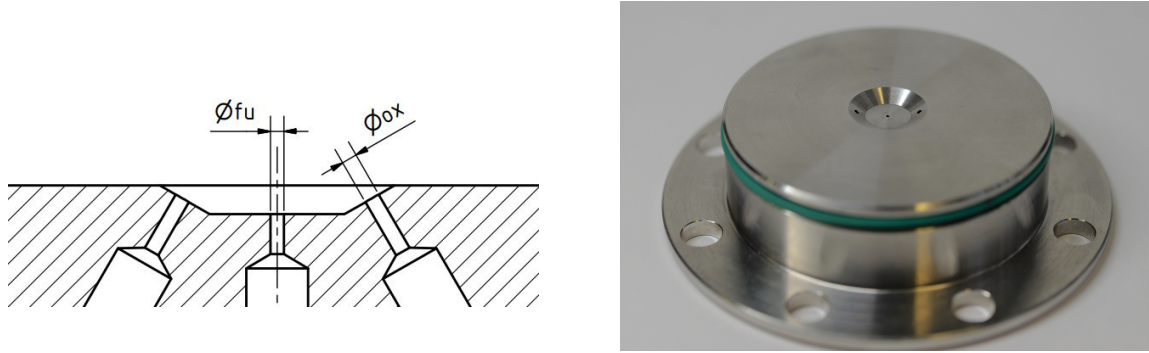


Figure 6.1: 2-on-1 Injector, left: drawing, right: picture

visibility on the single jets. The mass flows will be selected to reach injection velocities from 10-15 m/s, typical values for hypergolic thrusters [42]. A scheme and a picture of the injector are shown in figure 6.1; the drawing is appended in figure 9.4.

In addition to the 2-on-1 injector, other injectors were manufactured and tested: a 3-on-1 impinging injector and a swirl injector. These two injectors were developed by J. Witte during his master's thesis [179]. Details on the injectors can be found in the master's thesis. Further, the ignition behaviour of different fuels was investigated. An overview of the different fuels and injectors tested is given in 6.1.

Table 6.1: Test matrix with fuels and injectors

	Block 0	[EMIm][SCN]	E1C	E5C
2-on-1	x	x	x	x
3-on-1				x
swirl				x

## 6.2 Preparation

Before the first hit firing tests of the injectors, a calibration of the  $c_d$  value was conducted with cold flow tests.

### 6.2.1 Discharge coefficient calibration

The injectors were calibrated to determine the mass flow depending on the  $\Delta p$ . Especially of interest was the dependence of the tank's supply pressure on the mass flow through the injector because the tank supply pressure was the adjustable value at the test setup. Therefore, a 'global' discharge coefficient  $c_d$  value was determined with calibration tests. The calibration test used a calibration fluid such as water to simulate  $H_2O_2$  or a glycerol water mixture to simulate the ionic liquid. Water was used as a simulant for the oxidiser calibration. Water, or a mixture of glycerol and water in a ratio of 70 wt% to 30 wt%, was used for the fuel. This mixture has a viscosity of 23.1 mPa s at 20 °C [177], which is similar to the pure [EMIm][SCN] [50]. Also, the density of this mixture (1.18 g/cm<sup>3</sup>) is close to the pure [EMIm][SCN] (1.12 g/cm<sup>3</sup> at 20 °C) and therefore a suitable simulant.

The global  $c_d$  assumes a pressure reservoir and an injection orifice with a certain diameter. The injection orifice is the smallest dimension where the liquid has to flow through in the system. Therefore, the different pressure losses in the system between the pressurised fuel reservoir and the orifice are neglected and treated as a black box. It is assumed that the major contribution

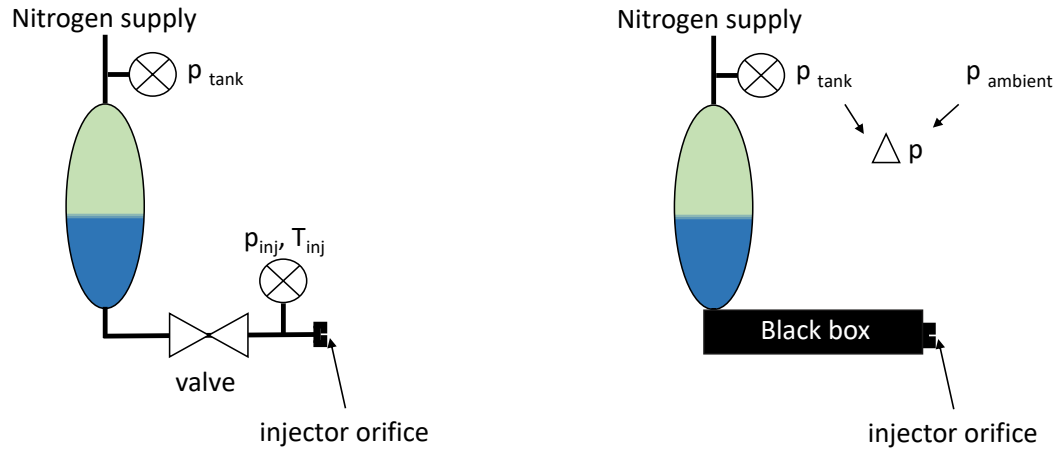
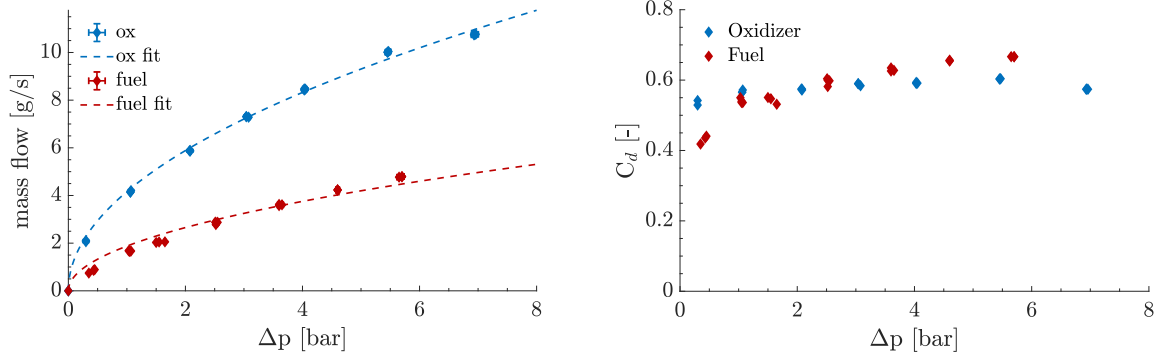


Figure 6.2: Discharge coefficient, left: real system, right: assumption

to the pressure loss is across the injection orifice. A scheme of this assumption is shown in figure 6.2. Only the supply pressure of the tanks can be set to a certain value, and hence, a corresponding mass flow results. Therefore, it stands to reason to have an estimation for the mass flow depending on the supply pressure.

Here, exemplary the calibration for the tests in section 6.3.2 for the 2-on-1 injector is shown. The calibration for the other injector configurations is in the appendix; see section 9.1. The calibration was conducted by filling the tank and lines until the injector, setting the desired pressure, and opening one of the flow control valves for 10 s (oxidizer) or 20 s (fuel). The simulant was captured in a beaker, and the weight difference before and after the test was determined. The average mass flow is the mass in the beaker divided by the opening time of the FCV. In figure 6.3 on the left side, the mass flow for different pressure differences between the fuel supply and ambient is shown. Every pressure step was repeated three times. The reproducibility was high for each point. The fit is a function with the square root of  $\Delta p$ , similar to equation (2.20). The fit is in good agreement with the actual measurements for the oxidiser. In the case of the fuel, the data points follow a different slope. With the mass flow and the pressure difference, the discharge coefficient can be calculated according to equation (2.20). The  $c_d$  dependent on the  $\Delta p$  is shown on the right side of figure 6.3. For the oxidizer, the  $c_d$  values are on one level for the different  $\Delta p$ . Therefore, the average value between 3 bar and 7 bar of  $\Delta p$  was used to calculate the operating points. The average  $c_d$  value was 0.589. For the fuel, the  $c_d$  values are not constant in the pressure range of interest caused by the fuel's high viscosity and the simulant. The viscosity generates relatively low Reynolds numbers: the Reynolds numbers in the injection orifice of the fuel range from 80 to 530. This means the flow is expected to be laminar or transitioning to a turbulent flow. The  $c_d$  can be assumed constant if the flow is fully turbulent [219]. This is not the case for the relatively high viscous fuel and simulant. Therefore, for calculating the mass flow of the fuel orifice, the actual  $c_d$  from 6.3 was taken. This also explains why the fuel's fit on the left of figure 6.3 differs from the slope of the data points. The calibration of the other injectors can be found in the appendix; see section 9.1.

Figure 6.3: Mass flow over  $\Delta p$  2-on-1 injector

### 6.3 Initial testing of green hypergolic fuels

Initial tests with the hypergolic fuel Block 0 were conducted before testing the novel ionic liquid fuels and hydrogen peroxide. The rationale behind this was to test a known alternative hypergolic fuel with hydrogen peroxide to gather first experience testing hypergols and the setup. Block 0 was chosen because extensive literature data is available [25, 26, 76], and the production is simple.

#### 6.3.1 Block 0

The very first tests with the hypergolic ignition test setup were conducted with the hypergolic fuel Block 0 and hydrogen peroxide. For the initial test, a 2-on-1 injector with a central fuel orifice diameter of 0.7 mm and two oxidizer orifices with 0.8 mm was used. The tests were described in [43].

Table 6.2: Block 0 operating condition and ignition delay time

$P_{\text{tank}}$ [bar]	oxidizer		$P_{\text{tank}}$ [bar]	fuel		ROF [-]	IDT [ms]
	$\dot{m}$ [g/s]	$v_{\text{inj}}$ [m/s]		$\dot{m}$ [g/s]	$v_{\text{inj}}$ [m/s]		
2	$12.5 \pm 0.4$	$8.8 \pm 1.1$	2	$4.4 \pm 0.4$	$12.4 \pm 1.2$	$2.9 \pm 0.3$	471.6
2.8	$16.8 \pm 0.6$	$11.8 \pm 1.4$	2.8	$5.7 \pm 0.5$	$16.3 \pm 1.6$	$2.9 \pm 0.3$	310.6
4.1	$22.1 \pm 0.8$	$15.5 \pm 1.9$	4.1	$6.3 \pm 0.5$	$17.8 \pm 1.8$	$3.5 \pm 0.3$	247.4
4.5	$23.5 \pm 0.8$	$16.4 \pm 2$	4.5	$6.4 \pm 0.5$	$18.1 \pm 1.8$	$3.7 \pm 0.3$	256.7
4.7	$24.1 \pm 0.9$	$16.9 \pm 2.1$	4.7	$6.3 \pm 0.5$	$17.8 \pm 1.8$	$3.9 \pm 0.3$	190

Table 6.2 displays the operating conditions and ignition delay time of the Block 0 tests. Different operating points with a targeted ROF of around 3 were tested. The ignition delay of Block 0 lies in the order of some 100 ms. The ignition occurred outside the field of view of the high-speed camera. After ignition, the flame propagated into the field of view. The long ignition delay is not very favourable for a smooth ignition of a combustion chamber. In literature, IDT values below 100 ms are reported at similar injection conditions but using a 1-on-1 injector [25, 26]. The difference could result from an unfortunate injector design or other parameters, which are not known at this stage. Pourpoint also mentioned that if "mixing [is] too efficient [it] prevents ignition" [26]. Because the promising hypergolic ionic liquid fuels were to be tested, no further attempt was undertaken to optimise the ignition of Block 0.

Table 6.3: Different operating points 2-on-1 injector during stationary conditions, tank supply pressure  $p_{\text{tank}}$ , mass flow  $\dot{m}$ , and injection velocity  $v_{\text{inj}}$  for oxidizer and fuel; resulting ROF

	oxidizer			fuel			ROF
	$p_{\text{tank}}$ [bar]	$\dot{m}$ [g/s]	$v_{\text{inj}}$ [m/s]	$p_{\text{tank}}$ [bar]	$\dot{m}$ [g/s]	$v_{\text{inj}}$ [m/s]	
OP 1	4.1	$17.6 \pm 0.6$	$12.3 \pm 1.5$	2.5	$2 \pm 0.2$	$8.7 \pm 1.2$	$8.9 \pm 1.1$
OP 2	5.2	$20.5 \pm 0.7$	$14.3 \pm 1.8$	3.5	$2.8 \pm 0.3$	$12.5 \pm 1.7$	$7.2 \pm 0.9$
OP 3	6.8	$24.0 \pm 0.9$	$16.8 \pm 2.1$	4.5	$3.5 \pm 0.4$	$15.5 \pm 2.2$	$6.8 \pm 0.8$
OP 4	8.5	$27.3 \pm 1.0$	$19.1 \pm 2.3$	5.5	$4.2 \pm 0.5$	$18.7 \pm 2.6$	$6.5 \pm 0.8$
OP 5	10.0	$29.9 \pm 1.1$	$21.0 \pm 2.6$	6.5	$4.7 \pm 0.5$	$21.0 \pm 2.9$	$6.3 \pm 0.7$

### 6.3.2 E5C

In this section, E5C was tested with two different impinging injectors. The test results are shown and discussed. The tests were conducted within the master's thesis of J. Witte [179].

#### 2-on-1 impinging injector

The first test with E5C was conducted using the 2-on-1 impinging injector described above. Several operating points (OP) were tested. The operation points depend on the pressure in the tanks. As a result of the pressure in the tanks, a certain mass flow will develop after the opening of the flow control valve. Therefore, the initial tank pressures of fuel and oxidiser were set before a test. The different operating points with the corresponding tank pressure, the calculated mass flow and injection velocity are shown in table 6.3. The mass flow is determined with the derived  $c_d$  values during the calibration tests and the tank supply pressure. The injection velocity is the mass flow divided by the cross-section of the orifice(s) and the density of the component, see equation (2.19). These values must be regarded as a rough estimation of the conditions during the stationary operation of the injection setup. Thus, the mass flow and injection velocity give the order in which the operation is conducted. In contrast, the ignition process occurs during the transient stage of operation, and the actual conditions during the ignition are not precisely known. The operating points all have a lean ROF due to an error in the conversion from the calibration test to the hot firings. The changing density between hydrogen peroxide and the simulant water was not considered during the initial determination of the operating points. At a given supply pressure, hydrogen peroxide's mass flow is higher than water's. Unfortunately, this error was detected after the tests were conducted and the data was analysed. The mistake shifted the ROF to values of 6.8 to 7.5. A more favourable ROF would have been around 4 due to the maximum  $I_{\text{sp}}$  close to this ROF. Nevertheless, the results are valuable because the ignition occurs during the highly transient conditions of the injection. During the transient stage, exact measurements of mass flow, injection velocities, and injection pressures are not very precise, but qualitative conclusions can be drawn.

A test with a successful ignition (test run 2019\_2on1\_HTP\_ECUSCN\_005\_001) of E5C in the HIT is shown in figure 6.4. Two high-speed cameras were utilised to record the test. As described in 2.3 the cameras watch the injector from two angles. The coloured high-speed camera (frames a) to g)) looks upright at the spray sheet developing when the flows of the oxidiser meet. This layout facilitates the recording of the spray sheet and the vapour generation and ignition being detected. The view of the monochrome camera is perpendicular to the spray sheet and looks at the plane where the three bores of the 2-on-1 impinging injectors are. With this view, the contact of fuel and oxidiser can be determined. Behind the glass cylinder are white LED

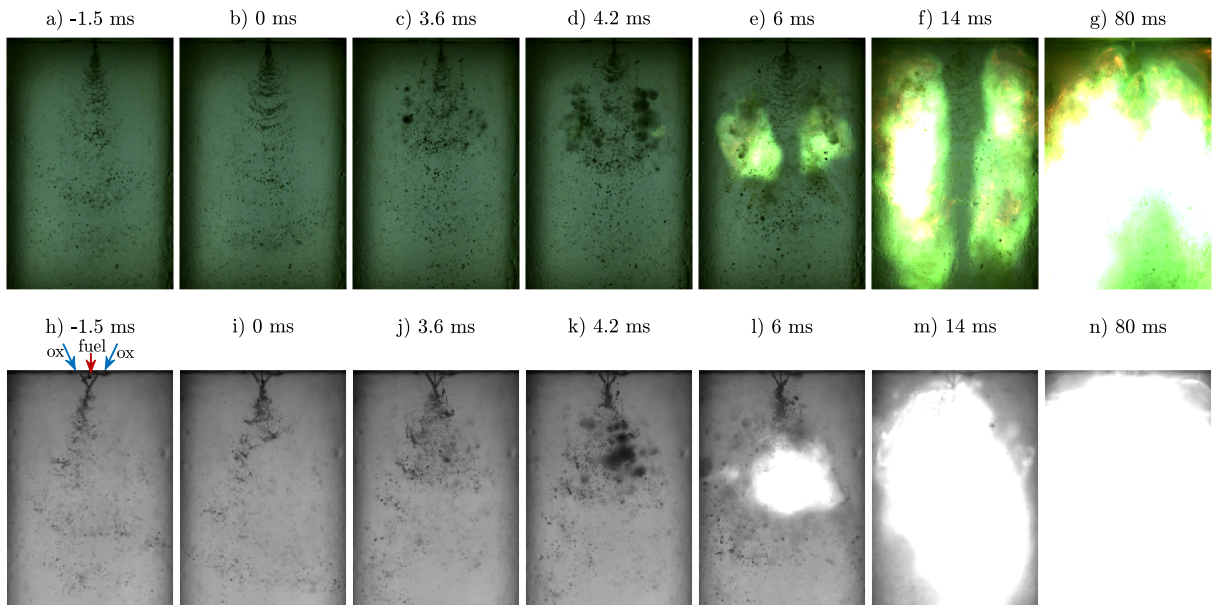


Figure 6.4: Ignition of E5C under flowing condition

panels located to illuminate the background. This facilitates the detection of the spray, jets, drops, and vapour generation. The flame emission can still be safely detected because it is much brighter than the LED panels.

The first frames (a) and h)) show the spray 1.5 ms before contact. The two jets of the oxidizer already met and produced smaller irregular drops. The spray sheet has not been developed yet because of the transient process. In frame h) between the oxidizer jets, the start of the fuel jet can be seen before the first contact. Frames b) and i) show the first contact of the fuel and oxidizer jets. This is also defined as 0 ms similar to the drop tests. After this, fuel and oxidizer start to mix, and at 3 ms, the first vapour generation becomes visible. The frames c) and j) display vapour around single drops shortly after the initial generation. Frames d) and k) show the state shortly after ignition at 4 ms. The initial flames are obvious in frame d) but can hardly be spotted in frame k). The initiation of the flame occurs in the vapour clouds of the border area of the spray sheet on both sides. After this, the flame propagates in the vapour phase frames (e)/f) and l)/m)) and a sustained combustion with a bright, green flame can be observed g) and n). The flame is still burning after 600ms after initial contact.

Figure 6.5 shows the pressure slopes during the previously presented test. The operating conditions correspond to OP5 with 10.1 bar oxidiser supply pressure (red / TNK\_O) and 6.5 bar fuel supply pressure (green / TNK\_F). The feed line pressures are also displayed for fuel (blue / FDL\_F) and hydrogen peroxide (black / FDL\_O). The feed line pressures are measured downstream of the flow control valve and upstream of the injector. The dotted vertical lines represent the moments when the control signal to the opening of the oxidiser valve was given, which is defined as 0s in this graph. Also, the fuel valve's opening signal and the ignition moment are marked. When the signal for the opening of the oxidiser valve is given, the pressure starts to rise about 30 ms later. This is caused by the delay of the signal commanding a relay to power the solenoid of the valve and the inertia of the plunger until it is mechanically opened. The fuel valve is commanded with a delay of 70 ms. The pressure also starts to rise 30 ms later. The delay of the opening commands of fuel and oxidiser was chosen to ensure a developing and



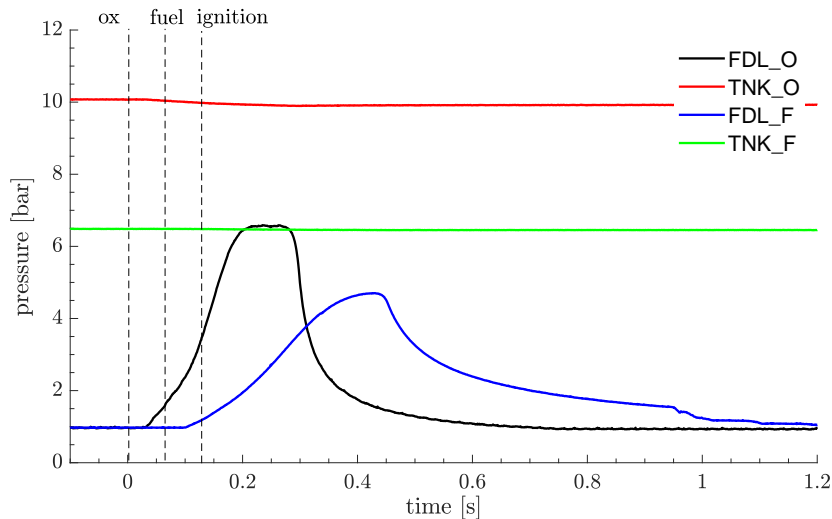


Figure 6.5: Pressure slopes HIT test

distinguishable flow of the oxidiser during the start-up. If the oxidiser starts to flow, a distinct determination of the initial contact of fuel and oxidiser can be assured. This is necessary because a two-phase flow is observed in the first milliseconds when the oxidiser starts. This would not allow a clear determination of the first contact of fuel and oxidiser. Ignition occurs 124 ms after the oxidiser valve is triggered. The moment of ignition is determined with the time stamp of the high-speed camera, which is triggered 100 ms before the ox valve. At the instance of ignition, the fuel pressure has only increased to 1.14 bar. Also, the oxidiser pressure is still increasing. This shows the highly transient character of hypergolic ignition. After the initial ignition, the flame propagates and continuously burns for 600 ms. The oxidiser reaches a plateau of 6.6 bar after 0.2s. The oxidiser pressure decreases after 0.28s because the valve is commanded to close. The transient of the fuel needs more time and reaches its maximum after 0.43s. After this, the pressure decreases again because the valve was commanded to close. The pressure decrease in the fuel is much slower than the oxidiser's. This behaviour may be related to the relatively high viscosity of the fuel and the small diameter of the injector and tubing. With this configuration, stationary conditions were not achieved in the short-time ignition tests. This was also not the aim of this investigation since the interest lies in the ignition delay.

The mass flow corresponds to the square root of the pressure difference in the injector, assuming a constant discharge coefficient. In this transient test, the assumption of a constant discharge coefficient is not valid due to the low-pressure differences and low resulting injection velocities. But a quantitative statement on the behaviour can be made. In addition, the ignition occurs in a very lean environment in this test. The pressure increase in the fuel is only 0.14 bar when ignition occurs, whereas the oxidizer pressure has already reached 3 bar. Figure 6.6 shows the different flame appearance during the test. The time stamps refer to the oxidizer valve opening signal. The pressure of the oxidizer increases faster than the fuel pressure, which means that the increase in oxidizer mass flow is also higher than for the fuel. Thereby, the mixture gets leaner, and the ROF rises. After the oxidizer reaches its pressure plateau, the rise in pressure of the fuel continues, which increases the fuel mass flow. Consequently, the ROF decreases again. At the plateau, the flame at 250 ms appears with a bright heart-shaped core, see figure 6.6 a). On top of the flame, the spay sheet is distinguishable. When the oxidizer valve closes, the oxidizer mass flow decreases, decreasing the ROF. During this, the bright area of the flame gets more intense, and the flame can propagate closer to the injector, see b) and c). The higher brightness could be related to the decreasing ROF, which passes through the stoichiometric conditions and



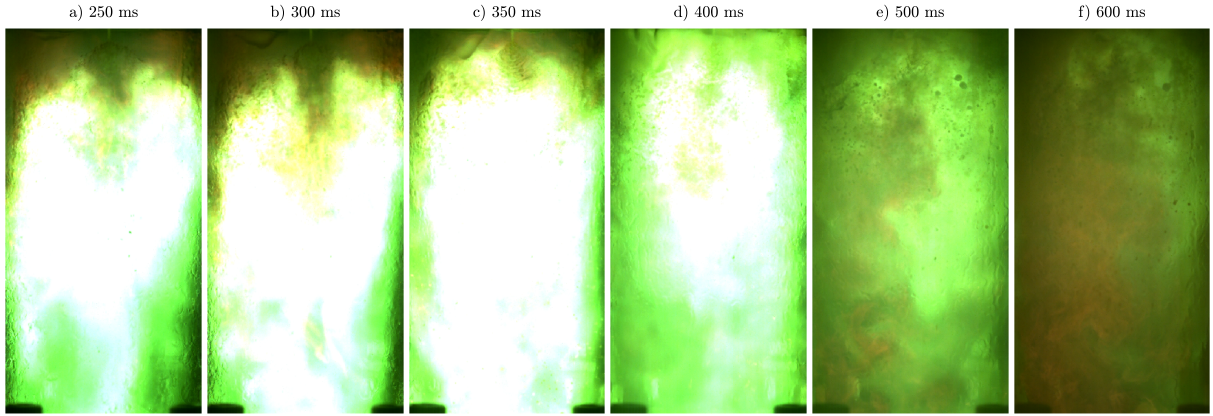


Figure 6.6: Flames during combustion, times from ox valve signal

Table 6.4: Ignition delay at different operating points, 2-on-1 injector, E5C 96.7 % H<sub>2</sub>O<sub>2</sub>

	IDT	SD <sub>IDT</sub>	TVG	SD <sub>TVG</sub>	IDT-TVG	n
	[ms]	[ms]	[ms]	[ms]	[ms]	[-]
OP 1	7.8	2.6	6.7	2.5	1.1	3
OP 2	7.4	0.7	6.4	0.7	1.0	3
OP 3	6.9	1.5	5.6	1.3	1.3	4
OP 4	5.6	1.4	4.6	1.2	1.1	4
OP 5	4.7	0.9	3.8	0.9	0.9	3

ends up in fuel-rich conditions. The rich flames in e) and f) appear less bright, and orange flame structures are visible. Through the whole ROF variation, the combustion is continuous and robust.

Table 6.4 lists the IDT, TVG and vapour phase duration of the different operating points and the 2-on-1 impinging injector. The tests were conducted at ambient temperatures between 22 °C and 28 °C. Each operating point was repeated at least three times. In total, 21 Tests were conducted. Ignition and continuous combustion were achieved in all tests. To the author's knowledge, these are the first successful hypergolic ignition tests with an injector setup and a hypergolic ionic liquid as fuel with hydrogen peroxide as oxidizer. For all operating points, the average ignition delay is below 10 ms. Further, with increasing pressure levels, the IDT decreases. The duration of the vapour phase reaction leading to the ignition is around 1 ms for all operating points.

The IDT in the injector tests is shorter for all operating points than the drop tests at similar ambient temperatures with 13 ms. The reason is that in the drop tests, the two components are brought into contact by dropping one component into a pool of the other component. In the baseline configuration, the falling drop reaches an impact velocity of about 1 m/s. In contrast, the injection velocities of the investigated operating points are between 10 and 20 m/s; see table 6.3. Therefore, the components have more kinetic energy when they meet. Besides, the vapour phase duration is almost similar in the different cases to the one in the drop tests. This indicates the reason for the shorter ignition delay lies in the liquid phase interactions. The injection of the components facilitates the mixing process. Therefore, mixing the two components is accelerated

at higher pressure levels, which also results in higher injection velocities. This leads to a faster ignition. The investigated 2-on-1 impinging injector is suitable for fast and reliable ignition of the hypergolic fuel E5C and enables sustained combustion over a broad range of ROF.

### 3-on-1 impinging injector

A second injector was designed and tested with E5C. The injector was designed within the master's thesis by J. Witte [179]. Table 6.5 lists the different operating points. These operating points were chosen to achieve an ROF of 4 to 4.5 under stationary conditions. It must be mentioned that these conditions are not achieved before the propellant ignites. Compared to the previous section, the injection velocities of the oxidizer are lower. This is a consequence because of a different construction of the 3-on-1 injector. It has a lower global  $c_d$  value. This is mainly caused because three holes with a smaller diameter generate a higher pressure drop than the two oxidizer bores of the 2-on-1 injector. The fuel orifice has the same diameter for both injectors, and the mass flow and injection velocities are similar for the two injectors. Slight variations result from a different lining configuration.

Table 6.5: Different operating points 3-on-1 injector during stationary conditions, tank supply pressure  $p_{\text{tank}}$ , mass flow  $\dot{m}$ , and injection velocity  $v_{\text{inj}}$  for oxidizer and fuel; resulting ROF

	oxidizer			fuel			ROF [-]
	$p_{\text{tank}}$ [bar]	$\dot{m}$ [g/s]	$v_{\text{inj}}$ [m/s]	$p_{\text{tank}}$ [bar]	$\dot{m}$ [g/s]	$v_{\text{inj}}$ [m/s]	
OP 1	5.2	$13.4 \pm 0.4$	$9.5 \pm 1.9$	4	$3.1 \pm 0.4$	$13.7 \pm 1.9$	$4.3 \pm 0.5$
OP 2	5.2	$13.4 \pm 0.4$	$9.5 \pm 1.9$	5.2	$3.7 \pm 0.4$	$16.2 \pm 2.2$	$3.7 \pm 0.4$
OP 3	6.8	$15.8 \pm 0.5$	$11.1 \pm 2.3$	4.8	$3.5 \pm 0.4$	$15.4 \pm 2.1$	$4.5 \pm 0.5$
OP 4	7.4	$16.6 \pm 0.5$	$11.7 \pm 2.4$	6.5	$4.2 \pm 0.5$	$18.6 \pm 2.6$	$4 \pm 0.5$
OP 5	8.4	$17.8 \pm 0.5$	$12.6 \pm 2.6$	5.7	$3.9 \pm 0.4$	$17.2 \pm 2.4$	$4.6 \pm 0.5$
OP 6	8.4	$17.8 \pm 0.5$	$12.6 \pm 2.6$	7.3	$4.5 \pm 0.5$	$19.9 \pm 2.8$	$4 \pm 0.5$
OP 7	10	$19.6 \pm 0.6$	$13.9 \pm 2.8$	6.5	$4.2 \pm 0.5$	$18.6 \pm 2.6$	$4.7 \pm 0.5$

Snapshots of the coloured high-speed camera during a test at operation point 6 are shown in figure 6.7 (006\_001). Further, in figure 6.8, different pressure slopes of this test are shown: feed line pressure of oxidizer (FDL\_O) and fuel (FDL\_F) downstream of the flow control valve and tank supply pressure of oxidizer (TND\_O) and fuel (TNK\_F). The opening signal of the oxidizer valve is defined as 0 for the displayed time reference in both figures. The opening signal of the oxidizer and fuel valve and the ignition time are marked in figure 6.8 with the dashed lines. The fuel valve signal has a programmed delay of 30 ms to ensure a developed flow of the hydrogen peroxide so that clear detection of the first contact between fuel and oxidizer is possible. The fuel and oxidiser supply pressures are similar to the test previously presented. However, due to the different configurations of the injectors, the oxidizer mass flow is lower, and the targeted ROF is achieved during stationary conditions.

Frame a) of figure 6.7 at 50.7 ms shows the initial contact of fuel and oxidizer. The generated vapour can be detected in the upper quarter of the frame b). At 56.1 ms, the initial ignition was observed, and the propagating flame is displayed in frame c). After the ignition, the flame propagated and continuous combustion is observed; see frames d) to f). The stationary feeding conditions are reached for fuel and oxidizer, and a bright greenish-yellowish flame can be seen in frame f). The presented test has an ignition delay of 5.4 ms and a liquid reaction phase of 4.7

ms. The ignition occurs during the transient phase, where the pressure and mass flow rise. The rising pressure gradients are steeper compared to figure 6.5. This is caused by a different lining configuration.

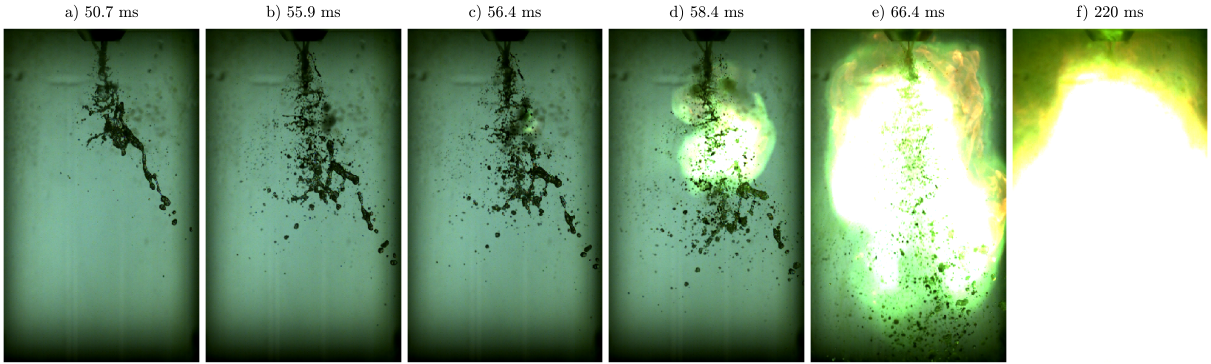


Figure 6.7: Ignition of E5C and H<sub>2</sub>O<sub>2</sub> with 3-on-1 injector times from ox valve signal

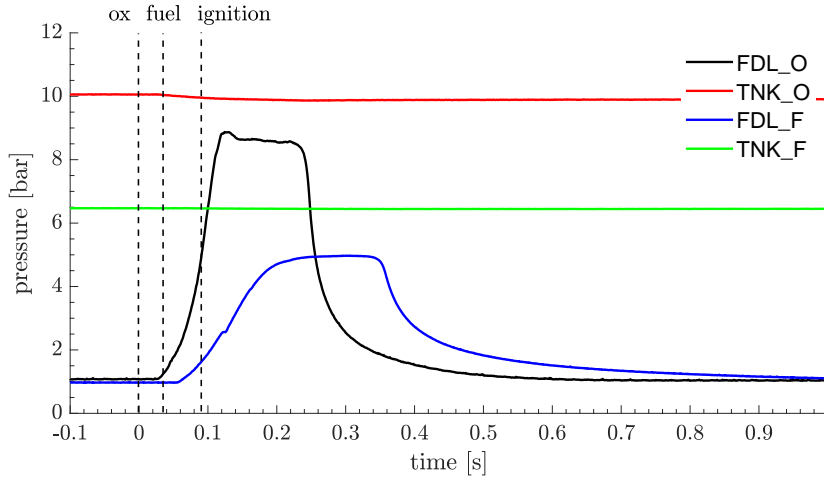


Figure 6.8: Pressure of E5C and H<sub>2</sub>O<sub>2</sub> with 3-on-1 injector times from ox valve signal

Table 6.6: Results of ignition tests with different operating points 3-on-1 injector

	IDT	SD <sub>IDT</sub>	TVG	SD <sub>TVG</sub>	IDT-TVG	n	remark
	[ms]	[ms]	[ms]	[ms]	[ms]	[-]	
OP 1	6.8	-	5.6	-	1.2	1	
OP 2	8.3	1.2	7.3	1.1	1.0	2	
OP 3	8.1	0.8	6.8	0.8	1.3	2	
OP 4 a	11.6	4.4	10.5	4.0	1.1	2	
OP 4 b	5.9	-	4.5	-	1.4	1	TNK-O at 9.2 bar
OP 5 a	7.5	-	6.7	-	0.8	1	standard
OP 5 b	12.0	1.4	9.8	0.5	2.2	2	fuel lead
OP 6	7.1	1.2	5.2	1.4	1.9	2	
OP 7	5.7	0.2	4.8	0.1	0.9	4	

Table 6.6 displays the results of the single tests performed with the 3-on-1 injector in terms of average IDT, TVG and vapour phase duration. Two different conditions were conducted at some operating points, such as for OP 3. Two tests were conducted with a fuel lead of 40 ms

and one test with the standard configuration. For OP 4, one of the tests was conducted with a misset oxidizer tank pressure (OP 4 b). For this test, oxidizer mass flow and injection velocity at stationary conditions would be expected at 18.7 g/s and 13.2 m/s. This would result in an ROF of 4.5.

Regarding IDT, most tests show a shorter IDT than the drop tests. The shortest IDT was achieved for OP 7, which has the highest supply pressures. Further, this operating point was repeated four times with good reproducibility. Other clear trends cannot be drawn because only a few repetitions were made. For OP 5, the ignition delay seems higher for the fuel lead operation than in the standard configuration. The two repetitions of the OP 4 differ in terms of ignition delay. The two tests had IDTs of 16 ms and 7.2 ms. The cause of the long IDT is not known. This test is regarded as an outlier. The duration of the vapour phase reaction until ignition is, for most of the tests, around 1 ms, which is similar to the results of the drop test and the 2-on-1 injector tests.

The 3-on-1 injector produces reliable ignitions and sustained combustion. The IDTs tend to be shorter than drop test values.

## 6.4 Second test campaign: fuel screening and low pressure ignition verification

The second test campaign was conducted inside the vacuum chamber of the M11.2. Hence, adjusting the ambient pressure inside the vacuum tank before the ignition test was possible. In contrast to the previously conducted injection test in this configuration, the propellant is sprayed into the open volume of the vacuum chamber. There is no confinement around the spray to avoid residues of the propellant contaminating the glass cylinder and blocking the view. Because the setup is inside the vacuum chamber, there is no access to the combustion chamber after every test run. The lining was reconfigured for this test series.

In the present configuration, three different fuels were tested:

- E5C
- E1C
- [EMIm][SCN]

For E5C, the impact of the ambient pressure on the IDT was investigated, and results will be presented. Furthermore, an ignition verification under flowing conditions for E1C was conducted, and the influence of the ambient pressure on the IDT was screened. In the end, an ignition verification of the pure [EMIm][SCN] at different operation points was conducted. All tests used the 2-on-1 impinging injector. Additionally, the ignition behaviour of a new injector configuration, namely a swirl injector, was tested with E5C. The tests investigating E5C and E1C with variation of the initial pressure were conducted within the master's thesis of J. Scholl [213].

### 6.4.1 E5C ambient pressure variation

E5C with 96.5 % hydrogen peroxide was tested by applying the 2-on-1 injector. This test series aimed to evaluate the ignition delay of E5C in a reduced pressure environment. At first, two different operating points were defined, and ignition tests were conducted at ambient pressure. The operating conditions for fuel and oxidizer during stationary operation are displayed in table 6.8. A ROF between 4 and 5 was targeted for this test series. The second operation point was chosen for the ambient pressure variation. The operation point OP 2a was only applied to the ambient pressure of 500 mbar because reducing the initial pressure on the pressure set in the

tank was not considered. For the lower ambient pressures, the tank pressure was corrected. Four reduced initial pressure steps were investigated, varying from 500, 100, 50, and 25 mbar.

Table 6.7: Operation points for tests with E5C and 2-on-1 injector at different ambient conditions,  $\Delta p$  pressure difference from tank to ambient,  $v_{inj}$  calculated injection velocity of the jet and resulting ROF

	oxidizer			fuel			ROF [-]
	$\Delta p$ [bar]	$\dot{m}$ [g/s]	$v_{inj}$ [m/s]	$\Delta p$ [bar]	$\dot{m}$ [g/s]	$v_{inj}$ [m/s]	
OP 1	6.0	$20.4 \pm 0.7$	$18.7 \pm 2.3$	5.4	$5 \pm 0.5$	$22.1 \pm 3$	$5.4 \pm 0.6$
OP 2	3.5	$26.7 \pm 0.9$	$14.3 \pm 1.8$	3.2	$4.3 \pm 0.5$	$19.1 \pm 2.6$	$4.7 \pm 0.5$
OP 2a	4.0	$21.8 \pm 0.8$	$15.3 \pm 1.9$	3.7	$4.6 \pm 0.5$	$20.5 \pm 2.8$	$4.7 \pm 0.5$

Table 6.8: Results of ignition tests with E5C and 2-on-1 injector at different pressure environments and operating conditions

	initial pressure [mbar]	IDT [ms]	$SD_{IDT}$ [ms]	TVG [ms]	$SD_{TVG}$ [ms]	IDT-TVG [ms]	n [-]
OP 1	987	6.6	0.8	5.0	0.3	1.6	2
OP 2	978	5.9	1.0	4.6	1.0	1.3	3
OP 2a	500	12.9	3.6	9.6	2.7	3.3	4
OP 2	100	25.0	1.3	7.3	1.1	17.7	4
OP 2	50	<i>38.8</i>	3.6	6.0	0.7	32.9	4
OP 2	25	<i>337.6</i>	76.2	7.0	1.9	330.6	3

Table 6.8 displays the results of the injection tests in terms of IDT, TVG and their difference with the according standard deviations. The value of the IDT in italic numbers for the two lowest pressures indicates that the initial ignition was not seen on the section recorded with the high-speed camera. The ignition took place below the field of view. The IDT is taken from the first sign that a flame is propagating, e.g., the flame is entering the field of view, or a glow of the flame illuminates the observed section. In those cases, the actual IDT is lower than the determined values, but the difference is expected to be in the order of several milliseconds. The trend of increased IDTs at lower pressure can be seen.

The IDT of operation points 1 and 2 are slightly different. Considering the low number of repetitions for OP 1 at this point, no difference in terms of IDT between the two configurations is expected. For better comparison with other fuels tested within this test campaign, OP 2 was chosen for further tests. Compared to the results of the initial tests, the ignition delay times are in the same order. A detailed comparison of the two test series is difficult due to the different configurations of the hypergolic injection setup. This leads to changes in the transient behaviour after the fuel and oxidizer valves are opened. Further, the spray is no longer confined by the glass cylinder, and the ROF is much closer to the theoretical  $I_{sp}$  optimum value. Ignition was achieved during all tests with lower initial pressures, and the IDT increased with decreasing pressure in the vacuum chamber. The highest IDT value is achieved at the lowest pressure level, with an average ignition delay of 337.6 ms. Tests with lower pressures were not conducted because ignition delays in the order of hundreds of milliseconds are not considered as desired. It can be expected that the limit, where ignition is not achieved any more, is close to 25 mbar because of the high increase of IDT between 50 and 25 mbar. Further tests at lower pressure also did not seem very useful because the spray behaviour of the oxidizer was very irregular. The

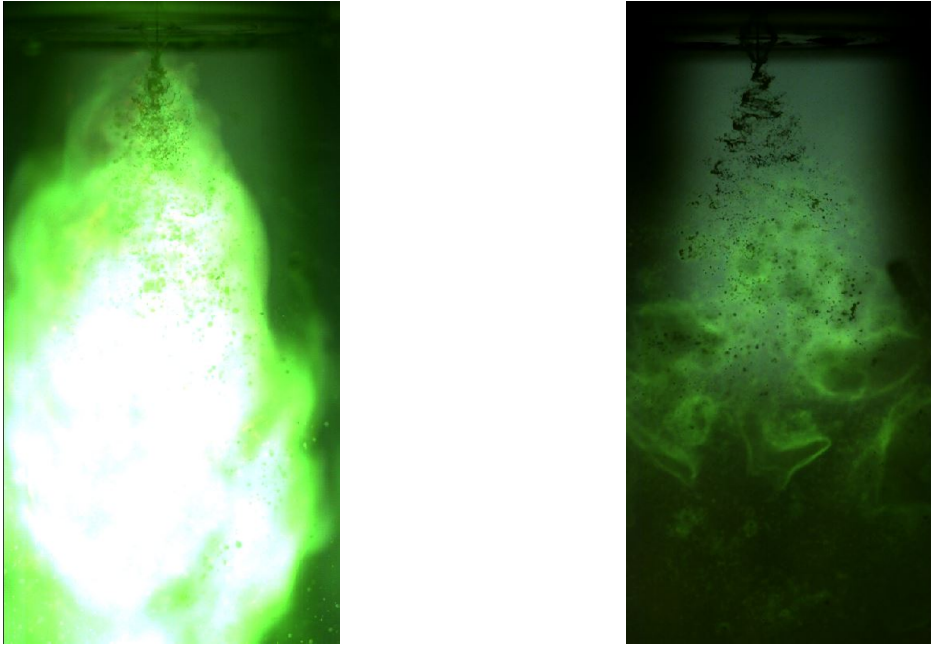


Figure 6.9: Flame during stationary condition at different pressures left: ambient pressure, right: 50 mbar

jets were disturbed by numerous gas bubbles resulting from the low-pressure environment and the occurrence of outgassing.

The TVG and the duration of the vapour phase reaction behave differently than the IDT. The TVG is highest at the pressure level of 500 mbar. For lower pressures, the TVG decreases again. The tests at 500 mbar have relatively high standard deviation. But compared to the increase of the IDT, the TVG stays at one level for the tested pressures below ambient pressure. In contrast, the average vapour phase reaction time increases with every pressure step. The vapour is generated, and the expansion of the vapour is faster compared to the ambient conditions. Because of the expansion, the density is lower, and a longer time is needed for the reacting substances to reach ignition temperature. This leads to a significant extension of the vapour phase reaction time.

Some aspects of the injection tests at reduced pressures differ from the drop tests under similar conditions; see figure 5.6. No significant change in IDT between ambient and 400 mbar was observed in the drop tests. The IDT in the drop tests increased by 10 ms at 100 mbar compared to ambient pressure. The injector tests show an increase of the IDT to 25 ms at 100 mbar, which is more than a factor of 4 compared to the IDT at ambient pressure. However, the TVG in the drop tests was consequently reduced with lower pressures.

The flame structure is different for the lower initial pressures. Figure 6.9 shows a flame at 1 bar (left) and a flame at 50 mbar (right). In those snapshots, the injection pressures have reached stationary conditions. The ambient flame is very bright, and some parts of the picture are overexposed. The flame starts to propagate close to the conjunction point of the injector jets. The flame at the reduced pressure is less bright. Therefore, the internal structure of the flame is visible. The injector jets decay into smaller drops after the conjunction point. A green flame around the drop can be seen some distance below the conjunction point. In addition, some drops are expanding and form large clouds. Those clouds have a green flame on their surface. The gas and vapour, of which the cloud consists, are consumed by the flame until the cloud disappears.



Table 6.9: Operation points for tests with E1C and 2-on-1 injector at different ambient conditions,  $\Delta p$  pressure difference from tank to ambient,  $v_{inj}$  calculated injection velocity of the jet and resulting ROF

	oxidizer			fuel			ROF [-]
	$\Delta p$ [bar]	$\dot{m}$ [g/s]	$v_{inj}$ [m/s]	$\Delta p$ [bar]	$\dot{m}$ [g/s]	$v_{inj}$ [m/s]	
OP 1	3.5	20.4 ± 0.7	14.3 ± 1.8	3.2	4.5 ± 0.5	20 ± 2.7	4.5 ± 0.5
OP 1a	4	21.8 ± 0.8	15.3 ± 1.9	3.7	3.7 ± 0.4	16.4 ± 2.2	5.9 ± 0.7
OP 2	6	26.7 ± 0.9	18.7 ± 2.3	5.4	5.3 ± 0.6	23.3 ± 3.1	5.1 ± 0.6
OP 3	8	30.9 ± 1.1	21.6 ± 2.7	7.2	5.7 ± 0.6	25.1 ± 3.4	5.4 ± 0.6

Table 6.10: Results of ignition tests with E1C and 2-on-1 injector at different ambient conditions and operating conditions

	initial pressure [mbar]	IDT [ms]	SD <sub>IDT</sub> [ms]	TVG [ms]	SD <sub>TVG</sub> [ms]	IDT-TVG [ms]	n [-]
OP 1	978	15.0	3.8	10.9	2.8	4.1	4
OP 1	N <sub>2</sub> @ 978	11.8	3.3	8.1	3.2	3.8	3
OP 2	978	30.7	9.4	15.6	4.4	15.1	3
OP 3	978	10.3	0.2	6.1	0.3	4.2	3
OP 1a	500	27.0	3.3	16.1	5.0	10.9	4
OP 1	100	55.5	4.0	13.7	3.6	41.8	3
OP 1	50	128.5	29.4	9.5	1.5	118.9	4
OP 1	27	-	-	-	-	-	2

#### 6.4.2 E1C pressure variation

E1C was tested with 96.5 % hydrogen peroxide with the 2-on-1 injector. The objective of this investigation was the ignition verification of E1C under flowing conditions, as well as the ignition behaviour in a reduced-pressure environment. Four operation points were investigated, and their parameters are shown in table 6.10. OP 1, OP 1a, and OP 2 are similar to the operation points previously reported for the E5C tests. OP 3 has a higher pressure difference and, hence, higher mass flows. After the successful ignition verification, tests under a reduced ambient pressure were conducted. Like the E5C tests, OP 1 and OP 1a were used during the pressure variation. Additionally, several tests were conducted in an inert nitrogen atmosphere at ambient pressure to investigate whether ambient air influences the ignition delay time.

The results of the ignition test are displayed in table 6.10. At ambient pressure, the ignition with OP 1 was successful. The average ignition delay was 15 ms, and the average TVG was 10.9 ms. When the supply pressure level was increased for OP 2, an IDT of 30.7 ms was achieved, and for OP 3, an IDT of 10.3 ms resulted. The high IDT at OP 2 was not expected. But during the tests, shortly after the tests at OP 2, the fuel bore was blocked. It is likely that some particles accumulated in the injector over several tests, influencing the fuel mass flow at OP 2. Also, the high-speed videos show that the fuel jet seems weaker in those tests. This contrasts with the higher pressure level because one would expect a higher mass flow and a strong fuel jet. The fuel feed line pressure evaluation also shows different behaviours in the transient phases. In the test data, the pressure decay after the closing of the valve is delayed. This argues for a partially blocked fuel orifice, which changed the pressure transients. Therefore, the IDT and TVG values of OP 2 are expected to not correspond to those that would have been achieved under nominal

operating conditions. It is more likely that for the pressure level of OP 2, the IDT is shortened or remains in the same order instead of being increased by a factor of two. The highest pressure level at OP 3 generates the shortest ignition delay times and the earliest vapour generation. These values were also highly reproducible. Several tests at OP 1 were conducted in an inert nitrogen atmosphere at ambient pressure ( $N_2@ 978$  mbar). The average ignition delay is 11.8 ms. This is slightly shorter than the OP 1 tests with air as the surrounding medium (IDT = 15 ms) but on the same level. Considering the standard deviations, it is not possible to identify a significant difference. The duration of the vapour phase of OP 1 in air and nitrogen and OP 3 is similar. This shows, again, that the difference in the IDT is related to the liquid phase interactions of fuel and oxidizer. With the higher pressure levels and consequently higher mass flows and injection velocities, the mixing process is accelerated, and hence the IDT is shortened.

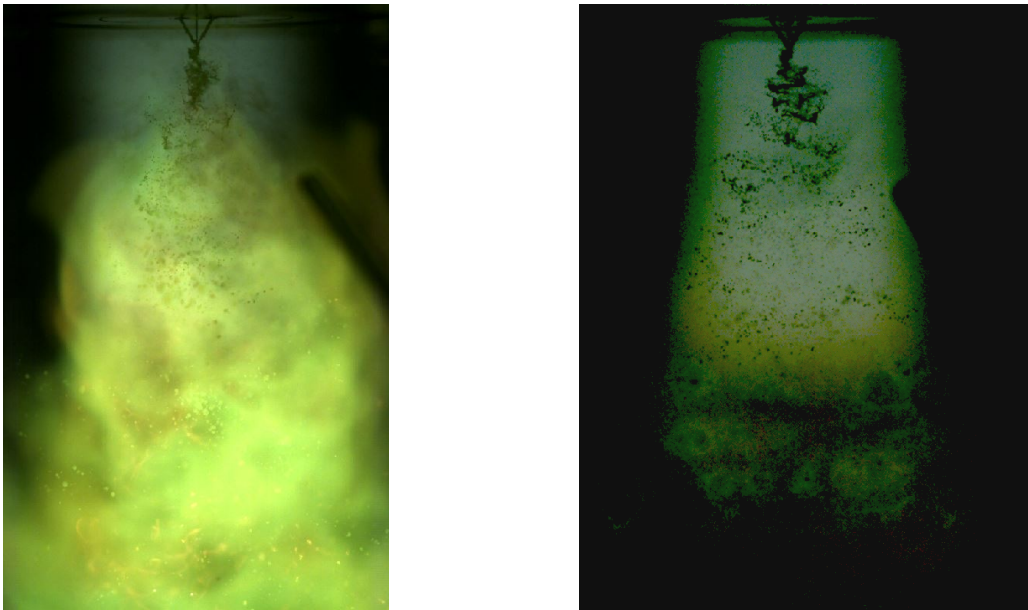


Figure 6.10: Flame during stationary condition at different pressures left: ambient pressure, right: 100 mbar

The reduction of the initial pressure leads to increased ignition delays. At 500 mbar, the IDT is roughly twice the value at ambient pressure. The TVG is also longer. For pressure steps of 100 and 50 mbar, again, the ignition occurred outside the high-speed camera's field of view. The instance for the determination of the ignition delay was taken from the first sign of a flame, such as the flame entering the field of view or the flame's glow. The actual IDT is expected to be in the order of several milliseconds shorter than the determined ignition delay. At the lowest initial pressure of 27 mbar, no ignition was observed. Therefore, the ignition limit of E1C is between 50 and 27 mbar. The TVG is slightly shortened for the lower pressure, and the vapour phase reaction time is significantly longer for every step with lower pressure.

The flame structure during the stationary operation is shown in figure 6.10 for ambient pressure (left) and 100 mbar (right). The flame at ambient pressure is more intense than at the reduced pressure. However, the flame is less bright than E5C fuel under similar conditions. The lower copper content reduces the brightness of the flame. The flame anchors close to the conjunction point of the injector jets. The low-pressure flame is paler. Here, combusting clouds can also be seen.



### 6.4.3 [EMIm][SCN] ignition verification

[EMIm][SCN] was tested to verify if the pure ionic liquid with an ignition delay in the order of some ten milliseconds can ignite under flowing conditions in an unconfined space. As of now, no hypergolic ignition using an injection setup of a pure ionic liquid and hydrogen peroxide has been reported. [EMIm][SCN] was tested with 96.5 % hydrogen peroxide and the 2-on-1 injector. Different operating points were tested, and their configuration is listed in table 6.12. The tests cover a wide range of pressure levels. The targeted ROF was between 4 and 5. The tests were all conducted with an oxidizer lead.

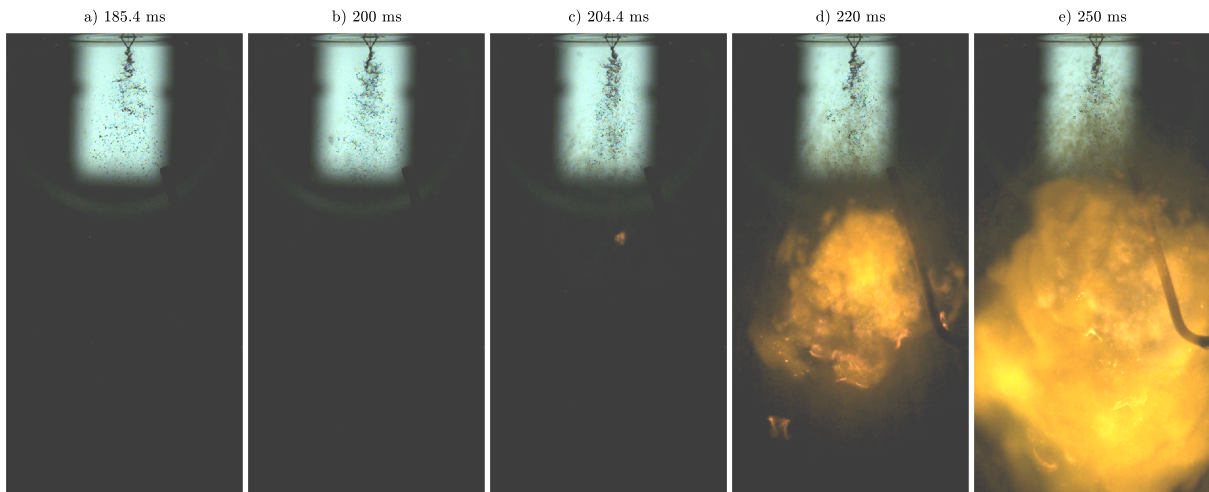


Figure 6.11: Ignition of [EMIm][SCN] and  $\text{H}_2\text{O}_2$  with 2-on-1 injector times from ox valve signal

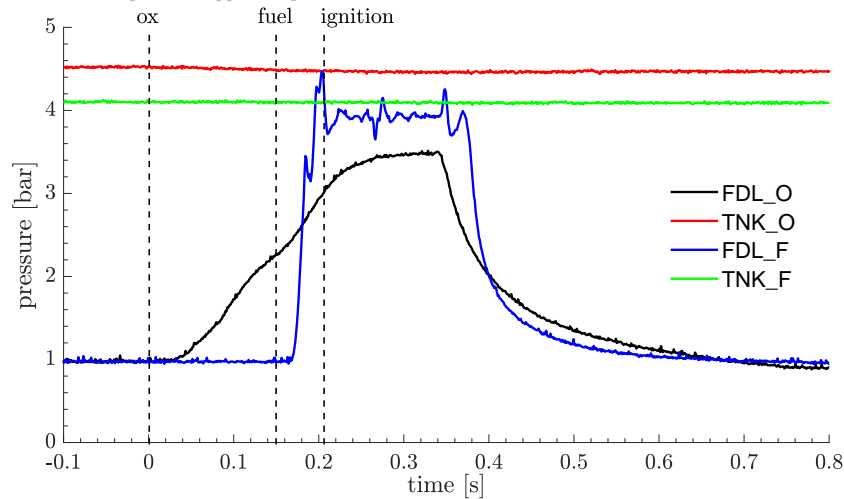


Figure 6.12: Pressure of [EMIm][SCN] and  $\text{H}_2\text{O}_2$  with 2-on-1 injector times from ox valve signal

Figure 6.11 shows an injection test with [EMIm][SCN] at OP 4 (test run 2020\_2-on-1\_001007\_EMIM). The time stamps refer to the opening signal of the oxidizer valve. The field of view for this test series is larger than the previously presented figures. At the top section, an LED panel is placed so that the injector jets and the spray are visible. The corresponding pressure plot is shown in figure 6.12. Here, the feed line pressures of fuel (FDL\_F) and oxidizer (FDL\_O) and their corresponding tank supply pressures (TNK\_F and TNK\_O) are shown. Besides, the opening signals of the oxidizer and fuel valve are marked with the dashed line as well as the instance of ignition. The oxidizer has a relatively gently inclined transient, whereas the fuel has

a sharp peak when the valve is opened. A check valve between the tank and the flow control valve delays the rise of the oxidizer pressure in the feed line. The check valve was installed for safety reasons. Because of the transient, the fuel valve is commanded 150 ms after the oxidizer valve to ensure a developed oxidiser flow.

The first frame of figure 6.11 shows the initial contact of fuel and oxidizer shortly after the fuel valve is opened. In the second frame, the first small vapour clouds can be seen. Frame c) shows the initial flame propagation 0.7 ms after ignition. After that, the flame propagates, and a sustained combustion can be observed, see d) and e). The flame is yellow to orange and less bright compared to E5C. In this test, the ignition delay is 18.3 ms, and the time to vapour generation is 13.3 ms.

Table 6.11: Operation points for tests with [EMIm] [SCN] and 2-on-1 injector,  $\Delta p$  pressure difference from tank to ambient,  $v_{inj}$  calculated injection velocity of the jet and resulting ROF

	oxidizer			fuel			ROF [-]
	$\Delta p$ [bar]	$\dot{m}$ [g/s]	$v_{inj}$ [m/s]	$\Delta p$ [bar]	$\dot{m}$ [g/s]	$v_{inj}$ [m/s]	
OP 1	2.3	12.4 ± 0.4	8.7 ± 1.1	2.2	2.9 ± 0.3	12.9 ± 1.7	4.3 ± 0.5
OP 2	3	15.4 ± 0.5	10.8 ± 1.3	2.8	3.6 ± 0.4	15.7 ± 2.1	4.3 ± 0.5
OP 3	3.5	17.3 ± 0.6	12.1 ± 1.5	3.3	4 ± 0.4	17.8 ± 2.4	4.3 ± 0.5
OP 4	4.5	20.4 ± 0.7	14.3 ± 1.8	4.1	4.2 ± 0.5	18.8 ± 2.5	4.8 ± 0.6
OP 5	6	24.4 ± 0.9	17.1 ± 2.1	5.5	4.5 ± 0.5	20.1 ± 2.7	5.4 ± 0.6
OP 6	7	26.7 ± 0.9	18.7 ± 2.3	6.4	5 ± 0.5	22.1 ± 3	5.4 ± 0.6

Table 6.12: Results of ignition tests with [EMIm] [SCN] and 2-on-1 injector at different operating conditions

	IDT [ms]	SD <sub>IDT</sub> [ms]	TVG [ms]	SD <sub>TVG</sub> [ms]	IDT-TVG [ms]	n [-]
OP 1	15.4	1.3	12.2	1.2	3.2	2
OP 2	14.6	1.6	11.0	2.1	3.7	3
OP 3	13.7	1.4	10.3	0.4	3.4	3
OP 4	19.2	1.4	13.7	1.4	5.4	4
OP 5	20.5	4.3	13.2	3.3	7.4	4
OP 6	23.4	5.8	13.1	1.3	10.3	4

The operation conditions of the injector tested with [EMIm][SCN] are displayed in table 6.11 and table 6.12 shows the results in terms of IDT, TVG and vapour phase. The shortest average IDT was achieved for OP 3 with 13.7 ms. In contrast to the catalytically promoted fuels, higher pressure levels do not facilitate a shorter IDT. Higher pressures have a contrary effect. The average IDTs for OP 4, 5 and 6 increase with each step. Also, for those high-pressure levels, the duration of the vapour phase until ignition occurs is increasing. The IDTs of OP 1,2 and 3 pressure levels are close together. For these operation points, the duration of the vapour phase reactions is similar to the drop tests.

The higher pressure levels lead to higher injection velocities and better atomisation, resulting in smaller drops that are spread wider. This may have a negative influence on the IDT since the reactions without additives need longer to initiate. A reason could be: the spray is wider spread and finer distributed due to higher injection velocities. In that case, the density of the

Table 6.13: Operating points swirl injector

	$P_{\text{tank, ox}}$ [bar]	$\dot{m}_{\text{Ox}}$ [g/s]	$P_{\text{tank, fuel}}$ [bar]	$\dot{m}_{\text{fuel}}$ [g/s]	ROF [-]
OP 1	6.3	$21.5 \pm 2.0$	6.3	$26.3 \pm 1.8$	$0.8 \pm 0.1$
OP 2	6.3	$21.5 \pm 2.0$	4.0	$19.8 \pm 1.3$	$1.1 \pm 0.1$
OP 3	6.3	$21.5 \pm 2.0$	2.5	$14 \pm 0.9$	$1.5 \pm 0.2$
OP 4	8.4	$25.4 \pm 2.4$	2.9	$15.8 \pm 1.1$	$1.6 \pm 0.2$
OP 5	10.8	$29.2 \pm 2.7$	3.4	$17.7 \pm 1.2$	$1.7 \pm 0.2$

hot reaction produced is lower, and more heat is lost to the surrounding medium. Therefore, ignition occurs later compared to the tests where the spray is less atomised.

This test series successfully demonstrated the hypergolic ignition of a pure ionic liquid and highly concentrated hydrogen peroxide. If the injection conditions are adequately selected, an ignition delay can be shorter than in drop tests. It could be possible that this ignition delay is sufficient to start a thruster without a hard start.

#### 6.4.4 Swirl injector

The dual swirl injector was tested with E5C and hydrogen peroxide. Different operating points were tested. The overview of the operating points is given in table 6.13. Due to the design of the swirl injector, the pressure loss of the injection bores is very low compared to the impinging injector. The fuel side especially had a very low pressure loss. The open swirl for the fuel has three tangential inlets with a diameter of 2 mm. This resulted from different design criteria according to Fu et al. [220]. Witte designed the swirl injector according to the mentioned model [179]. Because of the design specialities, reaching ROF values close to the  $I_{sp}$  maximum was impossible. To facilitate hypergolic ignition, the injector was designed with internal mixing. The inner simplex swirl of the oxidizer sits back, so the spray cone hits the wall of the outer open swirl for the fuel; see figure 6.13. Moreover, the swirls are counter-rotating to improve mixing.

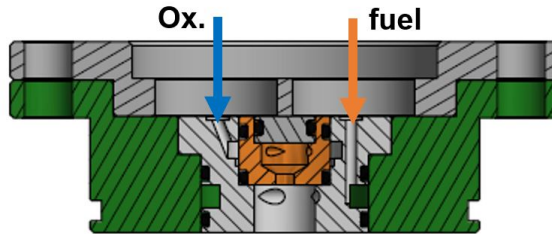


Figure 6.13: Swirl injector, taken from [179]

Because the double swirl has an internal mixing, it is impossible to determine the first contact of fuel and oxidizer with the high-speed camera. Therefore, two alternatives are possible. The first possibility is to define the moment of initial contact according to the start of pressure rise in the feed line. This overestimates the IDT because it is unknown when the fluid exits the feed line and comes into contact with the other component. The second alternative is to define contact when the first mixture exits the injector after the start-up phase. This is reasonably detectable but underestimates the IDT because the actual contact is not visible. The second method is expected to provide a better impression of the order of the IDT compared to the pressure data.

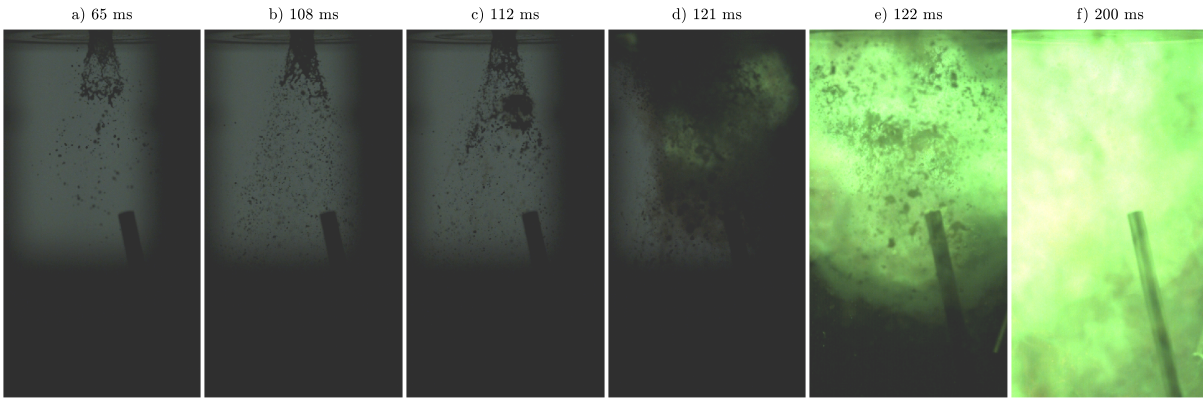


Figure 6.14: Ignition of E5C and  $\text{H}_2\text{O}_2$  with swirl injector at OP 3 times from ox valve signal

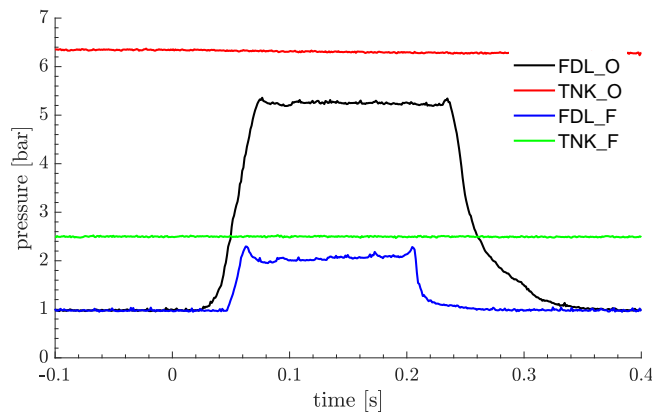


Figure 6.15: Pressure of E5C and  $\text{H}_2\text{O}_2$  with swirl injector at OP 3 from ox valve signal

Figure 6.14 shows snapshots of the high-speed camera and 6.15 the corresponding pressure plot of test SWIRL\_004\_002. The first frame shows the beginning of the spray, where only peroxide is sprayed. This spray changes at 104 ms, and the change is shown in frame b) 4 ms later (at 108 ms). At 104 ms, the first mixture of fuel and oxidizer leaves the injector. For the IDT determination based on high-speed imaging, 104 ms is the starting point. Frame c) shows the first vapour, which propagated at 111 ms. The ignition occurs in the vapour cloud at 120.8 ms, and the flame propagation afterwards is displayed in frames d) to f). After the ignition, an erratic combustion can be observed. The flame's anchor point is not visible and located inside the injector. From the pressure plot, it can be seen that the feeding line pressure reaches steady conditions. The IDT derived from the pressure starting point of the fuel pressure (variant 2) rise is 73.2 ms.

A second test of the swirl injector at OP 4 is shown in figure 6.16 and 6.17. The test runs smoothly with an IDT of 10.5 ms or 45.5 ms, respectively, the determination method. But at 170 ms, pressure peaks in the feeding line pressure occurs. Also, on the high-speed video, a very fast, bright flame propagation can be seen in figure 6.16 d) to e). The maximum value of the pressure peaks in the oxidizer feed line is 33.4 bar, and the maximum peak of the fuel is 8.1 bar. It is assumed that the actual pressure peaks are higher because the pressure transducer measures static pressure and the sampling rate of the pressure is 1 kHz. In contrast, the high-speed records indicate that this process propagates much faster. The explosions did not damage the setup and were unable to propagate into the oxidizer tank. Only 3 out of 12 conducted tests with the swirl

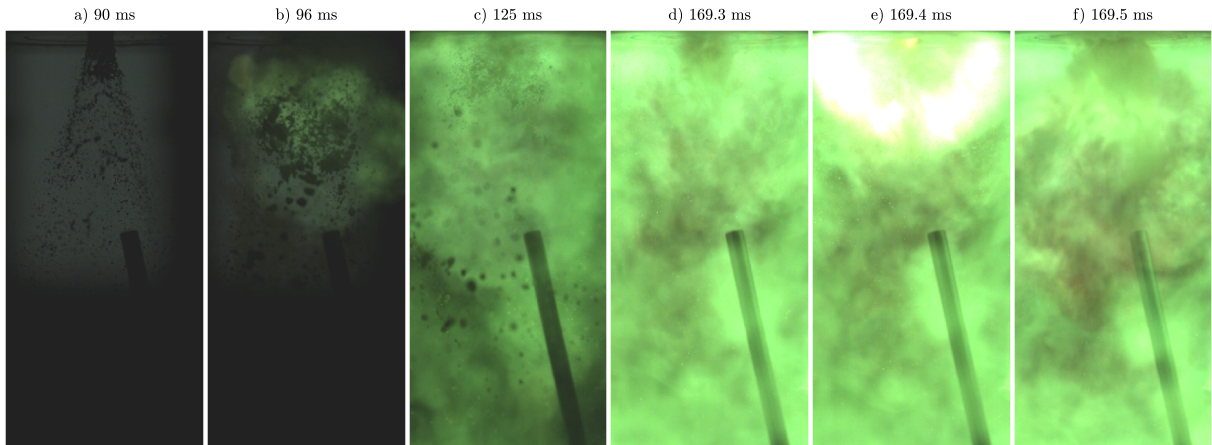


Figure 6.16: Ignition of E5C and H<sub>2</sub>O<sub>2</sub> with swirl injector at OP 4 times from ox valve signal

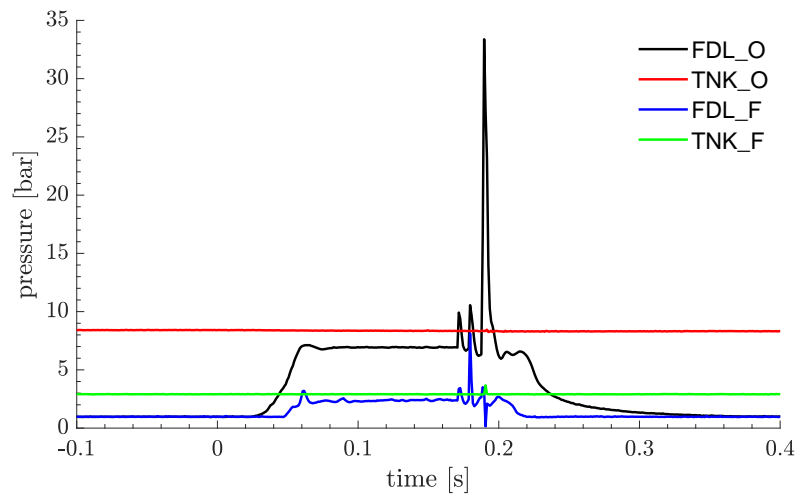


Figure 6.17: Pressure of E5C and H<sub>2</sub>O<sub>2</sub> with swirl injector at OP 4 from ox valve signal

injector did not produce any rapid events or pressure peaks in the feed lines. Because of the behaviour of the injector, the test campaign was stopped and not continued to avoid damage to the test bench and the setup.

Table 6.14: Results swirl injector  $IDT_{HS}$  - high speed recording,  $IDT_{pr}$  - pressure rise

	lead	$IDT_{HS}$ [ms]	SD [ms]	TVG [ms]	SD [ms]	$IDT_{HS-TVG}$ [ms]	$IDT_{pr}$ [ms]	SD [ms]	n
OP 1	ox	7.6		5.7		1.9	44.6		1
OP 2	ox	6.5		5.3		1.2	43.9		1
OP 3	ox	17.6	4.2	7.2	1.4	10.4	68.3	4.3	4
OP 3	fuel	12.8		9.5		3.3	50.2		1
OP 4	ox	10.1		6.0		4.1	45.5		1
OP 5	ox	12.3	0.3	7.4	1.3	4.9	55.2	1.2	2
OP 5	fuel	10.6		10.6		3.3	52.3		1

Table 6.14 shows the injection test results with the swirl injector in terms of IDT and TVG. Ignition was achieved in all tests, and the  $IDT_{HS}$  varies between 6.5 to 17.2 ms. The actual IDT

will be several milliseconds higher, but this gives a first order of the IDT. The  $IDT_{pr}$  determined with the pressure profile ranges from 44 to 68 ms. Ignitions were achieved for fuel and oxidizer leads. The TVG is slightly longer for fuel lead.

In conclusion, the double swirl injector can generate repeatable ignitions, but the combustion is highly erratic in the presented configuration. Several explosion events occurred with a partly propagated into the feed lines. A new iteration of swirl injectors needs to provide a significant pressure loss for a better operation.

## 6.5 Test anomalies

Apart from the experience with the double swirl injector, the impinging injector showed unexpected behaviour in a few cases. After three ignition tests with the 3-on-1 injector, a loud bang appeared, accompanied by a pressure peak in the oxidizer feeding line pressure. The anomalies occurred a few seconds after the FCV was closed, and the obvious combustion had stopped. Figures 6.18 and 6.19 show the data recorded during the test and anomaly of test 004\_001 conducted with the 3-on-1 injector, E5C fuel at OP 6. The actual ignition test went as planned, and an IDT of 6.1 ms was observed. A sudden bang occurred about 1.6 seconds after the test initially started. At this moment, the injection has already stopped. The data acquisition was still active at this moment. The nominal test can be seen between 0 and 1 s in the pressure readings. At 1.66 s, a peak in the oxidizer feed line is present. The maximum value reaches 50.2 bar. The data acquisition rate is 1 kHz, and the pressure rise from ambient pressure to 50.2 bar happens between 2 data points, so it is within 1 ms. The pressure transducer has an operating range from 0 to 50 bar. Therefore, the peak pressure value is expected to be much higher. The pressure decays within 0.2 s again. The temperature in the oxidizer feed line also shows a peak simultaneously. The temperature rises from ambient 23.8 °C to 98 °C and decays slowly. Figure 6.19 shows frames of the high-speed video around the measured peaks in pressure and temperature readings. The brightness of the single frames is increased to allow some visibility. At a), 1650 ms after the test started, the main combustion was over, but a glowing fume was inside the combustion chamber. Some milliseconds later, a slight jet of the oxidizer bores can be seen in b). A weak ignition occurs at the injector, see c). This ignition triggers the anomaly, and suddenly, the chamber is filled with a very bright combustion within 1.5 ms, see d) to h). The bright flame decays after 2 ms i), and vapour is ejected from the oxidizer bores, which can be seen in j).

Based on the high-speed recording and the pressure and temperature data, it is assumed that in the feed line of the oxidizer, an explosive decomposition of the hydrogen peroxide occurred. The decomposition event inside the feeding line is obvious by the high pressure and temperature rise in the feeding line sensors. The very short succession of the events indicates an explosive character. Overall, liquid hydrogen peroxide is hard to detonate, especially in lines with small diameters [221, 222]. On the other side, hydrogen peroxide vapour can detonate. Therefore, it is possible that after the test in at least one of the injector bores and lines, hydrogen peroxide vapour was present, and by the late ignition in the main chamber, an explosive decomposition in the injector was triggered. This decomposition converted the hydrogen peroxide in the lines. The exiting hot decomposition products ignited with the residual fuel-rich fumes in the combustion chamber, and a bright flame occurred. Luckily, this event did not cause severe damage to our setup, but the injector was deformed. Further tests were conducted successfully after the first anomaly until a second explosive event occurred.

The critical condition leading to these unintended events is suspected to be related to the presence of hydrogen peroxide vapour. The vapour formed during the shutdown of the injection test and rested in the injector close to the exit. Secondly, some residuals of the fuel that can trigger



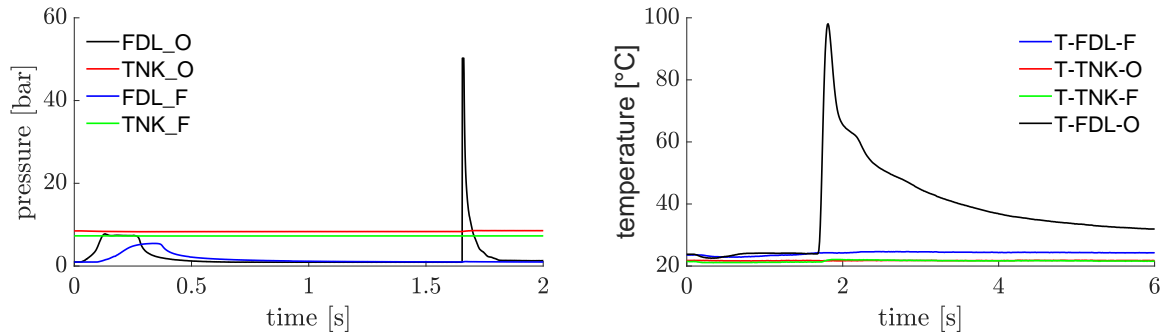


Figure 6.18: Pressure and temperature data of anomaly test 004\_001 3-on-1, left: pressure, right: temperature

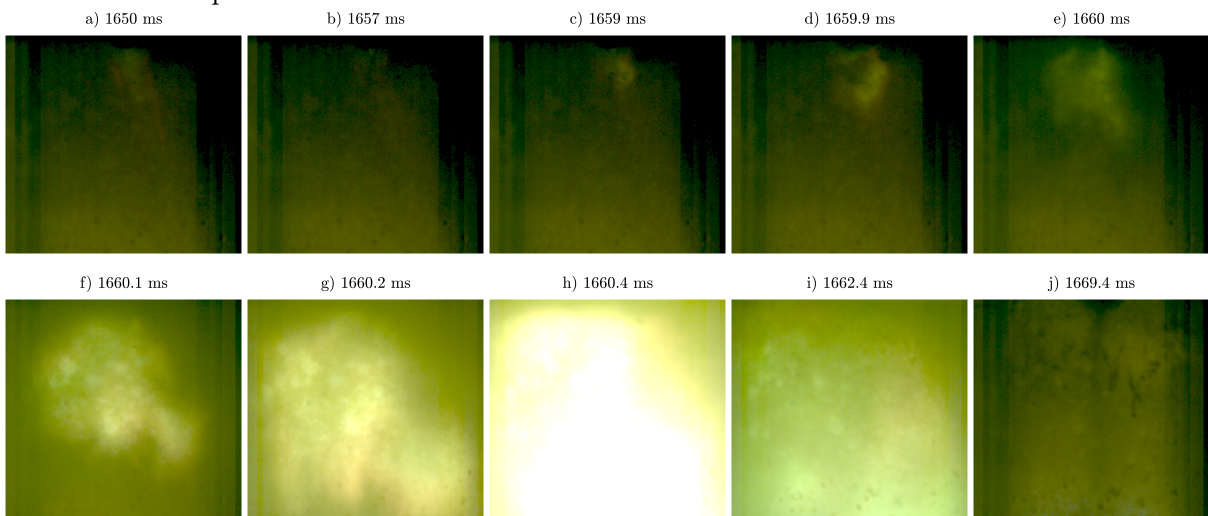


Figure 6.19: High speed recording of the anomaly with 3-on-1 injector during test 004\_001

decomposition need to be present. A purge of inert gas, such as nitrogen, could prohibit this condition. But this is not suitable for a later application. Such an event could severely damage the injector, thruster, or propulsion system, putting the spacecraft's mission in danger. Small dribble volumes and narrow lines can reduce the risk of the propagation of this decomposition. Also, the pressure decay to vacuum conditions in space prevents the condition of a resting vapour inside the injector. For further testing on the ground, a check valve was installed between the oxidizer tank and the flow control valve to prevent propagation of the decomposition reaction into the filled oxidizer tank. Also, lines with inner diameters between 2 and 4 mm were chosen to dampen the propagation of such a reaction.

The pressure peaks seen in the tests with the double swirl injector are also expected to be related to the described phenomenon. However, since they occurred during the normal operation of the injector, a permanent liquid flow was present in the feed lines. But in the injector head where oxidizer flow was distributed to the single swirl chamber inlets, it is thinkable that not all three bores were supplied with liquid oxidizer at all times. Because of this, a gaseous explosive decomposition could enter the injector head which caused the pressure peak. However, since the line supplying the injector was filled with liquid, the decomposition was unable to propagate upstream into the feeding line. Still, the pressure waves were transferred and measured at the feeding line pressure transducer. This is also supported because the temperature in the feeding line did not experience a peak compared to the anomalies.

## 6.6 Summary of the injector tests

This chapter presents the first successful hypergolic ignitions of an ionic liquid-based fuel with hydrogen peroxide under flowing conditions. 167 hot firings and numerous calibration tests were performed. As a baseline, a 2-on-1 impinging injector was applied. The ignition of the fuel E5C was characterised under different injection conditions, such as variation of supply pressure, following variant of mass flows and injection velocities. The ignition delay times were below 10 ms and shorter compared to the drop test presented in chapter 5, whereas the duration of the vapour phase is similar. This effect is mainly attributed to the enforced mixing of fuel and oxidiser due to the injection. For higher injection mass flows and velocities, the ignition delay tends to become shorter for E5C.

Two other injector configurations were tested with E5C. A 3-on-1 injector also provides fast and reliable ignitions. A double swirl injector with internal mixing of fuel and oxidiser showed reliable ignitions. However, the operation of the injector resulted in a rough combustion. The double swirl configuration needs to be redesigned.

Further, two other fuels, namely the pure [EMIm][SCN] and E1C, were tested with the 2-on-1 injector. Fast hypergolic ignitions were achieved with an IDT between 10 ms and 20 ms. For the neat [EMIm][SCN], higher mass flows and injection velocities can lead to increased ignition delay times.

The hypergolic ignition of E5C and E1C were tested in a low-pressure environment. E5C ignition at pressures down to 27 mbar, but the ignition delay in the order of several 100 ms. E1C ignited at 50 mbar but was unable to ignite at 25 mbar.

Some anomalies related to a sudden explosive decomposition event in the oxidiser feeding line occurred during the tests. To prevent them, the formation of  $\text{H}_2\text{O}_2$  vapour in the line after a test should be avoided.

Based on these results, E5C is a promising hypergolic propellant candidate. The ignition delay under flowing conditions in the order of several milliseconds, similar to conventional hypergolic propellants. Also, the ignition is robust at low-pressure environments. Impinging injectors can provide fast and reliable ignitions following stable combustion for the combination of E5C and hydrogen peroxide.





# 7 HIP\_11

This chapter gives an overview of important properties of the newly developed class of hypergolic fuels. The class of fuels is referred to as *HIP\_11* for **H**ypergolic **I**onic liquid **P**ropellant developed at the test facility M11 of the DLR Institute of Space Propulsion. The single fuel composition can be specified with the abbreviation introduced in chapter 5, for example *HIP\_11 E5C*. Part of the chapter will be a detailed register with essential properties of different HIP\_11 derivatives determined with own measurements or available from the literature. Moreover, an assessment of the ionic liquid propellant in a dual-mode propulsion system, where the IL is also applied in an electrical mode, is given.

## 7.1 Properties of HIP\_11

Certain properties are of high importance for the design of propulsion hardware. Essential properties were identified in chapter 4. The following sections are a compilation of crucial properties of HIP\_11.

### 7.1.1 Physical properties

#### Density

The density of the HIP\_11 propellant was determined with a density meter Easy D40 by *Mettler-Toledo* at ambient conditions for two fuel configurations: pure [EMIm][SCN] and E5C. The measurement was conducted at 298.15 K and repeated three times. The average density measurements with the according uncertainty are shown in 7.1. Additionally, this figure shows literature values of the density depending on the temperature for pure [EMIm][SCN] and different [Cu][SCN] concentrations (straight lines) by Zarca et al. [50]. Their investigation found a linear dependence between density and temperature in the range from 283.15 K to 353.15 K. The dotted line represents the density variation at 5 wt% [Cu][SCN]. Zarca did not determine this specific concentration. Therefore, the according slope and y-intercept at 5 wt% were calculated by linear interpolation of the two closest measurements, pure [EMIm][SCN] and 5.9 wt% [Cu][SCN] content.

With the increasing content of the copper additive, the density of the solution is increased. The measurements conducted for this thesis were taken at 298.15 K. The measured densities ([EMIm][SCN]:  $1.1113 \pm 0.0005$  g/cm<sup>3</sup>, E5C:  $1.1471 \pm 0.0006$  g/cm<sup>3</sup>) are close to the literature values. A slight difference occurred, but the difference is inside the uncertainty of the measurement. Therefore, no further measurements were conducted because the literature values are in good accordance with our measurements.

#### Viscosity

The viscosity was determined with an Ubbelohde viscometer at 298.3 K ([EMIm][SCN]:  $20.06 \pm 0.15$  mPa s, E5C:  $29.58 \pm 0.13$  mPa s). The results are displayed in figure 7.2. Literature data on the viscosity in dependence on temperature and the amount of additive is also shown in the plots. This data from Zarca et al. [50] is displayed with black and grey lines. Their viscosity measurements were conducted between 293.15 and 353.15 K. Their measurements correlate best with the Litovitz equation [223]. Therefore, the resulting fit has the form:

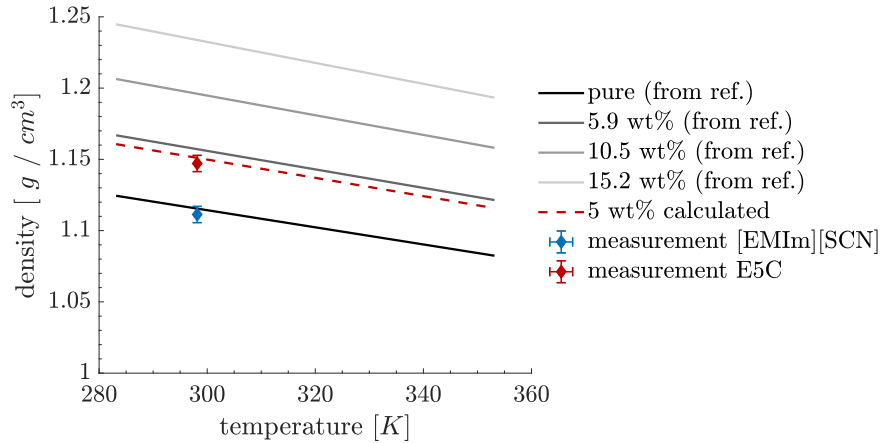


Figure 7.1: Lines: density of various concentrations of [Cu][SCN] dissolved in [EMIm][SCN] over temperature according to [50], dotted line interpolated values for 5 wt% [Cu][SCN] content, points: own measurements

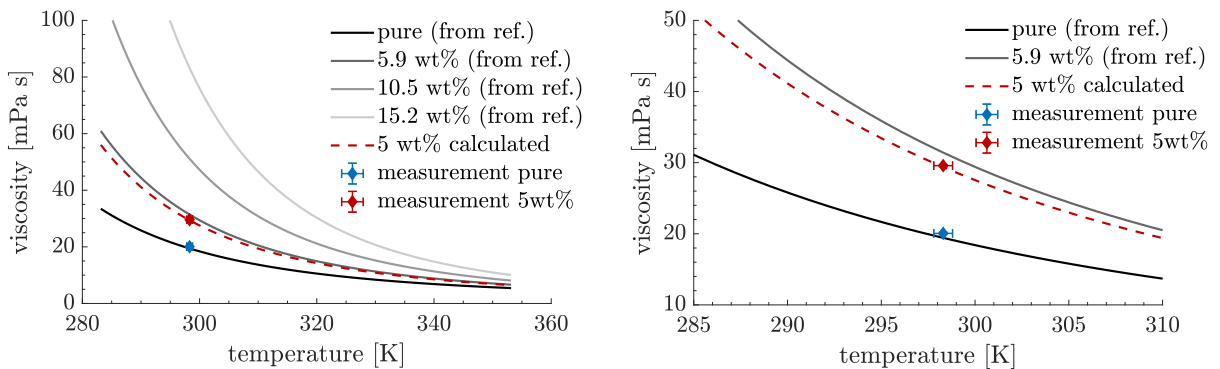


Figure 7.2: Lines: viscosity of various concentrations of [Cu][SCN] dissolved in [EMIm][SCN] over temperature according to [50], dotted line interpolated values for 5 wt% [Cu][SCN] content, points: own measurements; left: wide temperature range, right: zoom around the measurement

$$\eta [mPa s] = A * \exp\left(\frac{B}{T^3}\right) \quad (7.1)$$

where A and B are constants fitted to the measurements. The values for A and B used for the calculation were already mentioned in table 5.12. From the graph, a strong influence of the additive content and the temperature can be seen. Especially in the lower temperature range, the viscosity change is noticeable. This also substantially impacts the ignition delay times in drop tests, as discussed in 5.2.3. The viscosity measurements conducted for this thesis correspond to the literature values. Therefore, for the different initial temperatures, the literature model was used.

### FTIR spectrum

Figure 7.3 shows the characteristic FTIR spectra of the pure [EMIm][SCN] a) and E5C b). Furthermore, the difference between the two spectra is shown c) and the region around the characteristic thiocyanate band. The spectra of [EMIm][SCN] and E5C exhibit a high similarity.

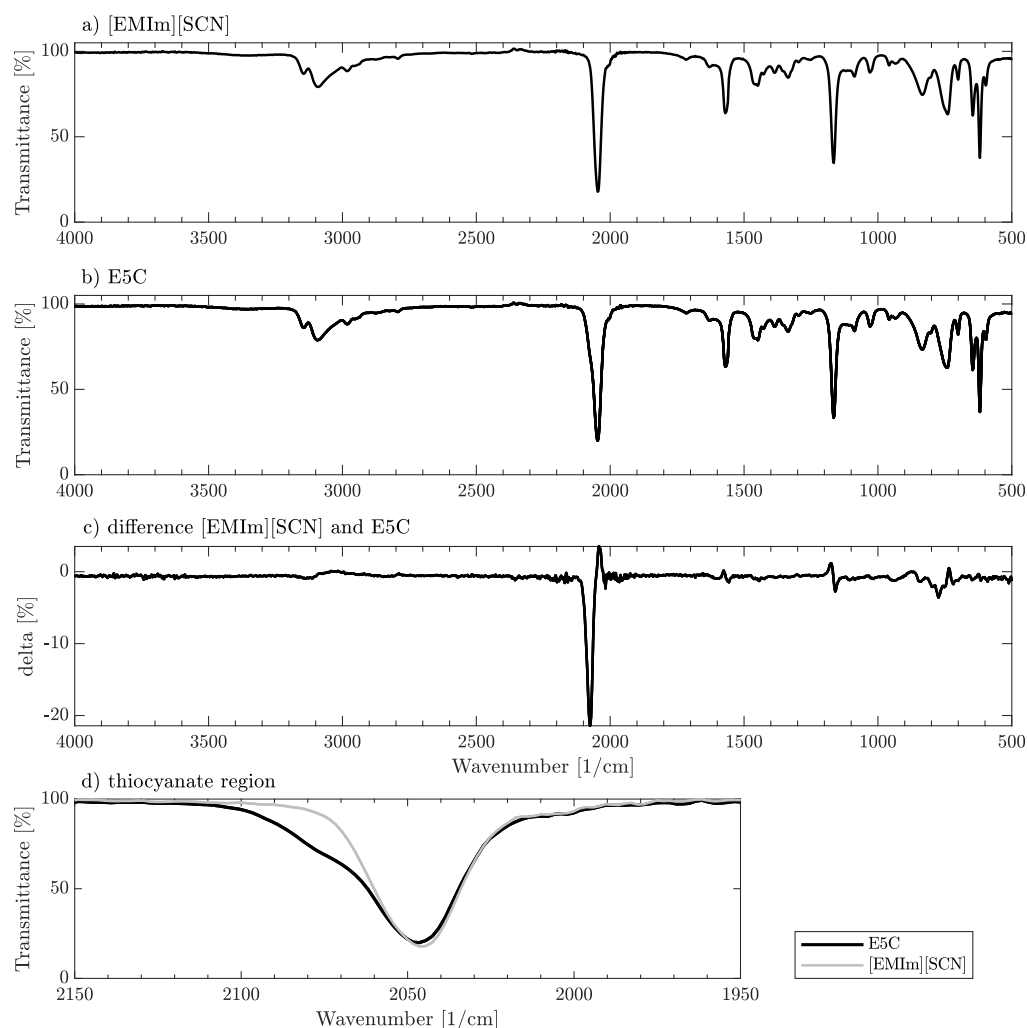


Figure 7.3: IR spectra from [EMIm][SCN] and E5C

At 2047  $1/\text{cm}$ , the characteristic thiocyanate band can be seen [224]. In d), this region is shown in more detail. The copper additive influences this band, and the peak is broader. This behaviour was also described by Cabeza et al. [224]. For complex copper thiocyanate anions, a double peak was observed in FTIR spectra at 2052 and 2069  $1/\text{cm}$ . The formation of a copper thiocyanate complex seems likely after the copper thiocyanate was dissolved in the [EMIm][SCN]. It is also expected that the large complex anion will increase viscosity. With the addition of a higher copper content, the amount of complex ions increases, and therefore, the ionic liquid becomes less viscous. The reactivity of the fuels with a complex copper anion is increased compared to the neat [EMIm][SCN]; see section 5.2.1.

### Surface tension

Table 7.1 shows the measured surface tension of [EMIm][SCN] and E5C and the according measuring temperature. The surface tensions are very similar. For E5C, the copper additive does not seem to affect the surface tension to a high degree. This also means that Weber numbers of

[EMIm][SCN] and E5C are similar if the drop size and drop velocity are identical. Interestingly,

Table 7.1: Surface tension of [EMIm][SCN] and E5C

	surface tension [mN /m]	temperature [°C]
[EMIm][SCN]	$46.3 \pm 0.26$	$25.5 \pm 0.1$
E5C	$47.2 \pm 0.11$	$24.5 \pm 0.1$

the surface tension differs from values found in the literature. Values between 53 and 58 mN /m are reported at ambient conditions [225–228]. Further, the influence of the temperature on the surface tension in a range from 298.15 to 338.15 K was very low. It decreased from 57.76 to 57.06 mN /m [228]. In our case, the surface tension of the IL was determined in the condition as purchased. So, no special drying or purification treatment was conducted. The purity specification of the [EMIm][SCN] is given with >98 %. But impurities may affect the surface tension to a quite high degree [226].

## 7.1.2 Thermodynamic properties

### TGA DSC

A thermogravimetric analysis (TGA) with differential scanning calorimetry (DSC) was conducted to determine the thermal properties of [EMIm][SCN] and E5C. Small amounts of the samples were heated in a nitrogen atmosphere at 10 K per minute. The results are plotted in figure 7.4 for a) [EMIm][SCN] and b) E5C. The black curves correspond to the normalised mass over the temperature, and the grey curves display the DSC signal over the temperature.

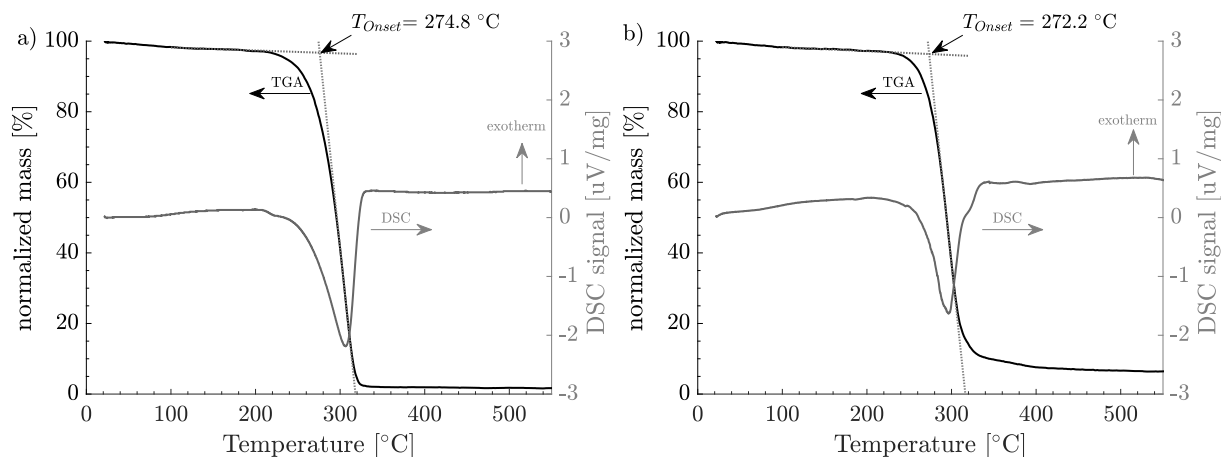


Figure 7.4: TGA/DSC of a) [EMIm][SCN] and b) E5C

For [EMIm][SCN], the mass starts to decrease rapidly around 210 °C. This decrease in mass is caused by the initiated thermal decomposition of the ionic liquid. It can be assumed that thermal decomposition of the [EMIm][SCN] occurs, not vaporisation. Chambreau et al. described this phenomenon: the thermal decomposition of thiocyanate ionic liquids is "strongly favoured over the vaporisation at moderate temperatures ( $T < 573$  K)" [57]. The onset temperature of the decomposition is determined as the section between the linear fit to the mass curve between 30 and 190 °C, and the tangential at the inflexion point of the fast decrease is 274.8 °C. The mass levels off at 2 % of the initial mass for temperatures above 330 °C. The E5C behaves similarly, and

the determined onset temperature is 272.2 °C. A difference can be seen at higher temperatures. The mass is reduced to a value of 6.4 % of the initial value. The higher final mass is attributed to the copper additive, which cannot react in the inert atmosphere and remains in the sample holder.

The DSC signal has a negative peak during the thermal decomposition of both fuels, with its maximum during the highest mass decrease. This indicates that the thermal decomposition process of both fuels is endothermic.

## Enthalpy of formation

The enthalpy of formation  $\Delta_f H^0$  is a necessary thermodynamic property to calculate the performance of the propellant combination in a combustor. For [EMIm][SCN], the enthalpy of formation is available from literature, and the value is  $52.8 \pm 2.3$  kJ/mol [191]. This value was reproduced with the equipment available at DLR with the method described by Ricker et al. [155, 157]. For the copper additive, the enthalpy of formation is not available in the literature. Therefore, colleagues from the chemical propellants' technology department determined the  $\Delta_f H^0$  of copper thiocyanate with their bomb calorimeter. The procedure to determine the enthalpy of formation is described in [155]. The resulting enthalpy of copper(I)thiocyanate formation is -98.0 kJ/mol.

### 7.1.3 Propulsive potential

The propulsive performance is an important factor for replacing conventional space propellants. In the initial screening, [EMIm][SCN] was found to be a high-performing potential fuel candidate. However, with an additive, the performance is expected to decrease due to the higher molecular mass of the metallic component in the additive. For the initial screening, the influence of additives on the performance was not of interest. Now, after identifying a suitable additive and characterising the additive, the performance can be calculated for different fuel compositions. The calculation is conducted with the NASA CEA code, assuming frozen supersonic expansion and an oxidiser concentration of 98 wt% hydrogen peroxide and 2 wt% water. As in 4.5, the reference case is the 400 N *ArianeGroup* thruster with a combustion chamber pressure  $p_c$  of 10.35 bar and an expansion ratio of the nozzle of  $\epsilon = 330$ . The calculation is executed similar as described in chapter 4.

Figure 7.2 shows the results of the performance calculation in terms of  $I_{sp}$ , adiabatic flame temperature, characteristic velocity and average molecular mass for three different fuels: [EMIm][SCN], E1C and E5C. The maximum values are presented in the table. Figure 7.2 a) shows the  $I_{sp}$  value, which refers to the expansion in vacuum over the ROF. As expected, the highest  $I_{sp}$  value has [EMIm][SCN] with 323.1 s at an ROF of 3.8. By adding 1 wt% [Cu][SCN], the maximum  $I_{sp}$  is 322.8 s. E5C has a maximum  $I_{sp}$  of 321.2 s at a ROF of 3.7. Consequently, by adding 5 wt% of the copper additive, the difference of the theoretical maximum  $I_{sp}$  of the neat IL is below 1 %. The negative effect on the  $I_{sp}$  of the additive is limited. In terms of performance, the addition of up to 5 wt% additive is reasonable and not connected to serious constraints limiting the performance. For the density-specific  $I_{sp}$ , no difference is noticeable in the first three digits. This is related to the slightly increasing density of the copper additive. Therefore, the  $I_{sp}$  decrease and the density increase level each other out in the investigated range. The adiabatic flame temperatures displayed in b) reach their maximum at the same ROF as the highest  $I_{sp}$ . The maximum values are 2820 K for E5C and 2829 K for [EMIm][SCN]. There is no significant difference. The characteristic velocities in dependence on the ROF are shown in c). The maximum values are 1595 m/s ([EMIm][SCN]) and 1586 m/s (E5C). The average molecular masses

of the exhaust gasses are displayed in d). It is obvious that the copper additive increases the average molecular mass.

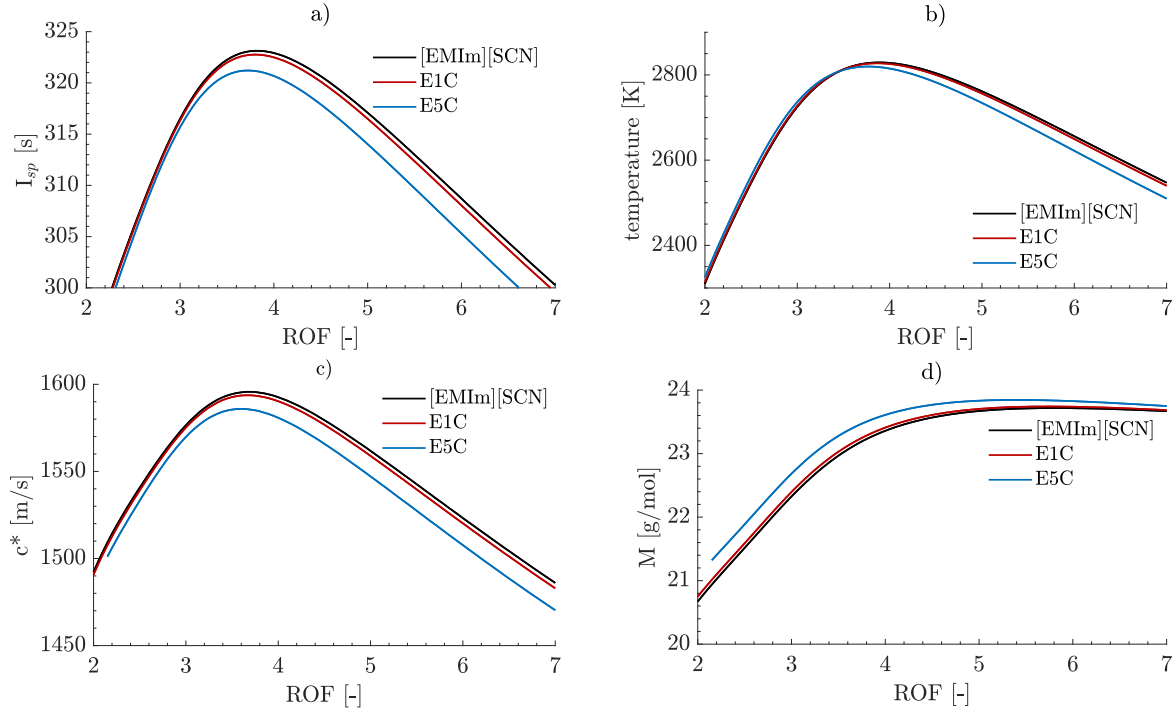


Figure 7.5: Performance variation depending on ROF for different fuels, a)  $I_{sp}$ , b) adiabatic temperature, c)  $c^*$ , d) average molecular mass of exhaust

Table 7.2: Maximum values of the theoretical performance

fuel	$I_{sp,max}$ [s]	ROF @ $I_{sp,max}$ [-]	$\rho I_{sp,sp,max}$ [s kg/m <sup>3</sup> ]	$T_c$ @ $I_{sp,max}$ [K]	$c^*$ @ $I_{sp,max}$ [m/s]	$M$ @ $I_{sp,max}$ [g/mol]
[EMIm] [SCN]	323.1	3.8	$437 \times 10^3$	2829	1595	23.2
E1C	322.8	3.8	$437 \times 10^3$	2826	1594	23.2
E5C	321.2	3.7	$437 \times 10^3$	2819	1586	23.4
MMH/NTO	339.3	1.8	$398 \times 10^3$	3124	1696	21.3

### Comparison with conventional propellants

The maximum performance values for a typical conventional hypergolic propellant combination, namely MMH/NTO, are in the table in figure 7.2. This propellant combination had a maximum  $I_{sp}$  of 339.1 s, which is about 5 % higher than the regarded alternative propellant combinations. On the contrary, the density specific  $I_{sp}$  of the alternative propellants is 10 % higher than the conventional. A more significant difference is the adiabatic flame temperature of 3124 K. Compared with this, the lower temperature of the alternatives can be advantageous in terms of cooling and material selection. On the other hand, the lower flame temperature is the main reason for the lower performance of green fuels compared to conventional hypergols. In conclusion, the performance of the presented alternative propellants is comparable with conventional hypergolic propellant combinations.

As shown, the copper additive has only a minor impact on the performance for an amount of up to 5 wt%. It must be considered that a metallic additive will form metallic oxides during the combustion. At typical temperatures in a nozzle, the oxides will become solid and form solid particles in the plume. This must be considered when designing a propulsion system. A thruster directed on an optical surface or solar panel should be avoided due to possible particles impacting at high velocity on these surfaces. Therefore, optimising the thruster design and propellant selection is necessary depending on the shortest IDT or impulse bit and plume composition. For a particle-free flow, using a neat ionic liquid would be beneficial, but this can have a negative consequence on the IDT and minimum impulse bit. Nevertheless, a high-performing, versatile group of fuels is found with the fuels based on [EMIm][SCN].

#### 7.1.4 Toxicity

In 4.3 requirements for a green propellant were defined. A critical requirement of green propellants is the reduced toxicity compared to conventional propellants. In section 1.2, hydrogen peroxide was identified as a suitable green oxidizer. It has a lower toxicity than NTO and a low vapour pressure at ambient conditions. Therefore, a SCAPE suit for handling is not necessary. The toxicity of ionic liquids must be considered. One property ionic liquids have in common is their neglectable vapour pressure at ambient conditions due to their ionic structure [56]. This is an advantage compared to the conventional propellants. Since the vapour pressure is so low at ambient conditions that it is not measurable, a recent publication presented vapour pressures of [EMIm][SCN] at an elevated temperature. The measured vapour pressure at 425 K was  $8.3 \times 10^{-5}$  Pa [229]. This is many orders lower than conventional liquids such as solvents or hydrocarbon fuels.

**Toxicity of the thiocyanate anion** The thiocyanate anion naturally occurs in certain foods and affects the human body. In high amounts, it is a toxic and harmful substance and can cause poisoning [230]. For example, potassium thiocyanate was used as a drug to treat hypertension [231], but its use was abandoned due to toxic side effects [232]. Thiocyanate can also be produced in the liver during the degradation of cyanides. Here, the enzyme rhodanase catalyses a reaction between thiosulfate and cyanide, producing thiocyanate. The thiocyanate is less toxic than cyanides and can be excreted from the body [232].

**Toxicity of the thiocyanate ionic liquids** The toxicity of ionic liquids is under investigation [192]. It was shown that the toxicity of different ILs has a few common principles. For example, the side chains of the imidazolium cation influence the toxicity. Longer hydrocarbon side chains increase toxicity, likely because of the lipophilic part of the molecules that can interact with cell membranes [233].

An investigation of the ecotoxicity towards the aquatic milieu with *Vibrio fischeri* was conducted by Delgado-Mellado et al. with [EMIm][SCN] and [BMIm][SCN] [193]. The ecotoxicity towards the water organisms ( $EC_{50}$ , 15 min) was 6310 mg/l for [EMIm][SCN] and 513 mg/l for [BMIm][SCN] [193]. According to the classification of the  $EC_{50}$  value by Passino and Smith, [EMIm][SCN] can be regarded as 'harmless' and [BMIm][SCN] as 'practically harmless' in terms of the ecotoxicity [234]. Further, the toxicity of [EMIm][SCN] is similar to acetone's, which is a prevalent solvent and used in many applications [193].

The safety data sheet of [EMIm][SCN] provided by *Iolitec* does not provide H-phrases with the remark that the substance is not yet fully tested. General measures are given standard for working with chemicals in a lab environment. A different safety data sheet [235] provides the following classification according to the CLP classification – Regulation(EC) No 1272/2008

- acute oral toxicity category 4



- acute dermal toxicity category 4
- acute inhalation toxicity - vapours category 4
- chronic aquatic toxicity category 3

The following H-phases are provided: harmful if swallowed (H302), harmful in contact with skin (H312) and Harmful if inhaled (H332). The acute toxicities are in category 4 of the GHS (Globally Harmonized System for Hazard Communication). This is the second lowest category.

The additive copper(I)thiocyanate (CAS: 1111-67-7) has the signal word "Warning" and is classified as hazardous to the aquatic environment (acute and chronic category 1; H400+H410) [236]. In conclusion, [EMIm][SCN] is significantly less toxic than conventional propellants. The additive is also uncritical in terms of toxicity. Therefore, it is suited as a 'green' alternative. Besides, due to the negligible vapour pressure, it can be handled easily with standard lab measures (such as protective glasses, face shield, gloves, and lab coat) and a SCAPE suit is not needed.

## 7.2 Perspective use of HIP\_11 in a multimode propulsion system

The term multimode in-space propulsion describes a spacecraft's propulsion system with at least two modes. For each mode, the same propellant is used, but the generation of thrust is based on different principles. For example, chemical and electrical propulsion methods could be combined using the same propellant. Also, a combination of two chemical modes is possible. This could be a combination of a hypergolic main apogee engine using HIP\_11 and a reaction control system with hydrogen peroxide monopropellant thrusters. The combination of electrical and chemical propulsion in a multimode system has become of recent interest [237]. In a combined chemical electrical multimode propulsion system, a low  $I_{sp}$  chemical and a high  $I_{sp}$  electrical mode are combined. Such a combination would also be possible with HIP\_11. The chemical modes could include a monopropellant mode using hydrogen peroxide and a hypergolic mode with HIP\_11. The electrical mode could be based on the ionic liquid fuel used in an electrical thruster.

Electrical thrusters using ionic liquids as propellant are called electrospray or colloid thrusters. Since an ionic liquid fuel is used, there is no need to ionise the propellant, unlike many other electrical propulsion concepts. The basic principle relies on applying a voltage between an emitter and an extractor, which generates an electric field. The ionic liquid wets the surface of the emitter. The extractor is some kind of porous structure or a fine grid. Because of the electric field, ions are extracted from the surface, accelerated, and passed through the extractor. This generates thrust. The emitter can be a structure with tips or capillaries to facilitate the extraction. The ions are extracted from the top of the tip or capillary. Because ionic liquids are not volatile, they can be provided passively to the emitter, making miniature valves or other flow control devices obsolete.

Many ionic liquids are suitable for the electrospray propulsion. Fonda-Marsland and Ryan proposed a criterion for potential high-performing ionic liquids in electrospray thruster [238]. The criterion is based on an ionic liquid's specific conductivity  $\kappa$  and surface tension  $\sigma$ . High surface tension and specific conductivity are beneficial for high thrust and  $I_{sp}$ . The criterion is defined as the square root of the product of conductivity and surface tension  $\sqrt{\kappa\sigma}$  [238]. For [EMIm][SCN], a value of 9.9 can be calculated with the specific conductivity  $\kappa=1.3 \text{ S m}^{-1}$  and surface tension  $\sigma=57.8 \text{ mN /m}$  [225]. This is a higher value than the commonly used 1-ethyl-3-methylimidazolium tetrafluoroborate ([EMIm][BF<sub>4</sub>]) [239] with 8.3 ( $\kappa=1.4 \text{ S m}^{-1}$  surface tension  $\sigma=49 \text{ mN /m}$  [225]). Ryan et al. already conducted preliminary tests using [EMIm][SCN] in an electrospray test setup and demonstrated the IL successfully [239]. Hence, electrospray propulsion with [EMIm][SCN] should be feasible.

In 2011, Donius and Rovey assessed different multimode propulsion systems and compared them to a conventional chemical and electrical propulsion combination [240]. In their study, they assumed a reference case with a 100 kg satellite, which has a mass budget of 35 kg for the propulsion module and predicted the maximum  $\Delta v$  depending on the ratio of the chemical and electrical mode. For the modelling, the masses of the different components of the propulsion system were estimated. Mainly, the power unit necessary for the cases using an electrospray thruster was a high mass penalty limiting the system's gain in  $\Delta v$ . Their assumption for the power unit was made based on state-of-the-art systems. Finally, they concluded that if the power units' efficiency can be increased in terms of specific power (watt per mass of the power unit), the overall total impulse and mission time can be improved compared to their reference cases. Such an increase in performance of the propulsion system can be expected for specific power values of more than 15 W/kg [240].

Today, electrospray propulsion systems are under development, and the first systems are flight-proven and available on the market. For example, Accion Systems offers an electrospray propulsion system called Tile 3 [138]. The system has a size of 1U and generates a nominal thrust of 0.45 mN at a power consumption of 20 W. The nominal  $I_{sp}$  is 1650 s [138]. The wet mass of the system is 1.25 kg. The specific power of this system (wet mass per power for simplification) is 16 W/kg. This indicates that the specific power of today's SoA electrospray systems has already reached competitive orders. It should be mentioned that Tile 3 is a closed system. It needs to be reconfigured for the use as part of a multimode system.

In the following, an exemplary calculation will be performed to estimate the potential of multimode propulsion. As a reference, a mission into geostationary orbit is chosen. The insertion into GEO from GTO is conducted with chemical bipropellant propulsion. The orbit keeping can be conducted chemically or electrically with an electrospray thruster. A dry mass is assumed, which includes the payload and the chemical propulsion system. The chemical propulsion system has an apogee motor powered with HIP\_11 at an assumed  $I_{sp}$  of 300 s. The RCS also uses HIP\_11 thrusters with an  $I_{sp}$  of 270 s. For the conventional case, an apogee motor with an  $I_{sp}$  of 320 s is assumed and 270 s of  $I_{sp}$  for the RCS. For the multimode case, the spacecraft is additionally equipped with electrospray thrusters of the Tile 3 type, assuming the thrusters run with [EMIm][SCN] at the same  $I_{sp}$  and power consumption [138]. Two different cases are compared. First, insertion and station keeping are conducted with chemical propulsion. Second, the insertion is accomplished with chemical propulsion, and the station keeping is performed with electrospray thrusters using [EMIm][SCN]. The velocity difference for insertion is assumed to be 1800 m/s and the station keeping with 50 m/s per year [241]. In the first step, the chemical mode is calculated. For the multimode case, the amount of electrospray thrusters is calculated based on the  $\Delta v$  for station keeping and the dry mass. This is fundamental because the electrospray thrusters need to provide the  $\Delta v$  for station keeping every year. Further, it is assumed that the spacecraft has a cuboid form and thrusters needed for the station keeping are placed on each side. If one thruster is sufficient to provide the  $\Delta v$ , in total, 6 thrusters are added on each side of the spacecraft. Based on the dry mass and the mass of the additional thrusters, the propellant mass for station keeping is calculated.

The results of the calculation are presented in table 7.3. Different satellite sizes are compared, as well as different mission durations. For a 100 kg class satellite, the mass saving by the multimode propulsion is 1.3 kg compared to a fully green chemical propulsion system. For heavier satellites, the advantage increases and lies in the order of ten per cent of the dry mass. The HIP\_11 propellant does not reduce masses over this mission duration compared to a conventional propulsion system in full chemical mode. For the lifetime of 15 years, the multimode brings a considerable mass reduction. The mass reduction is in the order of 15 % to 19 % of the initial dry mass. Further, the launch mass of the spacecraft is, for the multimode case, about 13 to 19 % reduced compared to the conventional chemical propellant.

Table 7.3: Different mission scenarios

Dry mass [kg]	chemical launch mass [kg]	multi mode launch mass [kg]	$\Delta m$ $m_{mm}-m_{chem}$ [kg]	conventional MMH/NTO [kg]
5 Year mission				
100	202.6	201.3	-1.3	193.7
500	1012.9	964.1	-48.8	928.0
1500	3038.8	2892.4	-146.4	2783.9
3500	7090.6	6734.9	-355.7	6482.3
15 yr mission				
100	244.7	207.6	-37.1	235.5
500	1223.4	994.4	-229.0	1177.5
1500	3670.2	2983.1	-687.0	3532.5
3500	8563.8	6942.2	-1617.6	8242.6

Adding an electrospray propulsion adds a mass penalty in terms of an additional thruster and power supply unit. This mass penalty is the main reason for the low differences in mass for small satellites and shorter mission durations. The electrical propulsion with the high  $I_{sp}$  can pay off for longer missions and heavier satellites. The power needed for the electrospray thruster is 20 W for the 100 kg satellite, increasing to 280 W for the heaviest satellites.

This is only a rough estimation. The mass budget for the single components is not recalculated for every case. For example, if several 100 kg less propellant is needed, the tank size and mass are also reduced. This will increase the advantage of larger satellites even more. Such an effect is not considered in the presented estimation. Further, the scaling of the electrospray thruster is expected to be more efficient than assuming several 1U thruster modules. On the other hand, redundancy is also not incorporated in the calculation, which will decrease the performance of light satellites.

The presented estimation is one application for multimode propulsion. For missions using a multimode, the advantage is higher mission efficiency. The total  $\Delta v$  is flexible if a propellant component is shared. If more propellant is used in electrical mode, higher  $\Delta v$  can be reached at the cost of power consumption and longer transfer durations. On the contrary, the chemical propulsion can provide fast manoeuvres.

### 7.3 Summary

In this chapter, the identified fuel candidates [EMIm][SCN] and E5C were characterised in terms of physical properties, thermodynamic properties, and propulsive performance. An initial toxicity assessment was conducted. Based on this characterisation, the HIP\_11 propellant is a suitable candidate as a green substitute for conventional hypergolic propellants.

Further, the application of the ionic liquid in a multimode propulsion system was assessed. As a reference case, a mission into geostationary orbit was assumed. In the multimode system, the insertion into the geostationary orbit would be completed in hypergolic chemical mode with HIP\_11. Electrospray thrusters propelled by the ionic liquid would perform the station keeping. The multimode system can provide mass savings compared to a fully chemical mission.

## 8 Conclusion and outlook

The objective of the present thesis was to overcome a gap in the present in-space propulsion. Due to the drawbacks of conventional propellants, "green" replacements are developed. There are green solutions that are already flight-ready and demonstrated in orbit, which can substitute hydrazine as a monopropellant, such as hydrogen peroxide or fuel blends with energetic materials. For bipropellants, the first solutions based on self-pressuring propellants such as nitrous oxide and light hydrocarbons are also already in space and on the market. Moreover, first solutions with hydrogen peroxide and a fuel in staged combustion mode are available. But as of now, there appears to be a gap in green hypergolic propellants. To overcome this gap, this thesis aimed to develop a green, hypergolic propellant that can be a candidate to substitute conventional hypergolic propellants.

### 8.1 Summary and conclusion

This thesis presents the development of a novel hypergolic combination based on hydrogen peroxide and ionic liquid fuels. Hydrogen peroxide was chosen as a green liquid oxidizer, and the group of ionic liquids was identified as promising. Ionic liquids have a neglectable vapour pressure, which allows for facilitated handling procedures compared to conventional propellants.

The development process started with a theoretical screening for suitable ionic liquid fuel candidates. The screening focused on commercially available ionic liquids. Several criteria were identified as relevant for applying an ionic liquid as fuel, and requirements for these criteria were defined. The relevant criteria include physical properties such as density and viscosity and thermal properties such as melting point and decomposition temperature. Further, the theoretical performance in terms of  $I_{sp}$  is relevant for the selection. Based on the catalogue of commercially available ionic liquids, suitable fuel candidates were identified: imidazolium ionic liquids with different anions. The considered anions included [DCA]<sup>-</sup>, [Ac]<sup>-</sup>, [MeOSO<sub>3</sub>]<sup>-</sup>, [SCN]<sup>-</sup>, [FeCl<sub>4</sub>]<sup>-</sup> and [TCM]<sup>-</sup>. The screened ionic liquids showed similar maximum theoretical performance between 300 and 330 s of  $I_{sp}$  with 98 % hydrogen peroxide at the selected conditions. Based on the screening, seven ionic liquids were purchased for further testing on hypergolic ignition with highly concentrated hydrogen peroxide.

In more than 900 drop tests, the hypergolic reaction between the ionic liquids and hydrogen peroxide was evaluated. [EMIm][MeOSO<sub>3</sub>], [BMIm][Ac] and [EMIm][DCA] have not shown an obvious reaction with hydrogen peroxide. [BMIm][FeCl<sub>4</sub>] and [BMIm][TCM] reaction with the hydrogen peroxide, but the ignition delay is in the order of several seconds, which is not suitable. [EMIm][SCN] and [BMIm][SCN] showed hypergolic ignitions with hydrogen peroxide, and the ignition delay times were between 30 and 60 ms. It was shown that the copper-based additive [Cu][SCN] dissolved in [EMIm][SCN] reduces the IDT. The shortest IDT around 13 ms was observed for a mixture of [EMIm][SCN] and 5 wt% [Cu][SCN] (E5C). Therefore, the substance [EMIm][SCN] and the mixture E5C were chosen as the most promising fuel candidates for further investigation.

In parallel, a study was conducted to assess the influence of different factors on the ignition delay

in drop test. The following factors were evaluated: drop height, drop order, amounts of drop and pool, surrounding medium, initial pressure, initial temperature,  $\text{H}_2\text{O}_2$  concentration. The results were:

- The drop height and different amounts for drops and pool did not significantly influence the ignition delay time in the tested boundaries.
- Test with Argon as an inert surrounding medium did not impact the IDT compared to tests in air.
- A falling drop of fuel into a  $\text{H}_2\text{O}_2$  pool generates significantly longer ignition delays compared to a  $\text{H}_2\text{O}_2$  drop falling into a fuel pool.
- The ignition delay depends on the ambient pressure. At lower pressure, the IDT increases. The influence was tested between 0.1 bar and 1 bar. [EMIm][SCN] did not ignite below 0.2 bar. E5C ignited down to 0.1 bar. At this pressure, the IDT was doubled compared to ambient conditions.
- The fuel's initial temperature significantly impacts the ignition delay in the drop tests. This is most likely related to the viscosity, which changes with temperature.
- The  $\text{H}_2\text{O}_2$  concentration has an impact on the ignition delay. The ignition delay increases for lower hydrogen peroxide concentrations. Reliable ignitions were observed down to 78%  $\text{H}_2\text{O}_2$  concentration. The IDT for [EMIm][SCN] and E5C is about four times higher for the low concentration compared to a concentration of 97 %.
- The shortest ignition delays of thiocyanate ILs were observed with [EMIm]<sup>+</sup> cation. Other cations, such as [AMIm]<sup>+</sup> or [BMIM]<sup>+</sup>, showed higher IDTs.

After the identification of suitable fuel candidates with ignition delay in the drop test in the order of 10 ms, the fuel candidates should be tested under more relevant conditions. For this, an injection setup with a suitable injector was implemented. E5C showed fast hypergolic ignitions in a 2-on-1 impinging injector. The ignition delay times were below 10 ms. Thereby, the IDTs were shorter than those IDTs measured in drop tests. A 3-on-1 impinging injector and a double swirl injector also provided reliable hypergolic ignitions. After the ignitions, the swirl injector showed a rough combustion behaviour. The ignition of E5C was also evaluated at low pressure conditions down to 27 mbar. The IDT increased with lower pressure, and the ignition delay was in the order of several 100 ms at 27 mbar.

Pure [EMIm][SCN] was also tested with the 2-on-1 injector, and successful ignitions were observed. The IDT was between 10 and 20 ms, shorter than drop tests.

Overall, it was shown that E5C provided fast, reliable and robust hypergolic ignitions with hydrogen peroxide. Therefore, E5C was selected as the most promising fuel candidate.

Finally, E5C and the neat [EMIm][SCN] were characterized by the determination of their physical (density, viscosity, surface tension, FTIR spectra) and thermodynamic properties (TGA, DSC). Further, the propulsive performance was calculated with CEA. [EMIm][SCN] has the highest  $I_{sp}$  of 323.1 s at a ROF of 3.8. E5C offers a maximum  $I_{sp}$  of 321.2 s. As a comparison, the  $I_{sp}$  of the conventional propellant MMH/NTO is 5 % higher at the same conditions. Regarding the density-specific impulse, [EMIm][SCN] and E5C offer a 10 % improvement compared to the conventional hypergolic propellant. Further, it was shown that [EMIM][SCN] and E5C are significantly less toxic than conventional propellants.

Ionic liquids can be used as propellant in electrospray thrusters. Therefore, a multimode propulsion system was considered with a high thrust hypergolic chemical mode and low thrust, high  $I_{sp}$

electric mode. Such a system could be applied in a geostationary satellite, where the manoeuvres for the delivery into GEO are conducted with the chemical mode. The electric mode is used in GEO for station keeping. It was shown that a multimode system can allow significant mass savings. For a 15-year mission, the launch mass of a spacecraft with a multimode propulsion system is in the order of 15 % to 19 % lower compared to a satellite with a fully chemical propulsion system.

To conclude, in this thesis, a novel group of hypergolic substances with hydrogen peroxide was identified, namely ionic liquids with the thiocyanate anion. Fuels based on [EMIm][SCN] have the potential to substitute conventional hypergolic propellants. However, further development is needed. Ionic liquids based on the thiocyanate anion have the potential to go to space.

## 8.2 Outlook

The tunability of ionic liquid offers a promising field of research. Ionic liquids can be tuned for shorter ignition delay times, higher performance or lower viscosity. Further ionic structures can be tested because their influence on hypergolic ignition is still unknown. Likewise, additives can be screened to shorten the IDT or increase the performance. Manganese, as well as non-metallic additives, could be an effective additives. The ignition process of hydrogen peroxide and thiocyanate ionic liquids is currently unknown. Understanding the path from liquid interaction, early liquid reaction, and vapour phase reaction until ignition cloud can help design new ionic liquids with superior performance.

On the other side, the HIP\_11 propellant is already competitive in terms of performance compared to conventional hypergolic propellants. In the last years, a battleship thruster was designed, and initial tests were performed to evaluate the performance of E5C with 98 %  $\text{H}_2\text{O}_2$  [242]. Figure 8.1 shows a hot firing with the battleship thruster.

Initial tests were performed with a 2-on-1 impinging injector based on the experiences gained

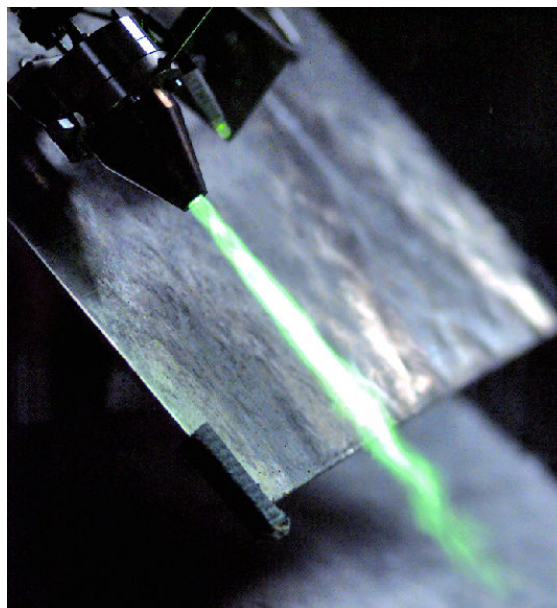


Figure 8.1: Hot firing test of battleship thruster with HIP\_11 E5C

during this thesis. Reliable ignitions and high  $c^*$  efficiencies (up to 95 %) were demonstrated [242].

Areas which need to be tackled to raise the TRL of the HIP\_11 technology include:

- the optimization of the injector for fast and reliable hypergolic ignition, efficient combustion and sufficient pressure loss
- the development of an appropriate cooling method for HIP\_11 allowing steady state firings and pulse mode
- the verification of vacuum ignition
- the development of a propulsion system with suitable components (tanks, tubes, valves, sensors, etc.) compatible with  $H_2O_2$  and the ionic liquid, suited for long-term space use

The final aim should be to increase the TRL of the HIP\_11 technology to validate the propellant combination in space.

# 9 Annex

## 9.1 Injectors

The following diagrams display the calibration tests of the different injector configuration. The  $c_d$  values were used to determine mass flows of the operation point during the hot firing tests described in chapter 6. Further, the technical drawing of the 2-on-1 injector is shown.

### $c_d$ of different injectors

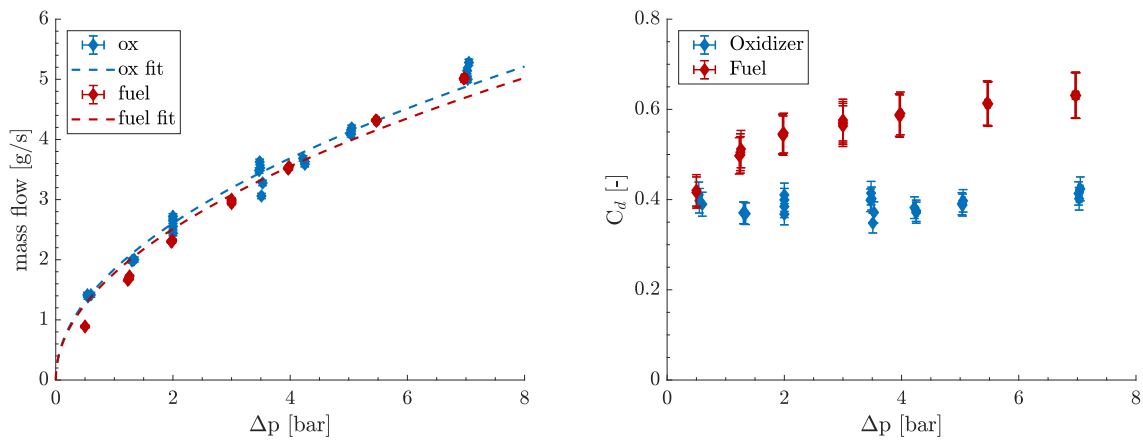


Figure 9.1: Pressure drop and  $c_d$  of 3on1 injector

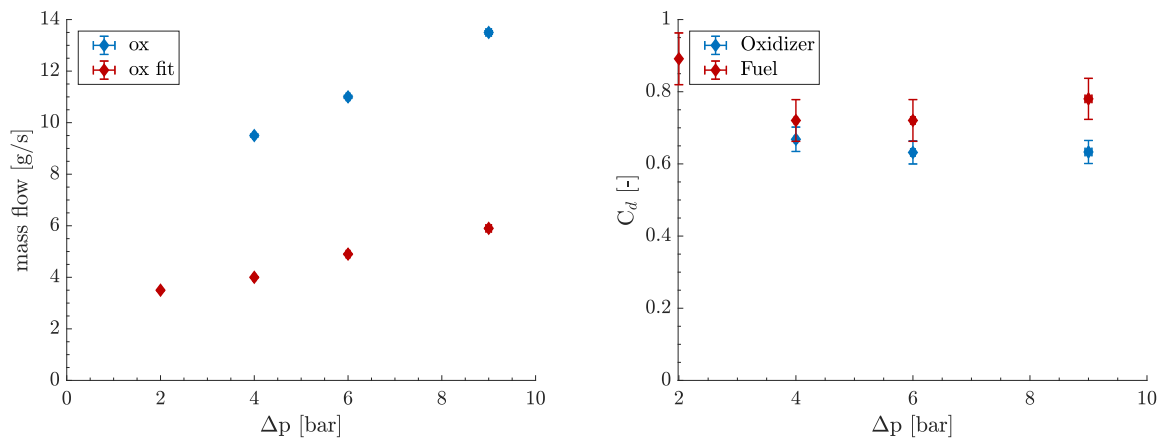


Figure 9.2: Pressure drop and  $c_d$  of 2on1 injector in 2nd test campaign





Table 9.1: Hypergolic ionic liquids with hydrogen peroxide (no DLR developments included), status from January 2023

Fuel Cation	Anion	Amount	Additive	IDT[ms]	conc. H2O2	condition	
[THTDP]	[Al(BH <sub>4</sub> ) <sub>4</sub> ] 2015			<30ms	90 und 98		[143]
[AMIm]	[DCA]	15%	Cu salt	9	94,7%	flow	[146]
[AMIm]	[DCA]	15%	Cu salt	11	90%	flow	[146]
[AMIm]	[DCA]	15%	Cu salt	22	80%	flow	[146]
Bhosale et al.	2019						
[EMIm]	BH <sub>4</sub>		solid	18,5	95%	fuel rich	[153]
[EMIm]	[BH <sub>3</sub> CN]			>1000	95%	fuel rich	[153]
[AEIm]	[BH <sub>3</sub> CN]			>1000	95%	fuel rich	[153]
Ammonium	Borane			8	95%		
Bhosale et al.	2020						
[EMIm]	[BH <sub>3</sub> CN]	5%	CuCl <sub>2</sub>	139	95%	ox rich	[63]
[EMIm]	[BH <sub>3</sub> CN]	5%	Co Ac	887	95%	ox rich	[63]
[EMIm]	[BH <sub>3</sub> CN]	5%	NaBH <sub>4</sub>	73	95%	ox rich	[63]
[EMIm]	[BH <sub>3</sub> CN]	5%	[MMIm] [Cu <sub>2</sub> I <sub>3</sub> ]	87	95%	ox rich 5ml H2O2	[63]
[EMIm]	[BH <sub>3</sub> CN]	2%	[MMIm] [Cu <sub>2</sub> I <sub>3</sub> ]	126	95%	ox rich	[63]
[EMIm]	[BH <sub>3</sub> CN]	5%	[MMIm] [Cu <sub>2</sub> I <sub>3</sub> ]	57	95%	ox rich 0,3 ml H2O2	[63]
[EMIm]	[BH <sub>3</sub> CN]	7%	[MMIm] [Cu <sub>2</sub> I <sub>3</sub> ]	50	95%	ox rich	[63]
[EMIm]	[BH <sub>3</sub> CN]	10%	[MMIm] [Cu <sub>2</sub> I <sub>3</sub> ]	41	95%	ox rich	[63]
[EMIm]	[BH <sub>3</sub> CN]	12%	[MMIm] [Cu <sub>2</sub> I <sub>3</sub> ]	38	95%	ox rich	[63]
[EMIm]	[BH <sub>3</sub> CN]	15%	[MMIm] [Cu <sub>2</sub> I <sub>3</sub> ]	29	95%	ox rich	[63]
[EMIm]	[BH <sub>3</sub> CN]	2%	[MMIm] [Cu <sub>2</sub> I <sub>3</sub> ]	47	95%	fuel rich	[63]
[EMIm]	[BH <sub>3</sub> CN]	5%	[MMIm] [Cu <sub>2</sub> I <sub>3</sub> ]	30	95%	fuel rich	[63]
[EMIm]	[BH <sub>3</sub> CN]	7%	[MMIm] [Cu <sub>2</sub> I <sub>3</sub> ]	21	95%	fuel rich	[63]
[EMIm]	[BH <sub>3</sub> CN]	10%	[MMIm] [Cu <sub>2</sub> I <sub>3</sub> ]	17	95%	fuel rich	[63]
[EMIm]	[BH <sub>3</sub> CN]	12%	[MMIm] [Cu <sub>2</sub> I <sub>3</sub> ]	14	95%	fuel rich	[63]
[EMIm]	[BH <sub>3</sub> CN]	15%	[MMIm] [Cu <sub>2</sub> I <sub>3</sub> ]	13	95%	fuel rich	[63]

continued on next page

## Hypergolic ionic liquids with hydrogen peroxide, status from January 2023

Fuel Cation	Anion	Amount	Additive	IDT[ms]	conc. H2O2	condition	
Bhosale et al.	2021						
[EMIm]	[BH <sub>3</sub> CN]	100%	Cu-P1	3.75	95%	solid	[154]
		100%	Cu-P2	8.5	95%	solid	[154]
		13%	Cu-P1	9.5	95%	fuel rich	[154]
Chinnam et al.	2018						
[EMIm]	[BH <sub>3</sub> CN]	0,08	[B <sub>12</sub> I <sub>12</sub> ] <sub>2</sub> [Cs]	> 4000	95%	fuel rich	[148]
		0,08	[B <sub>12</sub> I <sub>12</sub> ] <sub>2</sub> [Cu(en) <sub>2</sub> (CH <sub>3</sub> CN) <sub>2</sub> ]	1088	95%	fuel rich	[148]
		0,08	[B <sub>12</sub> I <sub>12</sub> ] <sub>2</sub> [FcCH <sub>2</sub> NEtMe <sub>2</sub> ]	24	95%	fuel rich	[148]
		0,08	[I] [FcCH <sub>2</sub> NEtMe <sub>2</sub> ]	17	95%	fuel rich	[148]
		0,08	[I] [Cu(en) <sub>2</sub> (CH <sub>3</sub> CN) <sub>2</sub> ]	243	95%	fuel rich	[148]
		0,08	Ferrocene	34	95%	fuel rich	[148]
		0,08	Triodopyrazole	> 1000	95%	fuel rich	[148]
		0,08		1420	95%	fuel rich	[148]
Wang et al.	2018						
[EMIm]	[BH <sub>3</sub> CN]			> 1000	95%	fuel rich	[147]
		0,1	[EMIm] <sub>4</sub> [Cu <sub>4</sub> I <sub>8</sub> ]	37	95%	fuel rich	[147]
		0,1	[EMIm] <sub>3</sub> [Cu <sub>8</sub> I <sub>14</sub> ]	36	95%	fuel rich	[147]
		0,1	[EMIm] <sub>2</sub> [Cu <sub>5</sub> I <sub>7</sub> ]	24	95%	fuel rich	[147]
		0,1	[MATA] [CuI <sub>2</sub> ]	38	95%	fuel rich	[147]
				> 300	95%	fuel rich	[147]
		0,1	[EMIm] <sub>4</sub> [Cu <sub>4</sub> I <sub>8</sub> ]	30	95%	fuel rich	[147]
		0,1	[EMIm] <sub>3</sub> [Cu <sub>8</sub> I <sub>14</sub> ]	23	95%	fuel rich	[147]
		0,1	[EMIm] <sub>2</sub> [Cu <sub>5</sub> I <sub>7</sub> ]	14	95%	fuel rich	[147]
		0,1	[MATA] [CuI <sub>2</sub> ]	28	95%	fuel rich	[147]
Wang et al.	2020						
[EMIm]	[DCA]	10%	P1	1000+	95%	fuel rich	[149]
		10%	P2	54	95%	fuel rich	[149]
		10%	P3	42	95%	fuel rich	[149]
		10%	P4	187	95%	fuel rich	[149]
		10%		78	95%	fuel rich	[149]

continued on next page

Hypergolic ionic liquids with hydrogen peroxide, status from January 2023

Fuel Cation	Anion	Amount	Additive	IDT[ms]	conc. H2O2	condition	
[EMIm]	[BH <sub>3</sub> CN]			1000+	95%	fuel rich	[149]
[EMIm]	[BH <sub>3</sub> CN]	10%	P1	38	95%	fuel rich	[149]
[EMIm]	[BH <sub>3</sub> CN]	10%	P2	31	95%	fuel rich	[149]
[EMIm]	[BH <sub>3</sub> CN]	10%	P3	144	95%	fuel rich	[149]
[EMIm]	[BH <sub>3</sub> CN]	10%	P4	55	95%	fuel rich	[149]
[EMIm]	[BH <sub>3</sub> CN]			1000+	95%	fuel rich	[149]
[EMIm]	[BH <sub>3</sub> CN]	10%	P1	89	95%	fuel rich	[149]
[EMIm]	[BH <sub>3</sub> CN]	10%	P2	56	95%	fuel rich	[149]
[EMIm]	DMPB			1000+	95%	fuel rich	[149]
[EMIm]	DMPB	10%	P1	175	95%	fuel rich	[149]
[EMIm]	DMPB	10%	P2	158	95%	fuel rich	[149]
Wang et al.							
[EMIm]	[DCA]	0,2	P-Al	34	90%	fuel rich	[151]
Zhao et al.							
[EMIm]	[BH <sub>3</sub> CN]		Cu[AIM] <sub>4</sub> [BH <sub>3</sub> CN] <sub>2</sub>	37	90%	fuel rich	[243]
[EMIm]	[BH <sub>3</sub> CN]		Cu[AIM] <sub>4</sub> [N(CN) <sub>2</sub> ] <sub>2</sub>	31	90%	fuel rich	[243]
[EMIm]	[BH <sub>3</sub> CN]		Mn[AIM] <sub>4</sub> [BH <sub>3</sub> CN] <sub>2</sub>	62	90%	fuel rich	[243]
[EMIm]	[BH <sub>3</sub> CN]		Mn[AIM] <sub>4</sub> [N(CN) <sub>2</sub> ] <sub>2</sub>	70	90%	fuel rich	[243]

end



## References

- [1] K. Chang. For Artemis mission to moon, NASA seeks to add billions to budget. *The New York Times*, May 13, 2019.
- [2] P. Berthe, A. Over, M. Picardo, and A. Byers. Orion European Service Module ESM development, integration and qualification status. In *AIAA SPACE and Astronautics Forum and Exposition*. American Institute of Aeronautics and Astronautics, September 2017. DOI: 10.2514/6.2017-5144.
- [3] L. Meland and F. Thompson. History of the Titan liquid rocket engines. In *25th Joint Propulsion Conference*. American Institute of Aeronautics and Astronautics, July 1989. DOI: 10.2514/6.1989-2389.
- [4] D. J. Kessler. Collisional cascading: the limits of population growth in low earth orbit. *Advances in Space Research*, 11(12):63–66, January 1991. DOI: 10.1016/0273-1177(91)90543-s.
- [5] ESA Clean Space Blog. Short introduction to ESA’s zero debris approach. January 12, 2023. URL: <https://blogs.esa.int/cleanspace/2023/01/12/short-introduction-to-esas-zero-debris-approach/>.
- [6] T. Hörger, D. Krishti, R.-J. Koopmanns, F. Lauck, F. Merz, L. Werling, C. Kirchberger, and J. Steelant. Green propellants for satellite propulsion: an updated literature survey in the frame of the ESA Project GreenRAIM. In *13th ISICP - International Symposium on Special Topics in Chemical Propulsion*, 2023.
- [7] G. P. Sutton and O. Biblarz. *Rocket Propulsion Elements, 7th Edition*. Wiley-Interscience, 2000, page 751. ISBN: 9780471326427.
- [8] P. Gadsby, R. Hermsen, J. Wink, and S. Powell. Development, qualification and flight heritage of the B20 20N class greenbi-propellant thruster. In *Space Propulsion Conference*, 2022.
- [9] IFA, Institute for Occupational Safety and Health of the German Social Accident Insurance. GESTIS Substance Database Entry: Hydrazin / Hydrazine. URL: <https://gestis.dguv.de/data?name=002010> (visited on 10/10/2022).
- [10] J. Malm. *Inclusion of substances of Very High Concern in the Candidate List*. European Chemicals Agency (EChA), Helsinki, 2011.
- [11] IFA, Institute for Occupational Safety and Health of the German Social Accident Insurance. GESTIS Substance Database Entry: Methylhydrazin/ Methylhydrazine. URL: <https://gestis.dguv.de/data?name=510635> (visited on 10/10/2022).
- [12] IFA, Institute for Occupational Safety and Health of the German Social Accident Insurance. GESTIS Substance Database Entry: N,N-Dimethylhydrazin / N,N-Dimethylhydrazine. URL: <https://gestis.dguv.de/data?name=003410> (visited on 10/10/2022).
- [13] D. F. Stai, F. Bizjak, and S. Stephanou. Thermodynamic properties of nitrogen tetroxide. *Journal of Spacecraft and Rockets*, 2(5):742–745, September 1965. DOI: 10.2514/3.28272.
- [14] IFA, Institute for Occupational Safety and Health of the German Social Accident Insurance. GESTIS Substance Database Entry: Distickstofftetroxid/ Dinitrogen tetraoxide. URL: <https://gestis.dguv.de/data?name=001950> (visited on 10/10/2022).

- [15] B. Nufer. A summary of NASA and USAF hypergolic propellant related spills and fires. In *SpaceOps 2010 Conference*. American Institute of Aeronautics and Astronautics, April 2010. DOI: 10.2514/6.2010-1994.
- [16] B. Nufer. Hypergolic propellants: the handling hazards and lessons learned from use. In *Joint JANNAF Interagency Propulsion Committee 25th Safety and Environmental Protection Joint Subcommittee Meeting*, number KSC-2010-045R, 2010.
- [17] ESA. Green propellant for space propulsion. 2001. URL: [https://www.esa.int/Applications/Observing\\_the\\_Earth/Green\\_Propellant\\_for\\_Space\\_Propulsion](https://www.esa.int/Applications/Observing_the_Earth/Green_Propellant_for_Space_Propulsion) (visited on 05/01/2023).
- [18] B. J. German, E. C. Branscome, A. P. Frits, N. C. Yiakas, and D. N. Mavris. An evaluation of green propellants for an ICBM post boost propulsion system. In *Missile Sciences Conference*. Georgia Institute of Technology, 2000.
- [19] K. Anflo, T. Gronland, and N. Wingborg. Development and testing of ADN-based monopropellants in small rocket engines. In *36th AIAA/ASME/SAE/ASEE Joint Propulsion Conference and Exhibit*. American Institute of Aeronautics and Astronautics, July 2000. DOI: 10.2514/6.2000-3162.
- [20] F. Valencia-Bel and M. Smith. Replacement of conventional spacecraft propellants with green propellants. *Space Propulsion Conference*, 2012.
- [21] IFA, Institute for Occupational Safety and Health of the German Social Accident Insurance. GESTIS Substance Database Entry: Salpetersäure / Nitric acid. URL: <https://gestis.dguv.de/data?name=001370> (visited on 10/10/2022).
- [22] IFA, Institute for Occupational Safety and Health of the German Social Accident Insurance. GESTIS Substance Database Entry: Lachgas / Nitrous oxide. URL: <https://gestis.dguv.de/data?name=004230> (visited on 10/10/2022).
- [23] IFA, Institute for Occupational Safety and Health of the German Social Accident Insurance. GESTIS Substance Database Entry: Wasserstoffperoxid / Hydrogen peroxide. URL: <https://gestis.dguv.de/data?name=002430> (visited on 10/10/2022).
- [24] B. McBride and S. Gordon. *Chemical Equilibrium and Applications*. NASA, 2004.
- [25] T. L. Pourpoint and W. E. Anderson. Hypergolic reaction mechanisms of catalytically promoted fuels with rocket grade hydrogen peroxide. *Combustion Science and Technology*, 179(10):2107–2133, September 2007. DOI: 10.1080/00102200701386149.
- [26] T. L. Pourpoint. *Hypergolic Ignition of a Catalytically Promoted Fuel with Rocket Grade Hydrogen Peroxide*. PhD Thesis, Purdue University, West Lafayette, Indiana, 2005.
- [27] A. Dadiou, R. Damm, and E. W. Schmidt. *Raketentreibstoffe*. Springer, Vienna, 1968. ISBN: 978-3-7091-7132-5. DOI: 10.1007/978-3-7091-7132-5.
- [28] H. Kang, S. Park, Y. Park, and J. Lee. Ignition-delay measurement for drop test with hypergolic propellants: reactive fuels and hydrogen peroxide. *Combustion and Flame*, 217:306–313, July 2020. DOI: 10.1016/j.combustflame.2020.04.017.
- [29] C. Hampton, K. Ramesh, and J. Smith. Importance of chemical delay time in understanding hypergolic ignition behaviors. In *41st Aerospace Sciences Meeting and Exhibit*. American Institute of Aeronautics and Astronautics, January 2003. DOI: 10.2514/6.2003-1359.
- [30] J. Smith, K. Ramesh, C. Hampton, and R. Dasarathy. Time resolved measurements and reactive pathways of hypergolic bipropellant combustion. AFRL Final Report, University of Alabama, Huntsville, March 31, 2006.

- [31] J. Li, X. Weng, C. Tang, Q. Zhang, W. Fan, and Z. Huang. The ignition process measurements and performance evaluations for hypergolic ionic liquid fuels: [EMIm][DCA] and [BMIm][DCA]. *Fuel*, 215:612–618, March 2018. DOI: 10.1016/j.fuel.2017.10.091.
- [32] J. Li, W. Fan, X. Weng, C. Tang, X. Zhang, Z. Huang, and Q. Zhang. Experimental observation of hypergolic ignition of superbase-derived ionic liquids. *Journal of Propulsion and Power*, 34(1):125–132, January 2018. DOI: 10.2514/1.b36441.
- [33] Y. Liu, Y. Guo, L. han Fei, Z. ming Mai, C. long Tang, Z. Wang, Y. tao Wu, and Z. hua Huang. Experimental study on hypergolic ignition and non-ignition for dicyanamide-based ionic liquids at low impact velocity conditions. *Energetic Materials Frontiers*, 2(4):241–248, December 2021. DOI: 10.1016/j.enmf.2021.08.004.
- [34] K. Kuo. *Principles of Combustion*. Wiley-Interscience, 2005. ISBN: 9780471046899.
- [35] S. Aggarwal. A review of spray ignition phenomena: present status and future research. *Progress in Energy and Combustion Science*, 24(6):565–600, January 1998. DOI: 10.1016/s0360-1285(98)00016-1.
- [36] L. J. Kapusta, L. Boruc, and J. Kindracki. Pressure and temperature effect on hypergolic ignition delay of triglyme-based fuel with hydrogen peroxide. *Fuel*, 287:119370, March 2021. DOI: 10.1016/j.fuel.2020.119370.
- [37] A. T. Black, M. P. Drolet, and T. L. Pourpoint. Early liquid and gas phase hypergolic reactions between monomethylhydrazine and nitrogen tetroxide or red fuming nitric acid. *Combustion Science and Technology*, 191(11):1990–2005, October 2018. DOI: 10.1080/00102202.2018.1540471.
- [38] I. Glassman, R. A. Yetter, and N. Glumac. *Combustion*. I. Glassman, R. A. Yetter, and N. Glumac, editors. Academic Press, Amsterdam, fifth edition edition, 2014. ISBN: 9780124079137.
- [39] V. D. Agosta, T. F. Seamans, and M. Vanpee. Development of a fundamental model of hypergolic ignition in space-ambient engines. *AIAA Journal*, 5(9):1616–1624, September 1967. DOI: 10.2514/3.4259.
- [40] H. Kang and S. Kwon. Development of 500 N scale green hypergolic bipropellant thruster using hydrogen peroxide as an oxidizer. In *51st AIAA/SAE/ASEE Joint Propulsion Conference*. American Institute of Aeronautics and Astronautics, July 2015. DOI: 10.2514/6.2015-4062.
- [41] D. J. Ladanyi and R. O. Miller. Comparison of ignition delays of several propellant combinations obtained with modified open-cup and small-scale rocket engine apparatus. *NACA Research Memorandum*, 1953.
- [42] H. Tani, Y. Daimon, M. Sasaki, and Y. Matsuura. Atomization and hypergolic reactions of impinging streams of monomethylhydrazine and dinitrogen tetroxide. *Combustion and Flame*, 185:142–151, 2017. DOI: 10.1016/j.combustflame.2017.07.005.
- [43] F. Lauck, J. Witte, M. Negri, D. Freudenmann, and S. Schleichriem. Design and first results of an injector test setup for green hypergolic propellants. In *AIAA Propulsion and Energy 2019 Forum*. American Institute of Aeronautics and Astronautics, August 2019. DOI: 10.2514/6.2019-4279.
- [44] R. Schalla and E. Flechter. The ignition behavior of various amines with white fuming nitric acid. *ARS Journal*, 29(1):33–39, January 1959. DOI: 10.2514/8.4673.
- [45] F. Lauck, M. Negri, D. Freudenmann, and S. Schleichriem. Selection of ionic liquids and characterization of hypergolicity with hydrogen peroxide. *International Journal of Energetic Materials and Chemical Propulsion*, 19, 2020. DOI: 10.1615/intjen.energetic.materials.chemprop.2019028004.



- [46] A. Spengler G.; Lepie. Über Raketentreibstoffe mit hypergolen Eigenschaften. *Zeitschrift für Flugwissenschaften*, 11, 1963.
- [47] R. Lecourt and F.-X. d'Herbigny. MMH/NTO injection and ignition in vacuum downstream from an aestus engine single injection element. *Aerospace Science and Technology*, 8(3):207–217, April 2004. ISSN: 1270-9638. DOI: 10.1016/j.ast.2003.11.001.
- [48] E. A. Hurlbert, R. J. Moreland, and S. Candel. Propellant ignition and flame propagation. In *Liquid Rocket Thrust Chambers*, pages 405–435. American Institute of Aeronautics and Astronautics, January 2004. DOI: 10.2514/5.9781600866760.0405.0435.
- [49] G. Spengler, A. Lepie, and J. Bauer. Measurements of ignition delays of hypergolic liquid rocket propellants. In *Spring Meeting, Western States Section - The Combustion Institute*, pages 64–12, 1964.
- [50] G. Zarca, I. Ortiz, and A. Urriaga. Novel solvents based on thiocyanate ionic liquids doped with copper(I) with enhanced equilibrium selectivity for carbon monoxide separation from light gases. *Separation and Purification Technology*, 196:47–56, 2018. ISSN: 1383-5866. DOI: <https://doi.org/10.1016/j.seppur.2017.06.069>. Ionic Liquids in Separation and Purification Technology - Papers presented at ILSEPT 2017.
- [51] T. Yuan, Y.-T. Chen, and J.-Y. Zhou. The auto-ignition of kerosene-based synthetic fuel/hydrogen peroxide propellants and its injector design. In *2018 Joint Propulsion Conference*. American Institute of Aeronautics and Astronautics, July 2018. DOI: 10.2514/6.2018-4775.
- [52] H. Kang, D. Jang, and S. Kwon. Demonstration of 500 N scale bipropellant thruster using non-toxic hypergolic fuel and hydrogen peroxide. *Aerospace Science and Technology*, 49:209–214, February 2016. DOI: 10.1016/j.ast.2015.11.038.
- [53] H. Kang, J. Won, S. W. Baek, and S. Kwon. Autoignition and combustion characteristics of sodium borohydride-based non-toxic hypergolic fuel droplet at elevated temperatures. *Combustion and Flame*, 181:149–156, July 2017. DOI: 10.1016/j.combustflame.2017.03.021.
- [54] E. Sebastiano, C. Cook, A. Hu, and M. Murugesu. Recent developments in the field of energetic ionic liquids. *Journal of Material Chemistry A*:8153–8173, 2014.
- [55] H. Kang, E. Lee, and S. Kwon. Suppression of hard start for nontoxic hypergolic thruster using H<sub>2</sub>O<sub>2</sub> oxidizer. *Journal of Propulsion and Power*, 33(5):1111–1117, September 2017. DOI: 10.2514/1.b36510.
- [56] H. Jenkins. Ionic liquids - an overview. *Science Progress*, 94(3):265–297, September 2011. DOI: 10.3184/003685011x13138407794135.
- [57] S. D. Chambreau, A. C. Schenk, A. J. Sheppard, G. R. Yandek, G. L. Vaghjiani, J. Maciejewski, C. J. Koh, A. Golan, and S. R. Leone. Thermal decomposition mechanisms of alkylimidazolium ionic liquids with cyano-functionalized anions. *The Journal of Physical Chemistry A*, 118(47):11119–11132, November 2014. DOI: 10.1021/jp5095855.
- [58] S. M. Davis and N. Yilmaz. Advances in hypergolic propellants: ignition, hydrazine, and hydrogen peroxide research. *Advances in Aerospace Engineering*, 2014:1–9, September 2014. DOI: 10.1155/2014/729313.
- [59] D. Zhang, D. Yu, P. Zhang, Y. Yuan, L. Yue, T. Zhang, and X. Fan. Hypergolic ignition modulated by head-on collision, intermixing and convective cooling of binary droplets with varying sizes. *International Journal of Heat and Mass Transfer*, 139:475–481, August 2019.
- [60] X. Weng, C. Tang, J. Li, Q. Zhang, and Z. Huang. Coulomb explosion and ultra-fast hypergolic ignition of borohydride-rich ionic liquids with WFNA. *Combustion and Flame*, 194:464–471, August 2018. DOI: 10.1016/j.combustflame.2018.05.015.

- [61] Y. Wu, Z. Wang, L. Fei, Y. Guo, Y. Liu, C. Tang, and Z. Huang. An experimental study on the hypergolic process enhanced by pre-ignition heat release: [AMIM][DCA]/furfuryl alcohol blends reacting with white fuming nitric acid. *Fuel*, 326:125103, October 2022. DOI: 10.1016/j.fuel.2022.125103.
- [62] H. Kang, S. Park, K. Lee, D. H. Lee, and J. Lee. Electrospray drop test method for green hypergolic propellants. *Journal of Spacecraft and Rockets*, 58(6):1920–1923, November 2021. DOI: 10.2514/1.a35113.
- [63] V. K. Bhosale, J. Jeong, J. Choi, D. G. Churchill, Y. Lee, and S. Kwon. Additive-promoted hypergolic ignition of ionic liquid with hydrogen peroxide. *Combustion and Flame*, 214:426–436, April 2020. DOI: 10.1016/j.combustflame.2020.01.013.
- [64] W. Florczuk and G. Rarata. Assessment of various fuel additives for reliable hypergolic ignition with 98 htp. *66th International Astronautical Congress (IAC)*, 2015.
- [65] W. Florczuk and G. Rarata. Performance evaluation of the hypergolic green propellants based on the htp for a future next generation space crafts, July 2017. DOI: <https://doi.org/10.2514/6.2017-4849>.
- [66] A. Thomas, S. D. Chambreau, and G. L. Vaghjiani. Ignition delay reduction with sodium addition to imidazolium-based dicyanamide ionic liquid. *The Journal of Physical Chemistry A*, 123(1):10–14, December 2018. DOI: 10.1021/acs.jpca.8b08678.
- [67] A. E. Thomas. *Green In-space Propellants: Ignition Chemistry of Hypergolic Ionic Liquids*. PhD thesis, 2019.
- [68] D. Hasan, D. Grinstein, A. Kuznetsov, B. Natan, Z. Schlagman, A. Habibi, and M. Elyashiv. Green comparable alternatives of hydrazines-based monopropellant and bipropellant rocket systems. In *Aerospace Engineering*. IntechOpen, November 2019. DOI: 10.5772/intechopen.82676.
- [69] Z. Schlagman, D. Komornik, R. Zvuloni, D. Hasan, R. Sagi, and B. Natan. Green hypergolic space propulsion. *Space Propulsion Conference 2022*, 2022.
- [70] K. Hatai and T. Nagata. Quantitative clarification of stable ignition region for HKP110 green hypergolic bipropellant. *Aerospace*, 9(3):129, March 2022.
- [71] H. Kim, H. Kang, and S. Kwon. Liquid sheet-sheet impinging structure for pintle injector with nontoxic hypergolic bipropellant. *Journal of Propulsion and Power*, 36(2):302–307, March 2020. DOI: 10.2514/1.b37645.
- [72] K.-S. Kim, S. Jung, and S. Kwon. Optical visualization of hypergolic burning spray structure using blue light spectrum. *Acta Astronautica*, 193:230–236, April 2022. DOI: 10.1016/j.actaastro.2022.01.007.
- [73] M. Long, W. Anderson, and R. Humble. Bicentrifugal swirl injector development for hydrogen peroxide and non-toxic hypergolic miscible fuels. In *38th AIAA/ASME/SAE/ASEE Joint Propulsion Conference & Exhibit*. American Institute of Aeronautics and Astronautics, July 2002. DOI: 10.2514/6.2002-4026.
- [74] J. D. Dennis, S. F. Son, and T. L. Pourpoint. Critical ignition criteria for monomethylhydrazine and red fuming nitric acid. *Journal of Propulsion and Power*, 31(4):1184–1192, July 2015. DOI: 10.2514/1.b35541.
- [75] T. L. Connell, G. A. Risha, R. A. Yetter, and B. Natan. Hypergolic ignition of hydrogen peroxide/gel fuel impinging jets. *Journal of Propulsion and Power*, 34(1):182–188, January 2018. DOI: 10.2514/1.b36571.

- [76] T. Yuan, Y. T. Chen, I. H. She, and B. Huang. Semi-hypergolic kerosene/hydrogen peroxide fuel system and its auto-ignition injector design. *51st AIAA / SAE / ASEE Joint Propulsion Conference*, July 2015. DOI: <https://doi.org/10.2514/6.2015-3847>.
- [77] J. J. Rusek, N. Anderson, B. M. Lormand, and N. L. Purcell. Non-toxic hypergolic miscible bipropellant. Patent (5,932,837) (USA). December 22, 1997.
- [78] B. L. Austin, S. D. Heister, and W. E. Anderson. Characterization of pintle engine performance for nontoxic hypergolic bipropellants. *Journal of Propulsion and Power*, 21(4):627–635, July 2005. DOI: 10.2514/1.7988.
- [79] R. Humble. Bipropellant engine development using hydrogen peroxide and a hypergolic fuel. In *36th AIAA/ASME/SAE/ASEE Joint Propulsion Conference and Exhibit*. American Institute of Aeronautics and Astronautics, July 2000. DOI: 10.2514/6.2000-3554.
- [80] Y. Cong, T. Zhang, T. Li, J. Sun, X. Wang, L. Ma, D. Liang, and L. Lin. Propulsive performance of hypergolic H<sub>2</sub>O<sub>2</sub>/kerosene bipropellant. *Journal of Propulsion and Power*, 20(1):83–86, January 2004. DOI: 10.2514/1.9189.
- [81] M. R. Long. *Swirl injectors for oxidizer-rich staged combustion cycle engines and hypergolic propellants*. PhD thesis, Purdue University, 2004.
- [82] A. Okninski, K. Sobczak, P. Surmacz, A. Kasztankiewicz, and M. Pakosz. The green dozen - twelve promising developments for european spacecraft and space transportation propulsion technology. *Space Propulsion Conference 2022*.
- [83] L. J. Maschio, E. P. de Araújo, L. G. F. Pereira, L. H. Gouvêa, and R. Vieira. Assessing the performance of a green liquid fuel hypergolic with hydrogen peroxide in a 50 N bipropellant thruster. *International Journal of Energetic Materials and Chemical Propulsion*, 20(1):21–30, 2021. DOI: 10.1615/intjenergeticmaterialschemprop.2020032684.
- [84] E. S. Shanley and F. P. Greenspan. Highly concentrated hydrogen peroxide. *Industrial & Engineering Chemistry*, 39(12):1536–1543, December 1947. DOI: 10.1021/ie50456a010.
- [85] W. C. Schumb, C. N. Satterfield, and R. L. Wentworth. *Hydrogen peroxide*. Reinhold Publishing Corporation, New York, 1955.
- [86] M. Ventura. Long term storability of hydrogen peroxide. In *41st AIAA/ASME/SAE/ASEE Joint Propulsion Conference & Exhibit*. American Institute of Aeronautics and Astronautics, July 2005. DOI: 10.2514/6.2005-4551.
- [87] S. Schuh, T. Bartok, R.-J. Koopmans, and C. A. Scharlemann. Results of material compatibility investigation of hydrogen peroxide. In *51st AIAA/SAE/ASEE Joint Propulsion Conference*. American Institute of Aeronautics and Astronautics, July 2015. DOI: 10.2514/6.2015-4252.
- [88] D. Davis, L. Dee, B. Greene, S. Hornung, M. McClure, and K. Rathgeber. *Fire, Explosion, Compatibility and Safety Hazards Of Hydrogen Peroxide*. NASA, Las Cruces, New Mexico, 2005.
- [89] Coherent Market Insights. Global hydrogen peroxide market to reach 6,624.4 KT by 2027. PRNewswire, editor. March 4, 2020. URL: <https://www.prnewswire.com/news-releases/global-hydrogen-peroxide-market-to-reach-6-624-4-kt-by-2027---coherent-market-insights-301016485.html> (visited on 05/01/2023).
- [90] C. W. Jones. *Applications of Hydrogen Peroxide and Derivatives*. J. H. Clark and M. J. Braithwaite, editors. The Royal Society of Chemistry, November 1999. DOI: 10.1039/9781847550132.

- [91] H. Walter. Report on rocket power plants based on T-substance. Technical report, NACA – Translation "Bericht Über die R-Triebwerke auf Grundlage des T-Stoffes" Schriften der Deutsche Akademie der Luftfahrtforschung Heft 1071 Nr. 82 1943, 1947.
- [92] G. Ventura and G. M. A brief history of concentrated hydrogen peroxide uses. In *35th AIAA/ASME/SAE/ASEE Joint Propulsion Conference and Exhibit*, Los Angeles, CA, 1999.
- [93] D. Baker. *NASA Mercury - 1956 to 1963 (Owners' Workshop Manual). An Insight into the Design and Engineering of Project Mercury - America's First Manned Space Programme*. Haynes Publishing Group P.L.C., 2017, page 208. ISBN: 9781785210648.
- [94] R. L. Sackheim and R. K. Masse. Green propulsion advancement: challenging the maturity of monopropellant hydrazine. *Journal of Propulsion and Power*, 30(2):265–276, March 2014. DOI: 10.2514/1.b35086.
- [95] J. D. Clark. *IGNITION! An Informal History of Liquid Rocket Propellants*. Rutgers University Press, New Brunswick, New Jersey, 1972.
- [96] B. A. Palyonov, A. I. Bessonov, A. I. Pastuhov, S. S. Shulkova, and G. P. Kalmykov. Green propellants in russia. In *Advanced Propulsion Systems and Technologies, Today to 2020*, pages 163–171. American Institute of Aeronautics and Astronautics, Reston, Virginia, April 2008. DOI: 10.2514/5.9781600866937.0163.0172.
- [97] R. Cort, E. Hurlbert, J. Riccio, and J. Sanders. Non-toxic on-orbit propulsion for advanced space vehicle applications. In *31st Joint Propulsion Conference and Exhibit*. American Institute of Aeronautics and Astronautics, July 1995. DOI: 10.2514/6.1995-2974.
- [98] D. Krejci, A. Woschnak, M. Schiebl, C. Scharlemann, K. Ponweiser, R. Brahmi, Y. Batonneau, and C. Kappenstein. Assessment of catalysts for hydrogen-peroxide-based thrusters in a flow reactor. *Journal of Propulsion and Power*, 29(2):321–330, March 2013. DOI: 10.2514/1.b34615.
- [99] C. Kappenstein, L. Pirault-Roy, M. Guérin, T. Wahdan, A. A. Ali, F. A. Al-Sagheer, and M. I. Zaki. Monopropellant decomposition catalysts. *Applied Catalysis A: General*, 234(1-2):145–153, August 2002. DOI: 10.1016/S0926-860X(02)00220-X.
- [100] S. Dolci, D. B. Dell'Amico, A. Pasini, L. Torre, G. Pace, and D. Valentini. Platinum catalysts development for 98% hydrogen peroxide decomposition in pulsed monopropellant thrusters. *Journal of Propulsion and Power*, 31(4):1204–1216, July 2015. DOI: 10.2514/1.b35590.
- [101] P. Surmacz. Green rocket propulsion research and development at the institute of aviation: problems and perspectives. *Journal of KONES. Powertrain and Transport*, 23(1):337–344, January 2016. DOI: 10.5604/12314005.1213534.
- [102] H. Kang, D. Lee, S. Kang, and S. Kwon. Effect of H<sub>2</sub>O<sub>2</sub> injection patterns on catalyst bed characteristics. *Acta Astronautica*, 130:75–83, January 2017. DOI: 10.1016/j.actaastro.2016.10.023.
- [103] P. Paszkiewicz, P. Wolanski, G. Rarata, L. Mezyk, and Z. a. Gut. Possibility of using thermal decomposition of hydrogen peroxide for low thrust propulsion system application. In *7th European Conference for Aeronautics and Space Sciences (EUCASS)*, 2017. DOI: 10.13009/EUCASS2017-626.
- [104] L. Mezyk, Z. Gut, K. Mohan, J. Kindracki, and G. Rarata. Initial research on thermal decomposition of 98% concentrated hydrogen peroxide in thruster-like conditions. *Engineering Science and Technology, an International Journal*, 31:101054, July 2022. DOI: 10.1016/j.jestch.2021.08.011.

- [105] H. Kang, J. W. Kim, J. R. Lee, and S. Kwon. A mixture of hydrogen peroxide and tetraglyme as a green energetic monopropellant. *Combustion and Flame*, 210:43–53, December 2019. DOI: 10.1016/j.combustflame.2019.08.016.
- [106] R. K. Palmer and J. J. Rusek. Low toxicity reactive hypergolic fuels for use with hydrogen peroxide. *2nd Int. Conference on Green Propellants for Space Propulsion*, 2004.
- [107] Benchmark Space Systems. Products. URL: <https://www.benchmarkspacesystems.com/products> (visited on 05/01/2023).
- [108] M. Negri, M. Wilhelm, and C. Hendrich. Development of ADN-based thruster technologies – an overview of the european project rheform. In *2018 Joint Propulsion Conference*. American Institute of Aeronautics and Astronautics, July 2018. DOI: 10.2514/6.2018-4751.
- [109] K. Anflo and B. Crowe. In-space demonstration of an ADN-based propulsion system. In *47th AIAA/ASME/SAE/ASEE Joint Propulsion Conference & Exhibit*. American Institute of Aeronautics and Astronautics, July 2011. DOI: 10.2514/6.2011-5832.
- [110] M. Persson, K. Anflo, and P. Friedhoff. Flight heritage of ammonium dinitramide (ADN) based high performance green propulsion (HPGP) systems. *Propellants, Explosives, Pyrotechnics*, 44(9):1073–1079, August 2019. DOI: 10.1002/prop.201900248.
- [111] R. A. Spores. GPIM AF-M315E propulsion system. In *51st AIAA/SAE/ASEE Joint Propulsion Conference*. American Institute of Aeronautics and Astronautics, July 2015. DOI: 10.2514/6.2015-3753.
- [112] C. H. McLean. Green propellant infusion mission: program construct, technology development, and mission results. In *AIAA Propulsion and Energy 2020 Forum*. American Institute of Aeronautics and Astronautics, August 2020. DOI: 10.2514/6.2020-3810.
- [113] R. K. Masse, R. Spores, and M. Allen. AF-M315E advanced green propulsion - GPIM and beyond. In *AIAA Propulsion and Energy 2020 Forum*. American Institute of Aeronautics and Astronautics, August 2020. DOI: 10.2514/6.2020-3517.
- [114] B. Marotta. On-orbit performance of the BCP-100 green propellant infusion mission. In *AIAA Propulsion and Energy 2020 Forum*. American Institute of Aeronautics and Astronautics, August 2020. DOI: 10.2514/6.2020-3826.
- [115] T. Katsumi and K. Hori. Successful development of HAN based green propellant. *Energetic Materials Frontiers*, 2(3):228–237, September 2021. DOI: 10.1016/j.enmf.2021.09.002.
- [116] L. Werling, Y. Joos, M. Wenzel, H. K. Ciezki, and S. Schlechtriem. A premixed green propellant consisting of N<sub>2</sub>O and C<sub>2</sub>H<sub>4</sub>: experimental analysis of quenching diameters to design flashback arresters. *International Journal of Energetic Materials and Chemical Propulsion*, 17(3):241–262, 2018.
- [117] L. K. Werling, T. Hörger, K. Manassis, D. Grimmeisen, M. Wilhelm, C. Erdmann, H. K. Ciezki, S. Schlechtriem, S. Richter, M. Torsten, E. Goos, J. Corina, C. Naumann, and U. Riedel. Nitrous oxide fuels blends: research on premixed monopropellants at the german aerospace center (DLR) since 2014. In *AIAA Propulsion and Energy 2020 Forum*. American Institute of Aeronautics and Astronautics, August 2020. DOI: 10.2514/6.2020-3807.
- [118] L. Werling and T. Hörger. Experimental analysis of the heat fluxes during combustion of a N<sub>2</sub>O–C<sub>2</sub>H<sub>4</sub> premixed green propellant in a research rocket combustor. *Acta Astronautica*, 189:437–451, December 2021. DOI: 10.1016/j.actaastro.2021.07.011.
- [119] L. Werling, N. Perakis, A. Bachmann, T. Methling, and C. Janzer. Numerical simulations of a research thruster operating with N<sub>2</sub>O/C<sub>2</sub>H<sub>4</sub> and comparison to experimental data. In *9th European Conference for Aerospace Sciences (EUCASS)*, 2022. DOI: 10.13009/EUCASS2022-6096.

- [120] J. Baker. A study of fast reactions in fuel-oxidant systems - ignition delay with rapidly mixed liquid reactants. Technical report, Illinois Inst of Tech Chicago, 1954.
- [121] B. Melof and M. Grubelich. Investigation of hypergolic fuels with hydrogen peroxide. In *37th Joint Propulsion Conference and Exhibit*. American Institute of Aeronautics and Astronautics, July 2001. DOI: 10.2514/6.2001-3837.
- [122] K.-S. Kim, V. K. Bhosale, and S. Kwon. Synergistic effect of a hybrid additive for hydrogen peroxide-based low toxicity hypergolic propellants. *Combustion and Flame*, 231:111450, September 2021. DOI: 10.1016/j.combustflame.2021.111450.
- [123] P. Wasserscheid and W. Keim. Ionische Flüssigkeiten - neue Lösungen für die Übergangsmetallkatalyse. *Angewandte Chemie*, 112(21):3926–3945, November 2000. DOI: 10.1002/1521-3757(20001103)112:21<3926::aid-ange3926>3.0.co;2-u.
- [124] M. C. Bubalo, K. Radošević, I. R. Redovniković, J. Halambek, and V. G. Srček. A brief overview of the potential environmental hazards of ionic liquids. *Ecotoxicology and Environmental Safety*, 99:1–12, January 2014. DOI: 10.1016/j.ecoenv.2013.10.019.
- [125] Q. Zhang and J. M. Shreeve. Energetic ionic liquids as explosives and propellant fuels: a new journey of ionic liquid chemistry. *Chemical Reviews*, 114(20):10527–10574, September 2014. DOI: 10.1021/cr500364t.
- [126] N. V. Plechkova and K. R. Seddon. Applications of ionic liquids in the chemical industry. *Chem. Soc. Rev.*, 37(1):123–150, 2008. DOI: 10.1039/b006677j.
- [127] A. J. Greer, J. Jacquemin, and C. Hardacre. Industrial applications of ionic liquids. *Molecules*, 25, November 2020. ISSN: 1420-3049. DOI: 10.3390/molecules25215207.
- [128] S. Schneider, T. Hawkins, M. Rosander, G. Vaghjiani, S. Chambreau, and G. Drake. Ionic liquids as hypergolic fuels. *Energy & Fuels*, 22(4):2871–2872, July 2008. DOI: 10.1021/ef800286b.
- [129] S. D. Chambreau, S. Schneider, M. Rosander, T. Hawkins, C. J. Gallegos, M. F. Pastewait, and G. L. Vaghjiani. Fourier transform infrared studies in hypergolic ignition of ionic liquids. *The Journal of Physical Chemistry A*, 112(34):7816–7824, August 2008. DOI: 10.1021/jp8038175.
- [130] M. Negri, M. Wilhelm, and H. K. Ciezki. Thermal ignition of ADN-based propellants. *Propellants, Explosives, Pyrotechnics*, 44(9):1096–1106, July 2019. DOI: 10.1002/prep.201900154.
- [131] K. Anflo and T.-A. Grönland. Towards green propulsion for spacecraft with adn-based monopropellants. In *38th AIAA/ASME/SAE/ASEE Joint Propulsion Conference*. American Institute of Aeronautics and Astronautics, July 2002. DOI: 10.2514/6.2002-3847.
- [132] K. Anflo and R. Möllerberg. Flight demonstration of new thruster and green propellant technology on the prisma satellite. *Acta Astronautica*, 65(9–10):1238–1249, November 2009. ISSN: 0094-5765. DOI: 10.1016/j.actaastro.2009.03.056.
- [133] B. S. Peter, R. A. Dressler, Y.-h. Chiu, and T. Fedkiw. Electrospray propulsion engineering toolkit (espet). *Aerospace*, 7(7):91, July 2020. ISSN: 2226-4310. DOI: 10.3390/aerospace7070091.
- [134] M. Gamero-Castano, V. Hruby, D. Spence, N. Demmons, R. McCormick, and C. Gaskaska. Micro newton colloid thruster system development for ST7-DRS mission. In *39th AIAA/ASME/SAE/ASEE Joint Propulsion Conference and Exhibit*. American Institute of Aeronautics and Astronautics, June 2003. DOI: 10.2514/6.2003-4543.

- [135] N. R. Demmons, D. Courtney, N. Alvarez, and Z. Wood. Component-level development and testing of a colloid micro-thruster (CMT) system for the LISA mission. In *AIAA Propulsion and Energy 2019 Forum*. American Institute of Aeronautics and Astronautics, August 2019. DOI: 10.2514/6.2019-3815.
- [136] J. Ziemer, C. Marrese-Reading, C. Dunn, A. Romero-Wolf, C. Cutler, S. Javidnia, T. Li, I. Li, G. Franklin, P. Barela, et al. Colloid microthruster flight performance results from space technology 7 disturbance reduction system. In *International Electric Propulsion Conference (IEPC) 2017*, number GSFC-E-DAA-TN47585, 2017.
- [137] Accion Systems Inc. Accion systems tile 2 in-space propulsion system to launch on the june 2021 spacex rideshare with astro digital and starfish space - press release. April 19, 2021. URL: <https://accion-systems.com/news/press/accion-systems-tile-2-in-space-propulsion-system-to-launch-on-the-june-2021-spacex-rideshare-with-astro-digital-and-starfish-space/> (visited on 01/03/2023).
- [138] Accion Systems Inc. Technical Specifications TILE 3. Technical report, 2021.
- [139] ION-X. Halo-100x. April 17, 2023. URL: <https://ion-x.space/product/> (visited on 04/17/2023).
- [140] Y. Zhang, H. Gao, Y.-H. Joo, and J. M. Shreeve. Ionic liquids as hypergolic fuels. *Angewandte Chemie International Edition*, 50(41):9554–9562, September 2011. DOI: 10.1002/anie.201101954.
- [141] Q. Zhang and J. M. Shreeve. Ionic liquid propellants: future fuels for space propulsion. *Chemistry - A European Journal*, 19(46):15446–15451, October 2013. DOI: 10.1002/chem.201303131.
- [142] Z. Zhang, Z. Zhao, B. Wang, and J. Zhang. Boron based hypergolic ionic liquids: a review. *Green Energy & Environment*, 6(6):794–822, December 2021. DOI: 10.1016/j.gee.2020.12.002.
- [143] S. Schneider, T. Hawkins, Y. Ahmed, M. Rosander, L. Hudgens, and J. Mills. Green bipropellants: hydrogen-rich ionic liquids that are hypergolic with hydrogen peroxide. *Angewandte Chemie*, 123(26):5886–5888, May 2011. DOI: 10.1002/ange.201101752.
- [144] S. Schneider, T. Hawkins, Y. Ahmed, and M. Rosander. Catalytic hypergolic bipropellants. Patent (US8758531B1). March 15, 2011.
- [145] Y.-S. Kim, G.-H. Son, T.-K. Na, and S.-H. Choi. Synthesis and physical and chemical properties of hypergolic chemicals such as n,n,n-trimethylhydrazinium and 1-ethyl-4-methyl-1,2,4-triazolium salts. *Applied Sciences*, 5(4):1547–1559, December 2015. DOI: 10.3390/app5041547.
- [146] V. Weiser, J. Hürttlen, U. Schaller, A. Imiolek, and S. Kelzenberg. Green liquid oxidizers basing on solutions of adn and an in hydrogen peroxide for hypergolic propellants with high performance. *7th EUCASS*, 2015.
- [147] K. Wang, A. K. Chinnam, N. Petrutik, E. P. Komarala, Q. Zhang, Q.-L. Yan, R. Dobrovetsky, and M. Gozin. Iodocuprate-containing ionic liquids as promoters for green propulsion. *Journal of Materials Chemistry A*, 6(45):22819–22829, 2018. DOI: 10.1039/c8ta08042a.
- [148] A. K. Chinnam, N. Petrutik, K. Wang, A. Shlomovich, O. Shamis, D. S. Tov, M. Sućeska, Q.-L. Yan, R. Dobrovetsky, and M. Gozin. Effects of closo-icosahedral periodoborane salts on hypergolic reactions of 70% H<sub>2</sub>O<sub>2</sub> with energetic ionic liquids. *Journal of Materials Chemistry A*, 6(41):19989–19997, 2018. DOI: 10.1039/c8ta03780a.

- [149] K. Wang, T. Liu, Y. Jin, S. Huang, N. Petrutik, D. Shem-Tov, Q.-L. Yan, M. Gozin, and Q. Zhang. Tandem-action ferrocenyl iodocuprates promoting low temperature hypergolic ignitions of green EILs-H<sub>2</sub>O<sub>2</sub> bipropellants. *Journal of Materials Chemistry A*, 8(29):14661–14670, 2020. DOI: 10.1039/d0ta04620e.
- [150] K. Wang, Z. Wang, X. Zhao, X. Qi, S. Song, Y. Jin, and Q. Zhang. Unearthing hidden hypergolic potential of energetic complexes with hydrogen peroxide. *Combustion and Flame*, 244:112235, October 2022. DOI: 10.1016/j.combustflame.2022.112235.
- [151] B. Wang, Z. Wang, Y. Jin, and K. Wang. Designing difunctional promoters for hypergolic ignitions of green bipropellants combining ionic liquids with H<sub>2</sub>O<sub>2</sub>. *Industrial & Engineering Chemistry Research*, 61(48):17433–17439, November 2022. DOI: 10.1021/acs.iecr.2c03065.
- [152] V. K. Bhosale, S. G. Kulkarni, and P. S. Kulkarni. Theoretical performance evaluation of hypergolic ionic liquid fuels with storable oxidizers. *New Journal of Chemistry*, 41(18):9889–9896, 2017. DOI: 10.1039/c7nj01748k.
- [153] V. K. Bhosale, J. Jeong, and S. Kwon. Ignition of boron-based green hypergolic fuels with hydrogen peroxide. *Fuel*, 255:115729, November 2019. DOI: 10.1016/j.fuel.2019.115729.
- [154] V. K. Bhosale, J. Gwak, K.-S. Kim, D. G. Churchill, Y. Lee, and S. Kwon. Rapid ignition of green bipropellants enlisting hypergolic copper (II) promoter-in-fuel. *Fuel*, 297:120734, August 2021. DOI: 10.1016/j.fuel.2021.120734.
- [155] S. C. Ricker, D. Freudenmann, and S. Schlechtriem. The impact of cation structures on hypergolicity of thiocyanate ionic liquids with hydrogen peroxide. *Energy & Fuels*, 35(19):16128–16133, September 2021. DOI: 10.1021/acs.energyfuels.1c02427.
- [156] S. C. Ricker, D. Brüggemann, D. Freudenmann, R. Ricker, and S. Schlechtriem. Protic thiocyanate ionic liquids as fuels for hypergolic bipropellants with hydrogen peroxide. *Fuel*, 328:125290, November 2022. DOI: 10.1016/j.fuel.2022.125290.
- [157] S. Ricker. *Synthese und Charakterisierung neuer hypergoler Raumfahrttreibstoffe basierend auf ionischen Flüssigkeiten mit Thiocyanatanionen als Brennstoffe und Wasserstoffperoxid als Oxidator*. under preparation. PhD thesis, Universität Stuttgart, 2024.
- [158] S. Park, K. Lee, H. Kang, Y. Park, and J. Lee. Effects of oxidizing additives on the physical properties and ignition performance of hydrogen peroxide-based hypergolic propellants. *Acta Astronautica*, 200:48–55, November 2022. DOI: 10.1016/j.actaastro.2022.07.051.
- [159] G. S. Gill and W. H. Nurick. *Liquid Rocket Engine Injectors*. NASA SP-8089, 1976.
- [160] B. R. Lawver. Photographic observation of reactive stream impingement. *Journal of Spacecraft and Rockets*, 17(2):134–139, March 1980. DOI: 10.2514/3.57719.
- [161] R. Stechman and D. Sumpter. Development history of the apollo reaction control system rocket engine. In *25th Joint Propulsion Conference*. American Institute of Aeronautics and Astronautics, July 1989. DOI: 10.2514/6.1989-2388.
- [162] R. Stechman. Development history of the 25 Lbf (110 Newton) space shuttle vernier thruster. In *26th Joint Propulsion Conference*. American Institute of Aeronautics and Astronautics, July 1990. DOI: 10.2514/6.1990-1837.
- [163] P. Gallier and X. Pages. 200N bipropellant thruster pulsed mode behavior. In *35th Joint Propulsion Conference and Exhibit*. American Institute of Aeronautics and Astronautics, June 1999. DOI: 10.2514/6.1999-2467.



- [164] R. Mahakali, F. Kuipers, A. Yan, W. Anderson, and T. Pourpoint. Development of reduced toxicity hypergolic propellants. In *47th AIAA/ASME/SAE/ASEE Joint Propulsion Conference and Exhibit*. American Institute of Aeronautics and Astronautics, July 2011. DOI: 10.2514/6.2011-5631.
- [165] B. K. Kan, S. D. Heister, and D. E. Paxson. Experimental study of pressure gain combustion with hypergolic rocket propellants. *Journal of Propulsion and Power*, 33(1):112–120, January 2017. ISSN: 1533-3876. DOI: 10.2514/1.B36195.
- [166] H. Kang and S. Kwon. Green hypergolic combination: diethylenetriamine-based fuel and hydrogen peroxide. *Acta Astronautica*, 137, August 2017. DOI: 10.1016/j.actaastro.2017.04.009.
- [167] L. Bayvel and Z. Orzechowski. *Liquid Atomization*. Routledge, January 2019. DOI: 10.1201/9780203748787.
- [168] M. Fick, G. Schulte, and D. Ehmman. Status and current developments of astriums 400 N bipropellant engine. In *39th AIAA/ASME/SAE/ASEE Joint Propulsion Conference and Exhibit*. American Institute of Aeronautics and Astronautics, June 2003. DOI: 10.2514/6.2003-4778.
- [169] U. Gotzig and E. Dargies. Development status of astriums new 22N bipropellant thruster family. In *39th AIAA/ASME/SAE/ASEE Joint Propulsion Conference and Exhibit*. American Institute of Aeronautics and Astronautics, June 2003. DOI: 10.2514/6.2003-4777.
- [170] G. Schulte, U. Gotzig, A. Horch, and T. Dreer. Further improvements and qualification status of astriums 10N bipropellant thruster family. In *39th AIAA/ASME/SAE/ASEE Joint Propulsion Conference and Exhibit*. American Institute of Aeronautics and Astronautics, June 2003. DOI: 10.2514/6.2003-4776.
- [171] G. Dressler and J. Bauer. TRW pintle engine heritage and performance characteristics. In *36th AIAA/ASME/SAE/ASEE Joint Propulsion Conference and Exhibit*. American Institute of Aeronautics and Astronautics, July 2000. DOI: 10.2514/6.2000-3871.
- [172] J. Balkenhohl. *Design, construction and commissioning of a reaction chamber for hypergolic propellants as well as first optical measurements of the flame emission*. Master’s thesis, Universität Stuttgart, 2019.
- [173] H<sub>2</sub>O<sub>2</sub> passivation procedure. Technical report, Solvay Chemicals technical publications, 2005.
- [174] ASTM International. Specification for chemical passivation treatments for stainless steel parts. DOI: 10.1520/a0967\_a0967m-17.
- [175] E. Lemmon, M. Huber, and M. McLinden. NIST standard reference database 23: reference fluid thermodynamic and transport properties-refprop, version 9.1. en, 2013.
- [176] J. M. Pringle, J. Golding, C. M. Forsyth, G. B. Deacon, M. Forsyth, and D. R. MacFarlane. Physical trends and structural features in organic salts of the thiocyanate anion. *Journal of Materials Chemistry*, 12(12):3475–3480, October 2002. DOI: 10.1039/b208372h.
- [177] N.-S. Cheng. Formula for the viscosity of a glycerol-water mixture. *Industrial & Engineering Chemistry Research*, 47(9):3285–3288, March 2008. DOI: 10.1021/ie071349z.
- [178] K. Takamura, H. Fischer, and N. R. Morrow. Physical properties of aqueous glycerol solutions. *Journal of Petroleum Science and Engineering*, 98-99:50–60, November 2012. DOI: 10.1016/j.petrol.2012.09.003.
- [179] J. Witte. *Auslegung und experimentelle Untersuchung von Injektoren für grüne hypergole Treibstoffe*. Master’s thesis, Universität Stuttgart, 2019.

- [180] M. F. Easton, A. G. Mitchell, and W. F. K. Wynne-Jones. The behaviour of mixtures of hydrogen peroxide and water. part 1.- determination of the densities of mixtures of hydrogen peroxide and water. *Trans. Faraday Soc.*, 48(0):796–801, 1952. DOI: 10.1039/TF9524800796.
- [181] Performance Specification: Propellant Hydrogen Peroxide. Technical report, Military Specifications and Standards, August 1, 2003.
- [182] I. T. Horvath and P. T. Anastas. Introduction: green chemistry. *Chemical Reviews*, 107, June 2007. DOI: 10.1021/cr0783784.
- [183] M. Matzke, J. Arning, J. Ranke, B. Jastorff, and S. Stolte. Design of inherently safer ionic liquids: toxicology and biodegradation. *Handbook of green chemistry*, 6, 2013.
- [184] J. D. Holbrey and K. R. Seddon. Ionic liquids. *Clean Technologies and Environmental Policy*, 1(4):223–236, December 1999. DOI: 10.1007/s100980050036.
- [185] Iolitec. *Ionic Liquids 2017*. Ionic Liquids Technologies GmbH, 2017.
- [186] S. B. Heimsch. *Azido liquids as potential hydrazine replacements in a hypergolic bipropulsion system*. PhD thesis, Ludwig-Maximilians-Universität München, 2020.
- [187] L. Werling, F. Lauck, E. Goos, J. Wischek, Y. Besel, and F. Valencia-Bel. Final Project Report; ESA TDE Activity: High Performance Propellant Development ESA Contract No. 4000130652/20/NL/MG. Technical report, 2022.
- [188] E. W. Schmidt. *Hydrazine and Its Derivatives: Preparation, Properties, Applications, 2 Volume Set*. WILEY, August 31, 2001. 2232 pages. ISBN: 0471415537.
- [189] C. Sun, S. Tang, and X. Zhang. Role of cation structures for energetic performance of hypergolic ionic liquids. *Energy & Fuels*, 31(9):10055–10059, August 2017. DOI: 10.1021/acs.energyfuels.7b01259.
- [190] T. Brinck. *Green Energetic Materials*. John Wiley and Sons, January 15, 2014. 304 pages. ISBN: 9781118676455.
- [191] D. H. Zaitsau, V. N. Emel’yanenko, S. P. Verevkin, and A. Heintz. Sulfur-containing ionic liquids. rotating-bomb combustion calorimetry and first-principles calculations for 1-ethyl-3-methylimidazolium thiocyanate. *Journal of Chemical & Engineering Data*, 55(12):5896–5899, November 2010. DOI: 10.1021/je1009366.
- [192] C.-W. Cho, T. P. T. Pham, Y. Zhao, S. Stolte, and Y.-S. Yun. Review of the toxic effects of ionic liquids. *Science of The Total Environment*, 786:147309, September 2021. DOI: 10.1016/j.scitotenv.2021.147309.
- [193] N. Delgado-Mellado, M. Ayuso, M. M. Villar-Chavero, J. Garcia, and F. Rodriguez. Ecotoxicity evaluation towards vibrio fischeri of imidazolium- and pyridinium-based ionic liquids for their use in separation processes. *SN Applied Sciences*, 1(8), July 2019. DOI: 10.1007/s42452-019-0916-3.
- [194] E. Landau. Voyager 1 fires up thrusters after 37 years. J. P. L. NASA, editor. December 1, 2017. URL: <https://www.nasa.gov/feature/jpl/voyager-1-fires-up-thrusters-after-37> (visited on 05/01/2023).
- [195] P. D. McCrary, G. Chatel, S. A. Alaniz, O. A. Cojocar, P. A. Beasley, L. A. Flores, S. P. Kelley, P. S. Barber, and R. D. Rogers. Evaluating ionic liquids as hypergolic fuels: exploring reactivity from molecular structure. *Energy & Fuels*, 28(5):3460–3473, April 2014. DOI: <https://doi.org/10.1021/ef500264z>.
- [196] K. G. Bogolitsyn, T. E. Skrebets, and T. A. Makhova. Physicochemical properties of 1-butyl-3-methylimidazolium acetate. *Russian Journal of General Chemistry*, 79(1):125–128, January 2009. ISSN: 1608-3350. DOI: 10.1134/S1070363209010198.

- [197] Viscosities of Acetate or Chloride-Based Ionic Liquids and Some of Their Mixtures with Water or Other Common Solvents 56(1) (December 2010). ISSN: 1520-5134. DOI: 10.1021/je1007235.
- [198] G. J. Kabo, Y. U. Paulechka, A. G. Kabo, and A. V. Blokhin. Experimental determination of enthalpy of 1-butyl-3-methylimidazolium iodide synthesis and prediction of enthalpies of formation for imidazolium ionic liquids. *The Journal of Chemical Thermodynamics*, 42(10):1292–1297, October 2010. DOI: 10.1016/j.jct.2010.05.007.
- [199] V. N. Emel'yanenko, D. H. Zaitsau, S. P. Verevkin, A. Heintz, K. Voß, and A. Schulz. Vaporization and formation enthalpies of 1-alkyl-3-methylimidazolium tricyanomethanides. *The Journal of Physical Chemistry B*, 115(40):11712–11717, September 2011. DOI: 10.1021/jp207335m.
- [200] E. J. González, B. González, N. Calvar, and Á. Domínguez. Physical properties of binary mixtures of the ionic liquid 1-ethyl-3-methylimidazolium ethyl sulfate with several alcohols at  $t = (298.15, 313.15, \text{ and } 328.15) \text{ k}$  and atmospheric pressure. *Journal of Chemical & Engineering Data*, 52(5):1641–1648, July 2007. DOI: 10.1021/je700029q.
- [201] A. Fernández, J. S. Torrecilla, J. García, and F. Rodríguez. Thermophysical properties of 1-ethyl-3-methylimidazolium ethylsulfate and 1-butyl-3-methylimidazolium methylsulfate ionic liquids. *Journal of Chemical & Engineering Data*, 52(5):1979–1983, August 2007. DOI: 10.1021/je7002786.
- [202] Z.-H. Zhang, Z.-C. Tan, L.-X. Sun, J.-Z. Yang, X.-C. Lv, and Q. Shi. Thermodynamic investigation of room temperature ionic liquid: the heat capacity and standard enthalpy of formation of emies. *Thermochimica Acta Vol. 447*:141–146, 2006.
- [203] M. Cruz, R. Borges, M. Godinho, C. Marques, E. Langa, A. Ribeiro, M. Lourenço, F. Santos, C. N. de Castro, M. Macatrão, M. Tariq, J. Esperança, J. C. Lopes, C. Afonso, and L. Rebelo. Thermophysical and magnetic studies of two paramagnetic liquid salts: [C4mim][FeCl4] and [P66614][FeCl4]. *Fluid Phase Equilibria*, 350:43–50, July 2013. DOI: 10.1016/j.fluid.2013.03.001.
- [204] M. S. Gruzdev, L. M. Ramenskaya, U. V. Chervonova, and R. S. Kumeev. Preparation of 1-butyl-3-methylimidazolium salts and study of their phase behavior and intramolecular interactions. *Russian Journal of General Chemistry*, 79(8):1720–1727, August 2009. DOI: 10.1134/s1070363209080246.
- [205] E. Vataščin and V. Dohnal. Thermodynamic properties of aqueous solutions of [EMIM] thiocyanate and [EMIM] dicyanamide. *The Journal of Chemical Thermodynamics*, 106, March 2017. DOI: 10.1016/j.jct.2016.12.008.
- [206] P. J. Carvalho, T. Regueira, L. M. N. B. F. Santos, J. Fernandez, and J. A. P. Coutinho. Effect of water on the viscosities and densities of 1-butyl-3-methylimidazolium dicyanamide and 1-butyl-3-methylimidazolium tricyanomethane at atmospheric pressure. *Journal of Chemical & Engineering Data*, 55(2):645–652, October 2009. DOI: 10.1021/je900632q.
- [207] E. Vataščin and V. Dohnal. Thermophysical properties of aqueous solutions of the 1-ethyl-3-methylimidazolium tricyanomethanide ionic liquid. *The Journal of Chemical Thermodynamics*, 89:169–176, October 2015. DOI: 10.1016/j.jct.2015.05.011.
- [208] Y. Yoshida, K. Muroi, A. Otsuka, G. Saito, M. Takahashi, and T. Yoko. 1-ethyl-3-methylimidazolium based ionic liquids containing cyano groups: synthesis, characterization, and crystal structure. *Inorganic Chemistry*, 43(4):1458–1462, January 2004. DOI: 10.1021/ic035045q.

- [209] S. Schneider, S. Deplazes, Y. Ahmed, and C. A. Franquera Beauchamp. Catalytic ignition of ionic liquid fuels by ionic liquids. *Briefing Charts, ACS Fall National Meeting, San Francisco, CA*, 2014.
- [210] F. Lauck, M. Negri, and D. Freudenmann. Hypergoles Zweistoffsystem für Raketentriebwerke. Patent (EP3766859B1). July 19, 2019.
- [211] F. Lauck, J. Balkenhohl, M. Negri, D. Freudenmann, and S. Schlechtriem. Green bipropellant development – a study on the hypergolicity of imidazole thiocyanate ionic liquids with hydrogen peroxide in an automated drop test setup. *Combustion and Flame*, 226:87–97, 2021. ISSN: 0010-2180. DOI: <https://doi.org/10.1016/j.combustflame.2020.11.033>.
- [212] M. G. Freire, A. R. R. Teles, M. A. A. Rocha, B. Schröder, C. M. S. S. Neves, P. J. Carvalho, D. V. Evtuguin, L. M. N. B. F. Santos, and J. A. P. Coutinho. Thermo-physical characterization of ionic liquids able to dissolve biomass. *Journal of Chemical & Engineering Data*, 56(12):4813–4822, 2011. DOI: [10.1021/je200790q](https://doi.org/10.1021/je200790q). eprint: <https://doi.org/10.1021/je200790q>.
- [213] J. Scholl. *Untersuchungen zum Zündverzögerung von hypergolen grünen Treibstoffen unter verschiedenen Umgebungsbedingungen*. Master’s thesis, Universität Stuttgart, 2020.
- [214] W. M. Haynes. *Handbook of Chemistry and Physics 94th Edition*. CRC Press, 2016. ISBN: 9781466571150.
- [215] Themor Fisher Scientific. 1-ethyl-3-methylimidazolium thiocyanate. *Sicherheitsdatenblatt*.
- [216] U. Domańska and M. Laskowska. Effect of temperature and composition on the density and viscosity of binary mixtures of ionic liquid with alcohols. *Journal of Solution Chemistry*, 38(6):779–799, April 2009. DOI: [10.1007/s10953-009-9410-7](https://doi.org/10.1007/s10953-009-9410-7).
- [217] A. E. Thomas, S. D. Chambreau, N. D. Redeker, A. A. Esparza, E. Shafirovich, T. Ribbeck, J. A. P. Sprenger, M. Finze, and G. L. Vaghjiani. Thermal decomposition and hypergolic reaction of a dicyanoborohydride ionic liquid. *The Journal of Physical Chemistry A*, 124(5):864–874, January 2020. DOI: [10.1021/acs.jpca.9b09242](https://doi.org/10.1021/acs.jpca.9b09242).
- [218] G. Elverum Jr and T. Morey. Criteria for optimum mixture-ratio distribution using several types of impinging-stream injector elements. Technical report, NASA Jet Propulsion Laboratory, 1959.
- [219] F. C. Johansen. Flow through pipe orifices at low reynolds numbers. *Proceedings of the Royal Society of London. Series A, Containing Papers of a Mathematical and Physical Character*, 126(801):231–245, January 1930. ISSN: 2053-9150. DOI: [10.1098/rspa.1930.0004](https://doi.org/10.1098/rspa.1930.0004).
- [220] Q.-F. Fu, L.-J. Yang, W. Zhang, and K.-D. Cui. Spray characteristics of an open-end swirl injector. *Atomization and Sprays*, 22(5):431–445, 2012. DOI: [10.1615/atomizspr.2012005646](https://doi.org/10.1615/atomizspr.2012005646).
- [221] M. Ventura, E. Wernimont, S. Heister, and S. Yuan. Rocket grade hydrogen peroxide (RGHP) for use in propulsion and power devices - historical discussion of hazards. In *43rd AIAA / ASME / SAE / ASEE Joint Propulsion Conference and Exhibit*. American Institute of Aeronautics and Astronautics, July 2007. DOI: [10.2514/6.2007-5468](https://doi.org/10.2514/6.2007-5468).
- [222] J. McCormick. Hydrogen peroxide rocket manual. *FMC Corporation. Propulsion Department*, 1965.
- [223] T. A. Litovitz. Temperature dependence of the viscosity of associated liquids. *The Journal of Chemical Physics*, 20(7):1088–1089, July 1952. DOI: [10.1063/1.1700671](https://doi.org/10.1063/1.1700671).

- [224] O. Cabeza, L. M. Varela, E. Rilo, L. Segade, M. Domínguez-Pérez, D. Ausín, I. [de Pedro], J. R. Fernández, J. González, M. P. Vazquez-Tato, Y. Arosa, E. López-Lago, R. [de la Fuente], J. J. Parajó, J. Salgado, M. Villanueva, V. Matveev, A. Ievlev, and J. A. Seijas. Synthesis, microstructure and volumetry of novel metal thiocyanate ionic liquids with [BMIM] cation. *Journal of Molecular Liquids*, 283:638–651, 2019. ISSN: 0167-7322. DOI: <https://doi.org/10.1016/j.molliq.2019.03.088>.
- [225] W. Kong, P. Cao, X. He, L. Yu, X. Ma, Y. He, L. Lu, X. Zhang, and Y. Deng. Ionic liquid based vibrational energy harvester by periodically squeezing the liquid bridge. *RSC Adv.*, 4(37):19356–19361, 2014. DOI: 10.1039/c4ra00629a.
- [226] R. Anantharaj and T. Banerjee. Phase behaviour of 1-ethyl-3-methylimidazolium thiocyanate ionic liquid with catalytic deactivated compounds and water at several temperatures: experiments and theoretical predictions. *International Journal of Chemical Engineering*, 2011:1–13, 2011. DOI: 10.1155/2011/209435.
- [227] H. Almeida, P. J. Carvalho, K. A. Kurnia, J. A. L. da Silva, J. A. P. Coutinho, and M. G. Freire. Surface tensions of ionic liquids: non-regular trend along the number of cyano groups. *Fluid Phase Equilibria*, 409:458–465, February 2016. DOI: 10.1016/j.fluid.2015.10.044.
- [228] U. Domańska, M. Królikowska, and M. Królikowski. Phase behaviour and physico-chemical properties of the binary systems 1-ethyl-3-methylimidazolium thiocyanate, or 1-ethyl-3-methylimidazolium tosylate water, or an alcohol. *Fluid Phase Equilibria*, 294(1-2):72–83, July 2010. DOI: 10.1016/j.fluid.2010.01.020.
- [229] D. H. Zaitsau, A. V. Yermalayeu, and S. P. Verevkin. Ionic liquids alkyl-imidazolium thiocyanates: comprehensive thermochemical study. *Journal of Molecular Liquids*, 321:114284, January 2021. DOI: 10.1016/j.molliq.2020.114284.
- [230] G. Cui, H. Yu, and Y. jie Ma. Ionic liquids as mobile phase additives for determination of thiocyanate and iodide by liquid chromatography. *Journal of Separation Science*, 42(9):1733–1739, March 2019. DOI: 10.1002/jssc.201801277.
- [231] W. Gorman, E. Messinger, and M. Herman. Toxicity of thiocyanates used in treatment of hypertension. *Annals of Internal Medicine*, 30(5):1054, May 1949. DOI: 10.7326/0003-4819-30-5-1054.
- [232] S. N. Vogel, T. R. Sultan, and R. P. Ten Eyck. Cyanide poisoning. *Clinical Toxicology*, 18(3):367–383, January 1981. DOI: 10.3109/15563658108990043.
- [233] J. Ranke, K. Mölter, F. Stock, U. Bottin-Weber, J. Poczobutt, J. Hoffmann, B. Ondruschka, J. Filser, and B. Jastorff. Biological effects of imidazolium ionic liquids with varying chain lengths in acute vibrio fischeri and WST-1 cell viability assays. *Ecotoxicology and Environmental Safety*, 58(3):396–404, July 2004. DOI: 10.1016/s0147-6513(03)00105-2.
- [234] D. Passino and S. Smith. Acute bioassays and hazard evaluation of representative contaminants detected in great lakes fish. *Environmental Toxicology and Chemistry*, 6(11):901–907, November 1987. DOI: 10.1002/etc.5620061111.
- [235] ThermoFisher Scientific. Sicherheitsdatenblatt 1-Ethyl-3-methylimidazolium thiocyanate. Technical report.
- [236] IFA, Institute for Occupational Safety and Health of the German Social Accident Insurance. Gestis substance database entry: kupferthiocyanat / copper thiocyanate. URL: <https://gestis.dguv.de/data?name=530220> (visited on 10/10/2022).
- [237] J. L. Rovey, C. T. Lyne, A. J. Mundahl, N. Rasmont, M. S. Glascock, M. J. Wainwright, and S. P. Berg. Review of multimode space propulsion. *Progress in Aerospace Sciences*, 118:100627, October 2020. DOI: 10.1016/j.paerosci.2020.100627.

- 
- [238] E. Fonda-Marsland and C. Ryan. Preliminary ionic liquid propellant selection for dual-mode micro-propulsion systems. In *53rd AIAA/SAE/ASEE Joint Propulsion Conference*. American Institute of Aeronautics and Astronautics, July 2017. DOI: 10.2514/6.2017-5019.
- [239] C. Ryan, A Daykin-Iliopoulos, J. Stark, A. Salaverri, E. Vargas, P. Rangsten, S. Dandavino, C. Ataman, S. Chakraborty, D. Courtney, et al. Experimental progress towards the microthrust mems electro-spray electric propulsion system. In *33rd International Electric Propulsion Conference*, number CONF, 2013.
- [240] B. R. Donius and J. L. Rovey. Ionic liquid dual-mode spacecraft propulsion assessment. *Journal of Spacecraft and Rockets*, 48(1):110–123, January 2011. DOI: 10.2514/1.49959.
- [241] G. Pace, A. Pasini, and L. Torre. PulCheR-pulsed chemical rocket with green high performance propellants: 30th month project overview. In *Challenges in european aerospace 5th CEAS Air and Space Conference*, 2015.
- [242] M. Negri and F. Lauck. Hot firing tests of a novel green hypergolic propellant in a thruster. *Journal of Propulsion and Power*, 38(3):467–477, May 2022. DOI: 10.2514/1.b38413.
- [243] X. Zhao, Z. Wang, X. Qi, S. Song, S. Huang, K. Wang, and Q. Zhang. Hunting for energetic complexes as hypergolic promoters for green propellants using hydrogen peroxide as oxidizer. *Inorganic Chemistry*, 60(22):17033–17039, October 2021. DOI: 10.1021/acs.inorgchem.1c02149.



# Curriculum vitae

## PERSONAL INFORMATION

**Name:** Felix Lauck  
**E-Mail:** flauck@posteo.de  
**Date of birth:** 10<sup>th</sup> May 1990  
**Nationality:** German



## PROFESSIONAL EXPERIENCE:

- 08.2023 – present** CTO and Co-Founder of InSpacePropulsion Technologies GmbH (ISPTech), a DLR spin-off
- 02.2020 – present** Research associate, Satellite and Orbital Propulsion department, German Aerospace Center (DLR), Institute of Space Propulsion, Lampoldshausen
- 02.2017 – 11.2024** PhD researcher, Propellants department, German Aerospace Center (DLR), Institute of Space Propulsion, Lampoldshausen  
Topic: Development of a green hypergolic propellant

## EDUCATION:

- 04.2014 – 10.2016** University of Stuttgart, Aerospace Engineering  
Degree: Master of Science  
Thesis: Experimental investigation of detonation and flame arrestors used for a premixed, green propellant consisting of nitrous oxide (N<sub>2</sub>O) and ethylene (C<sub>2</sub>H<sub>4</sub>)
- 10.2010 – 12.2013** University of Stuttgart, Aerospace Engineering  
Degree: Bachelor of Science  
Thesis: Experimental investigation of the bearing strength of joints reinforced by pressed-in tailored fibre placements
- 09.2000 – 07.2009** Hochwaldgymnasium Wadern  
Degree: Abitur